อิทธิพลของไอออนโลหะและการเปลี่ยนแปลงโครงรูปของตัวถูกละลายต่อการไฮเดรตของกรดอะมิโนขนาดเล็ก

นางสาวณัฐิญา ดียิ่ง

วิทยานิพนธ์นี้เป็นส่วนหนึ่งของการศึกษาตามหลักสูตรปริญญาวิทยาศาสตรดุษฎีบัณฑิต
สาขาวิชาเคมี
มหาวิทยาลัยเทคโนโลยีสุรนารี
ปีการศึกษา 2548

ISBN 974-533-535-5

INFLUENCE OF METAL ION AND SOLUTE CONFORMATION CHANGE ON HYDRATION OF SMALL AMINO ACID

Natthiya Deeying

A Thesis Submitted in Partial Fulfillment of the Requirements

for the Degree of Doctor of Philosophy in Chemistry

Suranaree University of Technology

Academic Year 2005

ISBN 974-533-535-5

INFLUENCE OF METAL ION AND SOLUTE CONFORMATION CHANGE ON HYDRATION OF SMALL AMINO ACID

Suranaree University of Technology has approved this thesis submitted in partial fulfillment of the requirements for the Degree of Doctor of Philosophy.

Thesis Examining Committee

(Assoc. Prof. Dr. Malee Tangsathitkulchai)
Chairperson

(Prof. Dr. Kritsana Sagarik)
Member (Thesis Advisor)

(Prof. Dr. Supot Hannongbua)
Member

Tongraar A.
(Assoc. Prof. Dr. Anan Tongraar)
Member

(Asst. Prof. Dr. Visit Vao-Soongnern)
Member

(Assoc. Prof. Dr. Saowanee Rattanaphani)
Vice Rector for Academic Affairs

S. Thammathaworn
(Assoc. Prof. Dr. Sompong Thammathaworn)
Dean of Institute of Science

ณัฐิญา ดียิ่ง : อิทธิพลของไอออนโลหะและการเปลี่ยนแปลงโครงรูปของตัวถูกละลายต่อการไฮเดรตของกรดอะมิโนขนาดเล็ก (INFLUENCE OF METAL ION AND SOLUTE CONFORMATION CHANGE ON HYDRATION OF SMALL AMINO ACID)
อาจารย์ที่ปรึกษา : ศาสตราจารย์ ดร.กฤษณะ สาคริก, 192 หน้า. ISBN 974-533-535-5

งานวิจัยเรื่องนี้เป็นงานวิจัยเชิงทฤษฎีที่ศึกษาอิทธิพลของไอออนโลหะและผลของการเปลี่ยนแปลงโครงรูปของตัวถูกละลายที่มีต่อโครงสร้าง พลังงาน และพลวัตของโมเลกุลน้ำในชั้นไฮเดรชันของกรดอะมิโน ซึ่งศึกษาโดยใช้อะลานีน (Alanine; Ala) สามโครงรูปและสารประกอบเชิงซ้อนที่เกิดจากไอออนลิเทียมกับอะลานีน (Li^+/Ala) เป็นแบบจำลอง ทั้งนี้เริ่มจากการสร้างศักย์ระหว่างโมเลกุลเทสท์พาร์ทิเคิล (Test particle model; T-model) สำหรับโมเลกุลที่เกี่ยวข้องทั้งหมด จากนั้นนำศักย์ระหว่างโมเลกุลเทสท์พาร์ทิเคิลที่คำนวณได้ไปใช้ในการจำลองโมเลกุลพลวัต (Molecular Dynamics (MD) Simulations) Ala ในน้ำ ($[\text{Ala}]_{aq}$) และ Li^+/Ala ในน้ำ ($[\text{Li}^+/\text{Ala}]_{aq}$) ที่อุณหภูมิ 298 K ผลการคำนวณโดยวิธีการจำลองโมเลกุลพลวัตแสดงว่า โครงข่ายพันธะไฮโดรเจน (H-bond networks) ของน้ำรอบๆ หมู่ฟังก์ชันของ Ala มีความแข็งแรงมากขึ้นเนื่องจากอิทธิพลของไอออนโลหะ ในขณะที่การหมุนพันธะ $\text{N}-\text{C}^{\alpha}$ จากมุม $\phi = 0$ ถึง 180 องศา ส่งผลเพียงเล็กน้อยและไม่เป็นไปในทิศทางเดียวกัน ผลการศึกษาแสดงว่าพลวัตของโมเลกุลน้ำในชั้นไฮเดรชันที่หนึ่ง (the first hydration shell) สามารถคาดคะเนหรือประมาณได้จากภูมิภาพพลังงานศักย์เฉลี่ยสุทธิ (total-average potential energy landscapes) และแผนภาพการแลกเปลี่ยนน้ำ (water exchange diagrams) ผลการศึกษาเสนอว่าสำหรับกระบวนการการแลกเปลี่ยนน้ำ โมเลกุลน้ำเคลื่อนที่ในช่องภายในชั้นไฮเดรชันช่วงเวลาหนึ่ง ก่อนที่จะออกไปจากช่องนั้น ณ ตำแหน่งใดๆ ผลที่ได้จากการศึกษาเชิงทฤษฎีได้ย้ำความจำเป็นในการนำโมเลกุลน้ำมาพิจารณาสร้างแบบจำลองในการคำนวณ

สาขาวิชาเคมี ลายมือชื่อนักศึกษา____________________
ปีการศึกษา 2548 ลายมือชื่ออาจารย์ที่ปรึกษา____________________

NATTHIYA DEEYING : INFLUENCE OF METAL ION AND SOLUTE CONFORMATION CHANGE ON HYDRATION OF SMALL AMINO ACID. THESIS ADVISOR : PROF. KRITSANA SAGARIK, Ph.D. 192 PP. ISBN 974-533-535-5

ALANINE/LITHIUM ION/CONFORMATION/HYDRATION

The influence of metal ion and solute conformation change on the structures, energetic and dynamics of water molecule in the hydration shell of amino acid was studied, using three forms of alanine (Ala) and Li^+/Ala as model molecules. The theoretical investigations were started with construction of the test-particle model (T-model) potentials for all molecules involved and followed by Molecular Dynamics (MD) simulations of $[Ala]_{aq}$ and $[Li^+/Ala]_{aq}$ at 298 K. The MD results showed that, the hydrogen bond (H-bond) networks of water at the functional groups of Ala are strengthened by the metal ion binding; whereas the rotation of the $N - C^{\alpha}$ bond from the angle $\phi = 0$ to 180 degree brings about smaller effects which cannot be generalized. It was also shown that, the dynamics of water molecule in the first hydration shell of amino acid could be estimated from the total-average potential energy landscapes and the water exchange diagrams. The MD results suggested to include an additional dynamic step in the water exchange process, in which water molecule moves inside a channel within the first hydration shell of solute, before leaving the channel at some point. The theoretical results reported in the present work iterated the necessity to include explicit water molecules in the model calculations.

School of Chemistry Student's Signature Natthiya Deeying

Academic Year 2005 Advisor's Signature K-Sagarik

ACKNOWLEDGEMENTS

I would like to take this opportunity to express my deeply grateful thank to my thesis advisor, Prof. Dr. Kritsana Sagarik for his guidance, valuable suggestions and encouragement during the period of my studying.

I would like to acknowledge the financial support from the Thailand Research Fund (TRF) through the Royal Golden Jubilee (RGJ) Ph.D. program (Grant No.PHD/0005/2542). Special thanks to the School of Chemistry and the School of Mathematics, Institute of Science, Suranaree University of Technology (SUT) for providing computer facilities.

I would like to particularly thank to Assoc. Prof. Dr. Anan Tongraar and Asst. Prof. Dr. Visit Vao-soongnern for their encouragement and help. Furthermore I would like to thank the thesis examining committee for their valuable suggestions and comments.

I am very grateful to all of my friends in the School of Chemistry, especially in computational chemistry research group for their friendship and help.

Finally, I wish to express my deepest gratitude to my parents, brothers, grandmother, grandfather and Mr. Chalermpon Chungtragunwong for their hearten, understanding and encouragement.

Natthiya Deeying

CONTENTS

Page

CHAPTER

CONTENTS (Continued)

Page

APPENDICES

LIST OF TABLES

Table **Page**

LIST OF FIGURES

LIST OF FIGURES (Continued)

Figure **Page**

LIST OF FIGURES (Continued)

LIST OF FIGURES (Continued)

LIST OF FIGURES (Continued)

LIST OF ABBREVIATIONS

° = degree
Å = angström
D = Debye
K = Kelvin
kJ/mol = kilojoule per mole
ps = picosecond
Ala = Alanine
Gly = Glycine
Alaz = Alanine zwitterion
Glyz = Glycine zwitterion
Li^+ = Lithium ion
Na^+ = Sodium ion
H_2O = Water
FA = Formamide
BA = Benzoic acid
$Gdm^+ - FmO^-$ = Guanidinium - Formate complex
$[Ala]_{aq}$ = Ala in aqueous solution
$[Li^+/Ala]_{aq}$ = Li^+ /Ala complex in aqueous solution
$[Li^+]_{aq}$ = Li^+ in aqueous solution
$[Na^+]_{aq}$ = Na^+ in aqueous solution

LIST OF ABBREVIATIONS (Continued)

$[NH_4^+]_{aq}$ = Ammonium ion in aqueous solution

$[H_3O^+]_{aq}$ = Hydronium ion in aqueous solution

H-bond = Hydrogen bond

NMR = Nuclear Magnetic Resonance

NOE = Nuclear Overhauser Effects

SCF = Self-Consistent Field

CHelpG = CHarges from ELectrostatic Potentials using a Grid based method

BSSE = Basis Set Superposition Error

NSE = Net Stabilization Effect

HF = Hartree-Fock

MP2 = Second-order Møller-Plesset

MP2CP = MP2 calculations with the counterpoise corrections

ΔE_{MP2} = MP2 interaction energy

ΔE_{MP2CP} = MP2CP interaction energy

T-model = Test-particle model

$\Delta E_{T-model}$ = T-model interaction energy

ΔE_{SCF}^{1} = First-order SCF interaction energy

ΔE^{r} = Higher-order energy term

ΔE_{REP} = Exchange repulsion energy

LIST OF ABBREVIATIONS (Continued)

ΔE_{ES} = Electrostatic energy

B(T) = Second virial coefficient

L = Simulation box length

MC = Monte Carlo

MD = Molecular Dynamics

NVE-MD = Microcanonical Ensemble-MD simulations

g(R) = Atom-atom pair correlation function

n(R) = Average running coordination number

PD = Probability distribution

PDO = The probability distribution for the oxygen atoms of water

PDH = The probability distribution for the hydrogen atoms of water

AWPD = The average solute-solvent interaction energy probability distribution

WWPD = The average solvent-solvent interaction energy probability distribution

AW-WWPD = The total-average interaction energy probability distribution

$\langle E_{aq}^{pot} \rangle$ = The average potential energy of aqueous solutions

$\langle E_{aq}^{solu\text{-}solv} \rangle$ = The average solute-solvent interaction energies

LIST OF ABBREVIATIONS (Continued)

$<E_{aq}^{solv\text{-}solv}>$ = The average solvent-solvent interaction energies

$<E_{aq}^{L}>$ = The average potential energy barriers to the diffusion of water molecules within and between the H-bond networks

$<E_{aq}^{T}>$ = The average potential energy barriers to the diffusion of water molecules between the H-bond networks and the outside

$A\text{-}H\cdots B$ = H-bond between the proton donor A and acceptor B

$\tau_{A-H\cdots Ow,max}$ = The longest H-bond lifetime between the proton donor A-H and the oxygen atom of water (Ow)

$\tau_{A-H\cdots Ow}$ = The H-bond lifetime between the proton donor A-H and the oxygen atom of water (Ow)

$\tau_{Li^{+}\cdots Ow}$ = The water residence times at Li^{+}

$\tau_{ex,A\text{-}H\cdots Ow}$ = The lifetimes of the water exchange intermediate complexes at H-bond

$\tau_{ex,Li^{+}\cdots Ow}$ = The lifetimes of the water exchange intermediate complexes at Li^{+}

$\Delta E^{AW\text{-}WW}$ = The total-interaction energies

$\Delta Ea^{AW\text{-}WW}$ = The activation interaction energy of the transition state complex

LIST OF ABBREVIATIONS (Continued)

$\Delta E_{\mathrm{av}}^{\mathrm{AW\text{-}WW}}$ = The average interaction energy of a specific water molecule in the first hydration shell

$\Delta E_{\mathrm{TS}}^{\mathrm{AW\text{-}WW}}$ = The interaction energy at the water exchange transition state

k_{ex} = The water exchange rate constant

τ_{res} = The water residence time

$< \tau_{\mathrm{rt}} >$ = The water residence times obtained from MD simulations of the Bovine Pancreatic Trypsin Inhibitor in aqueous solution

CHAPTER I

INTRODUCTION

One of the fundamental issues of chemistry is the relationship between the reaction of a molecule and its structure. Chemists have long sought the principle governing this fundamental relation with impressive success in a wide range of chemical problems. This close relationship between the reaction and molecular structure is especially important for biomolecules. Indeed, the structure of a biomolecule may be considered as the blueprint for its biochemical functions, and this intricate interplay between the reactivity and the structure of biomolecules is the underlying mechanism of life itself. For example, amino acid sequence of a protein basically determines its structure at various levels, providing its characteristic reaction. Pairing of nucleic acid bases in DNA by hydrogen bonding (H-bonding) gives rise to the double helix structure, and the sequence of the base is nothing other than the genetic information.

When one considers the structure and reaction of biomolecules, the effects of solvent must be taken into account. This is due to the fact that biomolecules exist and almost always react under the influence of solvent, mostly water (Robertson and Simons, 2001; Shishkin, Sukhanov, Gorb and Leszczynski, 2002; Sicinska, Paneth and Truhlar, 2002; Zwier, 2001). The interactions with water molecules may alter the relative stability of various conformers of the solute, or they may profoundly influence the reaction path of molecules, affecting the properties of the solute molecule both thermodynamically and kinetically. Studying the effects of solvation is usually quite difficult, because the solute-solvent interactions are of a molecular nature, and thus, must be treated at the molecular level.

In recent years, there has been considerable interest in the determination of thermodynamic, transport, surface properties etc., of proteins which could mimic some aspects of protein and provide insight into protein hydration (Chalikian, Sarvazyan and Breslauer, 1993; 1994; Chalikian, Sarvazyan, Funck, Cain and Breslauer, 1994; Glinski, Chavepeyer and Platten, 2000; Häckel, Hinz and Hedwig, 1999). Amino acids, such as glycine (Gly) and alanine (Ala), have been extensively used as models for studies of such systems (Chalikian *et al*., 1994; Glinski *et al*., 2000; Häckel *et al*., 1999), due to their moderate size. As a matter of fact, they are among the most important biological molecules, since they constitute the building blocks of peptides and proteins. Most of their outstanding properties are due to their amphoteric nature, which derives from the presence, in their structure, of two functional groups of different polarity, the amino (NH_2) and the carboxyl (COOH) groups. They are responsible, for example, of the existence of a tautomeric equilibrium between neutral and zwitterionic forms. In the gas phase, the neutral form is energetically favoured, while in the condensed phase, such as solutions of polar solvents and crystals, the ionic form is more stable (Almlöf, Kuick and Thomas, 1973; Iijima, Tanaka and Onuma, 1991). Theoretical works have been devoted to the investigation of the structure and stability of amino acids both in the gas phase and in solution by means of *ab initio* techniques (Ahn *et al*., 2003; Kwon, Kim and No, 1995; Tortonda, Pascual-Ahuir, Silla and Tuñón, 1996; 2003; Tuñón, Silla and Ruiz-López, 2000). They found that the most stable structure is different in solution and in the gas phase, mainly due to the very different dipole moment (Tortonda *et al*., 1996; Tuñón *et al*., 2000). Most interestingly, they proposed a tautomerization mechanism for the conversion from the neutral to zwitterionic forms, where the rate determining step was an equilibrium between two neutral conformers (Tuñón *et al*., 2000). This is due to the very small classical energy barrier associated to the proton transfer step from the carboxylic oxygen atom to the nitrogen atom, predicted from continuum and discrete models if correlation energy is taken into account (Kassab, Langlet, Evleth and Akacem, 2000; Tortonda *et al*., 1996; Tuñón, Silla, Millot, Martins-Costa and Ruiz-López, 1998). Thus, although amino acid chemistry in solution is dominated by the zwitterionic form, equilibria among neutral conformers is of relevant interest.

The two simplest amino acids, namely Gly and Ala are also a good test molecules to learn about solvent effects on the conformational equilibrium of biomolecules. In the gas phase, various experimental and theoretical evidences have led to the conclusion that both Gly and Ala exist in neutral forms (Donohue, 1950; Levy and Corey, 1941); whereas in aqueous solutions and crystals, they adopt zwitterionic forms (Donohue, 1950; Junk and Sevec, 1963; Levy and Corey, 1941; Takagi, Chihara and Seki, 1959), abbreviated in the present study as Glyz and Alaz, respectively. Matrix isolation IR spectroscopy (Reva *et al*., 1995; Stepanian, Reva, Radchenko and Adamowicz, 1998), microwave spectroscopy (Suenram and Lovas, 1980) and *ab initio* calculations (Ahn *et al*., 2003; Barone, Adamo and Lelj, 1995; Cao, Newton, Pranata and Schafer, 1995; Csazar, 1995; 1996; Gronert and O'Hair, 1995; Hu, Shen and Schaefer III, 1993, Stepanian *et al*., 1998) predicted at least three most stable conformations of Gly and Ala in the gas phase. They possess cyclic

N-H..O=C, N..H-O and N-H..O-H intramolecular H-bonds, generally regarded as structures **I**, **II** and **III**, as given in Figure 1.1, respectively.

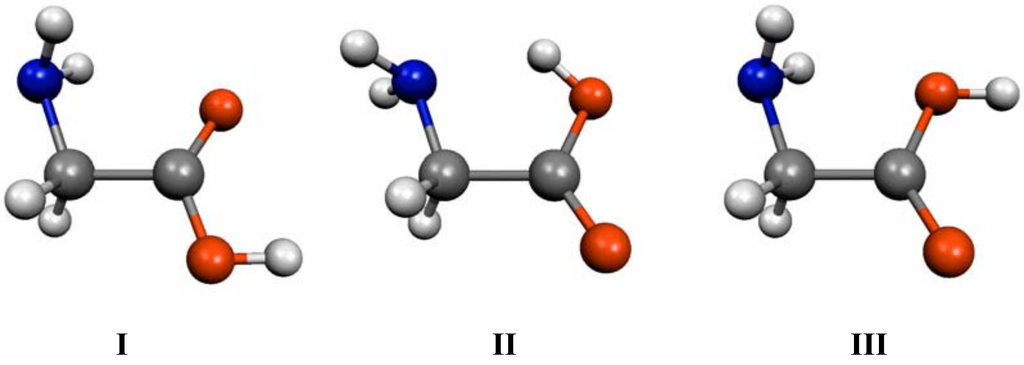

Figure 1.1 Three lowest energy conformers of Gly in the gas phase.

Structure **I** has been confirmed by *ab initio* calculations (Basch and Stevens, 1990; Bonaccorsi, Palla and Tomasi, 1984; Csazar, 1995; Ding and Krogh-Jespersen, 1992; Hu *et al*., 1993; Jensen and Gordon, 1991; Ramek and Cheng, 1992; Ramek, Cheng, Frey, Newton and Schäfer, 1991; Schäfer, Sellers, Lovas and Suenram, 1980; Sellers and Schäfer, 1978; Siam, Klimkowski, Ewbank, Van Alsenoy and Schäfer, 1984; Stepanian *et al*., 1998) and experiments (Reva *et al*., 1995; Stepanian *et al*., 1998) to represent the global minimum energy geometry; whereas structures **II** and **III** were reported to be local minimum energy geometries, with comparable relative stability (Hu *et al*., 1993; Jensen and Gordon, 1991). *Ab initio* calculations at MP2/6-31G(d) level predicted quite low interconversion energy barrier between structures **III** and **I**, only about 5.4 kJ/mol (Jensen and Gordon, 1991). The situation is different in aqueous solutions, in which structure **II** (Tortonda, Pascual-Ahuir, Silla and Tuñón, 2003) becomes the global minimum energy geometry and the proton transfer was suggested to take place readily between the O-H and N-H groups, forming Glyz and Alaz (Ahn *et al*., 2003; Stepanian *et al*., 1998).

It has been well established that metal ions play central roles in various processes in biological systems (Cerda and Wesdemiotis, 1996; Lippard and Berg, 1994). They are generally involved in enzyme regulation, stabilization of structures of reactive biomolecules (Cowan, 1993; Hughes, 1981; Kaim and Schwederski, 1994; Lippard and Berg, 1994) and transportation to transmembrane channels *etc.* (Dougherty and Stauffer, 1990; Kumpf and Dougherty, 1993; Miller, 1993; Zhong *et al*., 1998). Attempts have been made in the past decades to study structural and energetic aspects of metal ion-protein complexes in aqueous solutions and crystals (Lippard and Berg, 1994). These represent difficult tasks due to the fact that proteins are complicated multifunctional macromolecules with several possible conformations and binding sites. Based on theoretical and experimental studies, it appeared for example that, the positions of metal ion binding sites play critical roles in determining the locations of bond formations and disruptions in biochemical reactions (Leary, Zhou, Ogden and Williams, 1990). In aqueous solutions, the stability of proteins and the folding patterns of the peptide backbones have been pointed out to be affected by the presence of metal ion (Dyson and Wright, 2004). Since there have been many review articles taking into account the interactions in protein solutions in details (Gregory, ed., 1994), only some important theoretical and experimental aspects relevant to the present study will be briefly summarized.

The affinities of metal ions with small amino acids, such as Gly and Ala, as well as the dipeptides composed of these small amino acids such as Gly-Gly and Ala-Ala, in the gas phase have been investigated, using both experiments (Busch, Glish and McLuckey, 1988; Jockusch, Lemoff and Williams, 2001a; 2001b; Jockusch, Price and Williams, 1999; Moision and Armentrout, 2002; Strittmatter, Lemoff and Williams, 2000) and *ab initio* calculations (Jensen, 1992; Marino, Russo and Toscano, 2000; 2001; Remko and Rode, 2000; Strittmatter *et al*., 2000). The theoretical results obtained from the hybrid B3LYP exchange-correlation functional using extended basis sets revealed that, for Gly and Ala, the metal ion affinities decrease on going from Cu^+ to Li^+ and Na^+ and the values computed at this level of theory agree in general with experiments (Marino *et al*., 2000); except for Li^+, for which a deviation of about 29 kJ/mol was observed. It appeared that, in the gas phase, the metal ions considered by Marino *et al*. (2000) and Wyttenbach, Witt and Bowers (1999) prefer to bind simultaneously at the N and O atoms of Gly and Ala. This type of bidentate coordination has been found also in larger amino acid complexes, such as Li^+/valine (Li^+/Val) (Jockusch *et al*., 2001) and Na^+/phenylalanine (Na^+/Phe) (Siu, Ma and Tsang, 2001) *etc*.

The influence of metal ions on the stabilities of small H-bond complexes (Rode and Sagarik, 1982; Sagarik and Rode, 1981), as well as biologically active molecules, such as the base pairs of DNA (Sagarik and Rode, 1983a; 1983b), was reported based on theoretical studies. *Ab initio* calculations (Sagarik and Rode, 1981) showed that Li^+ transfers its electrostatic effects along the $O=C-N$ structure in the formamide (FA)-H_2O complex, leading to a net stabilization effect (NSE) at the neighboring N-H···Ow H-bond. This was supported by the results obtained from FTIR experiment (Du and Liang, 2000), which shows that, due to the condensing effects, Ag^+ and Zn^{2+} could give rise to an increase in the intermolecular H-bond interactions between adjacent molecules in the N-octadecanoyl–L-alanine monolayes;

whereas the expanding effects of Ca^{2+}, Cd^{2+}, Ni^{2+} and La^{3+} could lead to the formation of intramolecular H-bonds.

Structures, energetic and dynamics of water molecules in the first hydration shells of proteins have been pointed out to constitute basic information required to characterize their stability in aqueous solutions (Finney and Soper, 1994; Soper, 2000; Soper and Luzar, 1996). They have long been the subject of interest in both theoretical and experimental points of view (Bee, 1988; Dill, 1990; Frauenfelder, Parak and Young, 1988; Karplus and Faerman, 1994; Levitt and Park, 1993; Palma, Palma-Vittorelli and Parak, eds., 1993; Saenger, 1987), *e.g. ab initio* calculations, molecular dynamics (MD) and Monte Carlo (MC) simulations (Rozanska and Chipot, 2000; Saigal and Pranata, 1997), as well as X-ray (Levitt and Sharon, 1988; Van Gunsteren, Berendsen, Hermans, Hol and Postma, 1983) and NMR experiments (Otting, Liepinsh, Farmer II and Wüthrich, 1991; Otting, Liepinsh and Wüthrich, 1991; 1992; Otting and Wüthrich, 1989). In aqueous solutions and crystals, X-ray crystallography measures the extent to which specific hydration sites of proteins are occupied by water molecules, whereas the observations of the Nuclear Overhauser Effects (NOE) between individual protons of amino acid residues and those of sufficiently tightly bound water enable NMR experiments to monitor specific water molecules in the first hydration shells of proteins, before being replaced by another water molecule (Wüthrich, 1995). Through the measurements of NOE, the dynamics of individual water molecules in the first hydration shells of proteins could be determined with acceptable accuracy (Otting, Liepinsh, Farmer II and Wüthrich, 1991; Otting, Liepinsh and Wüthrich, 1991; 1992; Otting and Wüthrich, 1989), *e.g.* by measuring the residence times of specific water molecules. Although the residence times are sensitive to the definitions and methods employed in the investigations (Odelius and Laaksonen, 1999), the ones obtained from NMR experiments are compared well with those from MD simulations (Brunne, Liepinsh, Otting, Wüthrich and Van Gunsteren, 1993; Otting, Liepinsh, Farmer II and Wüthrich, 1991; Otting, Liepinsh and Wüthrich, 1991; 1992; Otting and Wüthrich, 1989). The residence times deduced from NMR experiments (Knapp and Muegge, 1993) suggested, for example, that the diffusion process of water molecules moving away from protein surface is heterogeneous; about 75% of the surface water diffuse four times slower and 25% diffuse fifteen times faster than in the bulk. It was also illustrated based on MD simulations that the average residence times of water at the side chain atoms of proteins are approximately 50% smaller than for the backbone atoms (Brunne *et al.*, 1993; Muegge and Knapp, 1995).

Theoretical methods employed in the studies of solutions fall into two categories (Orozco and Luque, 2000); microscopic methods consider solvent molecules and their interactions with solutes explicitly, whereas macroscopic ones take into account solvent as a continuum medium characterized by a dielectric constant. It has been shown that both approaches have advantages and disadvantages. The H-bond networks of water in the first hydration shells of solutes were investigated using an explicit water model and MD simulations (Sagarik, 1999; Sagarik, Chaiwongwattana and Sisot, 2004; Sagarik and Chaiyapongs, 2005; Sagarik and Dokmaisrijan, 2005; Sagarik and Rode, 2000). The MD results showed that, the H-bond networks in the first hydration shells of the zwitterionic form of Ala could be changed due to its conformation change (Sagarik and Dokmaisrijan, 2005); whereas the stability of the close-contact and solvent-separated guanidinium-formate

(Gdm^+- FmO^-) complexes could be affected by the structures of the H-bond networks. These pieces of information suggested the necessity to include explicit water molecules in the model calculation (Sagarik and Chaiyapongs, 2005).

In the present study, the effects of metal ion and solute conformation change on the structures, energetic and dynamics of water molecules in the first hydration shells of Ala were studied using MD simulations. The theoretical investigations were started with construction of the intermolecular potentials for the $Ala-H_2O$ and $Li^+/Ala-H_2O$ complexes using the test-particle model (T-model). They were applied in the calculations of equilibrium geometries and interaction energies of the $Ala-H_2O$ and $Li^+/Ala-H_2O$ complexes in the gas phase. *Ab initio* calculations at MP2 levels were performed to check some of the T-model results. The T-model potentials were then applied in MD simulations of $[Ala]_{aq}$ and $[Li^+/Ala]_{aq}$ at 298 K, from which the three-dimensional structures and energetic of the H-bond networks of water in the first hydration shells were analyzed and visualized (Clementi, 1980). The dynamics of water molecules in the H-bond networks, such as the water exchange processes and the water residence times, were systematically studied and discussed based on the total-average potential energy landscapes and probability distribution (PD) maps (Clementi, 1980; Sagarik and Chaiyapongs, 2005; Sagarik and Dokmaisrijan, 2005). The water exchanges in the first hydration shells in $[Ala]_{aq}$ and $[Li^+/Ala]_{aq}$ were further examined in details using the water exchange diagrams (Erras-Hanauer, Clark and Van Eldik, 2003; Helm and Merbach, 1999; Hermansson and Wojcik, 1998; Spångberg, Rey, Hynes and Hermansson, 2003), from which the water exchange pathways were identified and classified. The theoretical results obtained in the present investigations were discussed in comparison with available theoretical and experimental data of the same and similar systems.

CHAPTER II

RESEARCH METHODOLOGY

Although Glyz and Alaz dominate in aqueous solutions and crystals, the information on structures, energetic and dynamics of water molecules in the first hydration shells of their neutral forms could serve as model molecules in the studies of the hydration of the main chains, as well as the side chains of proteins (Cerda, Hoyan, Ohanessian and Wesdemiotis, 1998; Tortonda *et al*., 2003), which contain the N-H and C=O groups in general (Baker and Hubbard, 1984).

Since the main objectives of the present study were to investigate the effects of solute conformation change and metal ion on the hydration of model amino acid in its neutral forms, three possible structures of Ala were considered. They are denoted by Ala-A, Ala-B and Ala-C in Figure 2.1. Ala-A and Ala-B were chosen to illustrate the effects of conformation change, whereas Ala-C for the effects of metal ion. Ala-A represents the lowest minimum energy geometry of Ala in the gas phase, similar to structure **I** reported by Csazar (1995). The geometry of Ala-A was taken from Clementi, Cavallone and Scordamaglia (1977) and reoptimized using *ab initio* calculations at MP2/6-311G(d,p) level, shown in previous studies to be appropriate for the geometry optimizations of moderately strong H-bond systems, such as hydroxylamine (Sagarik, 1999) and benzoic acid (BA)-H_2O clusters (Sagarik and Rode, 2000). Structure of Ala-B is different from Ala-A, with the angle ϕ being 30 degree with respect to Ala-A. The structure of Ala-C is the same as structure **IVp**

Figure 2.1 a) – c) Structures and atom numbering systems of Ala-A, Ala-B and Ala-C, together with the reference planes employed in MD analyses. The dipole moments (μ) are computed from the point charges derived from the CHelpG scheme (Breneman and Wiberg, 1990).

d) – f) Reference planes **I**, **II** and **III** are on the YZ, XZ and XY planes, respectively.

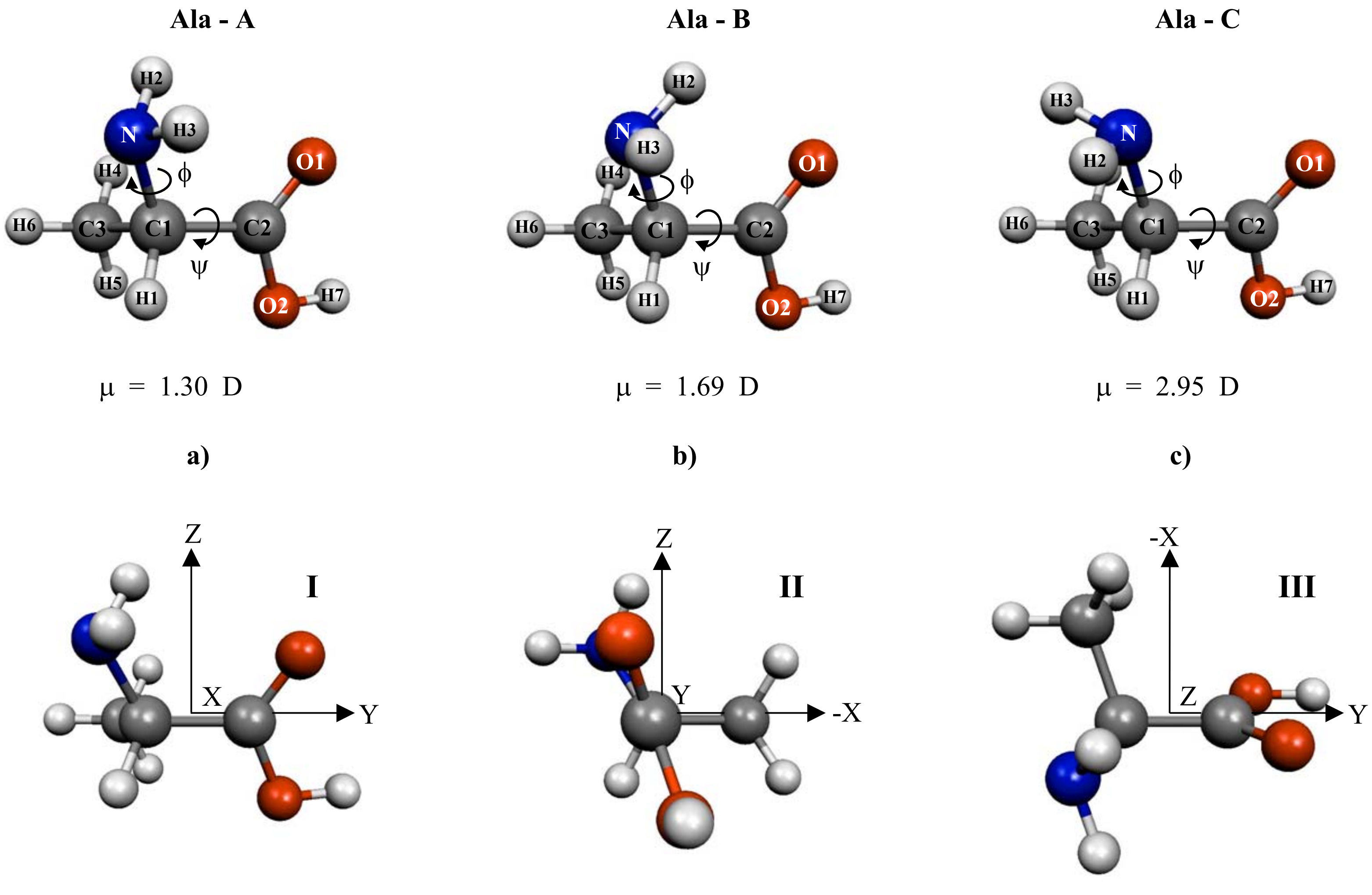

a) b) c)

d) e) f)

Figure 2.1

reported by Pacios and Gómez (2001), in which both N and O atoms are ready to form a bidentate coordination with metal ion (Jockusch *et al*., 2001; Siu *et al*., 2001). Since the electrostatic effects were expected to dominate in $\mathrm{Li^{+}/Ala\text{-}C}$, the basis set used in the geometry optimization was augmented with polarization and diffuse functions. The optimized geometries of Ala-A, Ala-B and Ala-C, as well as, $\mathrm{Li^{+}/Ala\text{-}C}$, were kept constants throughout the calculations. The optimal bond lengths, bond angles and torsion angles of Ala-A and $\mathrm{Li^{+}/Ala\text{-}C}$ are listed in Table A.1 (see Appendix A).

2.1 The T-model potentials

In the T-model (Böhm and Ahlrichs, 1982; 1985; Böhm, Ahlrichs, Scharf and Schiffer, 1984; Böhm, Meissner and Ahlrichs 1984; Hoinkis, Ahlrichs and Böhm, 1983), the interaction energy $(\Delta\mathrm{E_{T-model}})$ between molecules A and B is written as a sum of the first-order SCF interaction energy ($\Delta\mathrm{E^{1}_{SCF}}$) and a higher order term ($\Delta\mathrm{E^{r}}$),

$$\Delta\mathrm{E_{T-model}} = \Delta\mathrm{E^{1}_{SCF}} \;+\; \Delta\mathrm{E^{r}}. \tag{1}$$

$\Delta\mathrm{E^{1}_{SCF}}$ in Equation (1) accounts for the exchange repulsion and electrostatic energies which can be computed from *ab initio* first-order SCF calculations (Böhm and Ahlrichs, 1982). $\Delta\mathrm{E^{1}_{SCF}}$ takes the following analytical form:

$$\Delta\mathrm{E^{1}_{SCF}} = \sum_{i\in A}\sum_{j\in B}\left[\exp\left(\frac{-R_{ij}+\sigma_i+\sigma_j}{\rho_i+\rho_j}\right)+\frac{q_i q_j}{R_{ij}}\right], \tag{2}$$

i and j in Equation (2) label the sites of molecules A and B, respectively. σ_i, ρ_i and q_i are the site parameters; R_{ij} are the site-site distances. The exponential term in Equation (2) is responsible for the size and shape of molecules A and B, with the site parameters σ_i and ρ_i, determined by probing molecules A and B with a test particle (Hoinkis *et al*., 1983).

Since the structures and energetic of H-bond are determined to a large extent by the electrostatic energy, care must be exercised in the calculations of atomic charges, q_i and q_j in Equation (2). Within the framework of the T-model, atomic charges are determined from the requirement that a point charge model reproduces the electrostatic potentials of molecules A and B. The charges obtained from the electrostatic potentials at the points selected according to the CHelpG scheme (Breneman and Wiberg, 1990) has shown to work quite well with most H-bond systems considered (Sagarik, 1999; Sagarik, Chaiwongwattana and Sisot, 2004; Sagarik and Chaiyapongs, 2005; Sagarik and Dokmaisrijan, 2005; Sagarik and Rode, 2000). Therefore, the CHelpG scheme implemented in the Gaussian 98 package (Frisch *et al*., Computer software, 1998) was adopted in the present investigation. The electrostatic potentials employed in the calculations of the atomic charges were derived from *ab initio* calculations at MP2/6-311++G(d,p) levels. MP2/6-311++G (d,p) was applied successfully in the calculations of the electron densities and atomic charges in conformers of Gly (Csaszar, 1992; Pacios and Gómez, 2001), using various theoretical models including the CHelpG scheme. For the molecules and complex considered here, more than nine thousand electrostatic energies were employed in the calculations of the atomic charges. The dipole moments obtained from the CHelpG charges are also included in Figure 2.1.

The higher-order term $(\Delta \mathrm{E}^{\mathrm{r}})$ in Equation (1) takes into account the dispersion and polarization contributions of the T-model potentials. $\Delta \mathrm{E}^{\mathrm{r}}$ could be determined from both theoretical and experimental data and takes the following analytical form:

$$\Delta \mathrm{E}^{\mathrm{r}} = -\sum_{i \in A} \sum_{j \in B} C_{ij}^{6} F_{ij}\left(R_{ij}\right) R_{ij}^{-6} , \tag{3}$$

where

$$F_{ij}\left(R_{ij}\right) = \begin{cases} \exp[-(1.28\, R_{ij}^{0} / R_{ij} - 1)^{2}],\, R_{ij} < 1.28\, R_{ij}^{0}, \\ 1, \quad \text{elsewhere.} \end{cases} \tag{4}$$

R_{ij}^{0} in Equation (4) is the sum of the van der Waals radii of atoms i and j, and C_{ij}^{6} can be determined from the Slater-Kirkwood relation:

$$C_{ij}^{6} = C_{6} \frac{3}{2} \frac{\alpha_i \alpha_j}{(\alpha_i / N_i)^{1/2} + (\alpha_j / N_j)^{1/2}}, \tag{5}$$

α_i and N_i in Equation (5) denote the atomic polarizability and the number of valence electrons of atoms, respectively. C_6 in Equation (5) is the only unknown parameter. It can be determined in many ways (Sagarik, 1999; Sagarik, Chaiwongwattana and Sisot, 2004; Sagarik and Chaiyapongs, 2005; Sagarik and Dokmaisrijan, 2005; Sagarik and Rode, 2000). For example, one could calibrate the incomplete T-model potentials to the properties related to interaction energies, such as the second virial coefficients (B(T)), the experimental or theoretical dimerization energy. In many cases, C_6 are close to one and the variation within the range of 0.8 and 1.5 seems not significantly affect the potential energy surfaces. Since the value of C_6 for similar H-bond systems is 1.43 (Sagarik, Chaiwongwattana and Sisot, 2004; Sagarik and Dokmaisrijan, 2005), therefore, this value was adopted in the present investigation. The T-model parameters for Ala-A, Ala-B and Ala-C, as well as, $Li^+/Ala-C$ and water are summarized in Table A.2 (see Appendix A). The derivation of the T-model potential is shown schematically in Figure 2.2.

2.2 Equilibrium structures in the gas phase

In order to obtain information on the interaction energy surfaces, the computed T-model potentials were applied in the calculations of the equilibrium geometries and interaction energies of the $Ala-H_2O$ and $Li^+/Ala-H_2O$ 1 : n complexes, with $n = 1$ to 4. The equilibrium geometries in the gas phase could help visualize the three-dimensional arrangements of water molecules in $[Ala]_{aq}$ and $[Li^+/Ala]_{aq}$.

The absolute and local minimum energy geometries of the $Ala-H_2O$ 1 : n complexes were computed by placing Ala at the origin of the Cartesian coordinate system. Then, the coordinates of water molecules were randomly generated in the vicinities of Ala. Based on the T-model potentials, the absolute and local minimum energy geometries of the $Ala-H_2O$ 1 : n complexes were searched using a minimization technique. Some low-lying minimum energy geometries of the $Ala-H_2O$ 1 : 1 and 1 : 2 complexes are displayed and discussed. Additional minimum energy geometries are display in Appendix B.

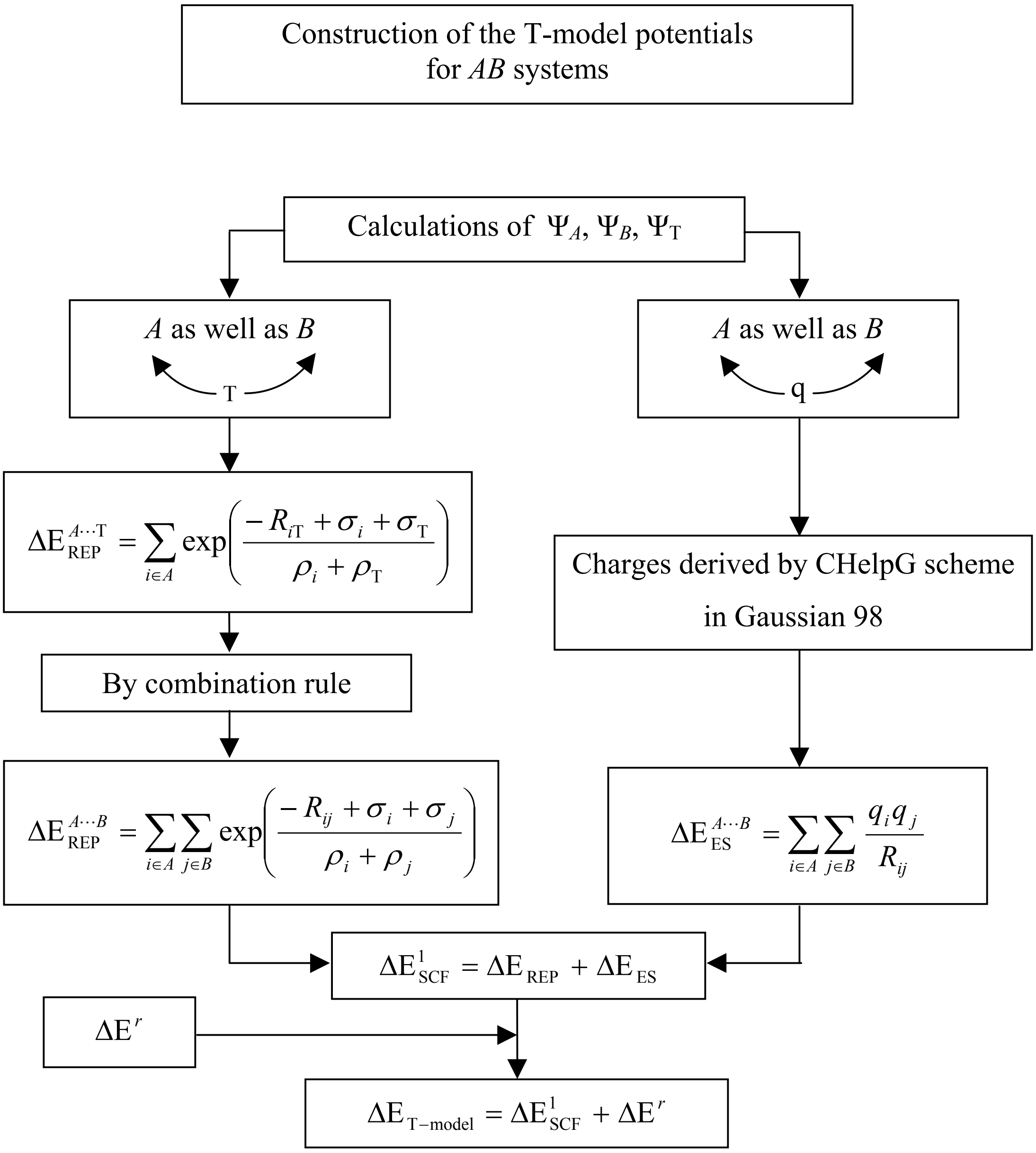

Figure 2.2 Construction of T-model potentials.

In order to sample check the T-model results, some of the equilibrium geometries were reoptimized using *ab initio* calculations at the MP2/6-311++G (2d,2p)//MP2/6-311G(d,p) level. In this case, the Berny optimization routine

(Schlegel, 1982) included in Gaussian 98 (Frisch *et al*., Computer software, 1998) were employed, by keeping the monomer geometries constant. In order to assess the quality of the basis sets, single-point counterpoise correction of the Basis Set Superposition Error (BSSE) was made on the optimized geometries. The same procedure was carried out for the $\mathrm{Li^+/Ala\text{-}H_2O}$ $1:n$ complexes. Since $\mathrm{Li^+}$ binds strongly with Ala-C, the equilibrium geometry of $\mathrm{Li^+/Ala\text{-}C}$ was kept constant; only the positions and orientations of water molecules were considered in *ab initio* geometry optimizations.

2.3 Molecular Dynamics simulations

The T-model potentials derived and tested in the previous section were employed in NVE-MD simulations of $[\mathrm{Ala}]_{\mathrm{aq}}$ and $[\mathrm{Li^+/Ala}]_{\mathrm{aq}}$. Four sets of MD simulations were performed at 298 K; regarded as MD-$[\mathrm{Ala\text{-}A}]_{\mathrm{aq}}$, MD-$[\mathrm{Ala\text{-}B}]_{\mathrm{aq}}$, MD-$[\mathrm{Ala\text{-}C}]_{\mathrm{aq}}$ and MD-$[\mathrm{Li^+/Ala\text{-}C}]_{\mathrm{aq}}$. In each MD run, a rigid solute and three hundred water molecules were put in a cubic box subject to periodic boundary conditions (Allen and Tildesley, 1989). The $\mathrm{C-C^{\alpha}-C}$ plane of Ala was coincident with the XY plane of the simulation box, see Figures 2.1d to 2.1f. The densities of all aqueous solutions were maintained at 1 g/cm^3; corresponding to the box length of 20.9 Å. The cut-off radius was half of the box length. About 50,000 MD steps of 0.0005 ps were devoted to equilibration and additional 100,000 steps to the property calculations. In order to study the electrostatic effects introduced by $\mathrm{Li^+}$ along the backbone of Ala-C and to simplify the analyses of the MD results, $\mathrm{Li^+/Ala\text{-}C}$ was treated as a supermolecule, which was not allowed to move in the course of MD simulations. The basic steps in MD simulations are illustrated in Figure 2.3.

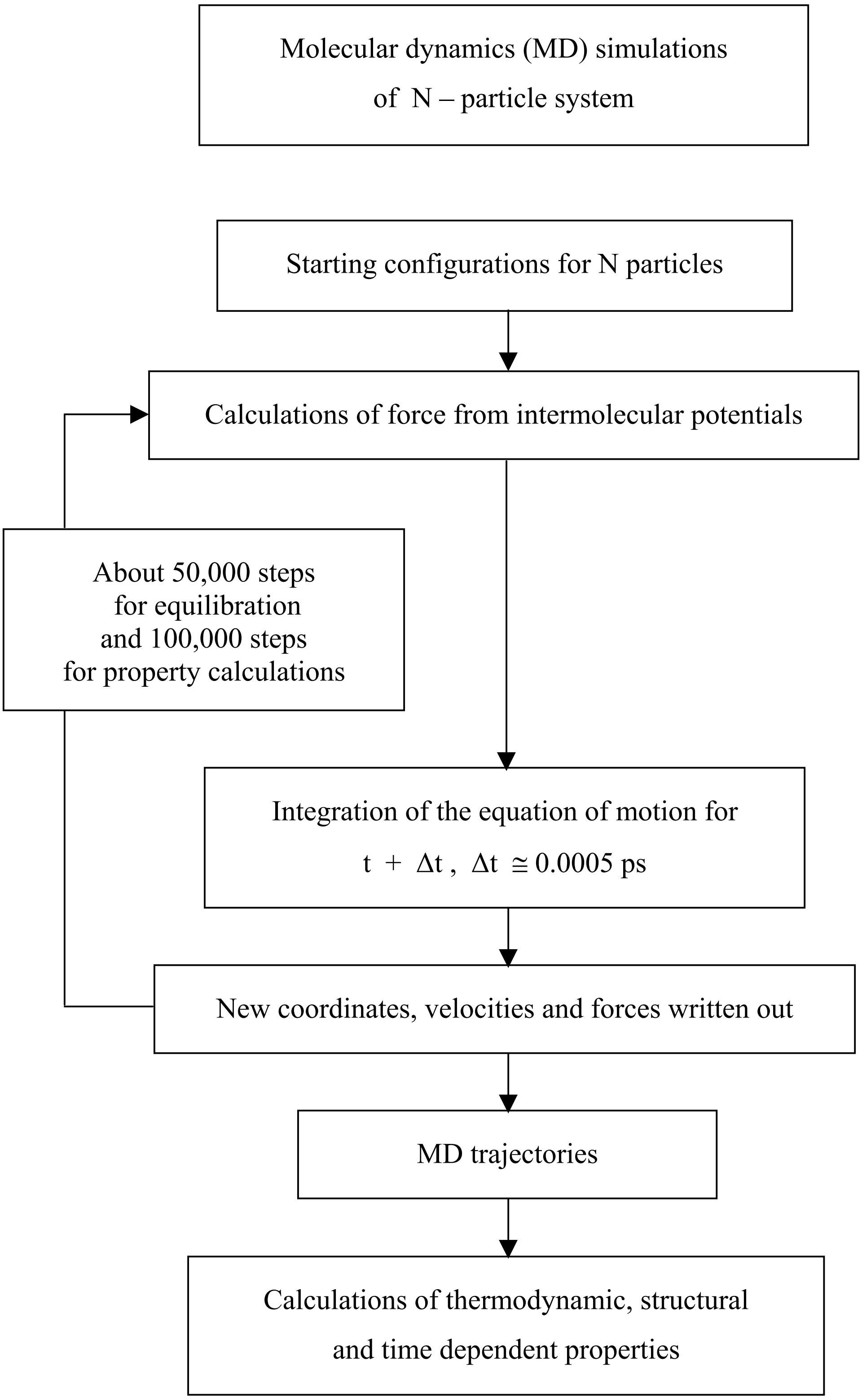

Figure 2.3 Basic steps in MD simulations of N-particle system.

The most basic one-dimensional views on the structures of $[\mathrm{Ala}]_{\mathrm{aq}}$ and $[\mathrm{Li}^{+}/\mathrm{Ala}]_{\mathrm{aq}}$ were obtained from the atom-atom pair correlation functions (g(R)) and the average running coordination number (n(R)). They were computed from the following equations:

$$g(R) = \frac{2V}{N^2}\left\langle \sum_{i<j} \delta\left(r - r_{ij}\right)\right\rangle \tag{6}$$

and

$$n(R) = 4\pi\rho \int g(r) r^2 dr \,, \tag{7}$$

where V is the volume, N is the total number of atoms; δ is the Dirac delta function; ρ is the number density of atoms in the total spherical volume; and r is radial distance. In order to characterize and visualize the three-dimensional structures of the H-bond networks of water, the probability distribution maps for the oxygen (PDO) and hydrogen (PDH) atoms of water were constructed from MD simulations (Sagarik and Chaiyapongs, 2005; Sagarik and Dokmaisrijan, 2005; Clementi, 1980). In the calculations of the PDO and PDH maps, three reference planes were defined with respect to the position and orientation of the solute molecule in the simulation box. The volumes above and below the reference planes were divided into layers with the thickness of 1 Å, as shown in Figure 2.4. In each layer, the PDO and PDH maps were computed separately, at the 61×61 grid intersections; by following the trajectories of the oxygen and hydrogen atoms of water in the course of MD simulations. The PDO and PDH maps were represented by contour lines, computed and displayed using the SURFER program (Golden Software, Computer software, 1997). The densities of the contour lines on the PDO and PDH maps are related to the probability of finding the oxygen and hydrogen atoms of water in the aqueous solutions.

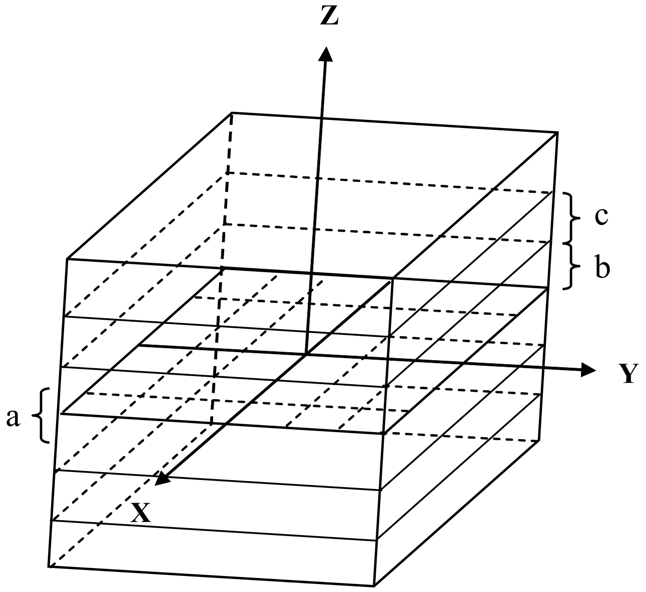

Figure 2.4 The volumes above and below the reference plane used in the calculations of PD maps.

Based on a similar approach, some average interaction energy PD maps were constructed from the MD trajectories. The average solute-solvent and solvent-solvent interaction energy PD maps, regarded as the AWPD and WWPD maps, respectively, were computed and represented by contour lines. The AWPD maps show the average interaction energies between water molecules at the grid intersections and solute, whereas the WWPD maps account for the average interaction energies between water molecules at the grid intersections and all other water molecules in aqueous solution. In the present case, only the negative interaction energies are displayed on the maps.

In order to visualize the total-average potential energy landscapes, as well as to provide basic energetic information to characterize the dynamics of water molecules in the H-bond networks, the total-average interaction energy PD (AW-WWPD) maps were constructed by combination of the AWPD and WWPD maps (Sagarik and Chaiyapongs, 2005; Sagarik and Dokmaisrijan, 2005; Clementi, 1980). The structures of the AWPD, WWPD and AW-WWPD maps were examined in details using cross section plots (Sagarik and Chaiyapongs, 2005; Sagarik and Dokmaisrijan, 2005), generated by taking vertical slices along predefined profile lines on their surfaces. The cross section plots derived from the longitudinal profile lines could be associated with the average potential energy barriers to the diffusion of water molecules within and between the H-bond networks ($< \Delta E_{aq}^{L} >$); whereas those obtained from the transverse profile lines could be attributed to the average potential energy barriers to the diffusion of water molecules between the H-bond networks and the outside ($< \Delta E_{aq}^{T} >$).

Attempt was further made to obtain detailed information on the water exchange processes in the first hydration shells of the solutes. Although not straightforward, it was shown that the dynamics of specific water molecules in the first hydration shells of solute, such as the longest H-bond lifetime ($\tau_{A-H\cdots Ow,max}$), could be anticipated at least qualitatively from the structures of the total-average potential energy landscapes (Sagarik and Chaiyapongs, 2005; Sagarik and Dokmaisrijan, 2005). Additionally, in the present case, water exchange diagrams

(Hermansson and Wojcik, 1998; Spångberg *et al.*, 2003), showing the distance between a specific water molecule and a functional group of solute as a function of MD simulation time, were constructed; from which the water residence times at Li^+ ($\tau_{Li^+\cdots Ow}$) and the H-bond lifetime ($\tau_{A-H\cdots Ow}$) at the functional groups were approximated. The lifetimes of the water exchange intermediate complexes at Li^+ and H-bond, denoted by $\tau_{ex,Li^+\cdots Ow}$ and $\tau_{ex,A\text{-}H\cdots Ow}$ respectively, were determined from the analysis of the water exchange diagrams. The five-water exchange pathways proposed by Langford and Gray (1996) were tentatively employed in the analysis of the water exchange processes. They have been applied successfully, for example, in $[Li^+]_{aq}$ (Hermansson and Wojcik, 1998; Spångberg *et al.*, 2003) and $[Na^+]_{aq}$ (Hermansson and Wojcik, 1998). In the course of MD simulations, the total-interaction energies ($\Delta E^{AW\text{-}WW}$) of selected water molecules were recorded and included in the water exchange diagrams.

2.4 Computer softwares and facilities

All calculations in the present study were performed at the School of Chemistry and the School of Mathematics, Institute of Science, Suranaree University of Technology (SUT). The following computers and standard computational chemistry softwares were used.

- Compaq alpha1000 XP1000.
- DEC alpha 600/5-266.
- LINUX cluster with eight nodes.
- COLUMBUS system programs developed by Ahlrichs *et al.* (1985).

- Gaussian 98 package (Frisch *et al*., Computer software, 1998).
- Moldy MD simulations program (Refson, Computer software, 1996).
- SURFER contouring program (Golden Software, Computer software, 1997).
- AMBER version 6 (Case *et al*., Computer software, 1999) *etc*.

CHAPTER III

RESULTS AND DISCUSSION

3.1 Equilibrium structures in the gas phase

Some absolute and low-lying minimum energy geometries for the Ala-A-H_2O, Ala-B-H_2O, Ala-C-H_2O and Li^+/Ala-C-H_2O 1 : *n* complexes, with *n* = 1 to 4, computed from the T-model potentials, are illustrated in Figures 3.1 to 3.4. $\Delta E_{T\text{-model}}$ and some characteristic distances and angles, together with the corresponding MP2 results, are included in the figures.

3.1.1 The Ala-H_2O complexes

The absolute minimum energy geometry of the Ala-A-H_2O 1 : 1 complex, obtained from the T-model potential, is structure **a** in Figure 3.1. Structure **a** consists of a cyclic H-bond, in which water acts simultaneously as proton donor and acceptor towards the C=O1 and O2-H7 groups, respectively. This type of cyclic H-bond has been commonly found in R-COOH-H_2O 1 : 1 complexes (Ahn *et al.*, 2003; Sagarik and Rode, 2000). $\Delta E_{T\text{-model}}$ of structure **a** is -41.4 kJ/mol, with the Ow-Hw···O1 and O2-H7···Ow H-bond distances of 2.93 and 2.85 Å, respectively. MP2/6-311++G(2d,2p)// MP2/6-311G(d,p) geometry optimization predicted the same structure, with slightly shorter Ow-Hw···O1 and O2-H7···Ow H-bond distances, in general. ΔE_{MP2} and ΔE_{MP2CP} of tructure **a** in Figure 3.1 are –41.4 and -34.3 kJ/mol, respectively. *Ab initio* calculations at the HF/6-31G(d,p) (Kwon, Kim and No, 1995)

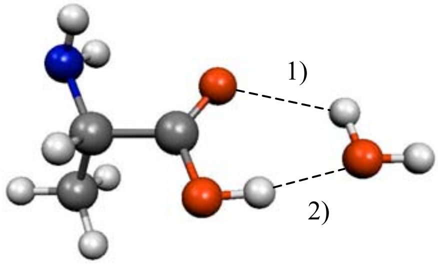

a)
$\Delta E_{T\text{-model}}$ = -41.4 kJ/mol
ΔE_{MP2} = -41.4 kJ/mol
ΔE_{MP2CP} = -34.3 kJ/mol

1) Ow···O = 2.93 [2.80] Å
Ow-Hw···O = 119.7° [134.9°]
2) O···Ow = 2.85 [2.74] Å
O-H···Ow = 165.4° [162.9°]

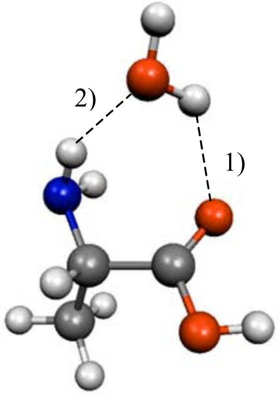

b)
$\Delta E_{T\text{-model}}$ = -29.3 kJ/mol
ΔE_{MP2} = -24.7 kJ/mol
ΔE_{MP2CP} = -19.4 kJ/mol

1) Ow···O = 2.99 [2.94] Å
Ow-Hw···O = 129.0° [154.0°]
2) N···Ow = 3.04 [3.14] Å
N-H···Ow = 152.8° [144.7°]

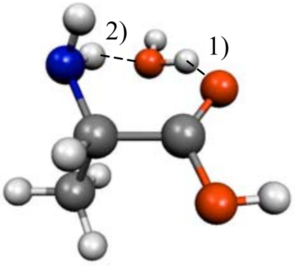

c)
$\Delta E_{T\text{-model}}$ = -29.1 kJ/mol
ΔE_{MP2} = -29.9 kJ/mol
ΔE_{MP2CP} = -21.9 kJ/mol

1) Ow···O = 2.95 [2.88] Å
Ow-Hw···O = 131.3° [153.9°]
2) N···Ow = 3.11 [3.17] Å
N-H···Ow = 163.1° [163.0°]

Figure 3.1 Equilibrium structures, interaction energies and some characteristic H-bond distances and angles of the Ala-H_2O 1 : 1 complexes in the gas phase, computed from the T-model potentials and MP2 calculations.

a) – c) Ala-A-H_2O 1 : 1 complexes.

d) – f) Ala-B-H_2O 1 : 1 complexes.

g) – i) Ala-C-H_2O 1 : 1 complexes.

MP2CP = MP2 calculations with single-point counterpoise correction.

[…] = values obtained from MP2/6-311++G(2d,2p)//MP2/6-311G(d,p).

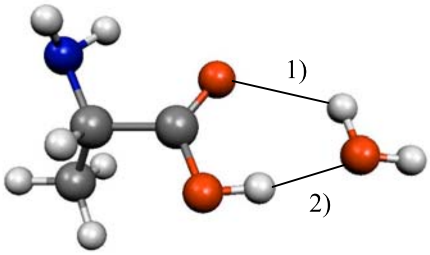

d)
$\Delta E_{\text{T-model}}$ = -41.4 kJ/mol
ΔE_{MP2} = -41.4 kJ/mol
ΔE_{MP2CP} = -34.4 kJ/mol

1) Ow···O = 2.93 [2.80] Å
Ow-Hw···O = 119.8° [134.3°]
2) O···Ow = 2.85 [2.74] Å
O-H···Ow = 165.4° [163.0°]

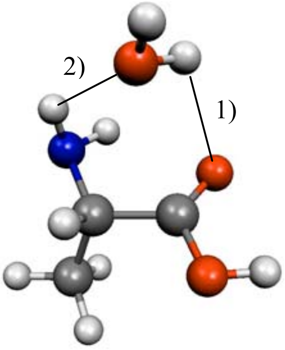

e)
$\Delta E_{\text{T-model}}$ = -28.9 kJ/mol
ΔE_{MP2} = -21.9 kJ/mol
ΔE_{MP2CP} = -16.4 kJ/mol

1) Ow···O = 3.12 [3.01] Å
Ow-Hw···O = 115.2° [138.0°]
2) N···Ow = 2.94 [3.05] Å
N-H···Ow = 124.5° [121.7°]

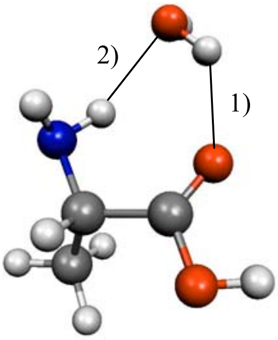

f)
$\Delta E_{\text{T-model}}$ = -25.0 kJ/mol
ΔE_{MP2} = -22.0 kJ/mol
ΔE_{MP2CP} = -16.6 kJ/mol

1) Ow···O = 2.95 [2.92] Å
Ow-Hw···O = 135.0° [156.1°]
2) N···Ow = 3.12 [3.28] Å
N-H···Ow = 153.7° [167.8°]

Figure 3.1 (continued)

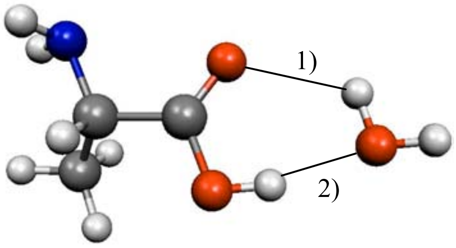

g)
$\Delta E_{\text{T-model}}$ = -41.1 kJ/mol
ΔE_{MP2} = -43.4 kJ/mol
ΔE_{MP2CP} = -36.2 kJ/mol

1) Ow···O = 2.92 [2.79] Å
Ow-Hw···O = 121.0° [137.2°]

2) O···Ow = 2.86 [2.74] Å
O-H···Ow = 164.8° [162.3°]

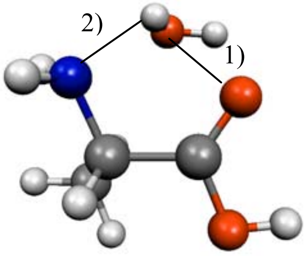

h)
$\Delta E_{\text{T-model}}$ = -30.0 kJ/mol
ΔE_{MP2} = -34.3 kJ/mol
ΔE_{MP2CP} = -27.5 kJ/mol

1) Ow···O = 3.05 [2.95] Å
Ow-Hw···O = 109.2° [98.5°]

2) Ow···N = 3.11 [2.89] Å
Ow-Hw···N = 132.6° [137.0°]

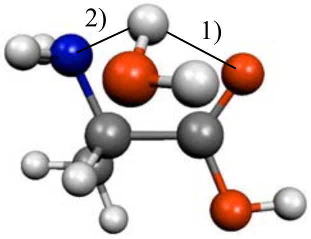

i)
$\Delta E_{\text{T-model}}$ = -28.9 kJ/mol
ΔE_{MP2} = -32.3 kJ/mol
ΔE_{MP2CP} = -26.0 kJ/mol

1) Ow···O = 3.15 [2.96] Å
Ow-Hw···O = 115.5° [94.1°]

2) Ow···N = 2.98 [2.83] Å
Ow-Hw···N = 108.9° [129.5°]

Figure 3.1 (continued)

and MP2/6-311++G(d,p) (Ahn *et al*., 2003) levels suggested the same equilibrium geometry. The Ow-Hw···O1 and O2-H7···Ow H-bond distances computed at the HF level are 2.78 and 2.67 Å, respectively.

The second and third low-lying minimum energy geometries of the Ala-A-H_2O 1 : 1 complex are represented by a cyclic H-bond, in which water molecule acts simultaneously as proton donor towards the C=O1 group and proton acceptor towards the N-H3 and N-H2 groups, respectively. $\Delta E_{T\text{-model}}$ of structures **b** and **c** are almost identical, -29.3 and -29.1 kJ/mol, respectively. The N-H3···Ow and Ow-Hw···O1 H-bond distances in structure **b** are 3.04 and 2.99 Å, respectively; whereas the N-H2···Ow and Ow-Hw···O1 H-bond distances in structure **c** are 3.11 and 2.95 Å, respectively. MP2/6-311++G(2d,2p)//MP2/6-311G(d,p) calculations suggested that structure **c** is slightly more stable than structure **b**. Three low-lying minimum energy geometries of the Ala-B-H_2O 1 : 1 complex, obtained from the T-model potential, are structures **d**, **e** and **f** in Figure 3.1. The H-bond structure at the COOH group seems not affected when the angle ϕ of Ala was rotated 30 degree about the $\mathrm{N\text{-}C}^{\alpha}$ bond. The H-bonding feature in structure **d** is almost identical to structure **a**, with the same interaction energy. The 30-degree rotation of the $\mathrm{N\text{-}C}^{\alpha}$ bond seems to bring about more visible effects to the N-H···Ow H-bonds; the interaction energy in structure **e** is slightly higher than structure **b**, whereas that of structure **f** is about 4 kJ/mol higher than structures **c**.

For the Ala-C-H_2O 1 : 1 complex, the cyclic H-bond in structure **g** is nearly identical to those in structures **a** and **d**. From chemical intuitions, one could expect that the N and O1 atoms in Ala-C might act simultaneously as proton acceptors towards both O-H groups of water molecule. In the present case, however, the approach of only one O-H group towards both N and O1 atoms was found in structures **h** and **i**, with the interaction energies of about -30 kJ/mol. Although this type of interaction is not very common, it was observed in protein crystals (Donohue, 1968) and has been regarded as a bifurcated or three-center H-bond (Jeffrey and Saenger, 1991). The term has been used to describe the situation, in which a single proton is shared between two H-bond acceptors. They were found, for example, in β–sheet structures of carboxypeptidase (Baker and Hubbard, 1984).

Since the characteristic structures of H-bonds in the Ala-B-H_2O and Ala-C-H_2O 1 : 2 complexes are similar to the Ala-A-H_2O 1 : 2 complexes, only some results on the latter are discussed. The lowest-lying minimum energy geometry for the Ala-A-H_2O 1 : 2 complex is structure **a** in Figure 3.2. For structure **a**, both water molecules act as proton donor and acceptor toward the COOH group, forming a larger cyclic H-bond structure. $\Delta E_{\text{T-model}}$ of structure **a** is -70.9 kJ/mol, with the Ow-Hw···O1 and O2-H7···Ow H-bond distances of 3.05 and 2.84 Å, respectively. Structures **b** and **c** in Figure 3.2 consist of two cyclic H-bonds, with the H-bond structures similar to those in the Ala-A-H_2O 1 : 1 complexes. Structures **b** and **c** possess comparable interaction energies. They are slightly higher than structure **a**. The structures of the Ala-A-H_2O 1 : 2 complexes derived from the T-model potentials agree in general with those reported by Ahn *et al*. (2003), in which the results of *ab initio* calculations with larger basis set on the Ala-H_2O 1 : n complexes, with n = 1 to 2, were reported.

a)

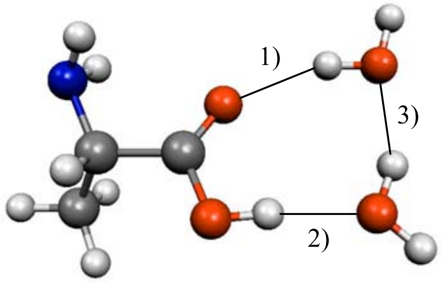

$\Delta E_{T\text{-model}}$ = -70.9 kJ/mol

1) Ow···O = 3.05 Å
Ow-Hw···O = 154.6°
2) O···Ow = 2.84 Å
O-H···Ow = 175.3°
3) Ow···Ow = 3.01 Å
Ow-Hw···Ow = 157.3°

b)

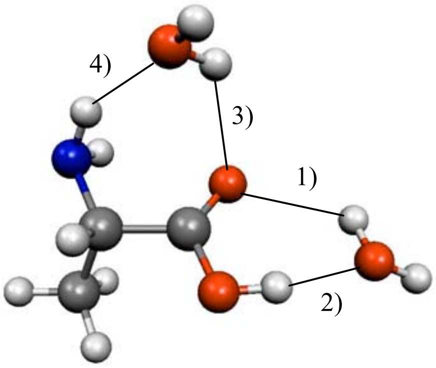

$\Delta E_{T\text{-model}}$ = -68.7 kJ/mol

1) Ow···O = 2.94 Å
Ow-Hw···O = 117.7°
2) O···Ow = 2.85 Å
O-H···Ow = 164.8°
3) Ow···O = 3.00 Å
Ow-Hw···O = 124.6°
4) N···Ow = 3.04 Å
N-H···Ow = 151.0°

c)

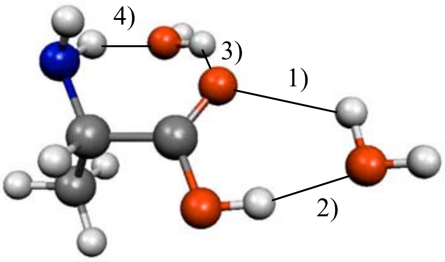

$\Delta E_{T\text{-model}}$ = -68.1 kJ/mol

1) Ow···O = 2.95 Å
Ow-Hw···O = 117.5°
2) O···Ow = 2.85 Å
O-H···Ow = 165.3°
3) Ow···O = 2.97 Å
Ow-Hw···O = 131.0°
4) N···Ow = 3.11 Å
N-H···Ow = 161.8°

Figure 3.2 Equilibrium structures, interaction energies and some characteristic H-bond distances and angles of the Ala-A-H_2O 1 : 2 complexes in the gas phase, computed from the T-model potentials.

3.1.2 The Li^+/Ala-H_2O complexes

The T-model and MP2 results on the Li^+/Ala-C-H_2O complexes are displayed in Figure 3.3. Figure 3.3a shows the equilibrium geometry of Li^+/Ala-C computed from MP2/6-311++G(2d,2p) calculations; the $Li^+\cdots O$ and $Li^+\cdots N$ distances are 1.92 and 2.08 Å, respectively, with ΔE_{MP2} of –261.1 kJ/mol. The binding energy justifies the approximation to keep the structure of Li^+/Ala-C constant in subsequence investigations. The $Li^+\cdots O$ and $Li^+\cdots N$ distances, as well as the binding energy, are comparable with those computed from B3LYP/6-311++G(d,p) calculations (Marino *et al*., 2000), 1.86 Å, 2.05 Å and -248.3 kJ/mol, respectively.

The bidentate coordination of Li^+ at the N and O1 atoms of Ala-C brings about significant effects at the COOH and NH_2 groups. Both T-model and MP2 calculations suggested structure **b**, in which water molecule binds directly at Li^+, to be the most favorable form of the Li^+/Ala-C-H_2O 1 : 1 complex, with $\Delta E_{T\text{-}model}$ and ΔE_{MP2} of –97.3 and –105.0 kJ/mol, respectively. The bidentate coordination directly affects the O2-H7···Ow H-bond structure and interaction energy. Structure **c** in Figure 3.3 consists of a linear O2-H7···Ow H-bond, compared to a cyclic H-bond in the Ala-C-H_2O 1 : 1 complex, structure **g** in Figure 3.1. The binding of Li^+ to Ala-C leads to an increase in the stability of the O2-H7···Ow H-bond, between 18 and 13 kJ/mol depending on the method used. Structures **d** and **e** in Figure 3.3 show the N-H2···Ow and N-H3···Ow H-bonds, which are also stabilized by the bidentate coordination of Li^+, with $\Delta E_{T\text{-}model}$ of about -50 kJ/mol.

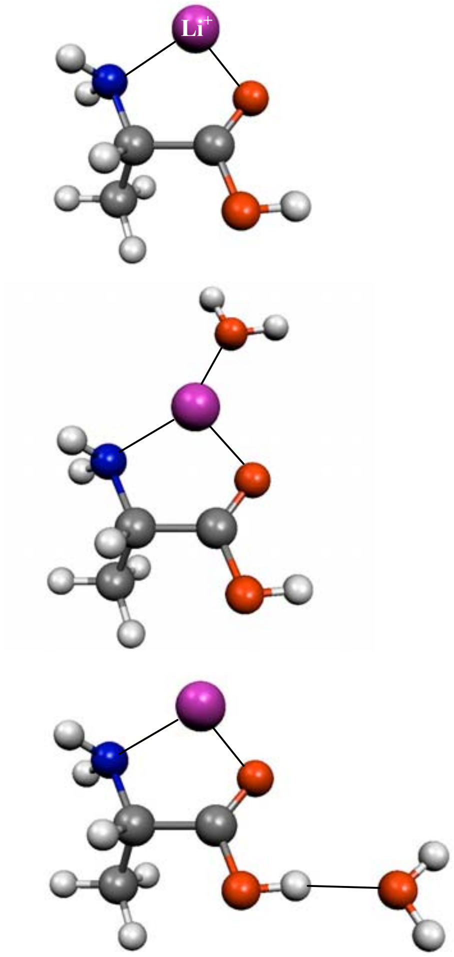

a)

ΔE_{MP2} = -261.1 kJ/mol

$Li^+\cdots O$ = 1.92 Å
$Li^+\cdots N$ = 2.08 Å

b)

$\Delta E_{T\text{-}model}$ = -97.3 kJ/mol
ΔE_{MP2} = -105.0 kJ/mol
ΔE_{MP2CP} = -98.2 kJ/mol

$Li^+\cdots Ow$ = 1.89 [1.88] Å

c)

$\Delta E_{T\text{-}model}$ = -59.1 kJ/mol
ΔE_{MP2} = -56.6 kJ/mol
ΔE_{MP2CP} = -50.2 kJ/mol

$O\cdots Ow$ = 2.77 [2.64] Å
$O\text{-}H\cdots Ow$ = 172.3° [173.6°]

Figure 3.3 Equilibrium structures, interaction energies and some characteristic distances and angles in the Li^+/Ala-C and Li^+/Ala-C-H_2O complexes in the gas phase, computed from the T-model potentials and MP2 calculations.

a) Li^+/Ala-C complex.

b) – e) Li^+/Ala-C-H_2O 1 : 1 complexes.

MP2CP = MP2 calculations with single-point counterpoise correction.

[…] = values obtained from MP2/6-311++G(2d,2p)//MP2/6-311G(d,p).

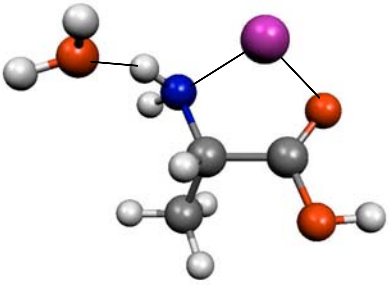

d)

$\Delta E_{T\text{-model}}$ = -52.8 kJ/mol
ΔE_{MP2} = -48.6 kJ/mol
ΔE_{MP2CP} = -44.0 kJ/mol

N···Ow = 2.93 [2.89] Å
N-H···Ow = 155.1° [155.5°]

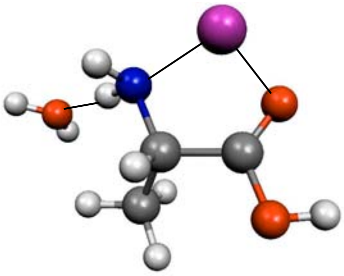

e)

$\Delta E_{T\text{-model}}$ = -50.8 kJ/mol
ΔE_{MP2} = -45.7 kJ/mol
ΔE_{MP2CP} = -41.0 kJ/mol

N···Ow = 3.01 [2.93] Å
N-H···Ow = 174.1° [172.6°]

Figure 3.3 (continued)

Similar results were obtained for the Li^+/Ala-C-H_2O 1 : 2, 1 : 3 and 1 : 4 complexes, shown in Figure 3.4; in which additional water molecule prefers to bind directly at Li^+, and subsequently at the O2-H7 and N-H2 groups. It appeared that, in the gas phase, not more than two water molecules can directly hydrate at Li^+, compared to four in the case of the Li^+/H_2O complex (Puchta, Galle, van Eikema Hommes, Pasgreta and van Eldik, 2004). The result is supported by *ab initio* calculations at B3LYP/6-311++G(d,p) and MP2/6-311++G(d,p) levels, as well as experiment, on the Li^+/Val-H_2O 1 : 2 and 1 : 3 complexes, in which only two water molecules interact solely at Li^+ and the third one at Val molecule (Jockusch *et al.*, 2001).

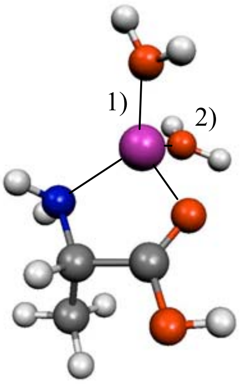

a)

$\Delta E_{\text{T-model}}$ = -176.2 kJ/mol

1) $Li^+\cdots Ow$ = 1.93 Å

2) $Li^+\cdots Ow$ = 1.93 Å

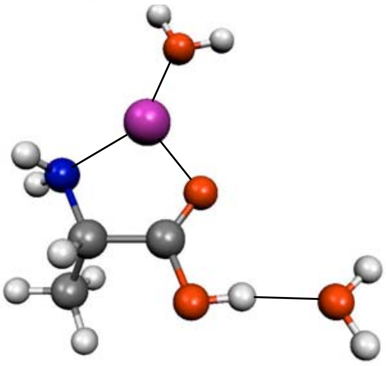

b)

$\Delta E_{\text{T-model}}$ = -154.9 kJ/mol

$Li^+\cdots Ow$ = 1.90 Å

$O\cdots Ow$ = 2.77 Å

$O\text{-}H\cdots Ow$ = 171.1°

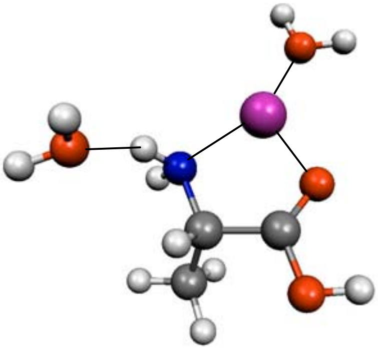

c)

$\Delta E_{\text{T-model}}$ = -147.9 kJ/mol

$Li^+\cdots Ow$ = 1.90 Å

$N\cdots Ow$ = 2.93 Å

$N\text{-}H\cdots Ow$ = 154.3°

Figure 3.4 Equilibrium structures, interaction energies and some characteristic distances and angles in the Li^+/Ala-C-H_2O complexes in the gas phase, computed from the T-model potentials.

a) – c) Li^+/Ala-C-H_2O 1 : 2 complexes.

d) Li^+/Ala-C-H_2O 1 : 3 complexes.

e) Li^+/Ala-C-H_2O 1 : 4 complexes.

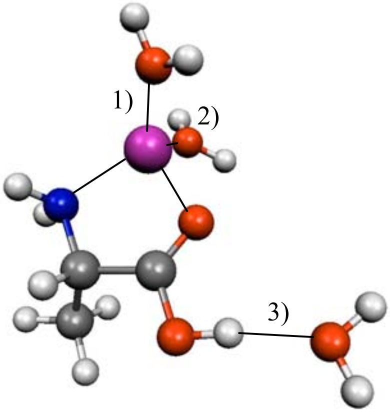

d)
$\Delta E_{\text{T-model}}$ = -232.9 kJ/mol

1) $Li^+\cdots Ow$ = 1.93 Å
2) $Li^+\cdots Ow$ = 1.93 Å
3) $O\cdots Ow$ = 2.77 Å
$O\text{-}H\cdots Ow$ = 170.7°

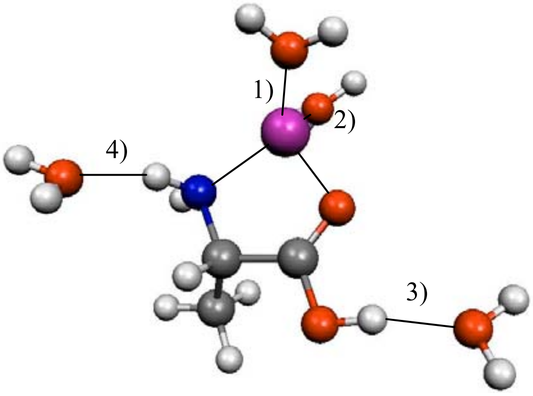

e)
$\Delta E_{\text{T-model}}$ = -281.2 kJ/mol

1) $Li^+\cdots Ow$ = 1.94 Å
2) $Li^+\cdots Ow$ = 1.93 Å
3) $O\cdots Ow$ = 2.77 Å
$O\text{-}H\cdots Ow$ = 170.6°
4) $N\cdots Ow$ = 3.00 Å
$N\text{-}H\cdots Ow$ = 155.9°

Figure 3.4 (continued)

Based on the results summarized in this section, one can conclude that the T-model potentials predicted reasonable gas-phase equilibrium structures and interaction energies for all the Ala-H_2O and Li^+/Ala-C-H_2O 1 : *n* complexes considered. They can be further applied in MD simulations of the aqueous solutions with confidence.

3.2 MD simulations

$<E_{aq}^{pot}>$, $<E_{aq}^{solu-solv}>$ and $<E_{aq}^{solv-solv}>$ obtained from MD-$[Ala-A]_{aq}$, MD-$[Ala-B]_{aq}$, MD-$[Ala-C]_{aq}$ and MD-$[Li^+/Ala-C]_{aq}$, are listed in Table 3.1, together with the MD simulation conditions.

Table 3.1 MD simulations parameters and the results for $[Ala]_{aq}$ and $[Li^+/Ala]_{aq}$.

MD	L	$<E_{aq}^{pot}>$	$<E_{aq}^{solu-solv}>$	$<E_{aq}^{solv-solv}>$
$[Ala\text{-}A]_{aq}$	20.8888	-30.74 ± 0.22	-0.6	-29.2
$[Ala\text{-}B]_{aq}$	20.8888	-30.92 ± 0.21	-0.6	-29.4
$[Ala\text{-}C]_{aq}$	20.8888	-30.89 ± 0.22	-0.7	-29.3
$[Li^+/Ala\text{-}C]_{aq}$	20.8977	-31.43 ± 0.22	-1.7	-28.9

L = simulation box lengths.

$<E_{aq}^{pot}>$ = average potential energy of aqueous solution.

$<E_{aq}^{solu-solv}>$ = average solute-solvent interaction energy.

$<E_{aq}^{solv-solv}>$ = average solvent-solvent interaction energy.

Energies in kJ/mol and distances in Å.

In order to limit the number of figures, only selected g(R), PDO and AW-WWPD maps, together with their cross section plots are displayed and used in the discussion. Additional results on MD-$[Ala-A]_{aq}$, MD-$[Ala-B]_{aq}$, MD-$[Ala-C]_{aq}$ and MD-$[Li^+/Ala-C]_{aq}$ are given in Appendix C. Characteristic high-density contours on the PD maps are labeled with letters; **A** at the O2-H7 group;

B and **C** at the lone-pair electrons of O1, above and below the COOH plane, respectively; **D** and **E** at H3 and H2, respectively; **F** at the C1-H1 group and; **G** at the CH_3 group. They represent the H-bond networks of water in the first hydration shells of Ala. In order to compare the average potential energy barriers to the diffusion of water molecules ($< \Delta E^{L}_{aq} >$ and $< \Delta E^{T}_{aq} >$) in the H-bond networks, the lowest energy minima in the cross section plots were set to zero.

3.2.1 $[Ala]_{aq}$

Since the structures of Ala-A and Ala-B are different only at the NH_2 group, one could expect that the structures and peak positions of g(R) for the COOH group are not substantially different. This is confirmed by the results in Figures 3.5a to 3.5d. For both $[Ala\text{-}A]_{aq}$ and $[Ala\text{-}B]_{aq}$, the positions of the main peaks of $g(R_{O2\cdots Ow})$ are seen at 2.91 Å. The integrations of $g(R_{O2\cdots Ow})$ to these peak positions suggested a little more than one water molecule (1.31 and 1.23, respectively) H-bonding directly at the O2-H7 group, which is compared well with 1.4 in the case of $[BA]_{aq}$ (Sagarik and Rode, 2000). It should be noted that, larger number of water molecule in close contact with the O2-H7 group in $[Ala\text{-}A]_{aq}$ does not necessarily mean that the O2-H7···Ow H-bond is stronger than in $[Ala\text{-}B]_{aq}$. To resolve this ambiguity, the results on $g(R_{O2\cdots Ow})$ have to be supplemented by the PDO maps. The O2-H7···Ow H-bond corresponds to the H-bond networks labeled with **A** on the PDO maps in Figures 3.6a, 3.6d, 3.6f and 3.6i. The contour density at **A** in $[Ala\text{-}B]_{aq}$ is higher than in $[Ala\text{-}A]_{aq}$, implying an increase in the degree of hydration at **A** upon the $N-C^{\alpha}$ bond rotation. For $[\text{Ala - A}]_{\text{aq}}$ and $[\text{Ala - B}]_{\text{aq}}$, the main peaks of $g(R_{\text{O1..Ow}})$ are seen at 3.11 and 3.16 Å, respectively, with about two water molecules (1.97 and 2.33, respectively) in close contact with O1. The two water molecules act as proton donor towards the lone-pair electrons of O1 and correspond to the H-bond networks labeled with **B** and **C** in Figures 3.6a, 3.6b and 3.6e for $[\text{Ala - A}]_{\text{aq}}$, and Figures 3.6f, 3.6g and 3.6j for $[\text{Ala - B}]_{\text{aq}}$. The contour densities at **B** and **C** in $[\text{Ala - B}]_{\text{aq}}$ are a little lower than in $[\text{Ala - A}]_{\text{aq}}$.

For $[\text{Ala - A}]_{\text{aq}}$, the position of the main peak of $g(R_{\text{N..Ow}})$ is located at 3.16 Å, with approximately two (1.92) water molecules H-bonding with both N-H groups. They are labeled with **D** and **E** on the PDO maps in Figures 3.6a to 3.6c. Since H2 and H3 are in different environment, due to the presence of the CH_3 group adjacent to H2, the structures of $g(R_{\text{H2}\cdots\text{Ow}})$ and $g(R_{\text{H3}\cdots\text{Ow}})$ in Figure 3.5b are quite different, for which the main peak of $g(R_{\text{H2}\cdots\text{Ow}})$ is more structured than $g(R_{\text{H3}\cdots\text{Ow}})$. This suggests that the N-H2···Ow H-bond could be more associated than the N-H3···Ow H-bond; in line with the PDO maps in Figure 3.6c, in which a more well define H-bond network at **E** compared to **D** is evident. The degree of hydration at the NH_2 group seems to be decreased when the angle ϕ varies from 0 to 30 degree. For $[\text{Ala - B}]_{\text{aq}}$, the main peak of $g(R_{\text{N}\cdots\text{Ow}})$ in Figure 3.5d is located at 3.11 Å, with lower number of water molecules (1.54) in close contact with both N-H groups compared to $[\text{Ala - A}]_{\text{aq}}$. Moreover, the main peak of $g(R_{\text{H2}\cdots\text{Ow}})$ in Figure 3.5d possesses nearly no structure, another indicator for a weaker N-H2···Ow H-bond upon the rotation. Comparison of the PDO maps in Figures 3.6c and 3.6h also shows

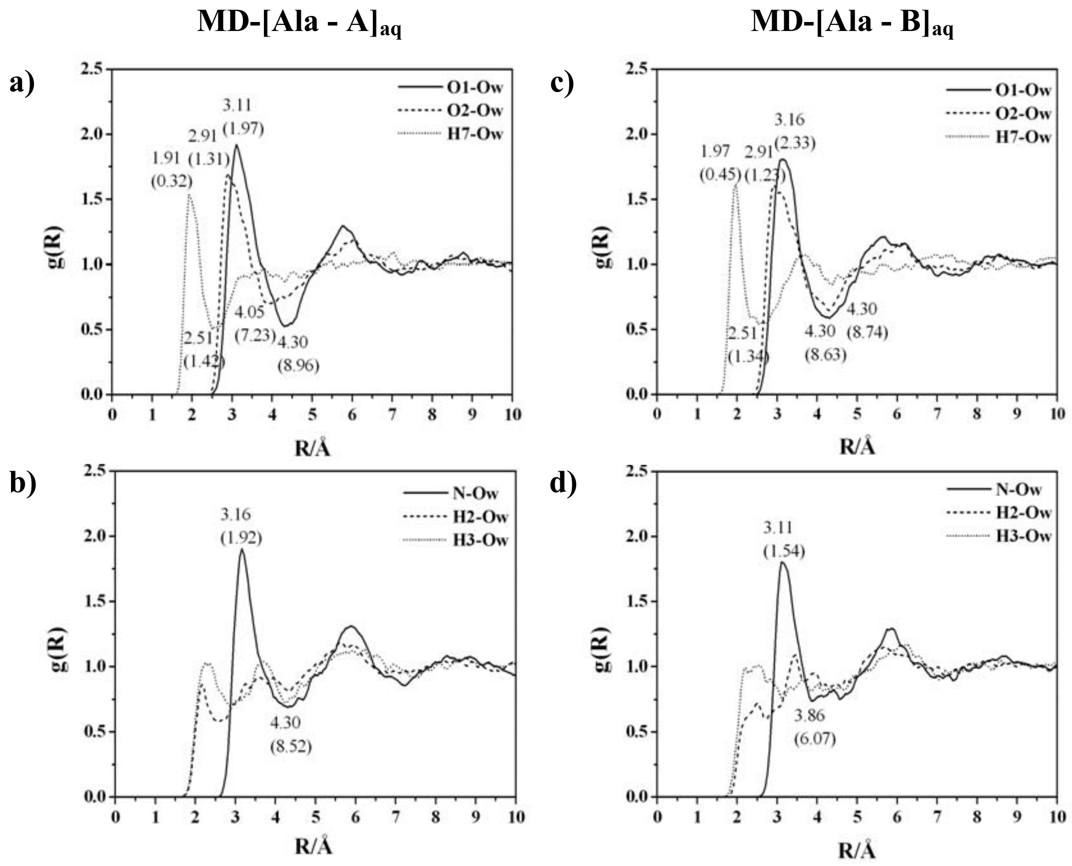

Figure 3.5 g(R) obtained from MD simulations at 298 K. Some characteristic distances are shown, with the average running coordination number (n(R)) in parenthesis.

a) – b) MD-[Ala - A]$_{aq}$

c) – d) MD-[Ala - B]$_{aq}$

e) – f) MD-[Ala - C]$_{aq}$

g) – i) MD-[Li$^+$/Ala - C]$_{aq}$

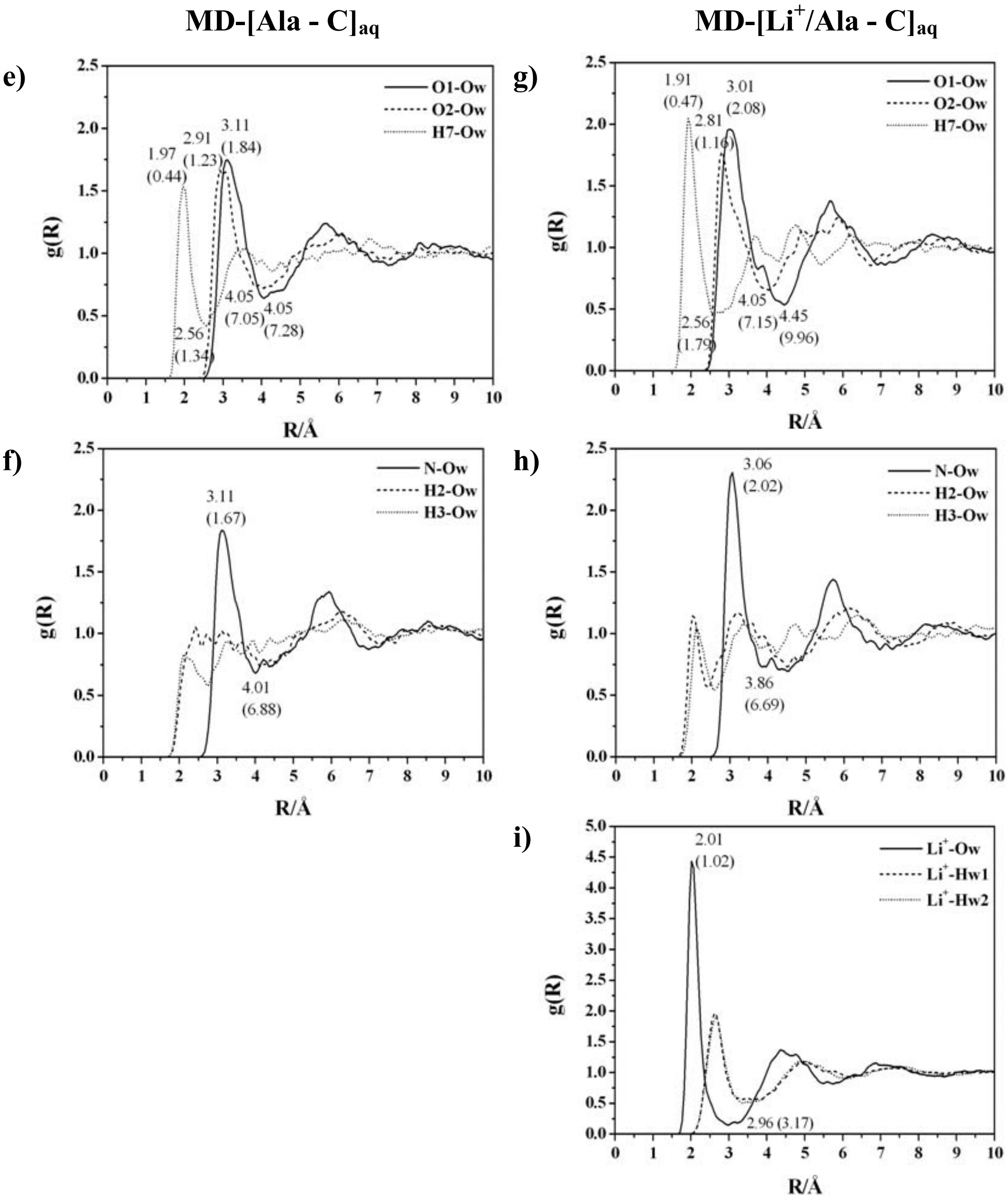

Figure 3.5 (continued)

decreases in the contour densities at **D** and **E**, due to the rotation of the $N-C^{\alpha}$ bond. This confirms the results of $g(R_{N\cdots Ow})$. The decrease in the degree of hydration at the NH_2 groups seems to be accompanied by an increase in the contour density at **F**, which means that the H-bond network at the C1-H1 group becomes stronger upon rotation; since in Ala-B, H3 is closer to H1, and the H-bond networks nearby can be partly overlap.

The structures and peak positions of g(R) for the COOH group are slightly modified when the angle ϕ is rotated 180 degree about the $N - C^{\alpha}$ bond. For $[Ala - C]_{aq}$, the main peak of $g(R_{O1 \cdots Ow})$ in Figure 3.5e is seen at 3.11 Å, with approximately two (1.84) water molecules in close contact with the C=O1 group. $g(R_{O2 \cdots Ow})$ in Figure 3.5 shows that the number of water molecules in close contact with the O2-H7 group is not much affected when the angle ϕ varies from 0 to 30 to 180 degree, respectively. However, an increase in the degree of hydration at the O2-H7 group is more evident from the PDO maps, on which the contour density at **A** in $[Ala - C]_{aq}$ is a little higher than in $[Ala - B]_{aq}$ and in $[Ala - A]_{aq}$, respectively. It is confirmed that the variation of the angle ϕ from 0 to 30 to 180 degree indeed destabilizes to the H-bond networks at the NH_2 groups. The structures of main peaks of $g(R_{H2 \cdots Ow})$ and $g(R_{H3 \cdots Ow})$ in Figure 3.5f are roughly the same as in Figure 3.5d. However, the 180-degree rotation of the NH_2 group creates an additional well define H-bond network, labeled with **I** in Figure 3.6n. This H-bond network is adjacent to **F**, spanning from H1 to the nearest H atom of the CH_3 group. The PDO maps also reveal a small H-bond network in the area between the N and O1 atoms in Ala-C, labeled with **H** in Figures 3.6k to 3.6m and 3.6o. This H-bond network seems to be an evidence showing the existence of the bifurcated H-bond, in which a water molecule acts as a proton donor towards both N and O1 atoms of Ala-C, see structure **h** and **i** in Figure 3.1.

Figure 3.6 Some PDO, AWPD and AW-WWPD maps obtained from MD simulations at 298 K.

a) - e) MD-$[Ala - A]_{aq}$

f) - j) MD-$[Ala - B]_{aq}$

k) - o) MD-$[Ala - C]_{aq}$

p) - t) MD-$[Li^+/Ala - C]_{aq}$

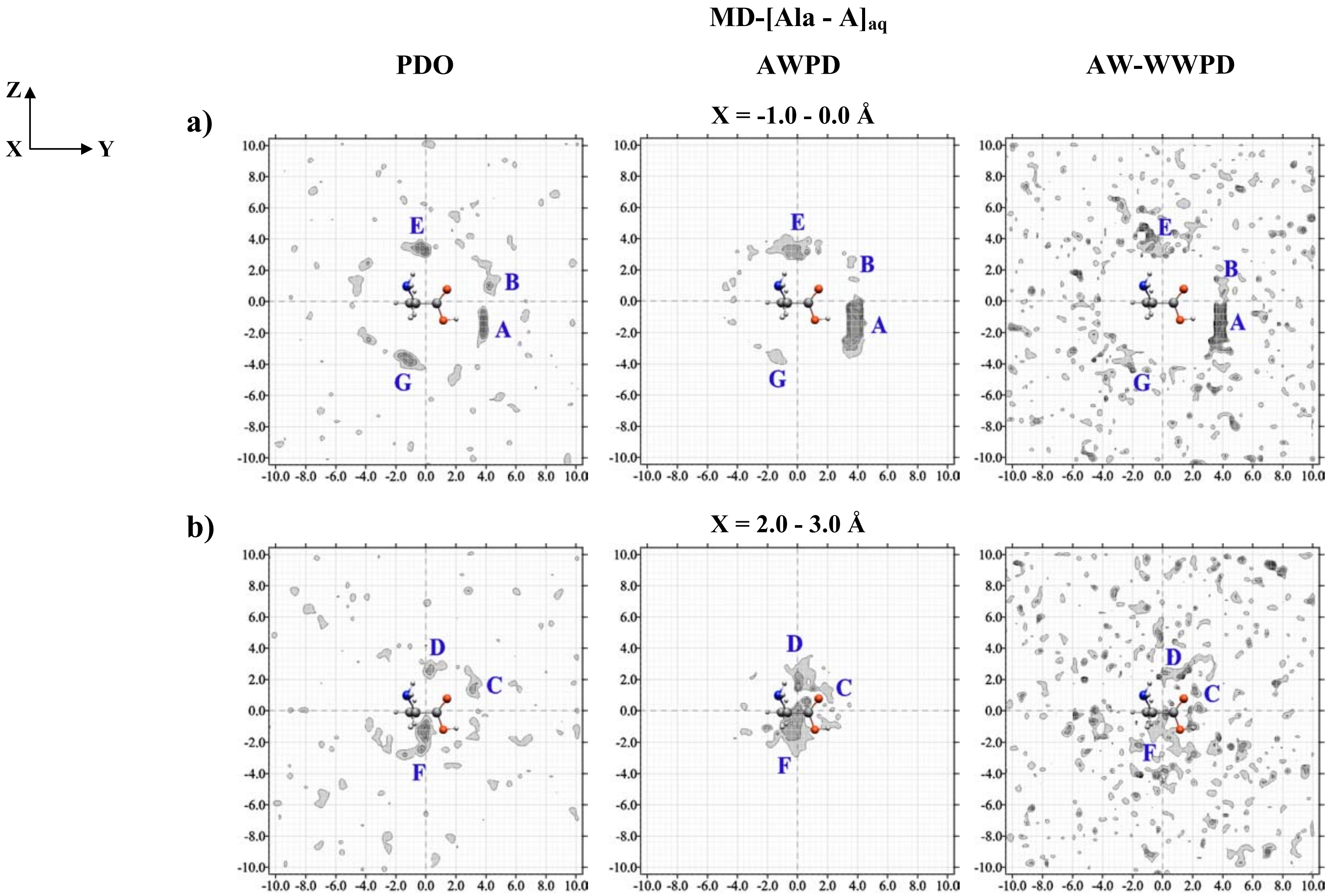
MD-[Ala - A]$_{aq}$
PDO
AWPD
AW-WWPD
Z
X
Y
a)
X = -1.0 - 0.0 Å
b)
X = 2.0 - 3.0 Å
A
B
C
D
E
F
G
10.0
8.0
6.0
4.0
2.0
0.0
-2.0
-4.0
-6.0
-8.0
-10.0
-10.0 -8.0 -6.0 -4.0 -2.0 0.0 2.0 4.0 6.0 8.0 10.0

Figure 3.6

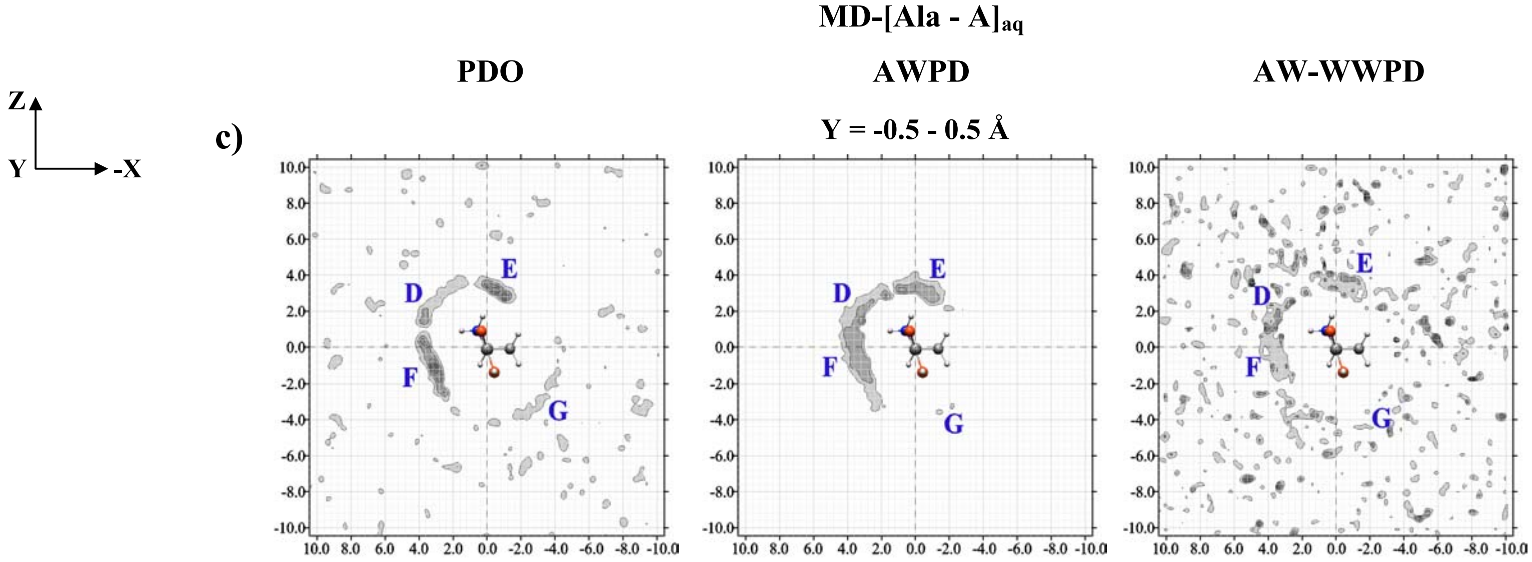

Figure 3.6 (continued)

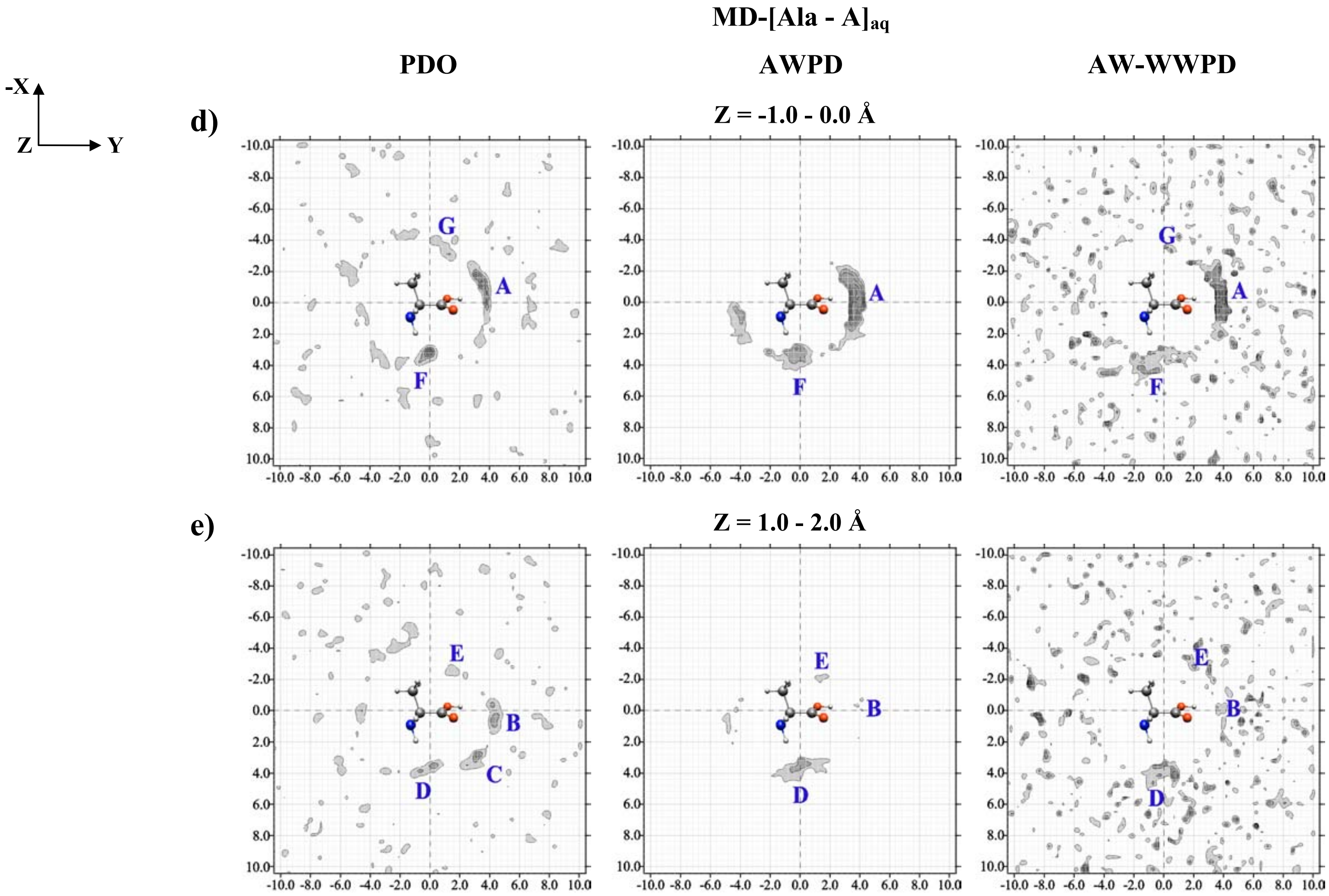

Figure 3.6 (continued)

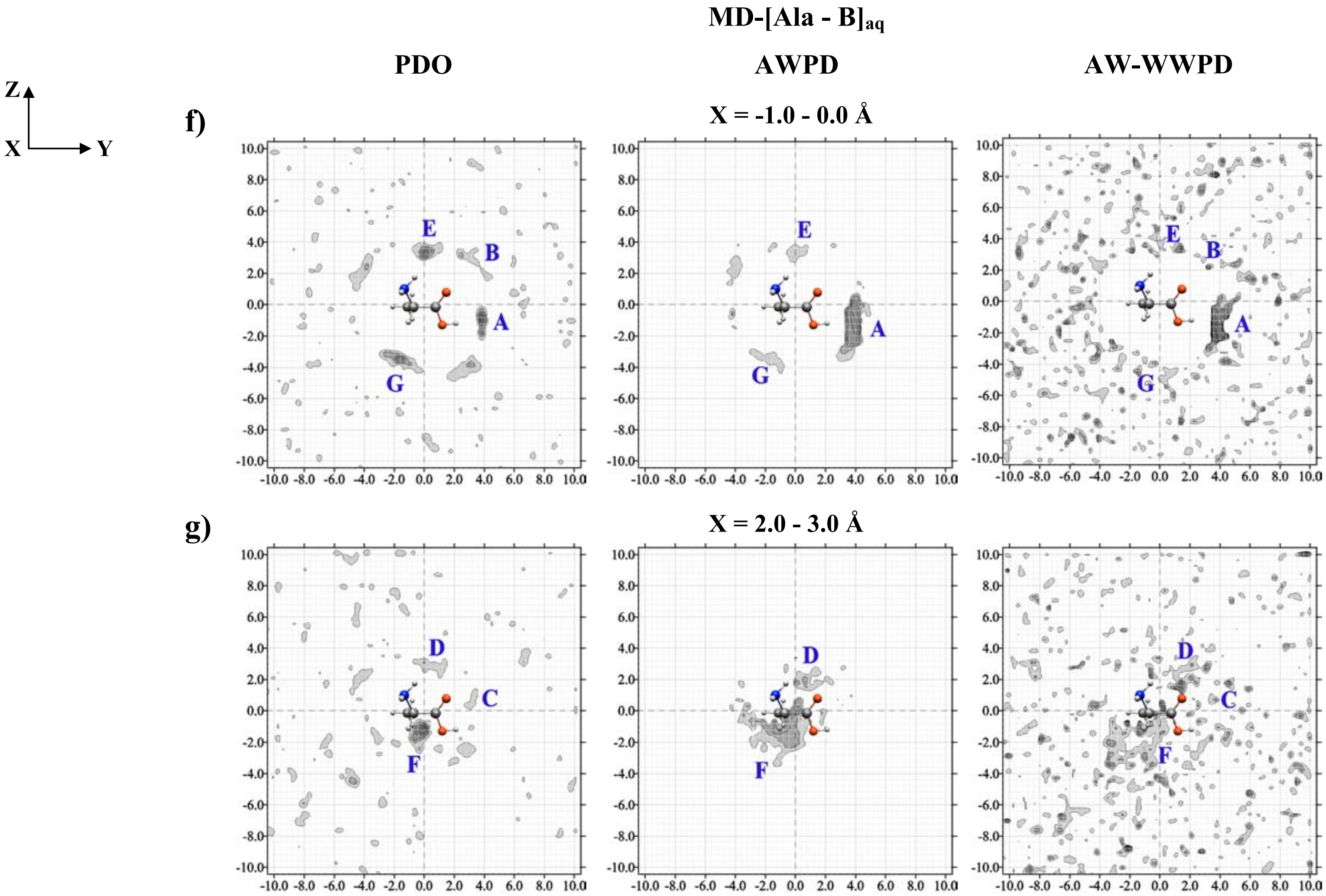

Figure 3.6 (continued)

MD-[Ala - B]$_{aq}$

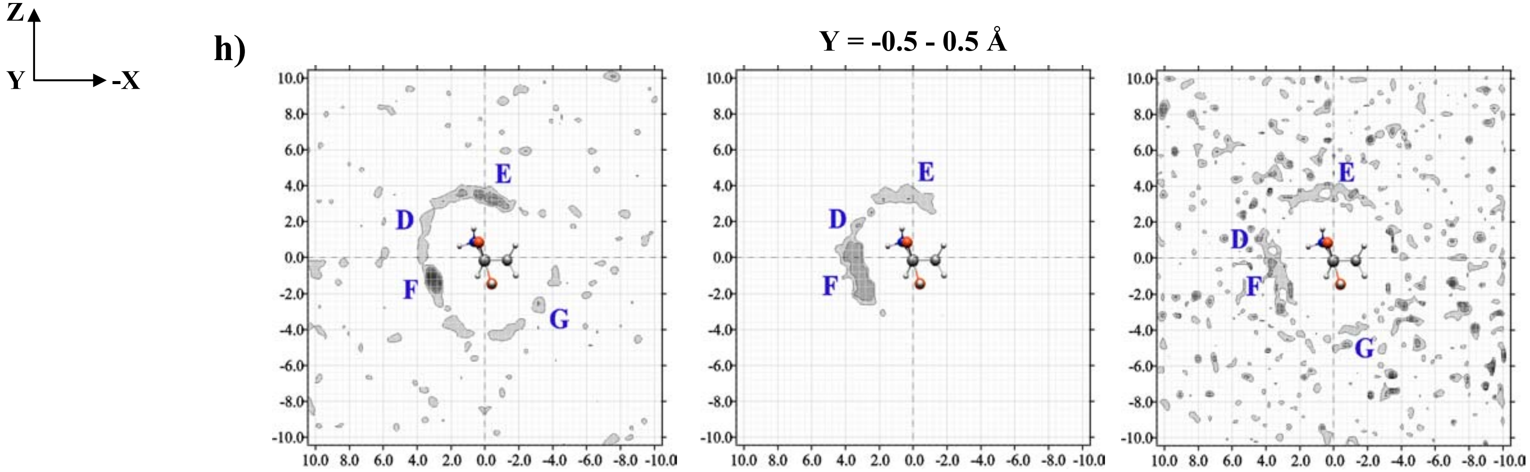
PDO

AWPD

AW-WWPD

Y = -0.5 - 0.5 Å

Figure 3.6 (continued)

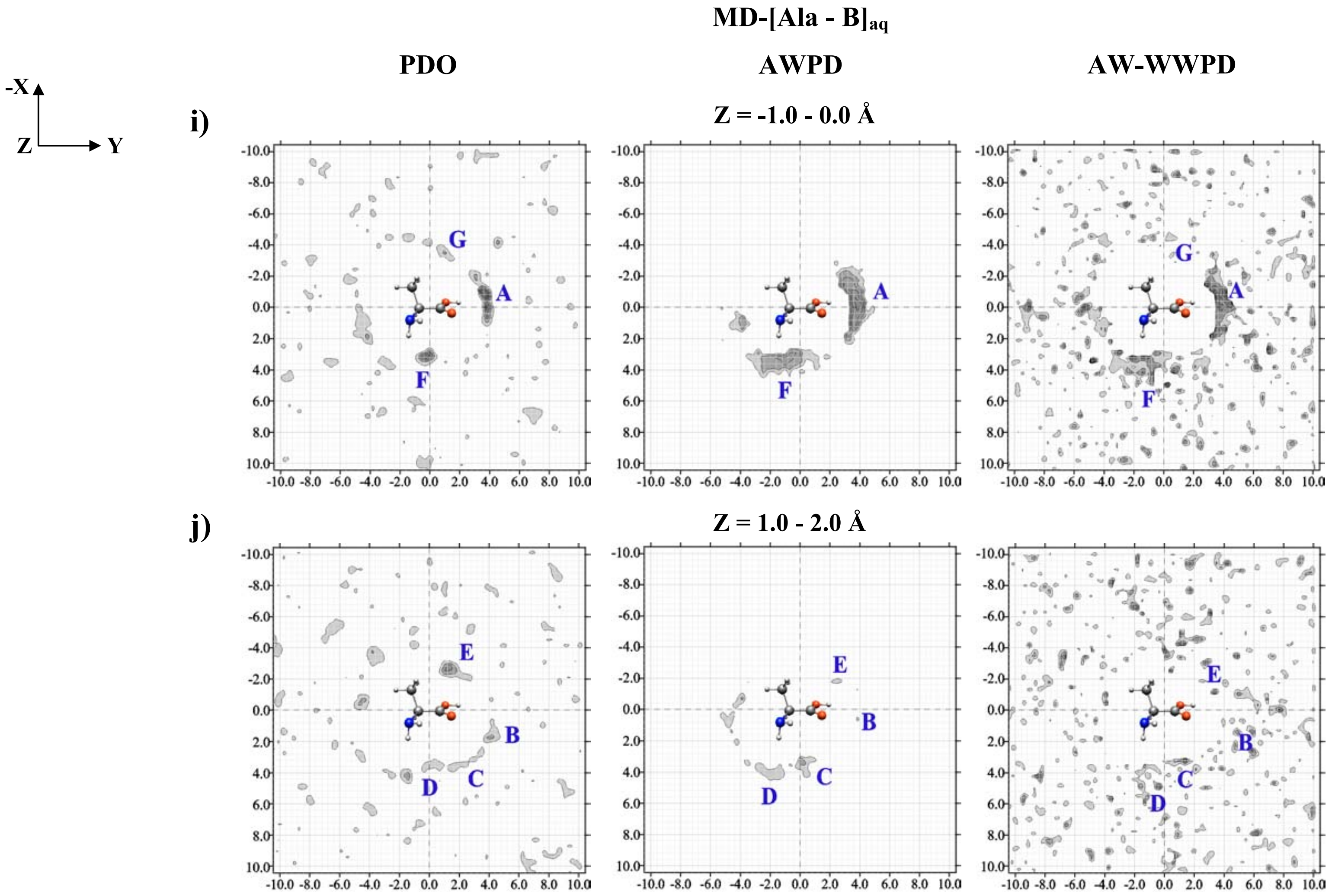

Figure 3.6 (continued)

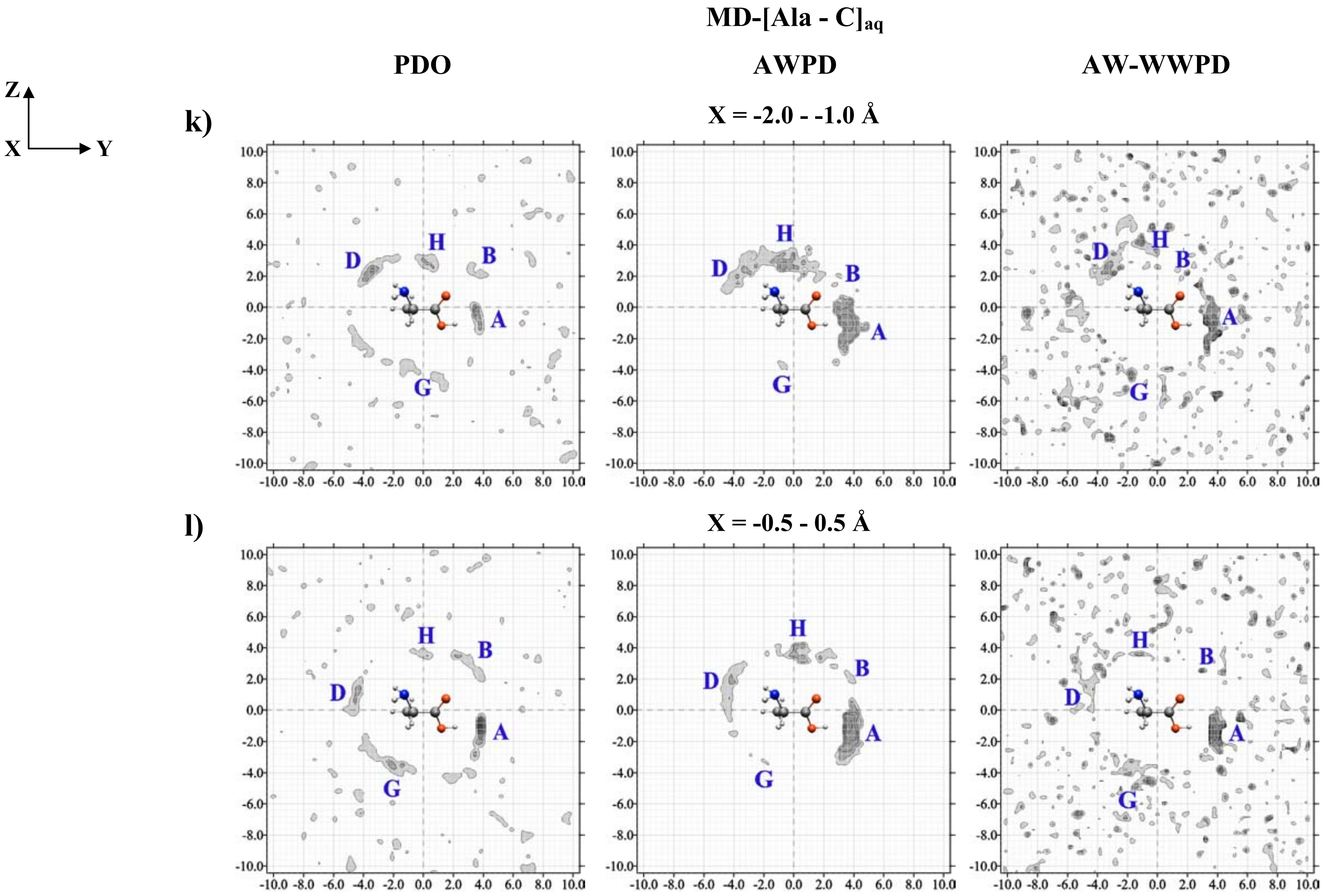

Figure 3.6 (continued)

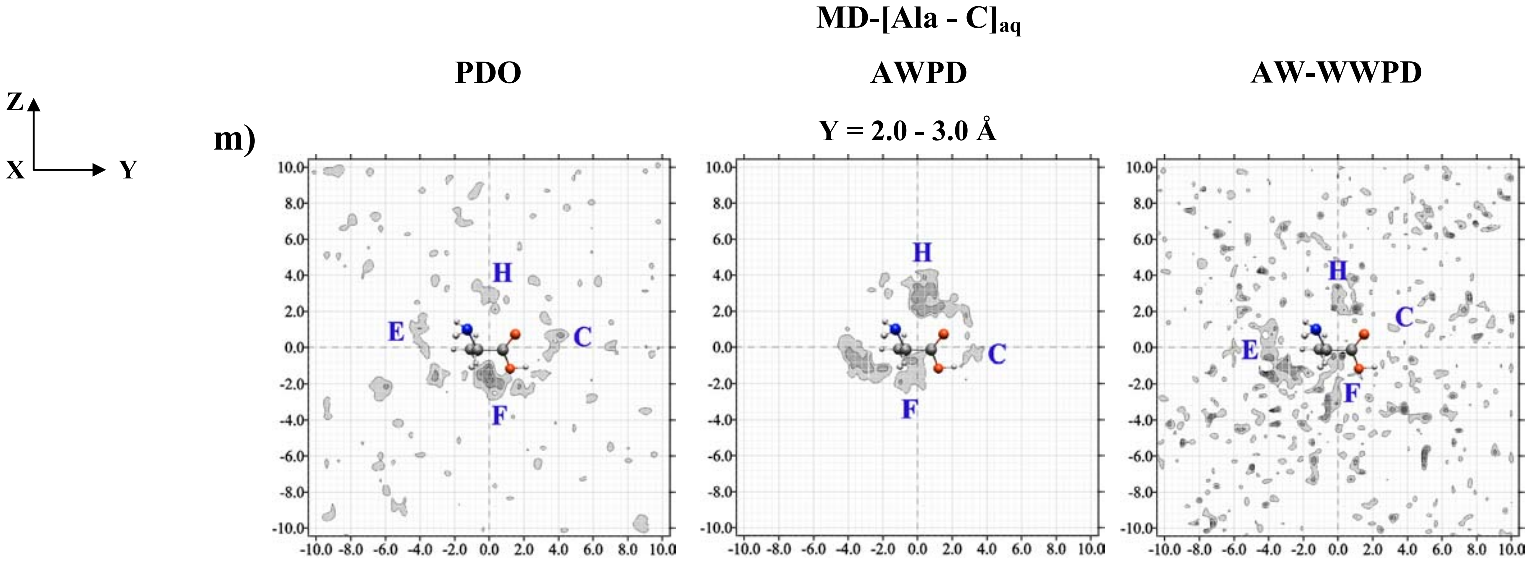

MD-$[Ala - C]_{aq}$

PDO AWPD AW-WWPD

m) Y = 2.0 - 3.0 Å

Figure 3.6 (continued)

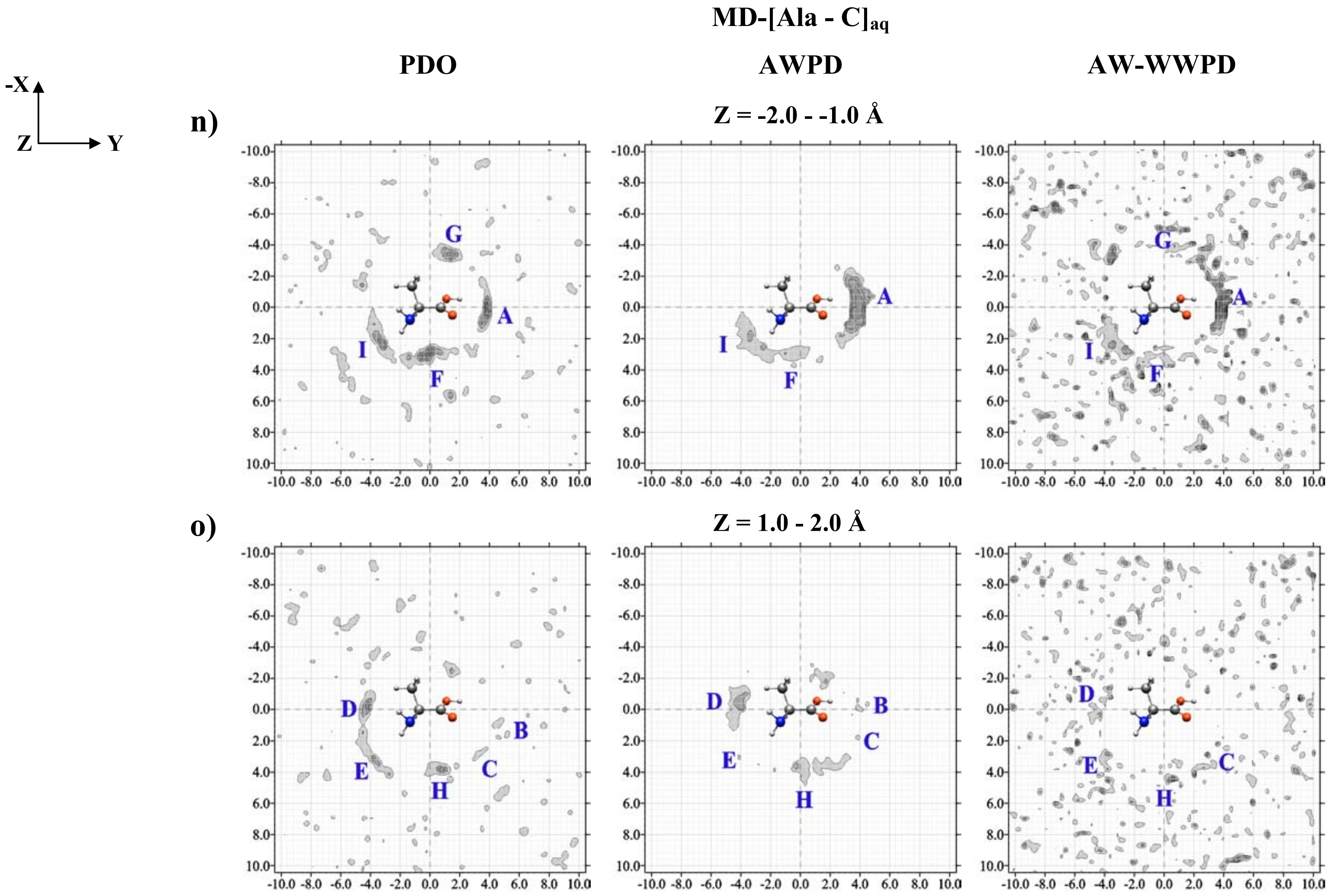

Figure 3.6 (continued)

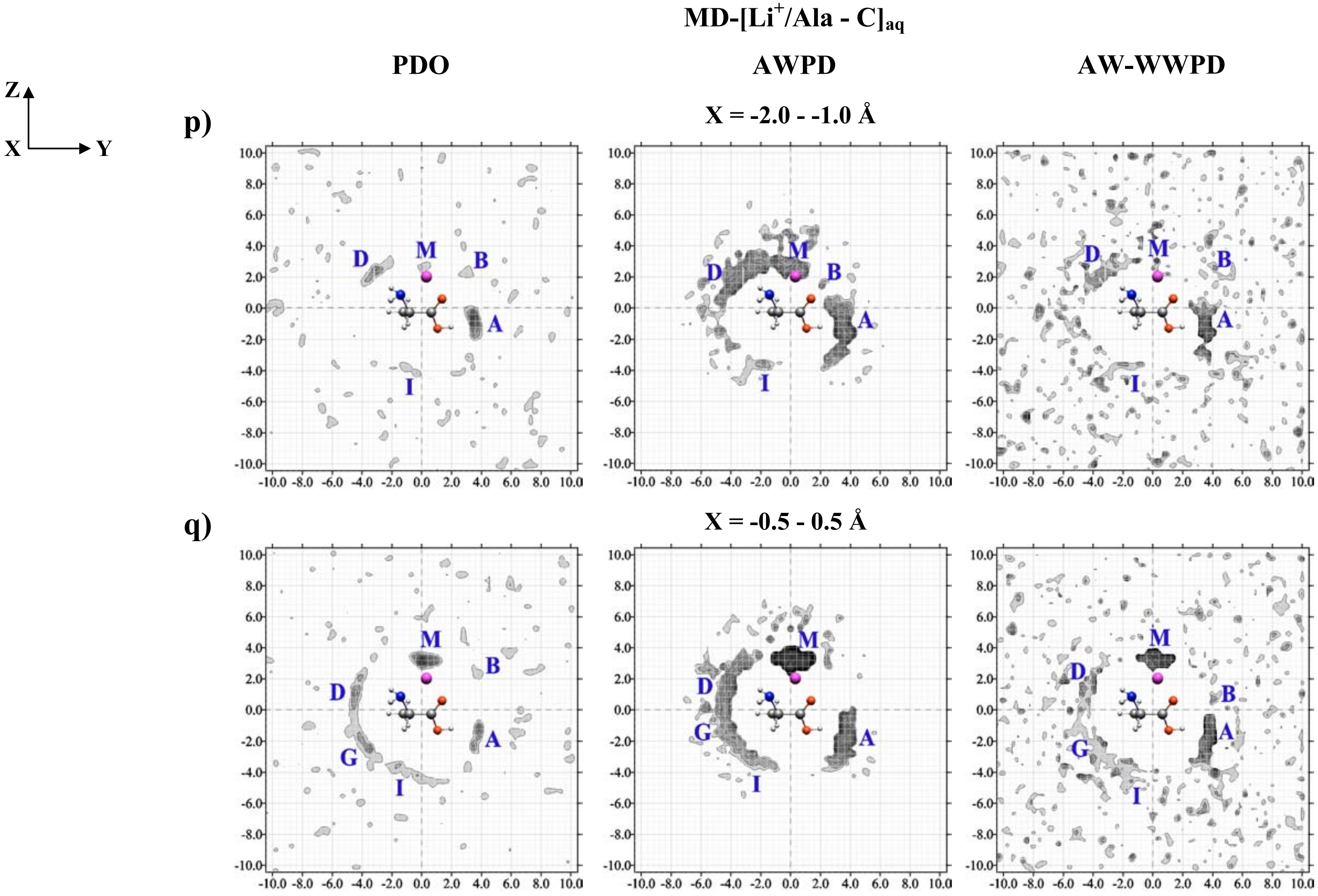

Figure 3.6 (continued)

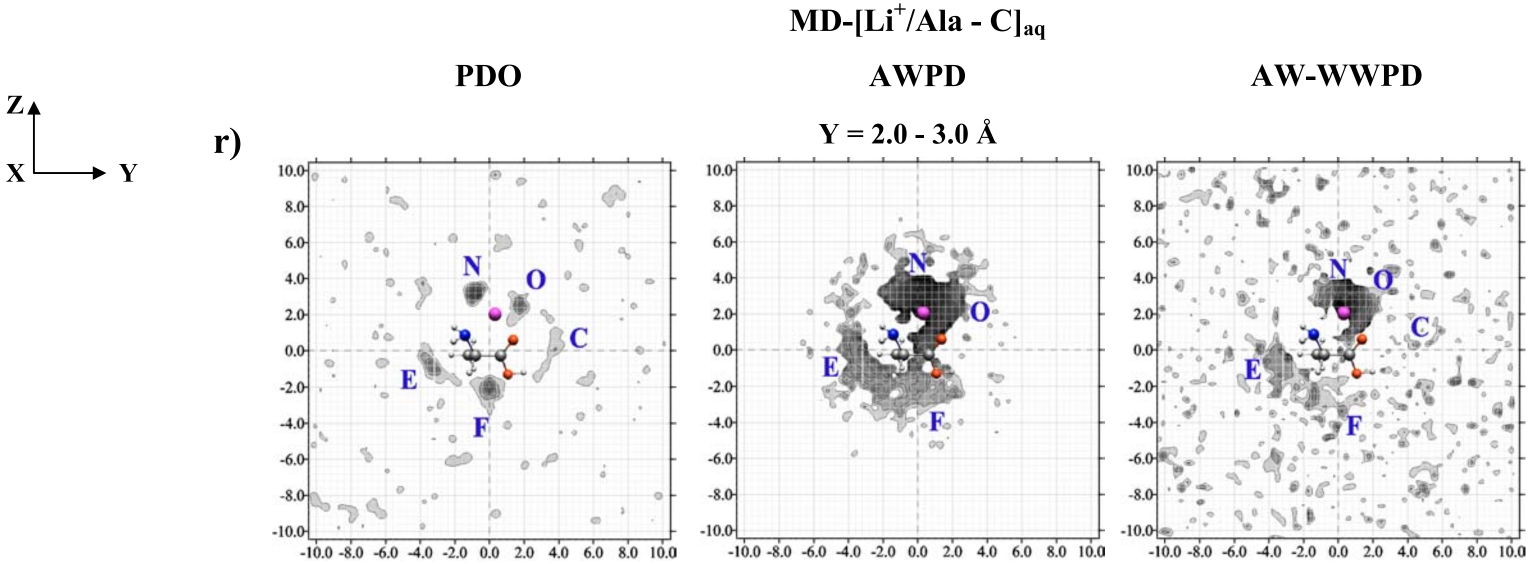

Figure 3.6 (continued)

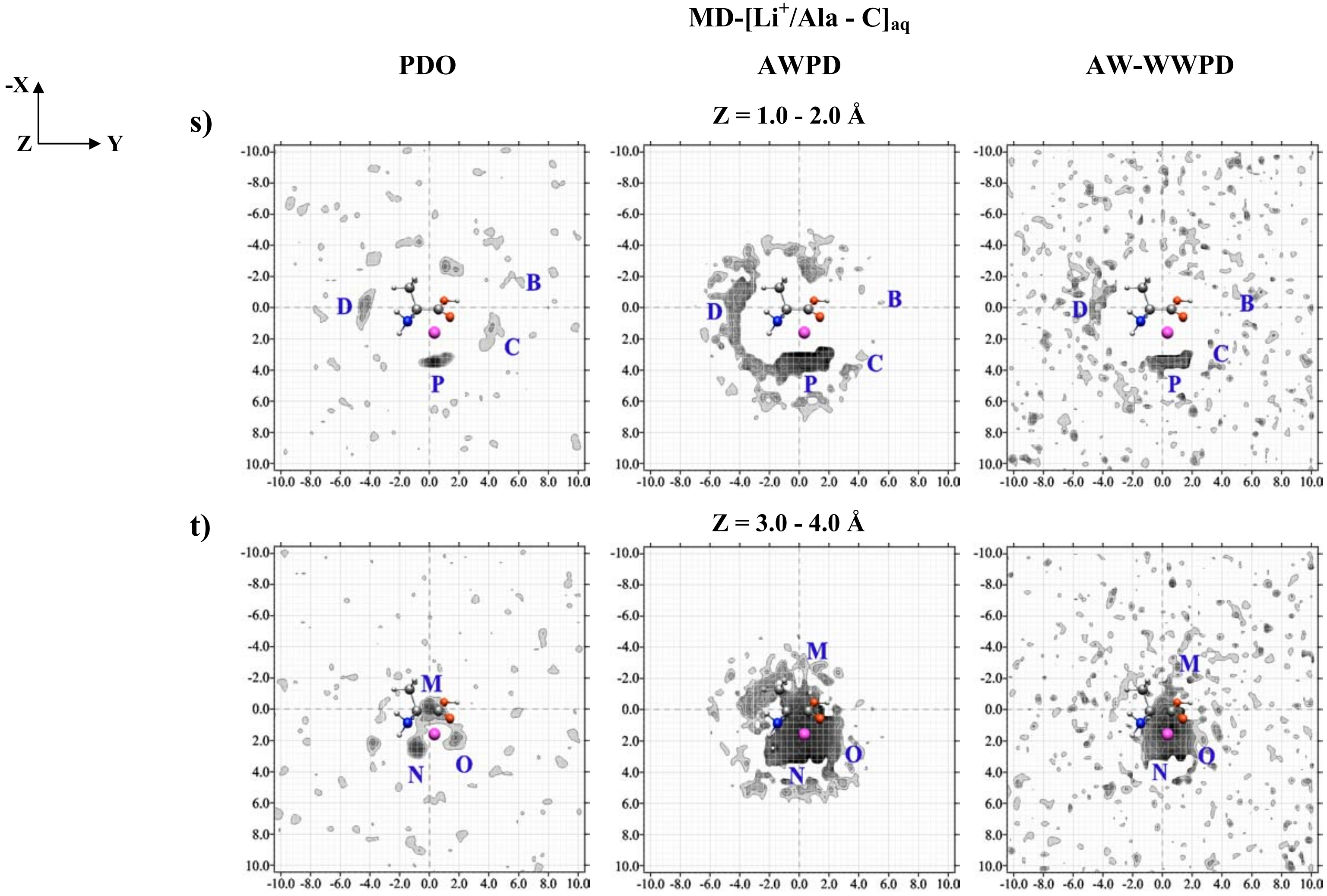

Figure 3.6 (continued)

The effects of conformation change on the hydration dynamics in $[\mathrm{Ala\text{-}A}]_{\mathrm{aq}}$, $[\mathrm{Ala\text{-}B}]_{\mathrm{aq}}$ and $[\mathrm{Ala\text{-}C}]_{\mathrm{aq}}$ are discussed using the cross section plots in Figure 3.7 and $\tau_{\mathrm{A-H\cdots B,\,max}}$ in Table 3.2. Since, on the PDO maps, the H-bond networks at **A** are the most well define, attention is focused on the behavior of water molecules forming H-bonds with the O2-H7 group. Selected water exchange diagrams are displayed in Figure 3.8, together with the corresponding $\Delta \mathrm{E}^{\mathrm{AW\text{-}WW}}$. The low-pass filter method (Middlehurst, 1993) was employed to smooth all the data plots in Figure 3.8. Additional water exchange diagrams are given in Appendix D. Some representative results of $\tau_{\mathrm{O2-H7\cdots Ow}}$ and $\tau_{\mathrm{ex,O2\text{-}H7\cdots Ow}}$, together with the water exchange pathways obtained from the analysis of the water exchange diagrams, are listed in Table 3.3. The energetic paths of the water exchange processes were explored by calculations of the activation interaction energy of the transition state complex ($\Delta \mathrm{Ea}^{\mathrm{AW\text{-}WW}}$), defined as the difference between the average interaction energy of a specific water molecule in the first hydration shell ($\Delta \mathrm{E}_{\mathrm{av}}^{\mathrm{AW\text{-}WW}}$) and its interaction energy at the water exchange transition state ($\Delta \mathrm{E}_{\mathrm{TS}}^{\mathrm{AW\text{-}WW}}$). These energy values can be extracted from the water exchange diagrams and some of them are given in Table 3.3. The derivations of $\Delta \mathrm{Ea}^{\mathrm{AW\text{-}WW}}$, as well as $\tau_{\mathrm{A-H\cdots Ow}}$ and $\tau_{\mathrm{ex,A\text{-}H\cdots Ow}}$, are also shown in Table 3.3. Attempt was further made to establish correlations among these energies and times. Some meaningful results are displayed in Figure 3.9.

Figure 3.7 Selected AW-WWPD maps and the cross section plots obtained from the transverse and longitudinal profile lines.

——— The total-average interaction energy.

– – – – – – – The average solute-solvent interaction energy.

- - - - - - - - - - - The average solvent-solvent interaction energy.

Energy values and distances are in kJ/mol and Å, respectively.

The lowest energy minima on the cross section plots are set to zero to estimate the transition energy barriers for water exchange.

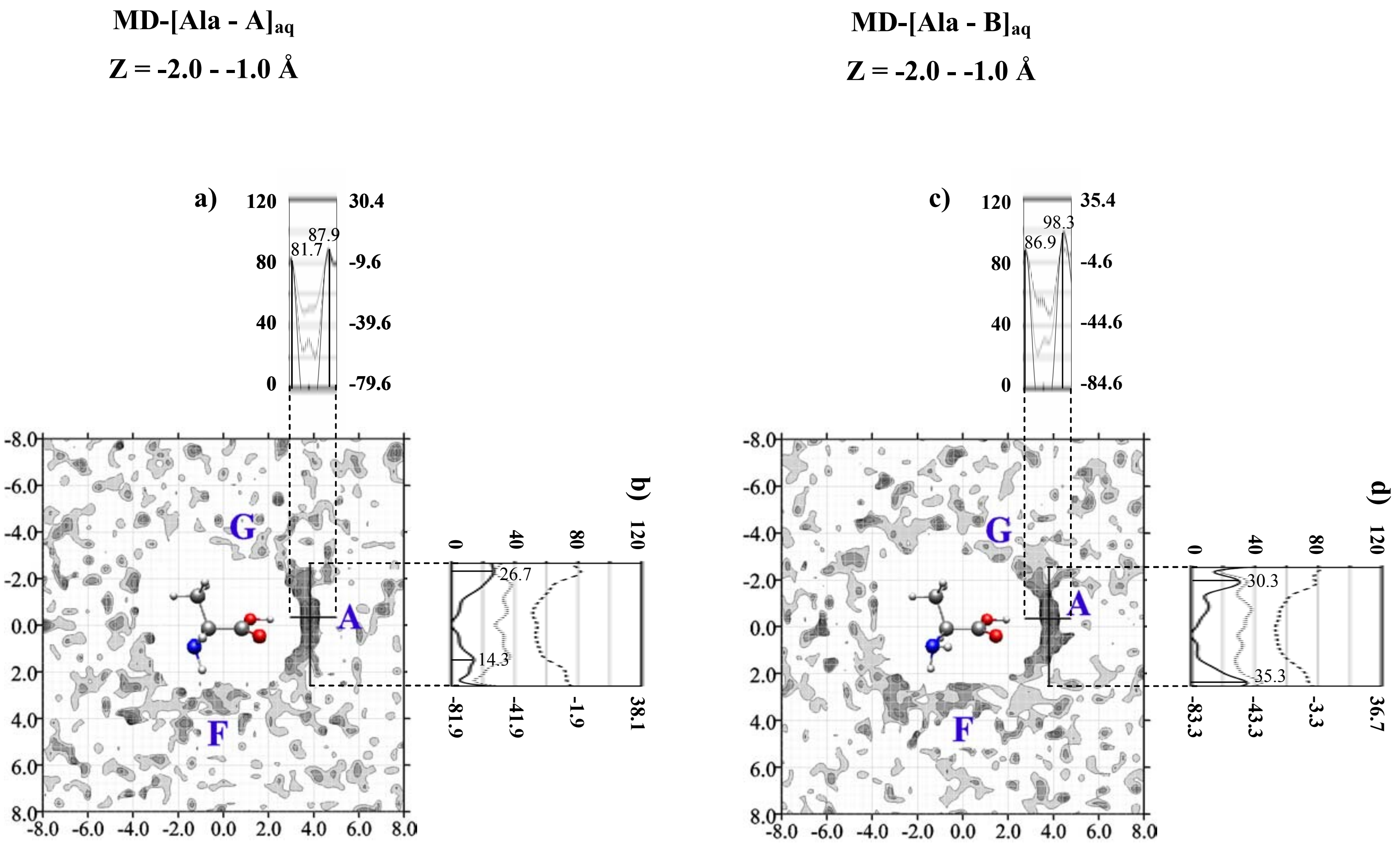
MD-[Ala - A]$_{aq}$
Z = -2.0 - -1.0 Å
MD-[Ala - B]$_{aq}$
Z = -2.0 - -1.0 Å
a)
120
80
40
0
30.4
-9.6
-39.6
-79.6
81.7
87.9
c)
120
80
40
0
35.4
-4.6
-44.6
-84.6
86.9
98.3
b)
0
40
80
120
-81.9
-41.9
-1.9
38.1
26.7
14.3
d)
0
40
80
120
-83.3
-43.3
-3.3
36.7
30.3
35.3
G
A
F
G
A
F
-8.0
-6.0
-4.0
-2.0
0.0
2.0
4.0
6.0
8.0
-8.0
-6.0
-4.0
-2.0
0.0
2.0
4.0
6.0
8.0

Figure 3.7

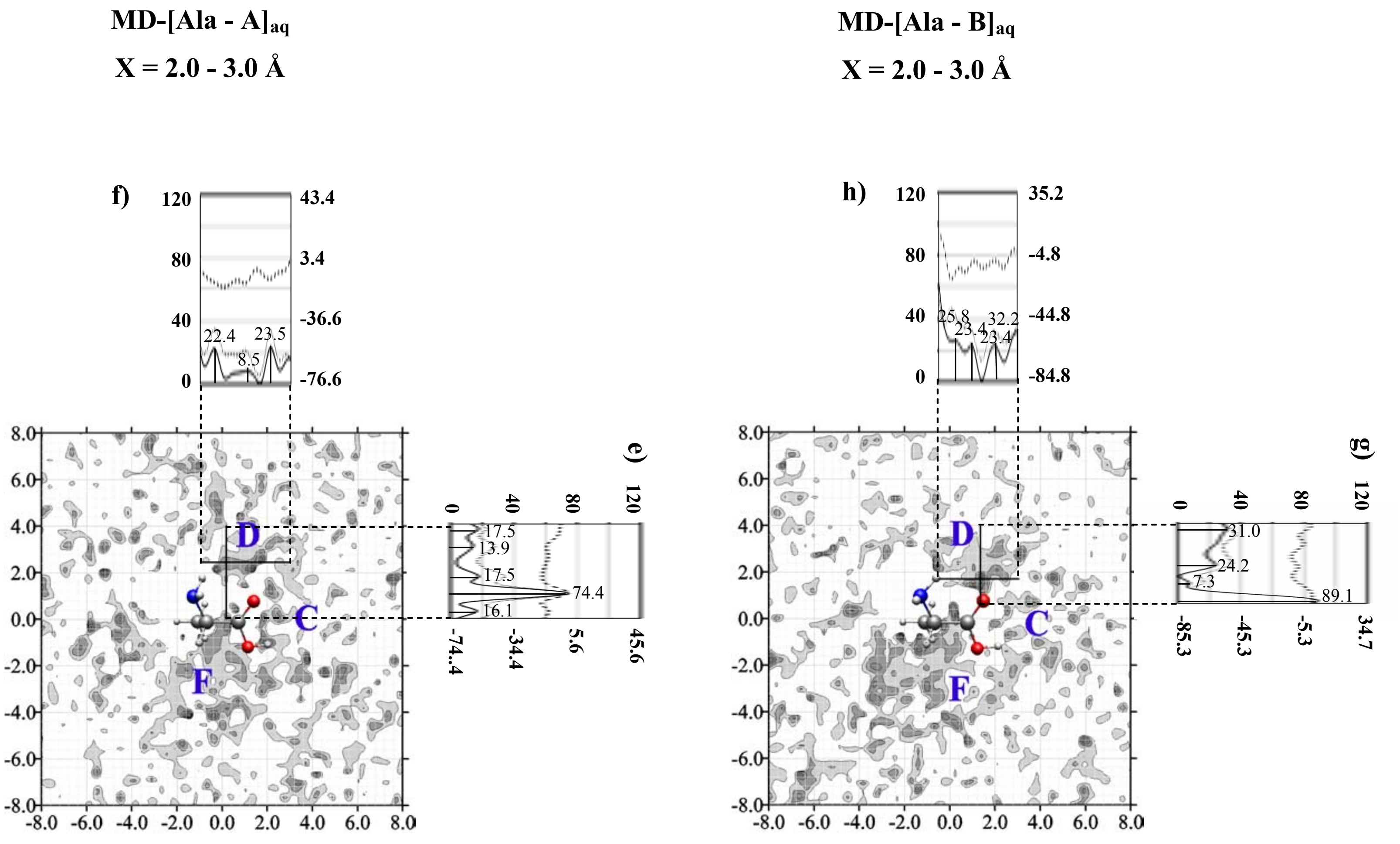

Figure 3.7 (continued)

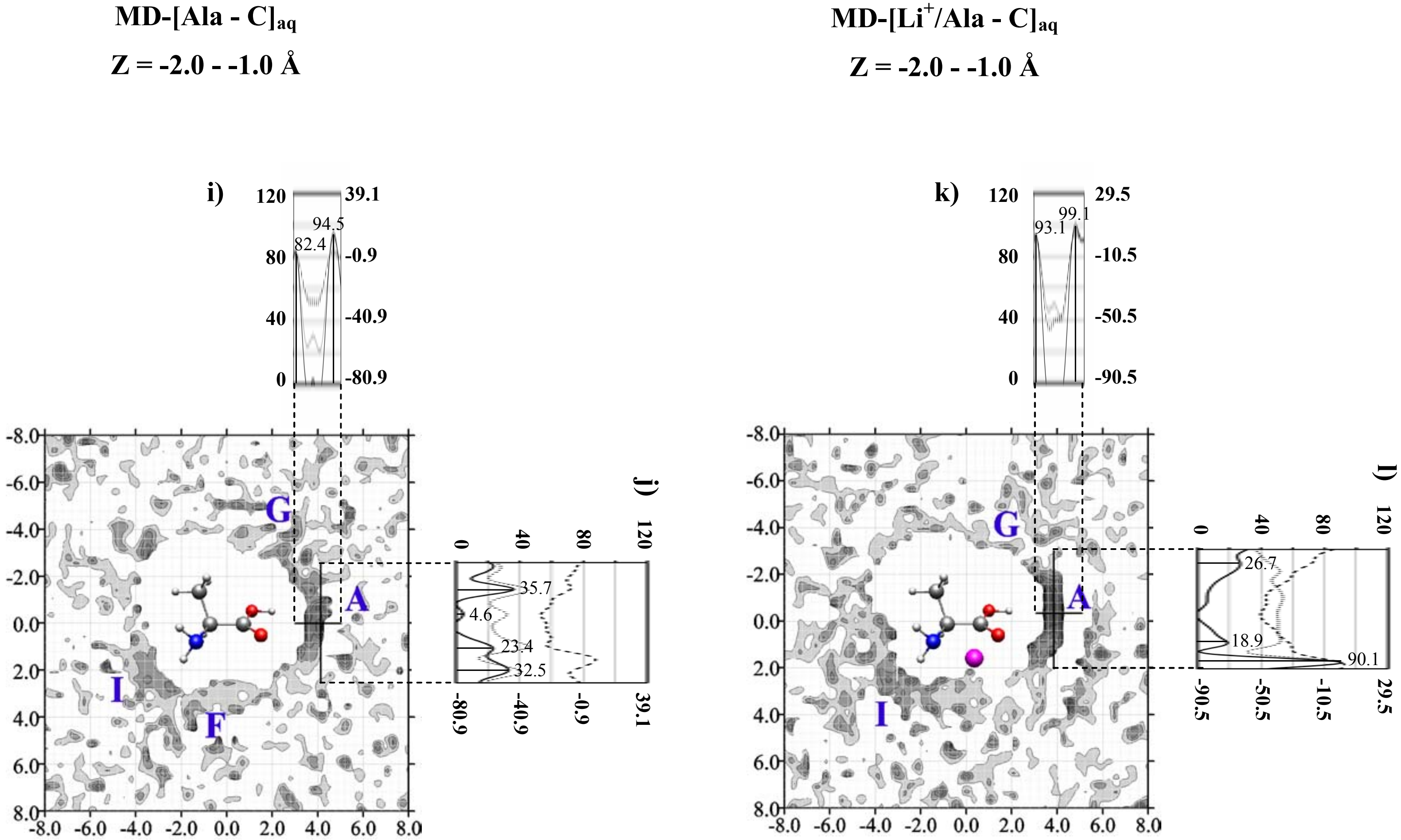

MD-[Ala - C]$_{aq}$

Z = -2.0 - -1.0 Å

MD-[Li$^+$/Ala - C]$_{aq}$

Z = -2.0 - -1.0 Å

Figure 3.7 (continued)

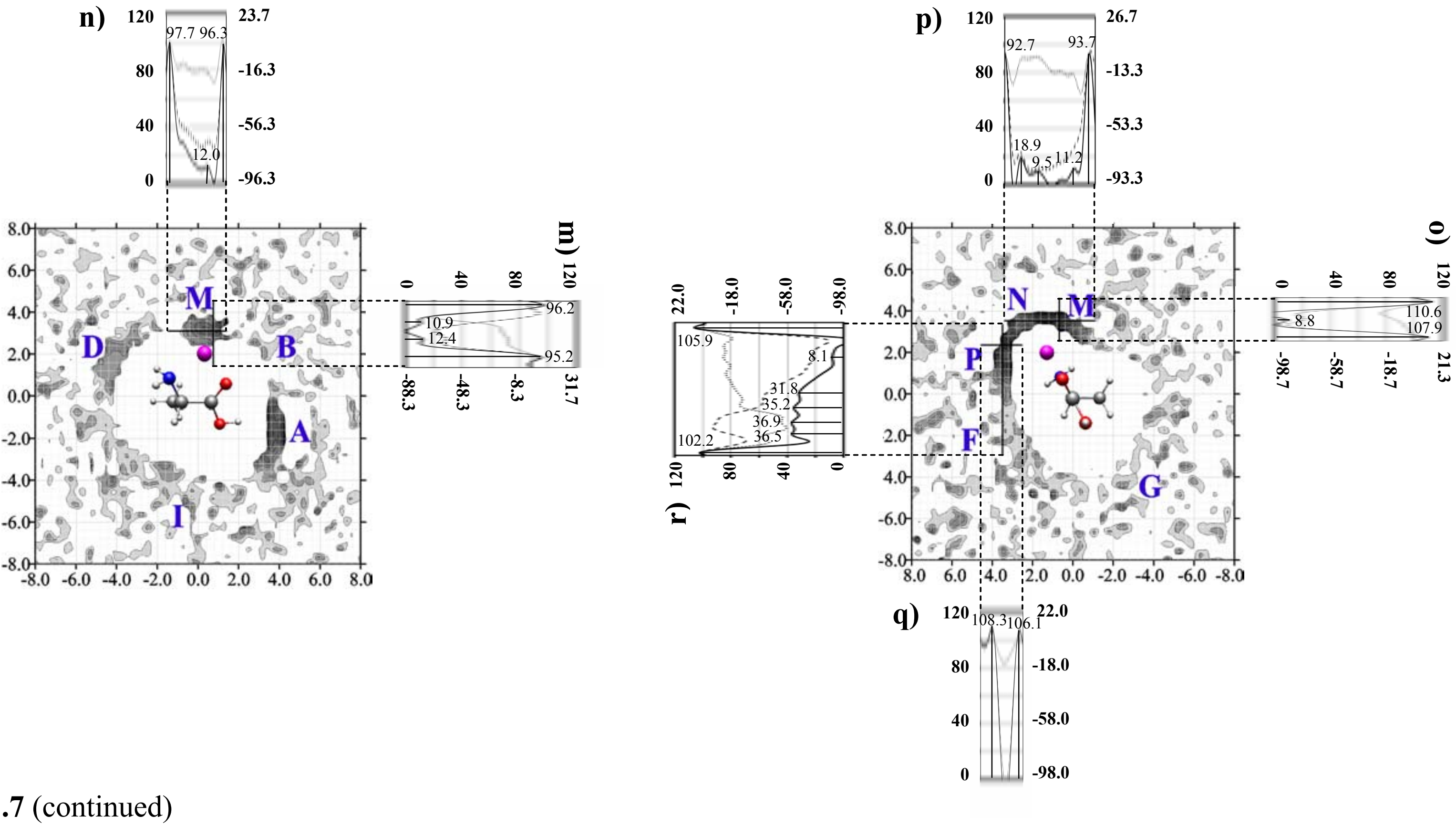

MD-[Li^+/Ala - C]$_{aq}$

X = -1.0 - 0.0 Å

MD-[Li^+/Ala - C]$_{aq}$

Y = -0.5 - 0.5 Å

Figure 3.7 (continued)

Table 3.2 The longest H-bond lifetimes ($\tau_{A-H\cdots Ow,max}$) and the longest water residence times ($\tau_{Li^+\cdots Ow,max}$), together with the water exchange rate constants ($k_{ex,A\text{-}H\cdots Ow}$ and $k_{ex,Li^+\cdots Ow}$) obtained from MD simulations of $[Ala]_{aq}$ and $[Li^+/Ala]_{aq}$, respectively. Time in ps and rate constant in ns^{-1}.

MD	O2-H7$\cdots$Ow		N-H$\cdots$Ow		Li$^+$$\cdots$Ow	
	$\tau_{O2-H7\cdots Ow,max}$	$k_{ex,O2\text{-}H7\cdots Ow}$	$\tau_{N-H\cdots Ow,max}$	$k_{ex,N\text{-}H\cdots Ow}$	$\tau_{Li^+\cdots Ow,max}$	$k_{ex,Li^+\cdots Ow}$
$[Ala - A]_{aq}$	19.63	50.9	13.12	76.2	-	-
$[Ala - B]_{aq}$	21.17	47.2	16.25	61.5	-	-
$[Ala - C]_{aq}$	20.37	49.1	17.19	58.2	-	-
$[Li^+/Ala - C]_{aq}$	28.03	35.7	17.99	55.6	38.02	26.3

Comparisons of the cross section plots in Figures 3.7a to 3.7d, and 3.7i and 3.7j show that the solute conformation changes from the angle $\phi = 0$ to 30 to 180 degree lead to visible effects on the structures of the total-average potential energy landscapes at **A**, especially in $[\mathrm{Ala-C}]_{\mathrm{aq}}$ compared to $[\mathrm{Ala-A}]_{\mathrm{aq}}$ and $[\mathrm{Ala-B}]_{\mathrm{aq}}$. For $[\mathrm{Ala-C}]_{\mathrm{aq}}$, the cross section plot derived from the longitudinal profile line in Figure 3.7j shows more structures compared to the others. This could reduce the mobility of water molecule inside the H-bond network at **A** in $[\mathrm{Ala-C}]_{\mathrm{aq}}$, compared to $[\mathrm{Ala-A}]_{\mathrm{aq}}$ and $[\mathrm{Ala-B}]_{\mathrm{aq}}$, as also suggested by the contour densities on the PDO maps. Since $< \Delta E_{\mathrm{aq}}^{\mathrm{T}} >$ could be correlated with $\tau_{\mathrm{A-H\cdots B,\,max}}$ (Sagarik and Chaiyapongs, 2005; Sagarik and Dokmaisrijan, 2005), one anticipates from the values of $< \Delta E_{\mathrm{aq}}^{\mathrm{T}} >$ in Figures 3.7a, 3.7c and 3.7i that $\tau_{\mathrm{O2-H7\cdots Ow,max}}$ in $[\mathrm{Ala-B}]_{\mathrm{aq}}$ is larger than $[\mathrm{Ala-C}]_{\mathrm{aq}}$ and $[\mathrm{Ala-A}]_{\mathrm{aq}}$, respectively. The values of $\tau_{\mathrm{O2-H7\cdots Ow,max}}$ in Table 3.2 confirm this anticipation namely, $\tau_{\mathrm{O2-H7\cdots Ow,max}}$ varies from 21.2 to 20.4 to 19.6 ps in $[\mathrm{Ala-B}]_{\mathrm{aq}}$, $[\mathrm{Ala-C}]_{\mathrm{aq}}$ and $[\mathrm{Ala-A}]_{\mathrm{aq}}$, respectively. By application of a simple relationship between the water exchange rate constant ($\mathrm{k_{ex}}$) and the water residence time (τ_{res}) namely, $\mathrm{k_{ex}} = 1/\tau_{\mathrm{res}}$ (Spångberg *et al.*, 2003), $\mathrm{k_{ex}}$ at the O2-H7 groups in $[\mathrm{Ala-B}]_{\mathrm{aq}}$, $[\mathrm{Ala-C}]_{\mathrm{aq}}$ and $[\mathrm{Ala-A}]_{\mathrm{aq}}$ are 47.2 and 49.1 and 50.9 ns^{-1}, respectively. A similar conclusion could be made for the H-bond networks at the NH_2 group, in which $< \Delta E_{\mathrm{aq}}^{\mathrm{T}} >$ at **D** in $[\mathrm{Ala-B}]_{\mathrm{aq}}$ is a little larger than $[\mathrm{Ala-A}]_{\mathrm{aq}}$, resulting in longer $\tau_{\mathrm{N-H3\cdots Ow,\,max}}$ in $[\mathrm{Ala-B}]_{\mathrm{aq}}$, see Figures 3.7e and 3.7g, as well as Table 3.2.

$\tau_{\text{N-H3}\cdots\text{Ow, max}}$ in $[\text{Ala - B}]_{\text{aq}}$ and $[\text{Ala - A}]_{\text{aq}}$ are 16.2 and 13.1 ps, respectively, corresponding to k_{ex} at the N-H3 groups of 61.5 and 76.2 ns^{-1}, respectively.

Literature survey showed that the water residence times or the H-bond lifetimes are sensitive to the definitions and the methods employed in the investigations, and the values in the literatures vary in a wide range (Sagarik and Chaiyapongs, 2005; Sagarik and Dokmaisrijan, 2005). Therefore, care must be exercised in comparison the present results with the others. The longest H-bond lifetimes reported here could be compared with results in $[\text{H}_2\text{O}]_{\text{aq}}$ (Sagarik and Chaiyapongs, 2005) and $[\text{Alaz}]_{\text{aq}}$ (Sagarik and Dokmaisrijan, 2005). $\tau_{\text{Ow-Hw}\cdots\text{Ow,max}}$ in $[\text{H}_2\text{O}]_{\text{aq}}$ is 8.7 ps, whereas $\tau_{\text{N-H}\cdots\text{Ow, max}}$ at the NH_3^+ group and $\tau_{\text{Ow-Hw}\cdots\text{O, max}}$ at the COO^- group in $[\text{Alaz}]_{\text{aq}}$ are 21.3 ps and 5.1 ps, respectively. They are quite reasonable, compared with the water residence times ($<\tau_{\text{rt}}>$) obtained from MD simulations of the Bovine Pancreatic Trypsin Inhibitor (BPTI) in aqueous solution (Brunne *et al*., 1993), in which $<\tau_{\text{rt}}>$ in $[\text{H}_2\text{O}]_{\text{aq}}$, at the amide protons (SC_HN) of asparagine (Asn) and at the hydroxyl proton (SC_HO) of serine (Ser) are approximately 10, 22 and 49 ps, respectively. In other words, the water residence time in pure water is smaller than at the N-H and O-H groups of proteins, respectively; which agrees qualitatively well with the present results.

The water residence times and the water exchange mechanisms in $[\text{Ala - A}]_{\text{aq}}$, $[\text{Ala - B}]_{\text{aq}}$ and $[\text{Ala - C}]_{\text{aq}}$ could be further discussed in details using the water exchange diagrams in Figures 3.8a to 3.8c and the results in Table 3.3a.

Figure 3.8 Selected water exchange diagrams for specific water molecule in the first hydration shell of the O2-H7 group and Li^+, together with the corresponding total interaction energy (ΔE^{AW-WW}), solute-solvent (ΔE^{AW}) and solvent-solvent (ΔE^{WW}) interaction energy, monitored in course of MD simulations. Some water exchange mechanisms proposed by Langford and Gray (1996) are also included in the figure.

a) - d) At the O2-H7 groups in $[\text{Ala-A}]_{aq}$, $[\text{Ala-B}]_{aq}$, $[\text{Ala-C}]_{aq}$ and $[\text{Li}^+/\text{Ala-C}]_{aq}$, respectively.

e) - g) At Li^+ in $[\text{Li}^+/\text{Ala-C}]_{aq}$.

h) Selected trajectories of water molecules at the O2-H7 group and Li^+ obtained from MD-$[\text{Li}^+/\text{Ala-C}]_{aq}$, denoted by **W151** and **W15**, respectively.

MD-[Ala – A]$_{aq}$

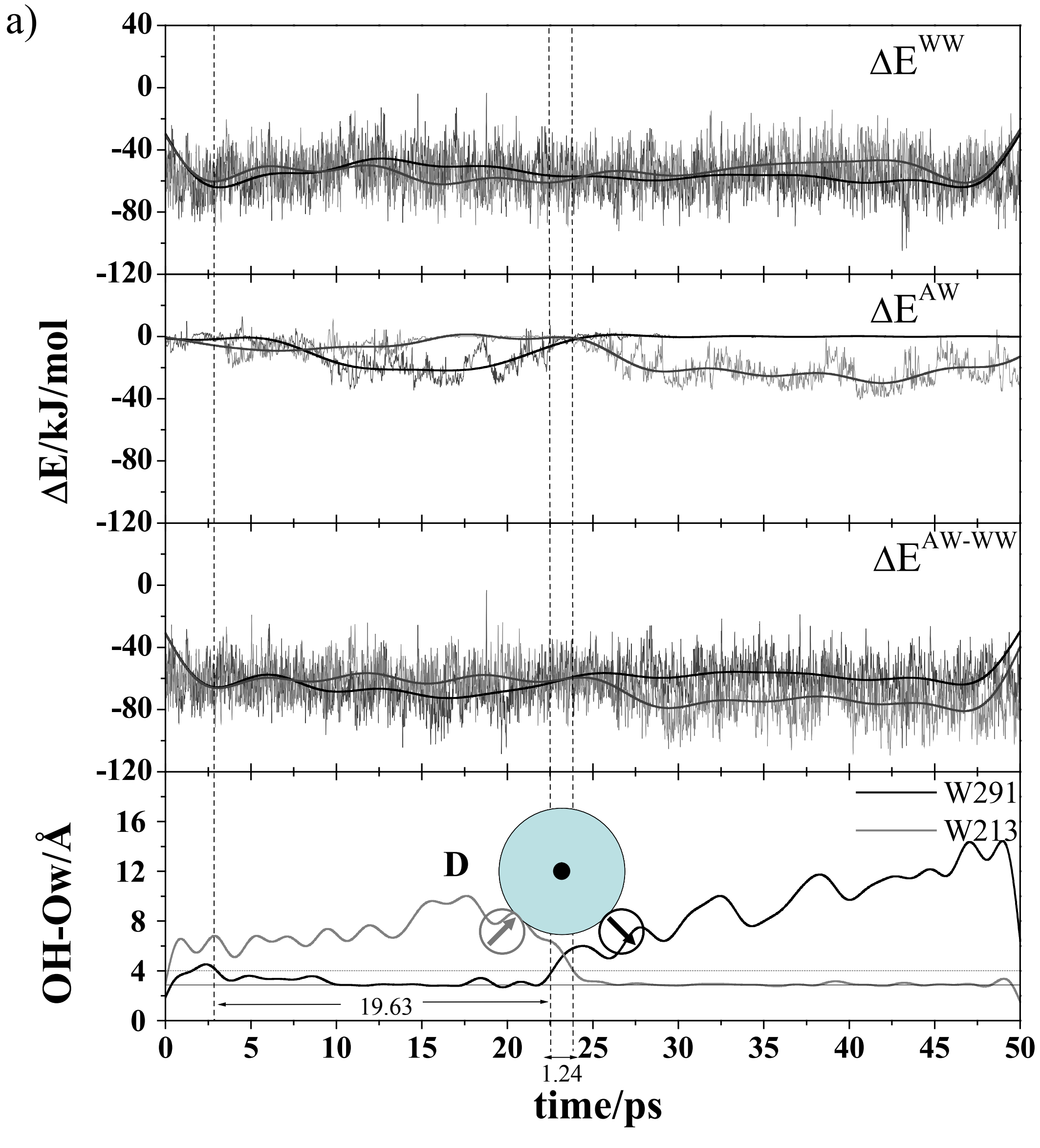

Figure 3.8

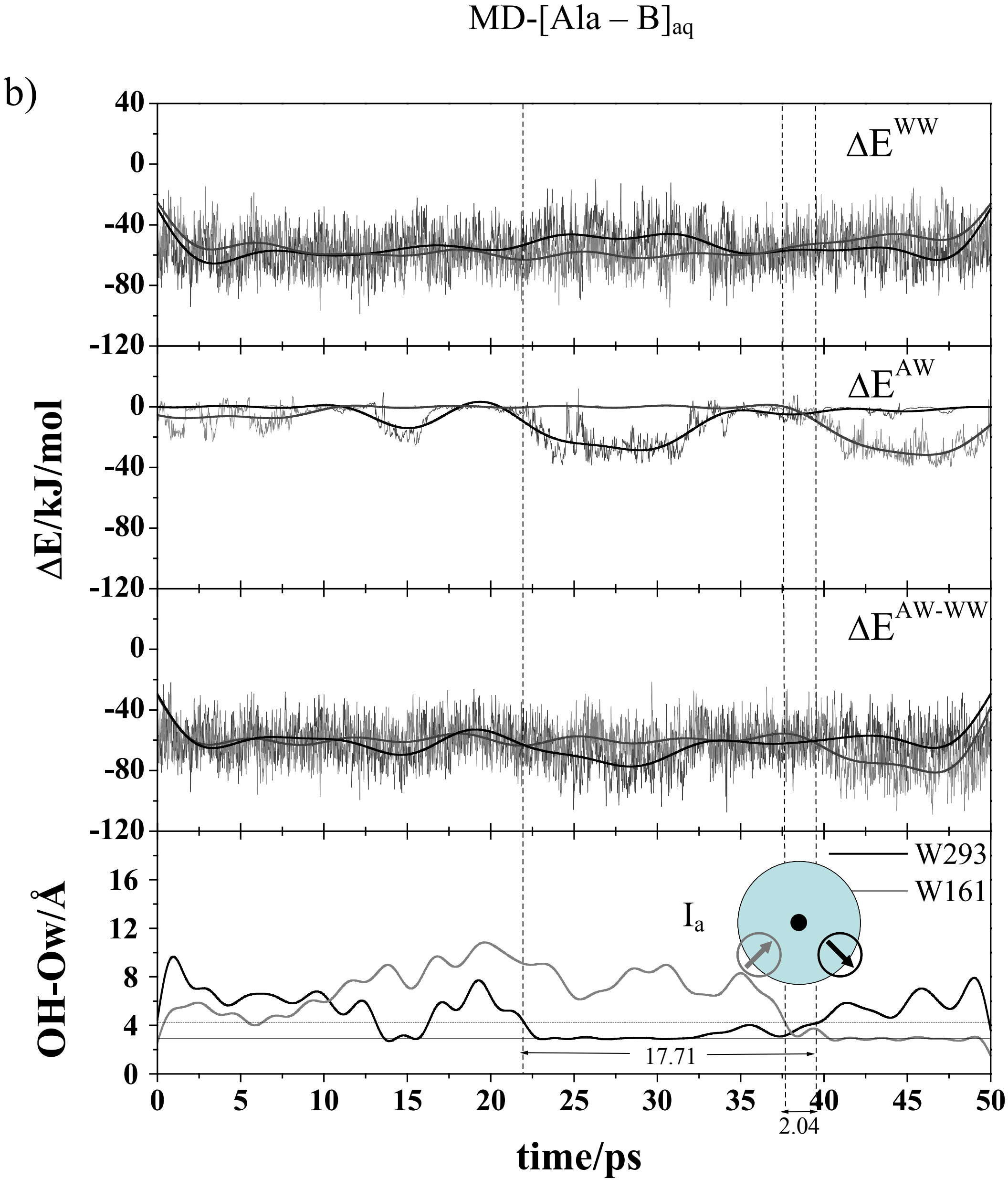

Figure 3.8 (continued)

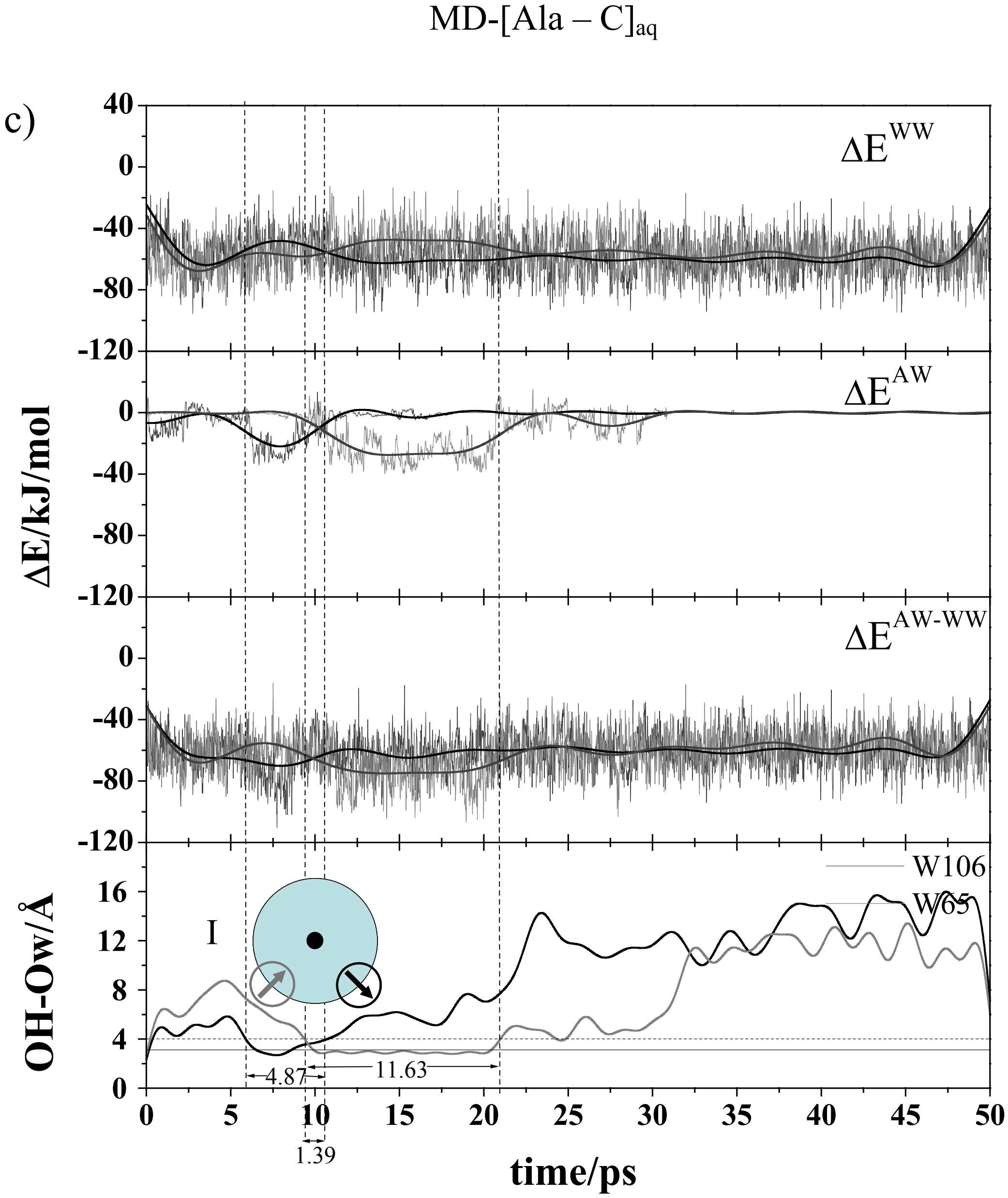

Figure 3.8 (continued)

MD-[Li^+/Ala – C]$_{aq}$

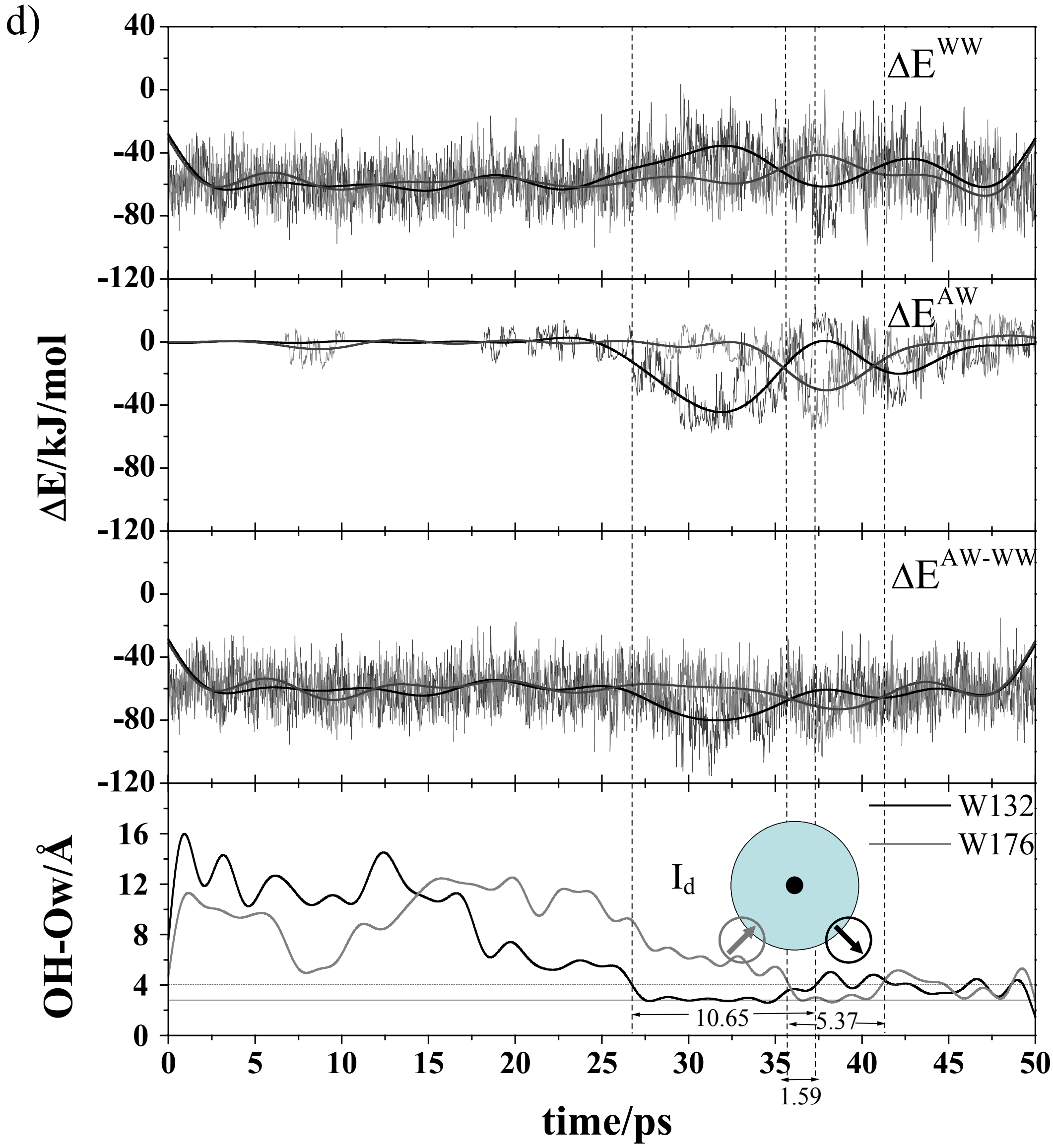

Figure 3.8 (continued)

MD-[Li$^+$/Ala – C]$_{aq}$

e)

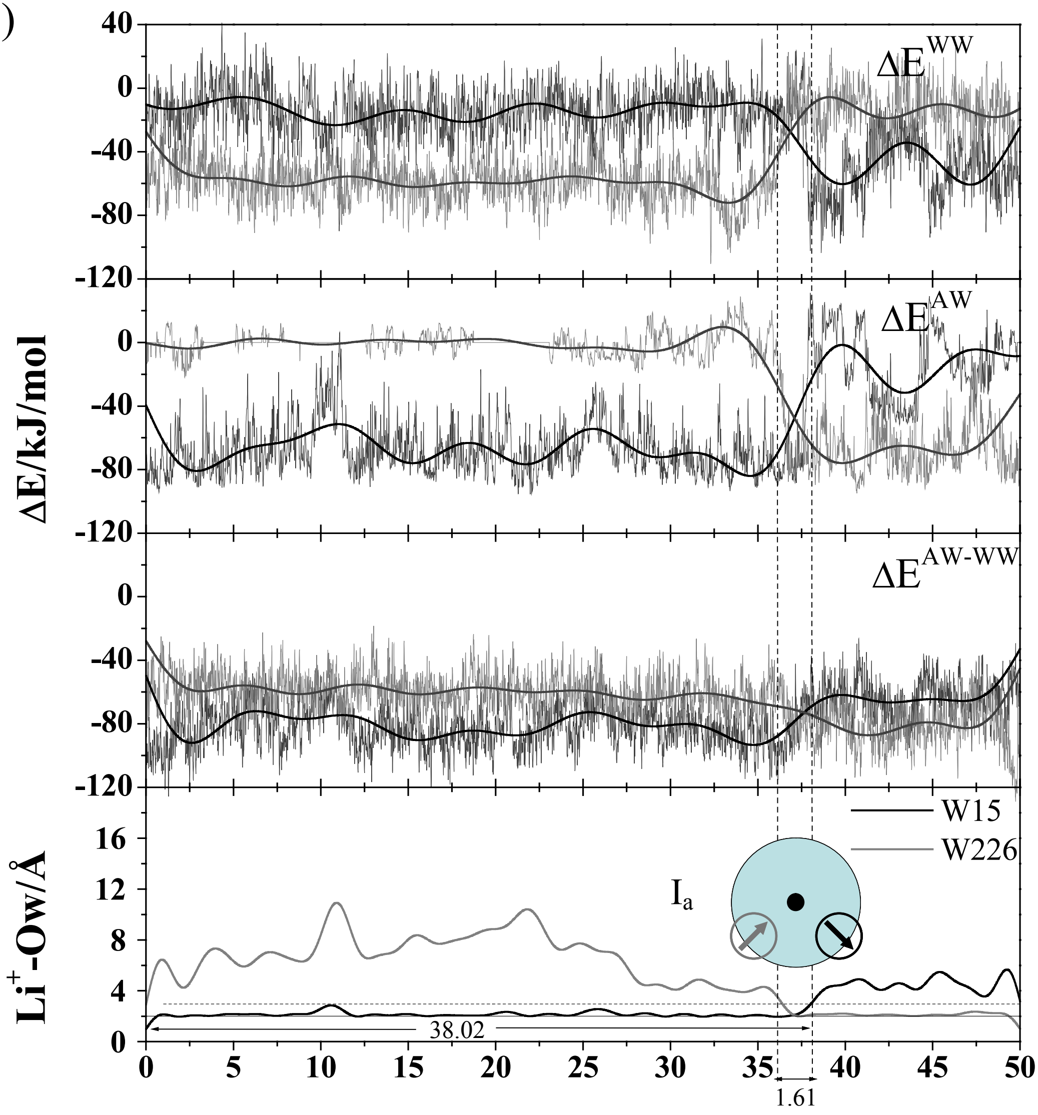

Figure 3.8 (continued)

MD-[Li^+/Ala – C]$_{aq}$

f)

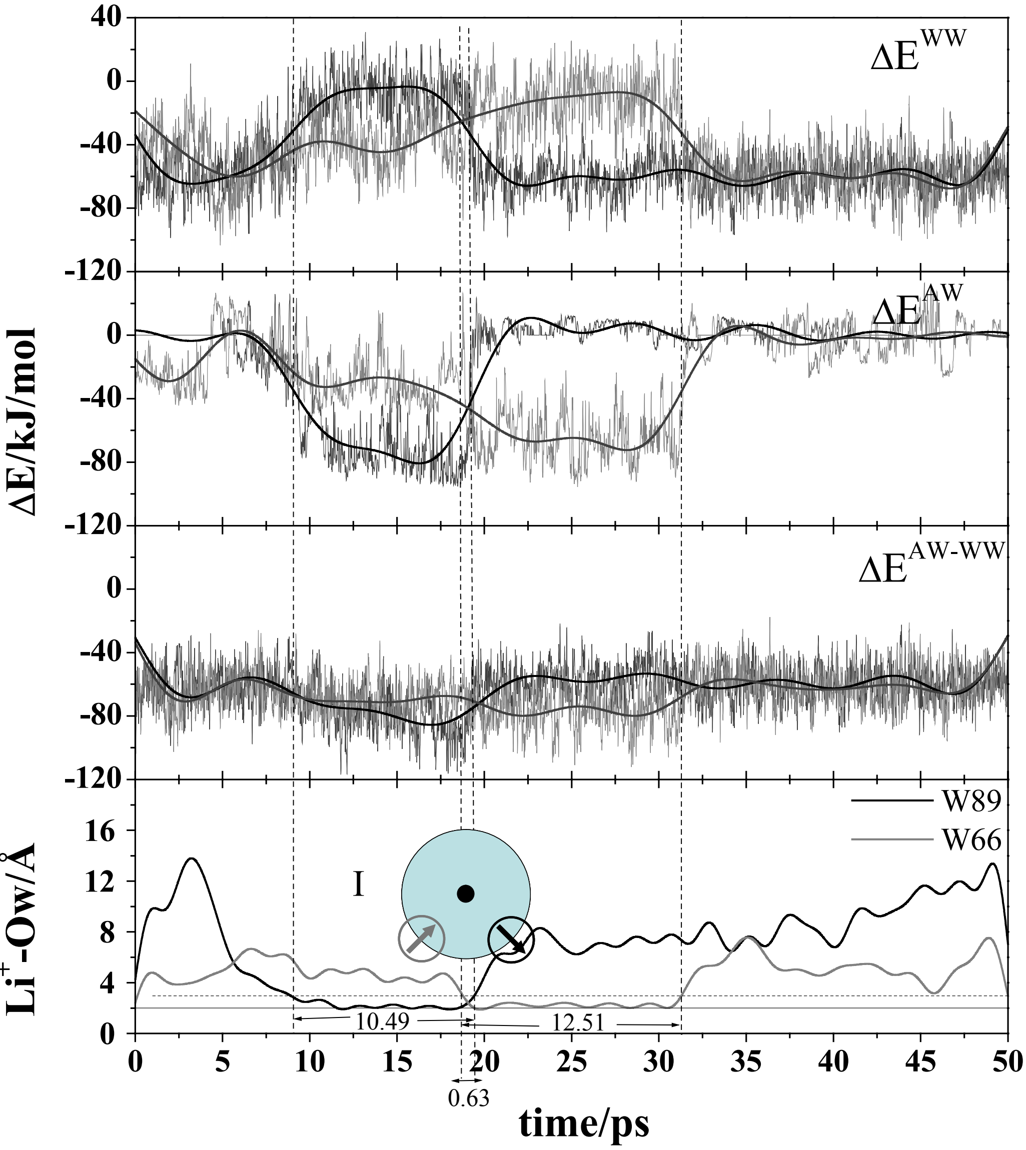

Figure 3.8 (continued)

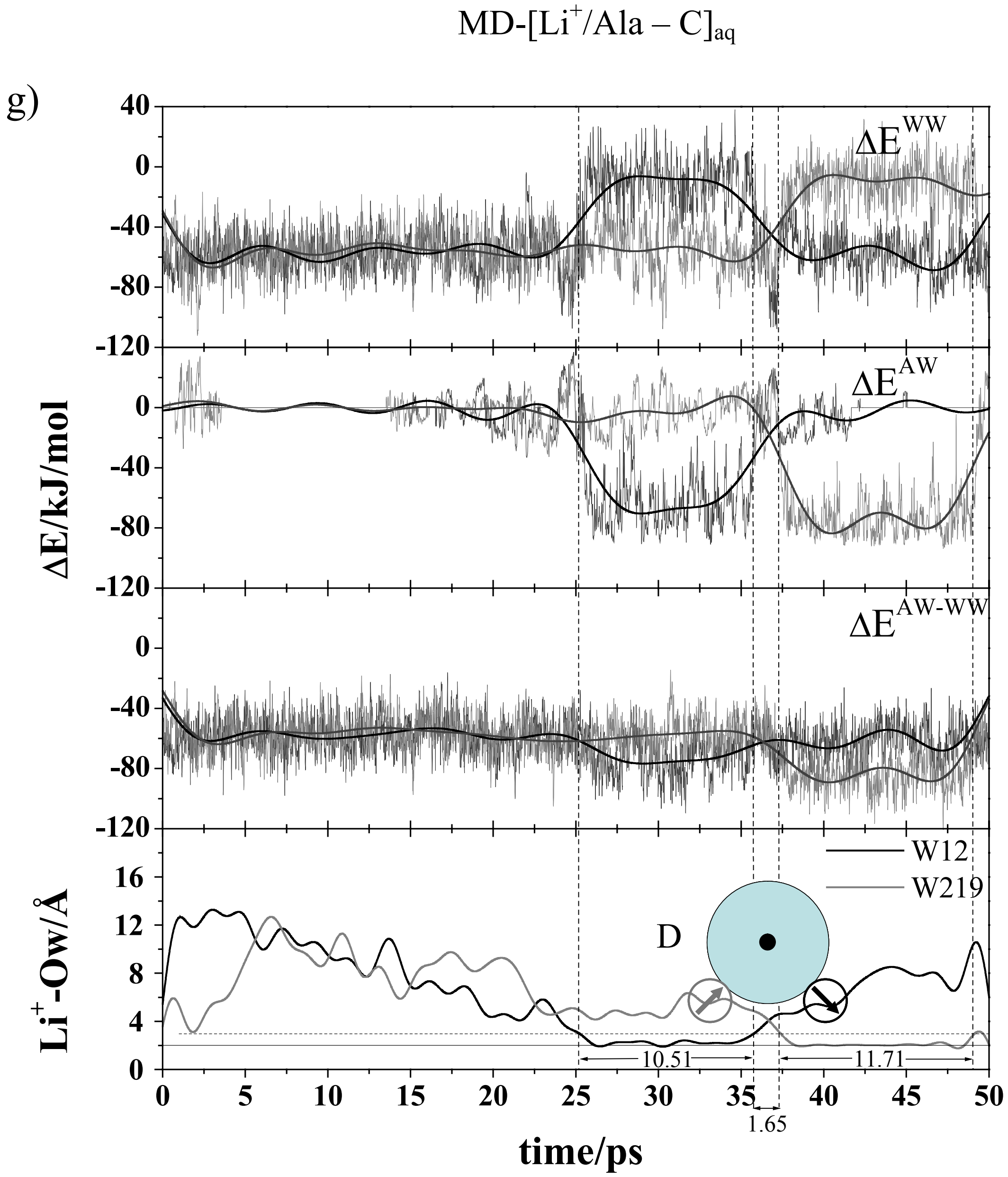

Figure 3.8 (continued)

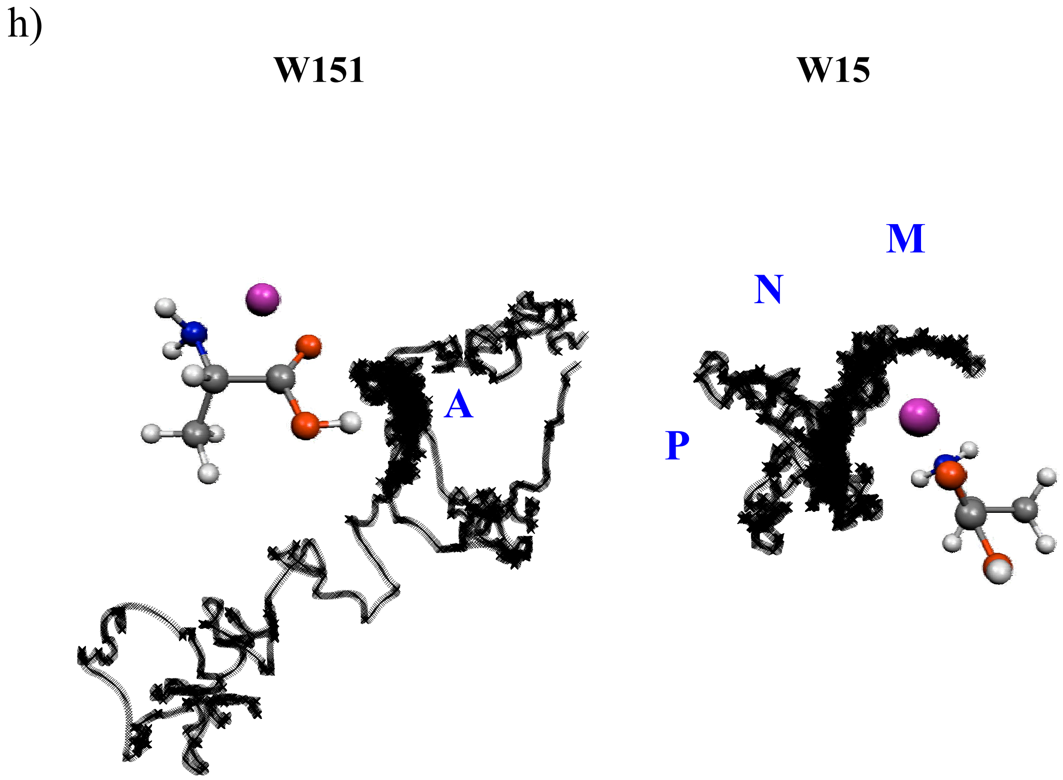

Figure 3.8 (continued)

Table 3.3 The results extracted from the water exchange diagrams, together with the derivation of $\tau_{A\text{-}H\cdots Ow}$, τ_{ex} and $\Delta Ea^{AW\text{-}WW}$. Simulation times in ps and energies in kJ/mol.

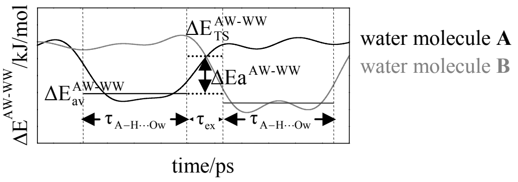

$$\Delta Ea^{AW\text{-}WW} = \Delta E_{av}^{AW\text{-}WW} - \Delta E_{TS}^{AW\text{-}WW}$$

a) O2-H7···Ow

mechanism*	water molecule A		water molecule B	$\Delta Ea^{AW\text{-}WW}$
	$\tau_{O2\text{-}H7\cdots Ow}$	$\tau_{ex,O2\text{-}H7\cdots Ow}$	$\tau_{O2\text{-}H7\cdots Ow}$	
MD-[Ala - A]$_{aq}$				
I_a	7.50	0.87	-	-
I	17.39	1.59	7.50	-
I_d	15.98	0.11	6.04	-
D	19.63	1.24	-	7.8
D	16.30	0.13	8.67	5.2
MD-[Ala - B]$_{aq}$				
I_a	17.71	2.04	-	6.4
I_a	8.29	0.89	4.73	-
I	16.67	0.79	8.30	-
I_d	3.50	1.23	21.17	-
I_d	15.17	0.45	9.11	-
D	3.78	1.20	5.31	-
D	3.37	0.72	8.29	-
MD-[Ala - C]$_{aq}$				
I_a	7.87	1.62	7.39	5.3
I_a	11.63	1.15	20.37	3.7
I_a	6.41	0.64	5.65	5.5
I	4.87	1.39	11.62	2.3
I_d	5.65	0.38	4.25	-
MD-[Li$^+$/Ala - C]$_{aq}$				
I_a	24.65	1.03	5.37	5.3
I_a	-	1.35	6.23	-
I	28.02	1.91	-	10.3
I	-	0.77	28.02	-
I_d	5.65	1.64	10.65	-
I_d	10.65	1.59	5.37	6.3
I_d	8.87	0.37	4.51	-
I_d	3.73	0.25	5.37	-
D	11.89	0.36	10.65	-
D	8.01	0.09	-	-

Table 3.3 (continued)

b) $Li^{+}\cdots Ow$

mechanism	water molecule A		water molecule B	$\Delta Ea^{AW\text{-}WW}$
	$\tau_{Li^{+}\cdots Ow}$	$\tau_{ex,Li^{+}\cdots Ow}$	$\tau_{Li^{+}\cdots Ow}$	
MD-$[Li^{+}/Ala - C]_{aq}$				
I_a	38.02	1.61	-	8.4
I_a	12.33	1.32	14.51	11.5
I	10.49	0.63	12.51	5.8
D	10.51	1.65	11.71	10.0

$\tau_{O2\text{-}H7\cdots Ow}$ = H-bond residence time at the O2-H7 group.

$\tau_{Li^{+}\cdots Ow}$ = water residence time at Li^{+} .

$\tau_{ex,O2\text{-}H7\cdots Ow}$ = lifetime of the water exchange intermediate complex at the O2-H7 group.

$\tau_{ex,Li^{+}\cdots Ow}$ = lifetime of the water exchange intermediate complex at Li^{+} .

$\Delta Ea^{AW\text{-}WW}$ = activation interaction energy for water exchange intermediate complex.

* The abbreviation for the water exchange mechanism taken from Langford and Gray (1996).

Due to the complexity of the solute structures, the water exchange mechanisms in $[\mathrm{Ala-A}]_{aq}$, $[\mathrm{Ala-B}]_{aq}$ and $[\mathrm{Ala-C}]_{aq}$ cannot be exactly the same as those in $[\mathrm{Li}^{+}]_{aq}$ (Hermansson and Wojcik, 1998; Spångberg *et al.*, 2003) and $[\mathrm{Na}^{+}]_{aq}$ (Hermansson and Wojcik, 1998). However, to simplify the discussion, the five-water exchange mechanisms proposed by Langford and Gray (1996) namely, the dissociative (**D**), associative (**A**) and interchange (**I**) mechanisms; the **I**-mechanism could be subdivided into two classes, depending on whether the interchange is associative-like or dissociative-like, regarded as $\mathbf{I_a}$ and $\mathbf{I_d}$ mechanisms, respectively, were primarily applied in this study.

Figures 3.8a to 3.8c show some predominant water exchange processes at the O2-H7 group of $[\mathrm{Ala-A}]_{aq}$, $[\mathrm{Ala-B}]_{aq}$ and $[\mathrm{Ala-C}]_{aq}$. It appeared from the analysis of the water exchange diagrams that, at the COOH groups, the **I**-mechanisms are more favored than the **D**-mechanism, with $\tau_{\mathrm{O2-H7\cdots Ow}}$ and $\tau_{\mathrm{ex,O2\text{-}H7\cdots Ow}}$ varying in quite wide ranges. The former is from 3.4 to 21.2 ps and the latter from 0.1 to 2.0 ps. Weak correlations were established between $\tau_{\mathrm{O2-H7\cdots Ow}}$ and $\Delta\mathrm{Ea}^{\mathrm{AW\text{-}WW}}$, as well as $\tau_{\mathrm{ex,O2\text{-}H7\cdots Ow}}$ and $\Delta\mathrm{Ea}^{\mathrm{AW\text{-}WW}}$. The trends of the correlation plots in Figures 3.9a and 3.9b support the anticipation made from the total-average potential energy landscapes and the cross section plots namely, the higher $\Delta\mathrm{Ea}^{\mathrm{AW\text{-}WW}}$ the longer $\tau_{\mathrm{O2-H7\cdots Ow}}$, and $\tau_{\mathrm{ex,O2\text{-}H7\cdots Ow}}$.

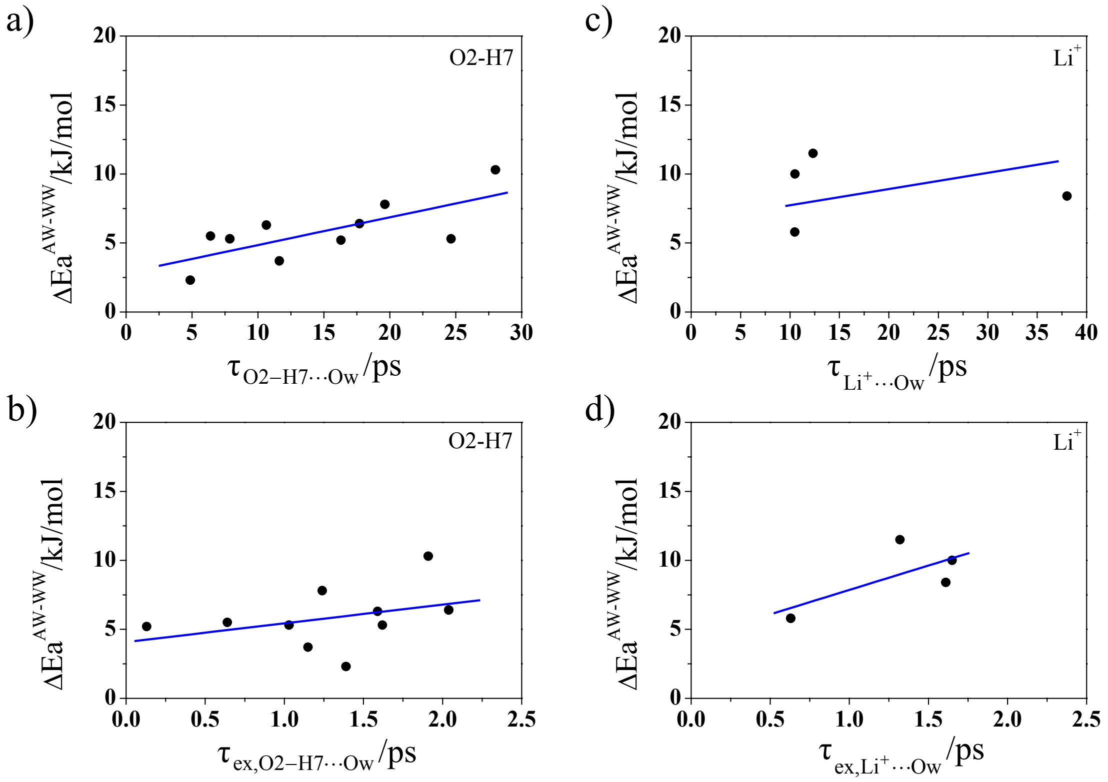

Figure 3.9 Selected correlation diagrams obtained from MD simulations of MD-$[Ala]_{aq}$ and MD-$[Li^{+}/Ala - C]_{aq}$ at 298 K

a) $\Delta E^{AW\text{-}WW}$ and $\tau_{O2-H7\cdots Ow}$

b) $\Delta E^{AW\text{-}WW}$ and $\tau_{ex,O2\text{-}H7\cdots Ow}$

c) $\Delta E^{AW\text{-}WW}$ and $\tau_{Li^{+}\cdots Ow}$

d) $\Delta E^{AW\text{-}WW}$ and $\tau_{ex,Li^{+}\cdots Ow}$

3.2.2 $[Li^{+}/Ala]_{aq}$

Since one of main objectives is to investigate the effects of Li^{+} on the H-bond networks of water in the first hydration shell of Ala, the discussion in the present section will be made based on the results of MD-$[Ala\text{-}C]_{aq}$ and MD-$[Li^{+}/Ala\text{-}C]_{aq}$. g(R) obtained from MD-$[Li^{+}/Ala\text{-}C]_{aq}$ show that the bidentate coordination of Li^{+} at the O1 and N atoms of Ala-C leads to a significant increase in the degree of hydration, especially at the COOH and NH_2 groups. In $[Li^{+}/Ala\text{-}C]_{aq}$, all g(R) related to the O2-H7···Ow and N-H···Ow H-bonds are in general more structured compared to those in $[Ala\text{-}C]_{aq}$. The positions of the main peaks of $g(R_{O2\cdots Ow})$, $g(R_{H7\cdots Ow})$ and $g(R_{N\cdots Ow})$ are also shifted to shorter distances; whereas those of $g(R_{H2\cdots Ow})$ and $g(R_{H3\cdots Ow})$ become more equivalent, compare Figures 3.5e and 3.5g, and Figures 3.5f and 3.5h, respectively. The integrations of $g(R_{O2\cdots Ow})$ and $g(R_{N\cdots Ow})$ to the first maxima showed that, upon the Li^{+} binding, the number of water molecule in close contact with the COOH and NH_2 groups are increased from 1.84 to 2.08, and from 1.7 to 2.0, respectively.

The structure of $g(R_{Li^{+}\cdots Ow})$ in Figure 3.5i indicates that, the first and second hydration shells of Li^{+}/Ala-C are not so well separated as in $[Li^{+}]_{aq}$ (Hermansson and Wojcik, 1998; Spångberg *et al*., 2003). This suggests that Li^{+} becomes softer due to the bidentate coordination with Ala, and water molecules in the first hydration shell of Li^{+} could be more dynamics. $g(R_{Li^{+}\cdots Ow})$ shows the first maximum and minimum at 2.01 and 2.96 Å, respectively. They are slightly longer than those in $[Li^{+}]_{aq}$ (Spångberg *et al*., 2003), 1.96, and 2.70 Å, respectively.

The integrations of $g(R_{Li^+\cdots Ow})$ to the first maximum and minimum yielded one (1.02) water molecule in close contact with Li^+, and about three (3.17) water molecules in the first hydration shell of Li^+/Ala-C. The number of water molecule in the first hydration shell is quite reasonable, compared with four (4.02) in the case of $[Li^+]_{aq}$ (Spångberg *et al*., 2003). The slightly larger first hydration shell with smaller number of water molecule in $[Li^+/Ala-C]_{aq}$ compared to $[Li^+]_{aq}$ could be attributed to the steric effects caused by the bidentate coordination at Li^+.

The hydration structures and the total-average potential energy landscapes at the H-bond networks of Ala-C are obviously affected by the Li^+ binding. Comparisons of the PDO maps in Figures 3.6l and 3.6p, and the total-average potential energy landscapes in Figures 3.7i to 3.7l, show that Li^+ can transfer its electrostatic effects to the O2-H7 group, leading to a more associated H-bond network at **A**, as well as higher average potential energy barriers for the diffusion of water molecule in the transverse direction ($<\Delta E^T_{aq}>$) in $[Li^+/Ala-C]_{aq}$ compared to $[Ala-C]_{aq}$. These lead to longer $\tau_{O2-H7\cdots Ow,max}$ in $[Li^+/Ala-C]_{aq}$, compared to $[Ala-C]_{aq}$, 28.0 and 20.4 ps, respectively. The values of $\tau_{O2-H7\cdots Ow,max}$ correspond to the water exchange rate constants (k_{ex}) of 35.7 and 49.1 ns^{-1}, respectively. The binding of Li^+ at the O1 and N groups of Ala-C also strengthens and lengthens the H-bond networks at the NH_2 group; the H-bond networks at **D**, **G** and **I** become more well defined and interconnected, as seen in Figures 3.6l and 3.6q. This further suggests that the hydration at the CH groups is increased upon the Li^+ binding, with the longest H-bond lifetime $\tau_{N-H3\cdots Ow,max}$ increasing from about 17 ps in $[Ala-C]_{aq}$ to about 18 ps in $[Li^+/Ala-C]_{aq}$.

The three water molecules in the first hydration shell of $\mathrm{Li^{+}/Ala\text{-}C}$ were found to distribute in four H-bond networks labeled with **M** to **P** on the PDO maps in Figures 3.6p to 3.6t, with quite high contour densities at **P** and **M**. The structures of the total-average potential energy landscapes and the cross section plots in Figures 3.7m to 3.7r show that water molecules in the first hydration shell of Li^{+} could be moving in narrow channels interconnecting the four H-bond networks, with $<\Delta E^{L}_{aq}>$ of about 10 kJ/mol. The structures of the cross section plots deduced from the transverse profile lines suggested longer water residence time at Li^{+} compared to those at the COOH and NH_2 groups, with $<\Delta E^{T}_{aq}>$ at **P** and **M** of 108 - 110 kJ/mol**,** respectively. $\tau_{Li^{+}\cdots Ow,max}$ derived from MD-$[\mathrm{Li^{+}/Ala\text{-}C}]_{aq}$ is about 38 ps, corresponding to the water exchange rate constant ($\tau_{ex,Li^{+}\cdots Ow}$) of 26.3 ns^{-1}, see Table 3.2. The value of $\tau_{Li^{+}\cdots Ow,max}$ is in reasonable agreement with those estimated by Lyubartsev *et al.* (2001) for $[Li^{+}]_{aq}$, to be between 20 and 50 ps.

Due to the limited number of complete water exchange events taking place in the first hydration shell of Li^{+}, the water exchange diagrams obtained from MD-$[\mathrm{Li^{+}/Ala\text{-}C}]_{aq}$ could not be examined as extensive as in $[\mathrm{Ala\text{-}A}]_{aq}$, $[\mathrm{Ala\text{-}B}]_{aq}$ and $[\mathrm{Ala\text{-}C}]_{aq}$. Some representative results are given in Figure 3.9 and their analyses in Table 3.3b. It appeared that, in $[\mathrm{Li^{+}/Ala\text{-}C}]_{aq}$, the **I**-mechanisms were observed more often than the **D**-mechanism, with $\tau_{Li^{+}\cdots Ow}$ and $\tau_{ex,Li^{+}\cdots Ow}$ varying from 10.5 to 38.0 ps and from 0.6 to 1.6 ps, respectively. This agrees well with the MD results by Hermansson *et al.* (1998), in which the $\mathbf{I_d}$- and **D**-mechanisms were reported to dominate in $[Li^{+}]_{aq}$.

Further investigations on MD trajectories, shown as examples in Figure 3.8h, revealed that, water molecule (**W151**) enters the first hydration shell of the O2-H7 group and moves randomly inside the average potential energy channel for a while, before leaving the channel at some point, and in general, water molecule could enter and leave the first hydration shell at various points in the channel. This implies that the frequency of the water exchange events taking place in the first hydration shell depends to some extent on this dynamic step. Therefore, this dynamic step should be included in the water exchange pathways of amino acid. The suggestion seems to comply with the observations made by Spångberg *et al.* (2003) that, a complete understanding of the water exchange mechanisms requires both hydration structures and dynamics, which are closely related to the interactions and momentum transfer between water molecules in the first and second hydration shells. The influence of water molecules in the second hydration shell has been illustrated in $[NH_4^+]_{aq}$ (Intharathep, Tongraar and Sagarik, 2005) and $[H_3O^+]_{aq}$ (Intharathep, Tongraar and Sagarik, accepted). Especially in the case of $[H_3O^+]_{aq}$, water molecules in the second hydration shell were shown to help promote the proton transfer from H_3O^+ to H_2O, through the formation of the Zundel complex ($H_5O_2^+$).

The MD trajectory in Figure 3.8h also shows that water molecule (**W15**) moves randomly inside the average potential energy channel interconnecting the H-bond networks at **M**, **N**, **O** and **P**, as in the case of the O2-H7 group, with the time interval between successive water exchange events of about 10 to 14 ps, see Figures 3.8e to 3.8g and Table 3.3b. Since the values of $\tau_{ex,Li^+\cdots Ow}$, shown in Table 3.3b, are considerably smaller than $\tau_{Li^+\cdots Ow}$ and vary only in a narrow range, between 0.6 and 1.6 ps, the diffusion of water molecule in the average potential energy channel could be considered as a rate-determining step and should be included in the water exchange process. The correlation diagrams in Figures 3.9c and 3.9d reveal the trends of $\tau_{\mathrm{Li^{+}\cdots Ow}}$ and $\Delta\mathrm{Ea}^{\mathrm{AW\text{-}WW}}$, and $\tau_{\mathrm{ex,Li^{+}\cdots Ow}}$ and $\Delta\mathrm{Ea}^{\mathrm{AW\text{-}WW}}$ similar to $[\mathrm{Ala}]_{\mathrm{aq}}$.

It should be noted that the water exchange mechanisms proposed by Langford and Gray (1996), as well as the others (Puchta *et al*., 2004), emphasize the stereochemistry (cis or tran) of each exchange event, by trying to correlate the five-water exchange mechanisms with the degree of contraction or expansion of the first hydration shell during the water exchange process. The present MD simulations focus attention also on the dynamics of water molecule in the first hydration shell of solute and suggests to include this dynamic aspect as an elementary step in the water exchange process. The MD analyses employed in the present work could, therefore, be applied in the study of the diffusion of water molecule at protein surfaces, known in general as the lateral and transversal diffusions (Knapp and Muegge, 1993).

CHAPTER IV

CONCLUSION

The effects of metal ion and solute conformation change on the structures, energetic and dynamics of water molecule in the first hydration shell of amino acid were examined, using alanine (Ala) and Li^+/Ala as model molecules. The present theoretical studies began with the constructions of the test-particle model (T-model) potentials for four forms of Ala, regarded as Ala-A, Ala-B, Ala-C and Li^+/Ala-C; Ala-B and Ala-C were generated from Ala-A by rotations of the N-C^α bond 30 and 180 degree, respectively. The T-model potentials were applied in the calculations of the optimal geometries of the Ala-H_2O 1 : n complexes in the gas phase, with $n = 1$ to 4. Some of the T-model results were examined using *ab initio* calculations at MP2 level of theory. The T-model potentials and MP2 calculations yielded comparable results. They suggested that, for all the Ala-H_2O complexes considered, water molecules prefer to form cyclic H-bonds at the COOH group, with similar H-bond structures and interaction energies. In the gas phase, the variation of the angle ϕ from 0 to 30 to 180 degree does not bring about significant change on the hydration at the COOH group; whereas some effects were observed at the NH_2 groups, especially when the angle $\phi = 180$ degree. A three-center or bifurcated H-bond, in which only one Ow-Hw group of water approaches simultaneously at the N and O1 atoms, was detected in the Ala-C-H_2O 1 : 1 complexes.

For Li^+/Ala-C, water molecule prefers to bind primarily at Li^+, and subsequently at the COOH and NH_2 groups. It appears that, in the gas phase, not more than two water molecules bind directly at Li^+, compared to four in the case of Li^+/H_2O. The number of water molecules is in good agreement with *ab initio* calculations on the Li^+/Val 1 : 2 and 1 : 3 complexes. The bidentate coordination of Li^+ at the N and O1 atoms of Ala-C brings about significant changes at both COOH and NH_2 groups, for which the structure of the O2-H7···Ow H-bond is most affected, with an increase in the H-bond interaction energy. The linear O-H···Ow H-bond becomes favorable upon the Li^+ binding. Based on the results discussed above, one can conclude that the T-model potentials predicted reasonable gas-phase equilibrium structures and interaction energies for all the Ala-H_2O and Li^+/Ala-C-H_2O 1 : *n* complexes and can be applied in MD simulations with confidence.

MD simulations were performed on $[\text{Ala-A}]_{aq}$, $[\text{Ala-B}]_{aq}$, $[\text{Ala-C}]_{aq}$ and $[Li^+/\text{Ala}]_{aq}$ at 298 K, using the T-model potentials. The MD results showed that the rotation of the $N-C^{\alpha}$ bond from the angle $\phi = 0$ to 30 to 180 degree brings about different effects to the H-bond networks, compared to the gas phase. MD-$[\text{Ala-A}]_{aq}$ and MD-$[\text{Ala-B}]_{aq}$ revealed that the variation of the angle ϕ from 0 to 30 degree strengthens the H-bond networks at the O2-H7 and C1-H1 groups and weakens the ones at the lone-pair electrons of O1 and the NH_2 groups. The stabilities of the H-bond networks at the COOH and NH_2 groups are further increased and decreased, respectively, when the angle ϕ is changed from 30 to 180 degree, with additional H-bond networks created upon the rotation. The dynamics of water molecules in the first hydration shells of solutes were illustrated again to be attributable from the structures of the total-average potential energy landscapes. Although not so straightforward, it was shown that, the values of the longest H-bond lifetimes could reflect the structures of the total-average potential energy landscapes and vice versa. The MD analyses employed in the present work could be applied in the investigation of the diffusion of water molecules at the protein surfaces, known in general as the lateral and transversal diffusions.

The structural and energetic results obtained from MD simulations showed that the bidentate coordination of Li^+ at N and O1 brings about considerable stabilization effects to all H-bond networks in $[Li^+/Ala]_{aq}$. It appeared that the H-bond networks at the O2-H7 and the NH_2 groups become more associated, with increases in the average potential energy barriers to the diffusion of water molecule between the H-bond network and the outside. Three water molecules are in the first hydration shell of Li^+. They seem to distribute in four associated H-bond networks, which are interconnected and form an average potential energy channel for the diffusion of water molecules. The analyses of the water exchange diagrams and MD trajectories in $[Li^+/Ala]_{aq}$ suggested to include an elementary dynamic step to the water exchange process, in which water molecule moves in a channel in the first hydration shell before leaving at some points in the channel.

It should be noted that the MD results reported in the present work were based on pair-wise additive intermolecular potentials, in which the many-body contributions were not taken into account. Although the electrostatic effects introduced by Li^+ are relatively strong, the treatment of Li^+/Ala as a supermolecule could partly compromise these effects, as shown in the case of $[Gdm^+ - FmO^-]_{aq}$. The inclusion of the cooperative effects in the model calculations is expected to result in slightly more associated H-bond networks, as well as longer water residence times, and should not bring about significant change in the reported results. The theoretical results presented here also iterate the necessity to include explicit solvent molecules in the model calculations. Since the microscopic nature of water molecules in aqueous solutions cannot be directly accessible from experiments, it is hoped that the present work could provide additional important information on the structures, energetic and dynamics of water molecules in the hydration shells of amino acids.

REFERENCES

REFERENCES

Ahlrichs, R., Böhm, H. J., Ehrhardt, C., Scharf, P., Schiffer, H., Lischka, H., and Schindler, M. (1985). Implementation of an electronic structure program system on the CYBER 205. **Journal of Computational Chemistry** 6: 200-208.

Ahn, D. S., Park, S. W., Jeon, I. S., Lee, M. K., Kim, N. H., Han, Y. H., and Lee, S. (2003). Effects of microsolvation on the structures and reactions of neutral and zwitterion alanine: Computational study. **The Journal of Physical Chemistry B** 107: 14109-14118.

Allen, M. P., and Tildesley, D. J. (1989). **Computer Simulation of Liquids.** New York: Oxford University Press.

Almlöf, J., Kuick, A., and Thomas, O. J. (1973). Hydrogen bond studies. 77. Electron density distribution in α-glycine: *X-N* difference Fourier synthesis vs *ab initio* calculations. **The Journal of Chemical Physics** 59: 3901-3906.

Baker, E. N., and Hubbard, R. E. (1984). Hydrogen bonding in globular proteins. **Progress in Biophysics and Molecular Biology** 44: 97-179.

Barone, V., Adamo, C., and Lelj, F. (1995). Conformational behavior of gaseous glycine by a density functional approach. **The Journal of Chemical Physics** 102: 364-370.

Basch, H., and Stevens, W. J. (1990). The structure of glycine-water H-bonded complexes. **Chemical Physics Letters** 169: 275-280.

Bee, M. (1988). **Applications of Quasielestic Neutron Scattering to Solid-State Chemistry, Biology and Material Science.** London: Adam Hilger.

Böhm, H. J., and Ahlrichs, R. (1982). A study of short-range repulsions. **The Journal of Chemical Physics** 77: 2028-2034.

Böhm, H. J., and Ahlrichs, R. (1985). Molecular dynamics simulation of liquid CH_2Cl_2 and $CHCl_3$ with new pair potentials. **Molecular Physics** 54: 1261-1274.

Böhm, H. J., Meissner, C., and Ahlrichs, R. (1984). Molecular dynamics simulation of liquid CH_3F, CHF_3, CH_3Cl, CH_2Cl_2, CH_3CN, CO_2 and CS_2 with new pair potentials. **Molecular Physics** 53: 651-672.

Böhm, H. J., Ahlrichs, R., Scharf, P., and Schiffer, H. (1984). Intermolecular potentials for CH_4, CH_3F, CHF_3, CH_3Cl, CH_2Cl_2, CH_3CN and CO_2. **The Journal of Chemical Physics** 81: 1389-1395.

Bonaccorsi, R., Palla, P., and Tomasi, J. (1984). Conformational energy of glycine in aqueous solutions and relative stability of the zwitterionic and neutral forms. An *ab initio* study. **Journal of the American Chemical Society** 106: 1945-1950.

Breneman, C. M., and Wiberg, K. B. (1990). Determining atom-centered monopoles from molecular electrostatic potentials. The need for high sampling density in formamide conformational analysis. **Journal of Computational Chemistry** 11: 361-373.

Brunne, R. M., Liepinsh, E., Otting, G., Wüthrich, K., and Van Gunsteren, W. F. (1993). Hydration of proteins: A comparison of experimental residence times of water molecules solvating the Bovine Pancreatic Trypsin inhibitor with theoretical model calculations. **Journal of Molecular Biology** 231: 1040-1048.

Busch, K. L., Glish, G. L., and McLuckey, S. A. (1988). **Mass Spectrometry/Mass Spectrometry.** New York: VCH Publishers.

Case, D. A., Pearlman, D. A., Caldwell, J. W., Cheatham III, T. E., Ross, W. S., Simmerling, C. L., Darden, T. A., Merz, K. M., Stanton, R. V., Cheng, A. L., Vincent, J. J., Crowley, M., Tsui, V., Radmer, R. J., Duan, Y., Pitera, J., Massova, I., Seibel, G. L., Singh, U. C., Weiner, P. K., and Kollman, P. A. (1999). **AMBER** (version 6) [computer software]. San Francisco: University of California.

Cerda, B. A., and Wesdemiotis, C. (1996). Li^+, Na^+, and K^+ binding to the DNA and RNA nucleobases. Bond energies and attachment sites from the dissociation of metal ion-bound heterodimers. **Journal of the American Chemical Society** 118: 11884-11892.

Cerda, B. A., Hoyan, S., Ohanessian, G., and Wesdemiotis, C. (1998). Na^+ binding to cyclic and linear dipeptides. Bond energies, entropies of Na^+ complexation, and attachment sites from the dissociation of Na^+-bound heterodimers and *ab initio* calculations. **Journal of the American Chemical Society** 120: 2437-2448.

Chalikian, T. V., Sarvazyan, A. P., and Breslauer, K. J. (1993). Partial molar volumes, expansibilities, and compressibilities of α,ω-aminocarboxylic acids in aqueous solutions between 18 and 55°C. **The Journal of Physical Chemistry** 97: 13017-13026.

Chalikian, T. V., Sarvazyan, A. P., and Breslauer, K. J. (1994). Hydration and partial compressibility of biological compounds. **Biophysical Chemistry** 51: 89-109.

Chalikian, T. V., Sarvazyan, A. P., Funck, T., Cain, C. A., and Breslauer, K. J. (1994). Partial molar characteristics of glycine and alanine in aqueous solutions at high pressures calculated from ultrasonic velocity data. **The Journal of Physical Chemistry** 98: 321-328.

Clementi, E. (1980). **Computational aspects for large chemical systems, Lecture Notes in Chemistry 19.** Berlin: Springer-Verlag.

Clementi, E., Cavallone, F., and Scordamaglia, R. (1977). Analytical potentials from "*ab initio*" computations for the interaction between biomolecules. 1. water with amino acids. **Journal of the American Chemical Society** 99: 5531-5545.

Cowan, J. A. (1993). **Inorganic Biochemistry.** New York: VCH Publishers.

Csaszar, A. G. (1992). Conformers of gaseous glycine. **Journal of the American Chemical Society** 114: 9568-9575.

Csazar, A. G. (1995). On the structures of free glycine and ∝-alanine. **Journal of Molecular Structure** 346: 141-152.

Csaszar, A. G. (1996). Conformers of gaseous ∝–alanine. **The Journal of Physical Chemistry** 100: 3541-3551.

Dill, K. A. (1990). Dominant forces in protein folding. **Biochemistry** 29: 7133-7155.

Ding, Y., and Krogh-Jespersen, K. (1992). The glycine zwitterion does not exist in the gas phase: results from a detailed ab initio electronic structure study. **Chemical Physics Letters** 199: 261-266.

Donohue, J. (1968). In A. Rich and N. Davidson (eds.). **Structure Chemistry and Molecular Biology** (p. 443). San Francisco: W.H. Freeman.

Dougherty, D. A., and Stauffer, D. A. (1990). Acetylcholine binding by a synthetic receptor: implications for biological recognition. **Science** 250: 1558-1560.

Du, X., and Liang, Y. (2000). Roles of metal complex and hydrogen bond in molecular structures and phase behaviors of metal *N*-octadecanoyl-L-alaninate langmuir-blodgett films. **The Journal of Physical Chemistry B** 104: 10047-10052.

Dyson, H. J., and Wright, P. E. (2004). Unfolded proteins and protein folding studied by NMR. **Chemical Reviews** 104: 3607-3622.

Erras-Hanauer, H., Clark, T., and Van Eldik, R. (2003). Molecular orbital and DFT studies on water exchange mechanisms of metal ions. **Coordination Chemistry Reviews** 238-239: 233-253.

Finney, J. L., and Soper, A. K. (1994). Solvent structure and perturbations in solutions of chemical and biological importance. **Chemical Society Reviews** 23: 1-10.

Frauenfelder, H., Parak, F., and Young, R. D. (1988). Conformational substates in proteins. **Annual Review of Biophysics and Biophysical Chemistry** 17: 451-479.

Frisch, M. J., Trucks, G. W., Schlegel, H. B., Scuseria, G. E., Robb, M. A., Cheeseman, J. R., Zakrzewski, V. G., Montgomery, J. A., Stratmann, R. E., Burant, J. C., Dapprich, S., Millam, J. M., Daniels, A. D., Kudin, K. N., Strain, M. C., Farkas, O., Tomasi, J., Barone, V., Cossi, M., Cammi, R., Mennucci, B., Pomelli, C., Adamo, C., Clifford, S., Ochterski, J., Petersson, G. A., Ayala, P. Y., Cui, Q., Morokuma, K., Malick, D. K., Rabuck, A. D., Raghavachari, K., Foresman, J. B., Cioslowski, J., Ortiz, J. V., Stefanov, B. B., Lui, G., Liashenko, A., Piskorz, P., Komaromi, I., Gomperts, R., Martin, R. L., Fox, D. J., Keith, T., Al-Laham, M. A., Peng, C. Y., Nanayakkara, A., Gonzalez, C., Challacombe, M., Gill, P. M. W., Johnson, B. G., Chen, W., Wong, M. W., Andres, J. L., Head-Gordon, M., Replogle, E. S., and Pople, J. A. (1998). **Gaussian 98** package (revision A.7) [Computer software]. Pittsburgh, PA, USA: Gaussian.

Glinski, J., Chavepeyer, G., and Platten, J. –K. (2000). Surface properties of aqueous solutions of L-leucine. **Biophysical Chemistry** 84: 99-103.

Gregory, R. B. (ed.). (1994). **Protein-Solvent Interactions.** New York: Marcel Dekker.

Gronert, S., and O'Hair, R. A. (1995). *Ab initio* studies of amino acid conformations. 1. The conformers of alanine, serine, and cysteine. **Journal of the American Chemical Society** 117: 2071-2081.

Häckel, M., Hinz, H. -J., and Hedwig, G. R. (1999). Partial molar volumes of proteins: amino acid side-chain contributions derived from the partial molar volumes of some tripeptides over the temperature range 10 – 90°C. **Biophysical Chemistry** 82: 35-50.

Helm, L., and Merbach, A. E. (1999). Water exchange on metal ions: experiments and simulations. **Coordination Chemistry Reviews** 187: 151-181.

Hermansson, K., and Wojcik, M. (1998). Water exchange around Li^+ and Na^+ in LiCl (aq) and NaCl(aq) from MD simulations. **The Journal of Physical Chemistry B** 102: 6089-6097.

Hoinkis, J., Ahlrichs, R., and Böhm, H. J. (1983). A simple treatment of intermolecular interactions: Synthesis of ab initio calculations and combination rules. **International Journal of Quantum Chemistry** 23: 821-834.

Hu, C. H., Shen, M., and Schaefer III, H. F. (1993). Glycine conformational analysis. **Journal of the American Chemical Society** 115: 2923-2929.

Hughes, M. N. (1981). **The Inorganic Chemistry of Biological Process** (2nd ed.). Chichester: John Wiley & Sons.

Iijima, K., Tanaka, K., and Onuma, S. (1991). Main conformer of gaseous glycine: molecular structure and rotational barrier from electron diffraction data and rotational constants. **Journal of Molecular Structure** 246: 257-266.

Intharathep, P., Tongraar, A., and Sagarik, K. (2005). Structure and dynamics of hydrated NH_4^+: An *ab initio* QM/MM molecular dynamics simulation. **Journal of Computational Chemistry** 26: 1329-1338.

Intharathep, P., Tongraar, A., and Sagarik, K. (2006). *Ab initio* QM/MM dynamics of H_3O^+ in water. **Journal of Computational Chemistry**, accepted.

Jeffrey, G. A., and Saenger, W. (1991). **Hydrogen bonding in biological structures.** Berlin: Springer-Verlag.

Jensen, F. (1992). Structure and stability of complexes of glycine and glycine methyl analogs with H^+, Li^+, and Na^+. **Journal of the American Chemical Society** 114: 9533-9537.

Jensen, J. H., and Gordon, M. S. (1991). Conformational potential energy surface of glycine: a theoretical study. **Journal of the American Chemical Society** 113: 7917-7924.

Jockusch, R. A., Lemoff, A. S., and Williams, E. R. (2001a). Effect of metal ion and water coordination on the structure of a gas-phase amino acid. **Journal of the American Chemical Society** 123: 12255-12265.

Jockusch, R. A., Lemoff, A. S., and Williams, E. R. (2001b). Hydration of valine-cation complexes in the gas phase: On the number of water molecules necessary to form a zwitterion. **The Journal of Physical Chemistry A** 105: 10929-10942.

Jockusch, R. A., Price, W. D., and Williams, E. R. (1999). Structure of cationized arginine ($Arg{\cdot}M^+$, M = H, Li, Na, K, Rb, and Cs) in the gas phase: Further evidence for zwitterionic arginine. **The Journal of Physical Chemistry A** 103: 9266-9274.

Junk, G., and Sevec, H. (1963). The mass spectra of the ∝-amino acids. **Journal of the American Chemical Society** 85: 839-845.

Kaim, W., and Schwederski, B. (1994). **Bioinorganic Chemistry: Inorganic Elements in the Chemistry of Life.** Chichester: John Wiley & Sons.

Karplus, P. A., and Faerman, C. (1994). Ordered water in macromolecular structure. **Current Opinion in Structural Biology** 4: 770-776.

Kassab, E., Langlet, J., Evleth, E., and Akacem, Y. (2000). Theoretical study of solvent effect on intramolecular proton transfer of glycine. **Journal of Molecular Structure (THEOCHEM)** 531: 267-282.

Knapp, E. W., and Muegge, I. (1993). Heterogeneous diffusion of water at protein surfaces: application. to BPTI. **The Journal of Physical Chemistry** 97: 11339–11343.

Kumpf, R. A., and Dougherty, D. A. (1993). A mechanism for ion selectivity in potassium channels: computational studies of cation-π interactions. **Science** 261: 1708-1710.

Kwon, O. Y., Kim, S. Y., and No, K. T. (1995). Determination of the proton transfer energies of glycine and alanine and the influence of water molecules. **Bulletin of the Korean Chemical Society** 16: 410-416.

Langford, C. H., and Gray, H. B. (1996). **Ligand Substitution Processes.** New York: W.A. Benjamin.

Leary, J. A., Zhou, Z., Ogden, S. A., and Williams, T. D. (1990). Investigations of gas-phase lithium-peptide adducts: tandem mass spectrometry and semiempirical studies. **Journal of the American Society of Mass Spectrometry** 1: 473-480.

Levitt, M., and Park, B. H. (1993). Water: now you see it, now you don't. **Structure** 1: 223-226.

Levitt, M., and Sharon, R. (1988). Accurate simulation of protein dynamics in solution. **Proceedings of the National Academy of Sciences of the United States of America** 85: 7557-7561.

Levy, H. A., and Corey, R. B. (1941). The crystal structure of DL-alanine. **Journal of the American Chemical Society** 63: 2095-2108.

Lippard, S. A., and Berg, J. M. (1994). **Principles of Bioinorganic Chemistry, University Science Books**. CA: Mill Valley.

Lyubartsev, A. P., Laasonen, K., and Laaksonen, A. (2001). Hydration of Li^+ ion. An *ab-initio* molecular dynamics simulation. **The Journal of Chemical Physics** 114: 3120-3126.

Marino, T., Russo, N., and Toscano**,** M. (2000). Gas-phase metal ion (Li^+, Na^+, Cu^+) affinities of glycine and alanine. **Journal of Inorganic Biochemistry** 79: 179-185.

Marino, T., Russo, N., and Toscano**,** M. (2001). Potential energy surfaces for the gas-phase interaction between $\propto$-alanine and alkali metal ions (Li^+, Na^+, K^+). A density functional study. **Inorganic Chemistry** 40: 6439-6443.

Middlehurst, J. (1993). In R. Harrison (ed.). **Practical Filter Design.** Brunswick: Prentice Hall.

Miller, C. (1993). Potassium selectivity in proteins: oxygen cage or in the Face. **Science** 261: 1692-1693.

Moision, R. M., and Armentrout, P. B. (2002). Experimental and theoretical dissection of sodium cation/glycine interactions. **The Journal of Physical Chemistry A** 106: 10350-10362.

Muegge, I., and Knapp, E. W. (1995). Residence times and lateral diffusion of water at protein surfaces: Application to BPTI. **The Journal of Physical Chemistry** 99: 1371-1374.

Odelius, M., and Laaksonen, A. (1999). Combined MD simulation-NMR relaxation studies of molecular motion and intermolecular interactions. In P. B. Baluena and J. M. Seminario (eds.). **Molecular Dynamics from Classical to Quantum Methods**. (Theoretical and computational chemistry, Vol. 7, pp. 281-324). Amsterdam: Elsevier.

Orozco, M., and Luque, F. J., (2000). Theoretical methods for the representation of solvent in biomolecular systems. **Chemical Reviews** 100: 4187-4225.

Otting, G., and Wuethrich, K. (1989). Studies of protein hydration in aqueous solution by direct NMR observation of individual protein-bound water molecules. **Journal of the American Chemical Society** 111: 1871-1875.

Otting, G., Liepinsh, E., and Wuethrich, K. (1991). Protein hydration in aqueous solution. **Science** 254: 974-980.

Otting, G., Liepinsh, E., and Wuethrich, K. (1992). Polypeptide hydration in mixed solvents at low temperatures. **Journal of the American Chemical Society** 114: 7093-7095.

Otting, G., Liepinsh, E., Farmer II, B. T., and Wuethrich, K. (1991). Protein hydration studied with homonuclear 3D (1)H NMR experiments. **Journal of Biomolecular NMR** 1: 209-215.

Pacios, L. F., and Gómez, P. C. (2001). Atomic charges in conformers of gaseous glycine. **Journal of Molecular Structure (THEOCHEM)** 544: 237-251.

Palma, M. U., Palma-Vittorelli, M. B., and Parak, F. (eds.). (1993). **Water-Biomolecule Interactions; Conference Proceedings** (Vol. 43). Bologna: SIF.

Puchta, R., Galle, M., van Eikema Hommes, N., Pasgreta, E., and van Eldik, R. (2004). Evidence for associative ligand exchange processes on solvated lithium cations. **Inorganic Chemistry** 43: 8227-8229.

Ramek, M., and Cheng, V. K. W. (1992). On the role of polarization functions in SCF calculations of glycine and related systems with intramolecular hydrogen bonding, **International Journal of Quantum Chemistry. Quantum Biology Symposium** 44: 15-26.

Ramek, M., Cheng, V. K. W., Frey, R. F., Newton, S. Q., and Schäfer, L. (1991). The case of glycine continued: some contradictory SCF result. **Journal of Molecular Structure (THEOCHEM)** 235: 1-10.

Refson, K. (1996). **Moldy** (revision 2.20 for release 2.14) [Computer software]. Oxford UK: Department of Earth Sciences, Oxford University.

Remko, M., and Rode, B. M. (2000). Bivalent cation binding effect on formation of the peptide bond. **Chemical Physics Letters** 316: 489-494.

Reva, I. D., Plokhotnichenko, A. M., Stepanian, S. G., Ivanov, A. Yu., Radchenko, E. D., Sheina, G. G., and Blagoi, Y.P. (1995). The rotamerization of conformers of glycine isolated in inert gas matrices. An infrared spectroscopic study. **Chemical Physics Letters** 232: 141-148.

Robertson, E. G., and Simons, J. P. (2001). Getting into shape: Conformational and supramolecular landscapes in small biomolecules and their hydrated clusters. **Physical Chemistry Chemical Physics** 3: 1-18.

Rode, B. M., and Sagarik, K. P. (1982). The influence of small monovalent cations on neighbouring N···H-O hydrogen bonds. **Chemical Physics Letters** 88: 337-341.

Rozanska, X., and Chipot, C. (2000). Modeling ion-ion interaction in proteins: A molecular dynamics free energy calculation of the guanidinium-acetate association. **The Journal of Chemical Physics** 112: 9691-9694.

Saenger, W. (1987). Structure and dynamics of water surrounding biomolecules. **Annual Review of Biophysics and Biophysical Chemistry** 16: 93-114.

Sagarik, K. (1999). Theoretical studies on hydrogen bonding in hydroxylamine clusters and liquid. **Journal of Molecular Structure (THEOCHEM)** 465: 141-155.

Sagarik, K., and Chaiyapongs, S. (2005). Structures and stability of salt-bridge in aqueous solution. **Biophysical Chemistry** 117: 18-39.

Sagarik, K., and Dokmaisrijan, S. (2005). A theoretical study on hydration of alanine zwitterions. **Journal of Molecular Structure (THEOCHEM)** 718: 31-47.

Sagarik, K. P., and Rode, B. M. (1981). The influence of small monovalent cations on neighbouring hydrogen bonds of aquo-protein complexes. **Zeitschrift Fur Naturforschung Section B** 36a: 1357-1360.

Sagarik, K. P., and Rode, B. M. (1983a). Quantum chemical investigations on group IA and IIA metal ion-DNA base complexes. **Inorganica Chimica Acta** 76: L209-L212.

Sagarik, K. P., and Rode, B. M. (1983b). The influence of small monovalent cations on the hydrogen bonds of base pair of DNA. **Inorganica Chimica Acta** 78: 81-86.

Sagarik, K., and Rode, B. M. (2000). Intermolecular potential for benzoic acid-water based on the test-particle model and statistical mechanical simulations of benzoic acid in aqueous solutions. **Chemical Physics** 260: 159-182.

Sagarik, K. P., Pongpituk, V., Chaiyapongs, S., and Sisot, P. (1991). Test-particle model potentials for hydrogen-bonded complexes: complexes formed from HCN, HF, H_2O, NH_3, $HCONH_2$, $HCONHCH_3$, guanine and cytosine. **Chemical Physics** 156: 439-456.

Saigal, S., and Pranata, J. (1997). Monte Carlo simulations of guanidinium acetate and methylammonium acetate ion pairs in water. **Bioorganic Chemistry** 25: 11-21.

Schäfer, L., Sellers, H. L., Lovas, F. J., and Suenram, R. D. (1980). Theory versus experiment: the case of glycine. **Journal of the American Chemical Society** 102: 6566-6568.

Schlegel, H. B. (1982). Optimization of equilibrium geometries and transition structures. **Journal of Computational Chemistry** 3: 214-218.

Sellers, H. L., and Schäfer, L. (1978). Investigations concerning the apparent contradiction between the microwave structure and the ab initio calculations of glycine. **Journal of the American Chemical Society** 100: 7728-7729.

Shishkin, O. V., Sukhanov, O. S., Gorb, L., and Leszczynski, J. (2002). The interaction of the most stable guanine tautomers with water. The structure and properties of monohydrates. **Physical Chemistry Chemical Physics** 4: 5359-5364.

Siam, K., Klimkowski, V. J., Ewbank, J. D., Van Alsenoy, C., and Schäfer, L. (1984). Ab initio studies of structural features not easily amenable to experiment : Part 39. Conformational analysis of glycine and alanine. **Journal of Molecular Structure (THEOCHEM)** 110: 171-182.

Sicinska, D., Paneth, P., Truhlar, D. G. (2002). How well does microsolvation represent macrosolvation? A test case: Dynamics of decarboxylation of 4-pyridylacetic acid zwitterion. **The Journal of Physical Chemistry B** 106: 2708-2713.

Siu, F. M., Ma, N. L., and Tsang, C. W. (2001). Cation-π interactions in sodiated phenylalanine complexes: Is phenylalanine in the charge-solvated or zwitterionic form?. **Journal of the American Chemical Society** 123: 3397-3398.

Soper, A. K. (2000). Probing the structure of water around biological molecules: concepts, constructs and consequences. **Physica B** 276-278: 12-16.

Soper, A. K., and Luzar, A. (1996). Orientation of water molecules around small polar and non-polar groups in solution: a neutron diffraction and computer simulation study. **The Journal of Physical Chemistry** 100: 1357-1367.

Spångberg, D., Rey, R., Hynes, J. T., and Hermansson, K. (2003). Rate and mechanisms for water exchange around Li^+(aq) from MD simulations. **The Journal of Physical Chemistry B** 107: 4470-4477.

Stepanian, S. G., Reva, I. D., Radchenko, E. D., and Adamowicz, L. (1998). Conformational behavior of ∝-alanine. Matrix-isolation infrared and theoretical DFT and ab initio study. **The Journal of Physical Chemistry A** 102: 4623-4629.

Strittmatter, E. F., Lemoff, A. S., and Williams, E. R. (2000). Structure of cationized glycine, gly·M^{2+} (M = Be, Mg, Ca, Sr, Ba), in the gas phase: Intrinsic effect of cation size on zwitterion stability. **The Journal of Physical Chemistry A** 104: 9793-9796.

Suenram, R. D., and Lovas, F. J. (1980). Millimeter wave spectrum of glycine. A new conformer. **Journal of the American Chemical Society** 102: 7180-7184.

SURFER for windows (version 6.04) [Computer software]. (1997). USA: Golden Software.

Takagi, S., Chihara, H., and Seki, S. (1959). Vapor pressure of molecular crystals. XIII. Vapor pressure of a-glycine crystal. The energy of proton transfer. **Bulletin of the Chemical Society of Japan** 32: 84.

Tortonda, F. R., Pascual-Ahuir, J. L., Silla, E., and Tuñón, I. (1996). Why is glycine a zwitterion in aqueous solution? Atheoretical study of solvent stabilising factors. **Chemical Physics Letters** 260: 21-26.

Tortonda, F. R., Pascual-Ahuir, J. L., Silla, E., and Tuñón, I. (2003). A theoretical study of solvent effects on the conformational equilibria of neutral glycine in aqueous solution. **Journal of Molecular Structure (THEOCHEM)** 623: 203-210.

Tuñón, I., Silla, E., and Ruiz-López, M. F. (2000). On the tautomerization process of glycine in aqueous solution. **Chemical Physics Letters** 321: 433-437.

Tuñón, I., Silla, E., Millot, C., Martins-Costa, M. T. C., and Ruiz-López, M. F. (1998). **The Journal of Physical Chemistry A** 102: 8673.

Van Gunsteren, W. F., Berendsen, H. J. C., Hermans, J., Hol, W. G. J. , and Postma, J. P. M. (1983). Computer simulation of the dynamics of hydrated protein crystals and its comparison with X-ray data. **Proceedings of the National Academy of Sciences of the United States of America** 80: 4315-4319.

Wüthrich, K. (1995) Hydration of biological macromolecules in solution: Surface structure and molecular recognition. In K. Wüthrich (ed.). **NMR in Structural Biology**. (World Scientific Series in 20 th Century Chemistry, Vol. 5, pp. 647-655). Singapore: World Scientific.

Wyttenbach, T., Witt, M., and Bowers, M. T. (1999). On the question of salt bridges of cationized amino acids in the gas phase: glycine and arginine. **International Journal of Mass Spectrometry** 182-183: 243-252.

Zhong, W. G., Gallivan, J. P., Zhang, Y. N., Li, L. T., Lester, H. A, and Dougherty, D. A. (1998). From *ab initio* quantum mechanics to molecular neurobiology: A cation- π binding site in the nicotinic receptor. **Proceedings of the National Academy of Sciences of the United States of America** 95: 12088-12093.

Zwier, T. S. (2001). Laser spectroscopy of jet-cooled biomolecules and their water-containing clusters: Water bridges and molecular conformation. **The Journal of Physical Chemistry A** 105: 8827-8839.

APPENDICES

APPENDIX A

SUPPLEMENTARY DATA IN THE CONSTRUCTION OF T-MODEL POTENTIALS

Table A.1 Optimized geometries of Ala-A and Li^+/Ala-C.

a) Ala-A

Bond lenght (Å)		Bond angle (°)		Torsion angle (°)	
N-C1	1.455	N-C1-C2	113.2	N-C1-C2-O1	345.2
N-H2	1.017	N-C1-C3	109.8	N-C1-C2-O2	166.6
N-H3	1.016	C1-C2-O1	125.2	N-C1-C3-H4	63.9
C1-C2	1.523	C1-C2-O2	111.6	N-C1-C3-H5	184.0
C1-C3	1.531	C3-C1-C2	108.9	N-C1-C3-H6	305.2
C1-H1	1.096	O1-C2-O2	123.1	C1-C2-O2-H7	177.9
C2-O1	1.210	H1-C1-N	108.8	C2-C1-N-H2	55.2
C2-O2	1.354	H1-C1-C2	107.3	C2-C1-N-H3	301.7
C3-H4	1.095	H1-C1-C3	108.7	C3-C1-N-H2	293.2
C3-H5	1.092	H2-N-H3	104.9	C3-C1-N-H3	179.7
C3-H6	1.091	H2-N-C1	107.9	C3-C1-C2-O1	107.7
O2-H7	0.967	H3-N-C1	109.2	C3-C1-C2-O2	289.0
		H4-C3-C1	109.8	O1-C2-O2-H7	359.3
		H4-C3-H5	108.6	H2-N-C1-C2*	55.2
		H4-C3-H6	108.5	H3-N-C1-C2*	301.7
		H5-C3-C1	111.1		
		H5-C3-H6	109.8		
		H6-C3-C1	108.9		
		H7-O2-C2	105.3		

* For Ala-B: H2-N-C1-C2 = 25.2° and H3-N-C1-C2 = 271.7°.

Table A.1 (continued)

b) Li^+/Ala-C

Bond lenght (Å)		Bond angle (°)		Torsion angle (°)	
N-C1	1.455	N-C1-C2	113.3	N-C1-C2-O1	355.1
N-H2	1.017	N-C1-C3	109.8	N-C1-C2-O2	176.6
N-H3	1.015	C1-C2-O1	125.3	N-C1-C3-H4	63.9
C1-C2	1.523	C1-C2-O2	111.6	N-C1-C3-H5	184.1
C1-C3	1.531	C3-C1-C2	108.9	N-C1-C3-H6	305.2
C1-H1	1.096	O1-C2-O2	123.1	C1-C2-O2-H7	177.9
C2-O1	1.209	H1-C1-N	108.8	C2-C1-N-H2	240.2
C2-O2	1.355	H1-C1-C2	107.3	C2-C1-N-H3	126.7
C3-H4	1.095	H1-C1-C3	108.7	C3-C1-N-H2	118.2
C3-H5	1.092	H2-N-H3	104.9	C3-C1-N-H3	4.8
C3-H6	1.091	H2-N-C1	108.0	C3-C1-C2-O1	117.6
O2-H7	0.968	H3-N-C1	109.2	C3-C1-C2-O2	299.1
N-Li^+	2.084	H4-C3-C1	109.9	O1-C2-O2-H7	359.4
O1-Li^+	1.922	H4-C3-H5	108.6	H2-N-C1-C2	240.2
		H4-C3-H6	108.5	H3-N-C1-C2	126.7
		H5-C3-C1	111.2	Li^+-N-C1-C2	3.0
		H5-C3-H6	109.8	Li^+-N-C1-C3	241.0
		H6-C3-C1	108.9	Li^+-O1-C2-C1	3.6
		H7-O2-C2	105.3	Li^+-O1-C2-O2	181.9
		N-Li^+-O1	89.3		

Table A.2 The T-model parameters obtained in the present work. Values are in atomic units.

Atom	Ala		Ala-A1)	Ala-C	Li$^+$/Ala-C		
	σ_i	ρ_i	q_i	q_i	σ_i	ρ_i	q_i
N	0.872299	0.362166	-0.993974	-1.042373	0.821177	0.387189	-1.254643
C1	1.496078	0.141245	0.501155	0.658525	0.827197	0.254253	0.510936
C2	0.294074	0.441821	0.602757	0.644678	0.243146	0.455488	0.613046
C3	1.062553	0.332897	-0.208891	-0.356863	1.014861	0.345991	-0.293042
O1	1.065449	0.266077	-0.550352	-0.533676	1.097223	0.257941	-0.578908
O2	1.058922	0.262881	-0.668386	-0.688801	1.041841	0.263546	-0.591467
H1	0.236792	0.237799	-0.005677	-0.085362	0.117132	0.263520	0.009138
H2	0.080085	0.217743	0.356028	0.354061	0.103890	0.194786	0.455304
H3	0.154128	0.196440	0.344797	0.361700	0.001927	0.225998	0.449684
H4	0.096367	0.269607	0.061143	0.099206	0.172461	0.246050	0.088411
H5	0.197438	0.235875	0.041397	0.087435	0.182215	0.227755	0.114356
H6	0.176430	0.238824	0.061901	0.052534	0.175520	0.236752	0.101378
H7	0.021343	0.206374	0.458104	0.448934	0.024090	0.197010	0.493005
Li$^+$	-	-	-	-	0.580043	0.162498	0.882803

1) q_i for Ala-A and Ala-B are the same.

Table A.2 (continued)

Atom	H_2O2)		
	σ_i	ρ_i	q_i
O	1.284091	0.200370	-0.451660
H	-0.318644	0.331849	0.514110
D3)	-	-	-0.576560

2) Values taken from Sagarik *et al.* (1991).
3) Dummy charge.

APPENDIX B

SUPPLEMENTARY RESULTS FOR THE T-MODEL POTENTIALS

Table B.1 Interaction energies of Ala-A-H_2O 1 : 1 complexes derived from the T-model potentials and *ab initio* calculations. Energy in kJ/mol.

Method	Structure			Mean	SD
	a	**b**	**c**		
T-model	-41.36	-29.33	-29.12		
SCF-A	-40.69	-24.58	-25.88		
SCFCP-A	-29.84	-14.52	-15.28		
BSSESCF-A	10.85	10.06	10.61	10.51	0.40
MP2-A	-53.27	-33.88	-36.76		
MP2CP-A	-32.09	-15.88	-17.53		
BSSEMP2-A	21.18	18.00	19.23	19.47	1.61
SCF-B	-31.50	-16.84	-17.70		
SCFCP-B	-28.05	-14.23	-15.07		
BSSESCF-B	3.45	2.61	2.63	2.90	0.48
MP2-B	-40.76	-24.23	-27.00		
MP2CP-B	-30.41	-16.37	-18.34		
BSSEMP2-B	10.35	7.86	8.66	8.96	1.27
SCF-C	-39.13	-23.72	-25.16		
SCFCP-C	-28.17	-13.64	-14.29		
BSSESCF-C	10.96	10.09	10.88	10.64	0.48
MP2-C	-55.62	-36.97	-40.66		
MP2CP-C	-35.13	-19.10	-21.20		
BSSEMP2-C	20.48	17.87	19.46	19.27	1.32
SCF-D	-29.63	-15.46	-16.33		
SCFCP-D	-27.25	-13.47	-14.29		
BSSESCF-D	2.38	1.99	2.04	2.13	0.21
MP2-D	-41.38	-24.74	-27.85		
MP2CP-D	-34.34	-19.41	-21.85		
BSSEMP2-D	7.04	5.34	6.00	6.13	0.86

SCF-X = SCF calculations using X basis set
SCFCP-X = SCF-X with BSSE correction
BSSESCF-X = SCFCP-X - SCF-X
MP2-X = MP2 calculation using X basis set
MP2CP-X = MP2-X with BSSE correction
BSSEMP2-X = MP2CP-X - MP2-X
X = A = *ab initio* calculations with the MP2/6-311G(d,p)
B = *ab initio* calculations with the MP2/6-311++G(d,p)//MP2/6-311G(d,p)
C = *ab initio* calculations with the MP2/6-311G(2d,2p)//MP2/6-311G(d,p)
D = *ab initio* calculations with the MP2/6-311++G(2d,2p)//MP2/6-311G(d,p)

Table B.2 Interaction energies of Ala-B-H_2O 1 : 1 complexes derived from the T-model potentials and *ab initio* calculations. Energy in kJ/mol.

Method	Structure			Mean	SD
	a	**b**	**c**		
T-model	-41.44	-28.92	-24.97		
SCF-A	-40.84	-19.54	-22.44		
SCFCP-A	-30.06	-10.35	-12.27		
BSSESCF-A	10.78	9.19	10.17	10.04	0.80
MP2-A	-53.40	-29.44	-32.01		
MP2CP-A	-32.35	-12.66	-13.41		
BSSEMP2-A	21.05	16.78	18.59	18.81	2.14
SCF-B	-31.73	-12.84	-14.58		
SCFCP-B	-28.23	-10.32	-11.97		
BSSESCF-B	3.50	2.52	2.62	2.88	0.54
MP2-B	-40.95	-21.90	-21.21		
MP2CP-B	-30.58	-13.63	-13.92		
BSSEMP2-B	10.36	8.28	7.29	8.64	1.57
SCF-C	-39.14	-18.78	-20.84		
SCFCP-C	-28.26	-9.30	-11.17		
BSSESCF-C	10.88	9.48	9.67	10.01	0.76
MP2-C	-55.57	-32.00	-33.95		
MP2CP-C	-35.24	-15.46	-16.16		
BSSEMP2-C	20.34	16.54	17.79	18.22	1.93
SCF-D	-29.70	-11.39	-13.09		
SCFCP-D	-27.32	-9.43	-11.10		
BSSESCF-D	2.38	1.95	1.99	2.11	0.23
MP2-D	-41.38	-21.91	-22.00		
MP2CP-D	-34.39	-16.37	-16.58		
BSSEMP2-D	6.99	5.54	5.42	5.98	0.87

SCF-X = SCF calculations using X basis set
SCFCP-X = SCF-X with BSSE correction
BSSESCF-X = SCFCP-X - SCF-X
MP2-X = MP2 calculation using X basis set
MP2CP-X = MP2-X with BSSE correction
BSSEMP2-X = MP2CP-X - MP2-X
X = A = *ab initio* calculations with the MP2/6-311G(d,p)
B = *ab initio* calculations with the MP2/6-311++G(d,p)//MP2/6-311G(d,p)
C = *ab initio* calculations with the MP2/6-311G(2d,2p)//MP2/6-311G(d,p)
D = *ab initio* calculations with the MP2/6-311++G(2d,2p)//MP2/6-311G(d,p)

Table B.3 Interaction energies of Ala-C-H_2O 1 : 1 complexes derived from the T-model potentials and *ab initio* calculations. Energy in kJ/mol.

Method	Structure			Mean	SD
	a	**b**	**c**		
T-model	-41.14	-29.98	-28.87		
SCF-A	-42.58	-32.56	-29.92		
SCFCP-A	-31.41	-18.87	-17.41		
BSSESCF-A	11.17	13.69	12.51	12.46	1.26
MP2-A	-55.34	-47.28	-43.63		
MP2CP-A	-33.45	-23.21	-21.20		
BSSEMP2-A	21.89	24.07	22.43	22.80	1.14
SCF-B	-33.17	-23.03	-21.91		
SCFCP-B	-29.72	-19.35	-18.33		
BSSESCF-B	3.46	3.68	3.58	3.57	0.11
MP2-B	-42.45	-36.14	-33.76		
MP2CP-B	-31.91	-25.36	-23.76		
BSSEMP2-B	10.55	10.78	10.01	10.44	0.40
SCF-C	-41.21	-30.24	-27.32		
SCFCP-C	-29.97	-16.46	-15.23		
BSSESCF-C	11.24	13.78	12.09	12.37	1.29
MP2-C	-57.90	-49.24	-44.45		
MP2CP-C	-36.82	-25.47	-23.39		
BSSEMP2-C	21.08	23.78	21.06	21.97	1.56
SCF-D	-31.57	-19.69	-18.87		
SCFCP-D	-29.17	-17.21	-16.50		
BSSESCF-D	2.40	2.48	2.37	2.42	0.06
MP2-D	-43.39	-34.33	-32.35		
MP2CP-D	-36.18	-27.53	-26.01		
BSSEMP2-D	7.21	6.80	6.35	6.79	0.43

SCF-X = SCF calculations using X basis set
SCFCP-X = SCF-X with BSSE correction
BSSESCF-X = SCFCP-X - SCF-X
MP2-X = MP2 calculation using X basis set
MP2CP-X = MP2-X with BSSE correction
BSSEMP2-X = MP2CP-X - MP2-X
X = A = *ab initio* calculations with the MP2/6-311G(d,p)
B = *ab initio* calculations with the MP2/6-311++G(d,p)//MP2/6-311G(d,p)
C = *ab initio* calculations with the MP2/6-311G(2d,2p)//MP2/6-311G(d,p)
D = *ab initio* calculations with the MP2/6-311++G(2d,2p)//MP2/6-311G(d,p)

Table B.4 Interaction energies of Li$^+$/Ala-C-H_2O 1 : 1 complexes derived from the T-model potentials and *ab initio* calculations. Energy in kJ/mol.

Method	Structure				Mean	SD
	a	**b**	**c**	**d**		
T-model	-97.28	-59.10	-52.76	-50.77		
SCF-A	-122.15	-57.53	-51.23	-48.39		
SCFCP-A	-109.88	-49.34	-44.64	-41.11		
BSSESCF-A	12.27	8.19	6.59	7.28	8.58	2.54
MP2-A	-131.18	-70.88	-61.18	-58.57		
MP2CP-A	-107.02	-55.07	-49.13	-45.44		
BSSEMP2-A	24.17	15.82	12.05	13.13	16.29	5.48
SCF-B	-110.43	-49.58	-44.04	-40.95		
SCFCP-B	-105.42	-45.06	-40.86	-37.56		
BSSESCF-B	5.01	4.52	3.18	3.39	4.03	0.88
MP2-B	-113.97	-60.71	-52.75	-49.54		
MP2CP-B	-100.11	-49.28	-44.39	-41.04		
BSSEMP2-B	13.86	11.43	8.36	8.50	10.54	2.63
SCF-C	-117.21	-53.46	-47.27	-44.41		
SCFCP-C	-105.50	-45.62	-39.45	-36.23		
BSSESCF-C	11.71	7.84	7.82	8.18	8.89	1.89
MP2-C	-124.09	-68.50	-60.47	-57.75		
MP2CP-C	-102.42	-53.90	-46.51	-43.10		
BSSEMP2-C	21.68	14.60	13.96	14.65	16.22	3.65
SCF-D	-105.19	-45.25	-39.19	-36.24		
SCFCP-D	-102.89	-43.04	-37.68	-34.69		
BSSESCF-D	2.30	2.21	1.52	1.55	1.89	0.42
MP2-D	-104.95	-56.62	-48.62	-45.69		
MP2CP-D	-98.20	-50.21	-44.05	-40.99		
BSSEMP2-D	6.75	6.41	4.58	4.70	5.61	1.13

SCF-X = SCF calculations using X basis set
SCFCP-X = SCF-X with BSSE correction
BSSESCF-X = SCFCP-X - SCF-X
MP2-X = MP2 calculation using X basis set
MP2CP-X = MP2-X with BSSE correction
BSSEMP2-X = MP2CP-X - MP2-X
X = A = *ab initio* calculations with the MP2/6-311G(d,p)
B = *ab initio* calculations with the MP2/6-311++G(d,p)//MP2/6-311G(d,p)
C = *ab initio* calculations with the MP2/6-311G(2d,2p)//MP2/6-311G(d,p)
D = *ab initio* calculations with the MP2/6-311++G(2d,2p)//MP2/6-311G(d,p)

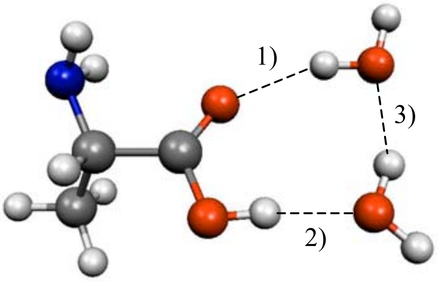

a)

$\Delta E_{\text{T-model}}$ = -70.9 kJ/mol

1) Ow···O = 3.05 Å
Ow-Hw···O = 154.6°

2) O···Ow = 2.84 Å
O-H···Ow = 175.3°

3) Ow···Ow = 3.01 Å
Ow-Hw···Ow = 157.3°

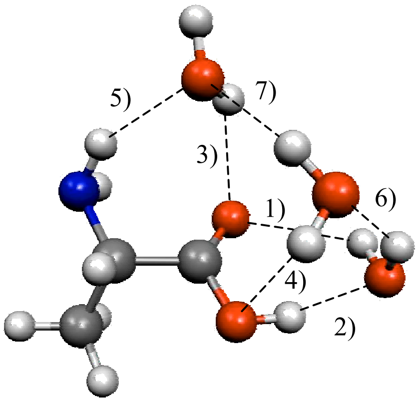

b)

$\Delta E_{\text{T-model}}$ = -105.2 kJ/mol

1) Ow···O = 2.94 Å
Ow-Hw···O = 114.6°

2) O···Ow = 2.82 Å
O-H···Ow = 162.0°

3) Ow···O = 2.96 Å
Ow-Hw···O = 125.4°

4) O···Ow = 3.04 Å
O-H···Ow = 105.6°

5) N···Ow = 3.09 Å
N-H···Ow = 150.4°

6) Ow···Ow = 2.97 Å
Ow-Hw···Ow = 140.7°

7) Ow···Ow = 3.07 Å
Ow-Hw···Ow = 150.5°

Figure B.1 Equilibrium structures, interaction energies and some characteristic distances and angles in the Ala-A-H_2O complexes in the gas phase, computed from the T-model potentials.

a) Ala-A-H_2O 1 : 2 complexes.

b) Ala-A-H_2O 1 : 3 complexes.

c) Ala-A-H_2O 1 : 4 complexes.

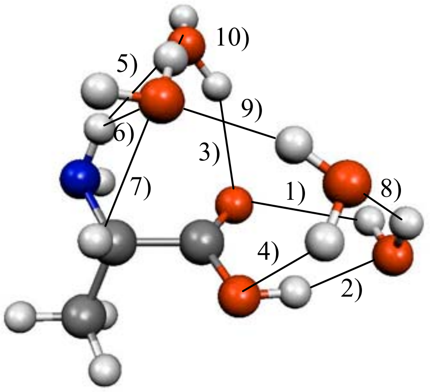

c)

$\Delta E_{T\text{-model}}$ = -143.3 kJ/mol

1) Ow···O = 3.03 Å
Ow-Hw···O = 116.6°

2) O···Ow = 2.83 Å
O-H···Ow = 164.6°

3) Ow···O = 3.04 Å
Ow-Hw···O = 140.7°

4) O···Ow = 2.94 Å
O-H···Ow = 103.9°

5) N···Ow = 3.08 Å
N-H···Ow = 141.4°

6) N···Ow = 3.11 Å
N-H···Ow = 124.7°

7) C···Ow = 3.00 Å
C-H···Ow = 105.2°

8) Ow···Ow = 2.94 Å
Ow-Hw···Ow = 138.1°

9) Ow···Ow = 3.08 Å
Ow-Hw···Ow = 161.5°

10) Ow···Ow = 2.94 Å
Ow-Hw···Ow = 144.5°

Figure B.1 (continued)

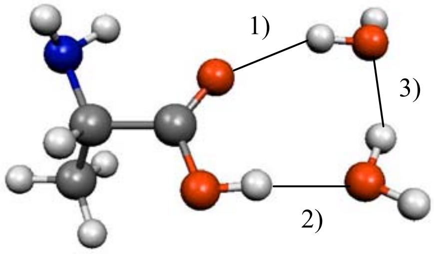

a)

$\Delta E_{\text{T-model}}$ = -71.0 kJ/mol

1) Ow···O = 3.05 Å
Ow-Hw···O = 154.1°

2) O···Ow = 2.84 Å
O-H···Ow = 175.6°

3) Ow···Ow = 3.01 Å
Ow-Hw···Ow = 157.4°

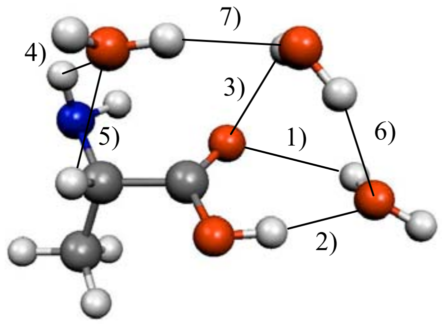

b)

$\Delta E_{\text{T-model}}$ = -106.0 kJ/mol

1) Ow···O = 2.94 Å
Ow-Hw···O = 113.9°

2) O···Ow = 2.86 Å
O-H···Ow = 165.1°

3) Ow···O = 3.03 Å
Ow-Hw···O = 127.5°

4) N···Ow = 3.00 Å
N-H···Ow = 125.9°

5) C···Ow = 2.93 Å
C-H···Ow = 106.1°

6) Ow···Ow = 3.11 Å
Ow-Hw···Ow = 137.8°

7) Ow···Ow = 3.02 Å
Ow-Hw···Ow = 154.6°

Figure B.2 Equilibrium structures, interaction energies and some characteristic distances and angles in the Ala-B-H_2O complexes in the gas phase, computed from the T-model potentials.

a) Ala-B-H_2O 1 : 2 complexes.

b) Ala-B-H_2O 1 : 3 complexes.

c) Ala-B-H_2O 1 : 4 complexes.

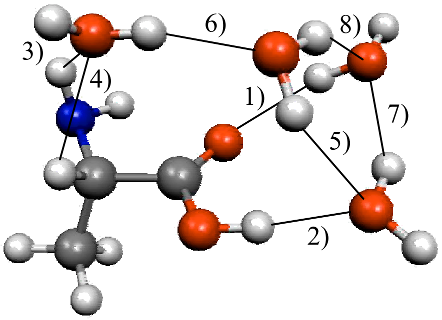

c)

$\Delta E_{\text{T-model}}$ = -143.4 kJ/mol

1) Ow···O = 2.98 Å
Ow-Hw···O = 148.5°

2) O···Ow = 2.84 Å
O-H···Ow = 166.3°

3) N···Ow = 2.97 Å
N-H···Ow = 127.3°

4) C···Ow = 2.94 Å
C-H···Ow = 105.3°

5) Ow···Ow = 3.07 Å
Ow-Hw···Ow = 133.2°

6) Ow···Ow = 3.03 Å
Ow-Hw···Ow = 168.7°

7) Ow···Ow = 3.01 Å
Ow-Hw···Ow = 149.2°

8) Ow···Ow = 3.10 Å
Ow-Hw···Ow = 150.1°

Figure B.2 (continued)

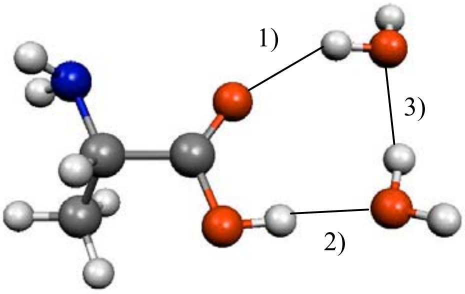

a)

$\Delta E_{\text{T-model}}$ = -72.2 kJ/mol

1) Ow···O = 3.01 Å
Ow-Hw···O = 148.8°

2) O···Ow = 2.85 Å
O-H···Ow = 178.2°

3) Ow···Ow = 3.04 Å
Ow-Hw···Ow = 162.8°

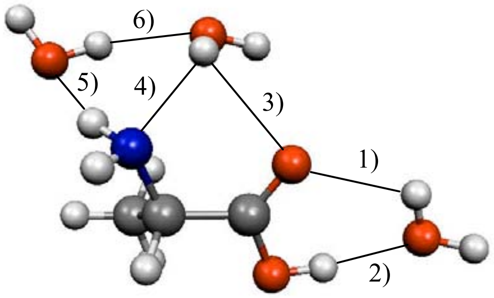

b)

$\Delta E_{\text{T-model}}$ = -107.7 kJ/mol

1) Ow···O = 2.94 Å
Ow-Hw···O = 117.8°

2) O···Ow = 2.86 Å
O-H···Ow = 164.8°

3) Ow···O = 3.11 Å
Ow-Hw···O = 115.1°

4) Ow···N = 3.10 Å
Ow-Hw···N = 135.9°

5) N···Ow = 3.08 Å
N-H···Ow = 162.2°

6) Ow···Ow = 3.00 Å
Ow-Hw···Ow = 149.7°

Figure B.3 Equilibrium structures, interaction energies and some characteristic distances and angles in the Ala-C-H_2O complexes in the gas phase, computed from the T-model potentials.

a) Ala-C-H_2O 1 : 2 complexes.

b) Ala-C-H_2O 1 : 3 complexes.

c) Ala-C-H_2O 1 : 4 complexes.

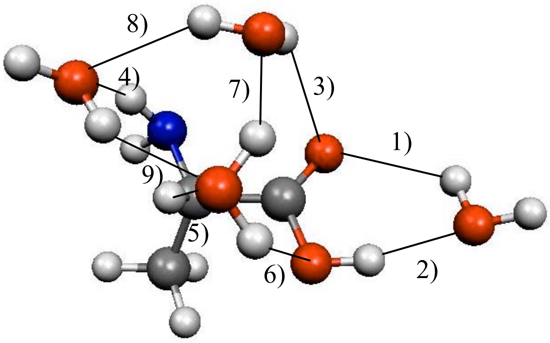

c)

$\Delta E_{\text{T-model}}$ = -146.0 kJ/mol

1) Ow···O = 2.94 Å
Ow-Hw···O = 119.1°

2) O···Ow = 2.85 Å
O-H···Ow = 164.9°

3) N···Ow = 3.07 Å
N-H···Ow = 125.0°

4) C···Ow = 3.05 Å
C-H···Ow = 144.2°

5) Ow···Ow = 3.26 Å
Ow-Hw···Ow = 138.9°

6) Ow···Ow = 3.12 Å
Ow-Hw···Ow = 127.1°

7) Ow···Ow = 2.95 Å
Ow-Hw···Ow = 139.4°

8) Ow···Ow = 3.04 Å
Ow-Hw···Ow = 139.6°

9) Ow···Ow = 3.03 Å
Ow-Hw···Ow = 153.2°

Figure B.3 (continued)

APPENDIX C

SUPPLEMENTARY RESULTS FOR MD SIMULATIONS

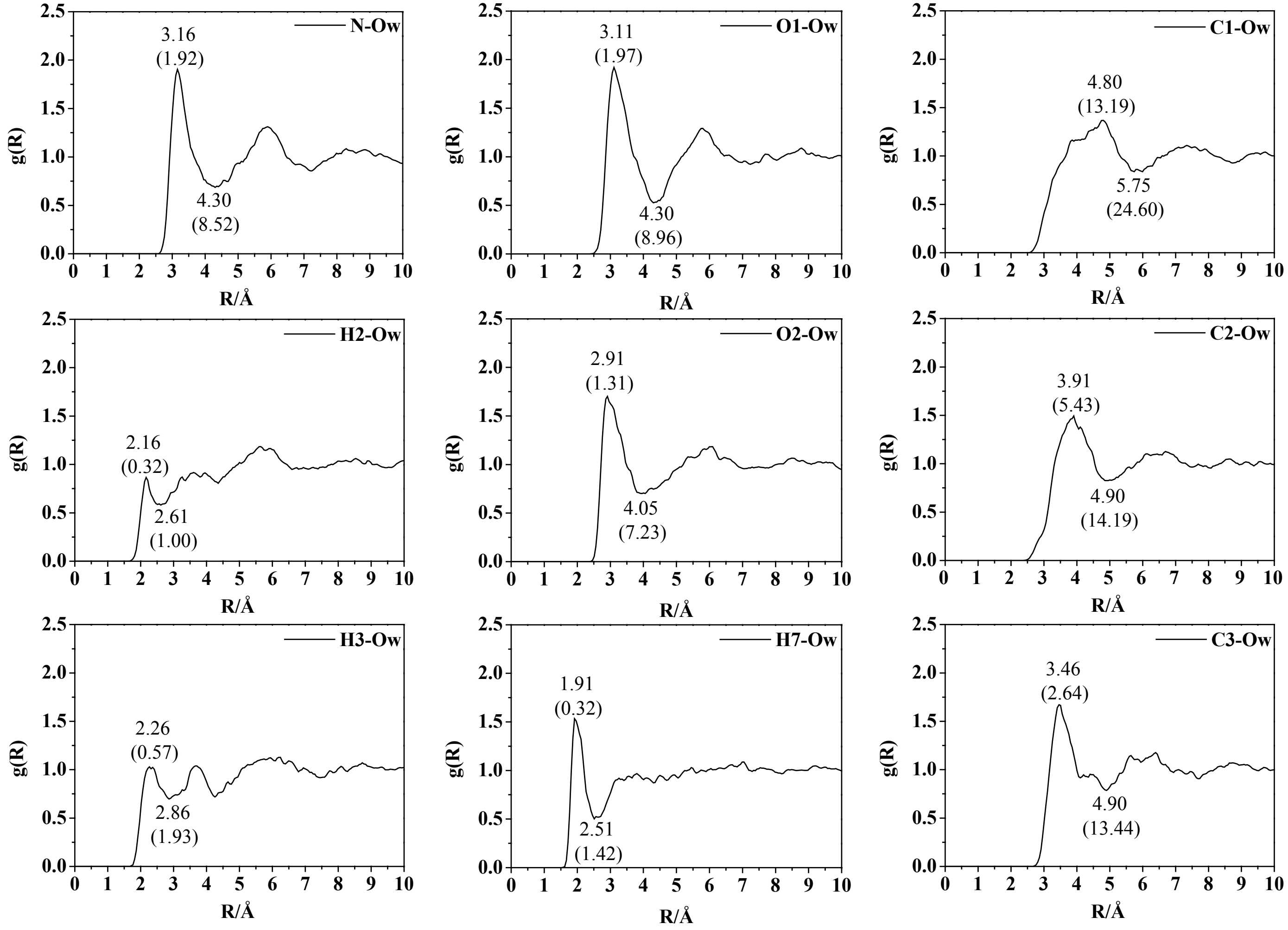

Figure C.1 g(R) obtained from MD-[Ala - A]$_{aq}$. Some characteristic distances are shown, with n(R) in parenthesis.

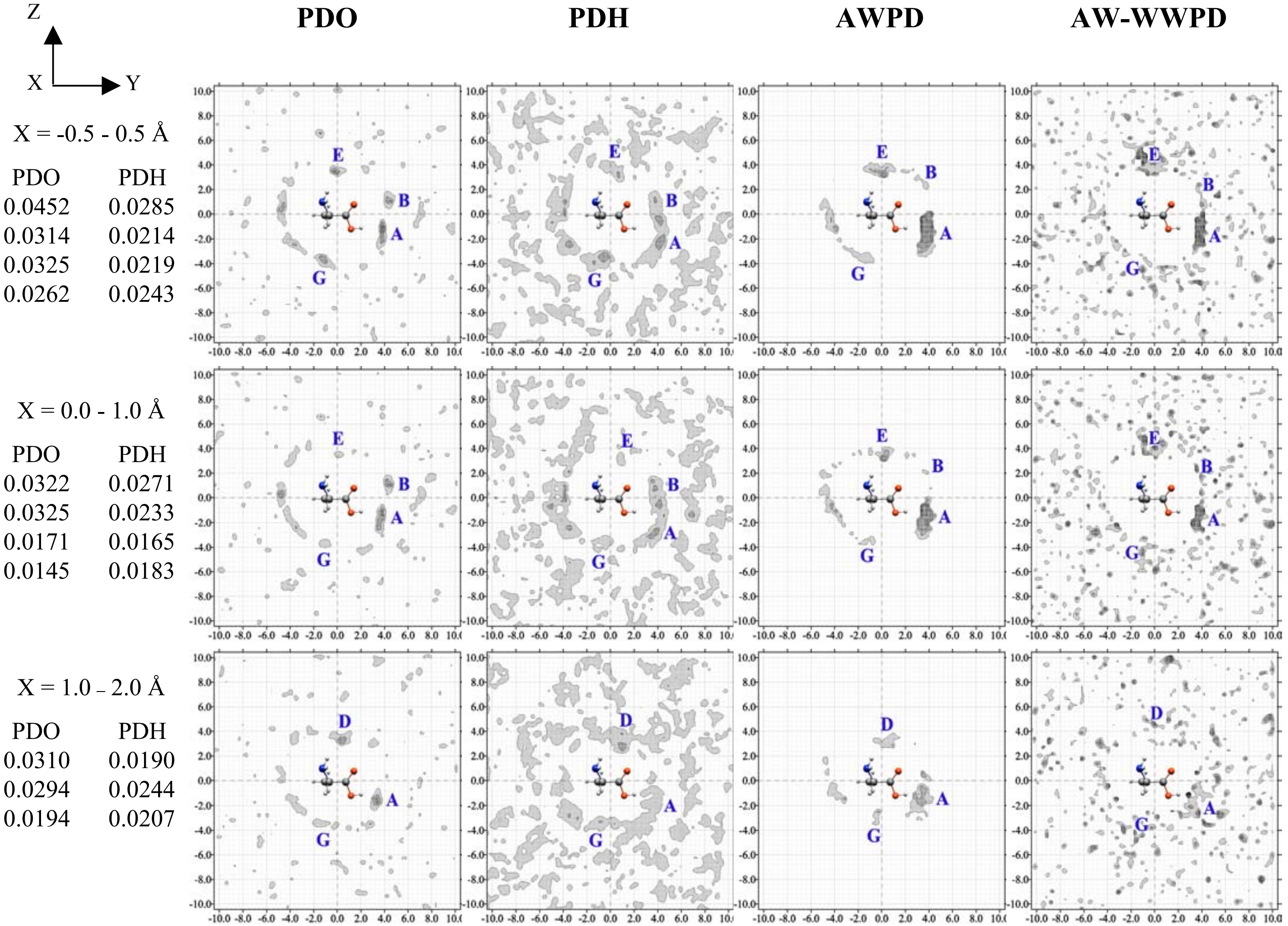

a) X = -0.5 - 0.5 Å

	PDO	PDH
A	0.0452	0.0285
B	0.0314	0.0214
E	0.0325	0.0219
G	0.0262	0.0243

	AWPD	AW-WWPD
A	-34.1043	-80.2889
B	-13.6695	-71.7175
E	-20.8298	-78.3113
G	-13.7349	-79.0547

b) X = 0.0 - 1.0 Å

	PDO	PDH
A	0.0322	0.0271
B	0.0325	0.0233
E	0.0171	0.0165
G	0.0145	0.0183

	AWPD	AW-WWPD
A	-30.7063	-80.5580
B	-12.2053	-75.9301
E	-20.8390	-77.4471
G	-11.5868	-75.7125

c) X = 1.0 – 2.0 Å

	PDO	PDH
A	0.0310	0.0190
D	0.0294	0.0244
G	0.0194	0.0207

	AWPD	AW-WWPD
A	-17.5217	-97.5841
D	-13.8112	-76.5166
G	-16.2938	-66.0313

Figure C.2 The PDO, PDH, AWPD and AW-WWPD maps with respect to reference plane I obtained from MD-[Ala - A]$_{aq}$.

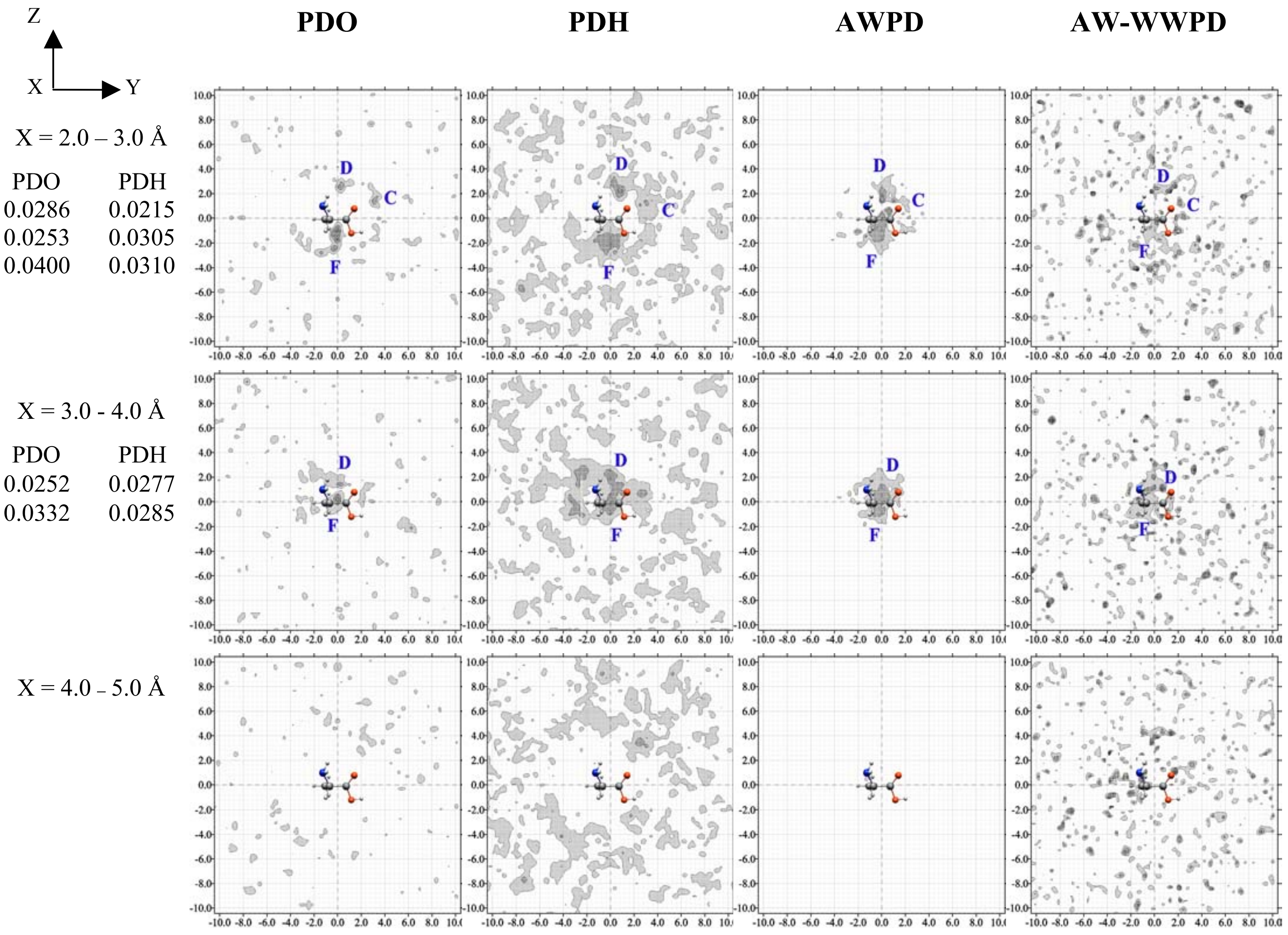

d) X = 2.0 – 3.0 Å

	PDO	PDH
C	0.0286	0.0215
D	0.0253	0.0305
F	0.0400	0.0310

	AWPD	AW-WWPD
C	-13.6894	-73.2773
D	-24.6433	-78.6247
F	-23.2564	-71.0927

e) X = 3.0 - 4.0 Å

	PDO	PDH
D	0.0252	0.0277
F	0.0332	0.0285

	AWPD	AW-WWPD
D	-14.8417	-86.2054
F	-19.2997	-72.8409

f) X = 4.0 – 5.0 Å

Figure C.2 (continued)

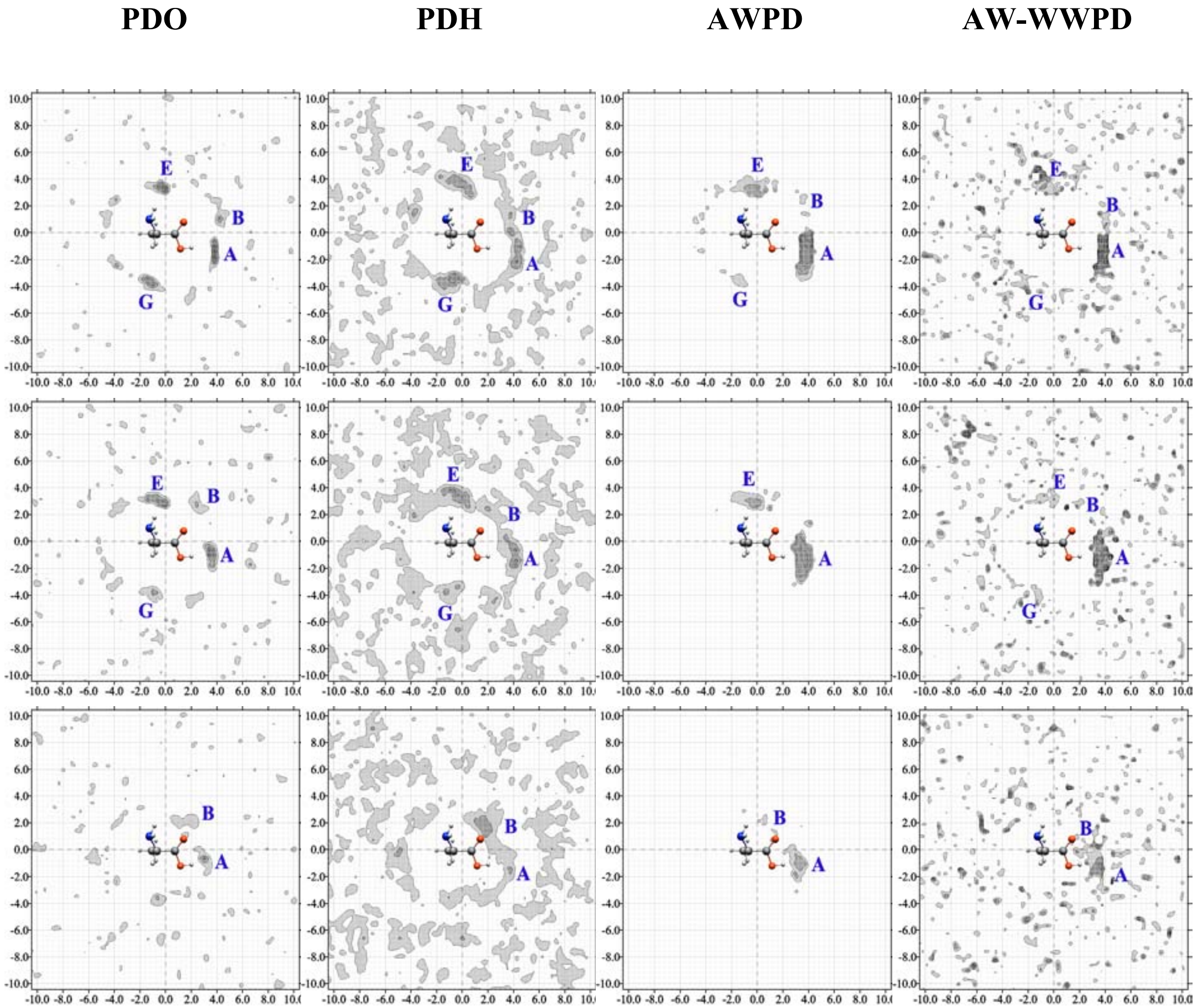

g) X = -1.0 - 0.0 Å

	PDO	PDH
A	0.0439	0.0313
B	0.0308	0.0212
E	0.0463	0.0298
G	0.0376	0.0379

	AWPD	AW-WWPD
A	-32.4997	-83.1577
B	-12.6003	-73.7109
E	-20.2133	-79.9264
G	-13.6676	-75.4141

h) X = -2.0 - -1.0 Å

	PDO	PDH
A	0.0432	0.0326
B	0.0221	0.0218
E	0.0379	0.0334
G	0.0233	0.0225

	AWPD	AW-WWPD
A	-26.4597	-79.6779
B	-	-69.3243
E	-18.7929	-70.5771
G	-	-67.6241

i) X = -3.0 – -2.0 Å

	PDO	PDH
A	0.0324	0.0326
B	0.0193	0.0284

	AWPD	AW-WWPD
A	-17.3977	-74.6710
B	-11.2072	-66.2534

Figure C.2 (continued)

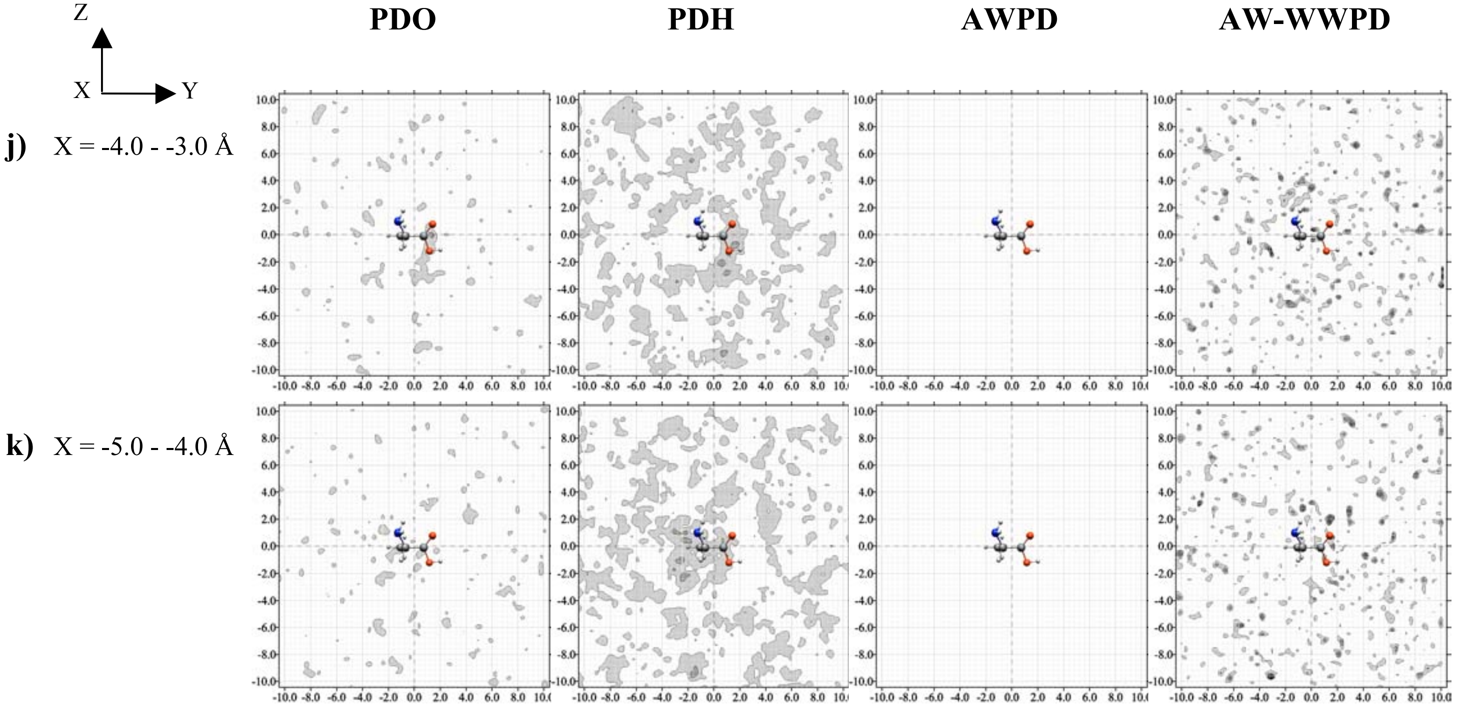

Figure C.2 (continued)

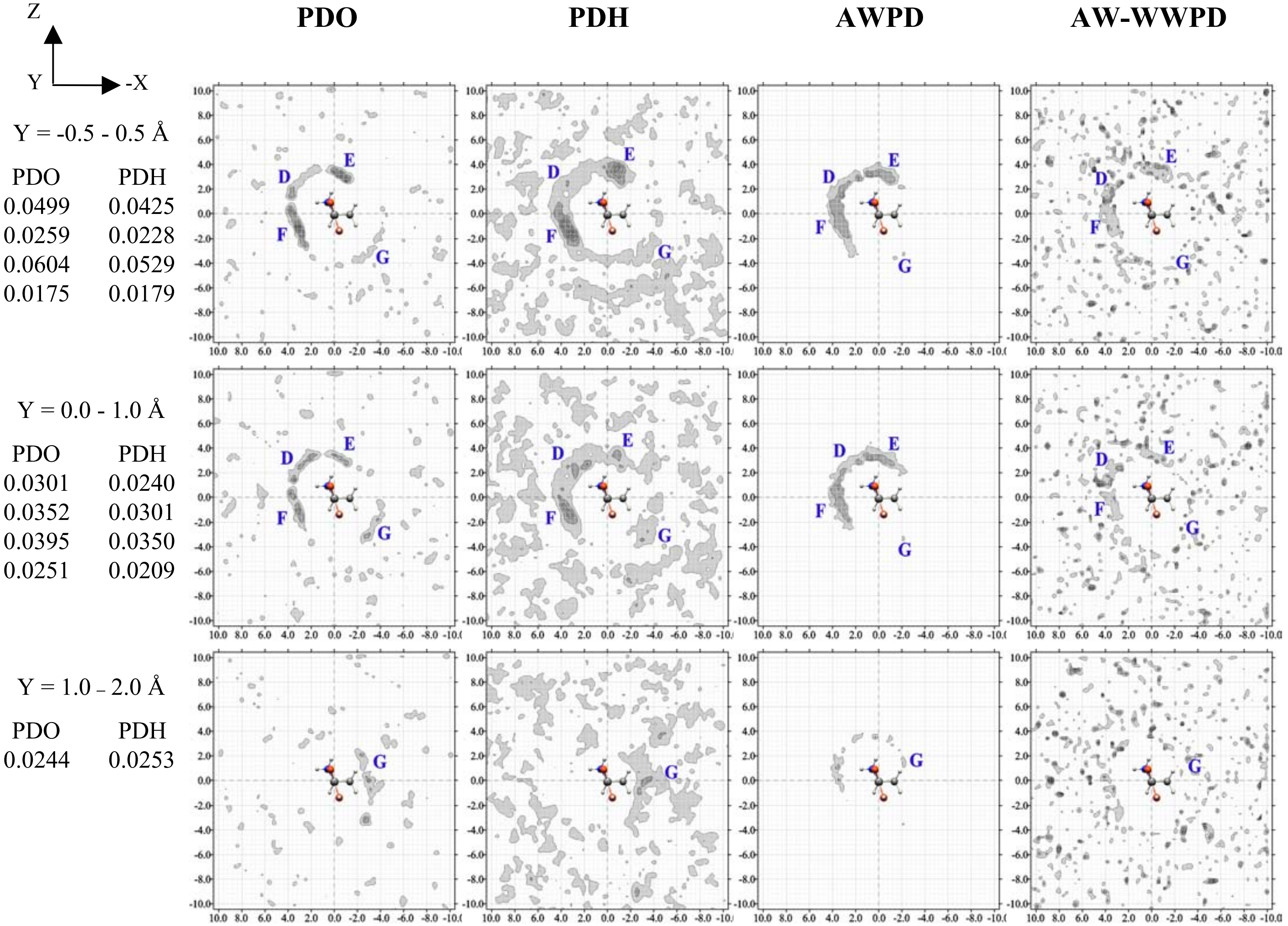

a) Y = -0.5 - 0.5 Å

	PDO	PDH
E	0.0499	0.0425
D	0.0259	0.0228
F	0.0604	0.0529
G	0.0175	0.0179

	AWPD	AW-WWPD
E	-22.3004	-72.6447
D	-20.2496	-73.0915
F	-22.6693	-73.8021
G	-11.1191	-74.2386

b) Y = 0.0 - 1.0 Å

	PDO	PDH
E	0.0301	0.0240
D	0.0352	0.0301
F	0.0395	0.0350
G	0.0251	0.0209

	AWPD	AW-WWPD
E	-22.3188	-73.2915
D	-18.4461	-72.2117
F	-20.1680	-70.4189
G	-10.3106	-72.9384

c) Y = 1.0 – 2.0 Å

	PDO	PDH
G	0.0244	0.0253

	AWPD	AW-WWPD
G	-11.2246	-73.6568

Figure C.3 The PDO, PDH, AWPD and AW-WWPD maps with respect to reference plane II obtained from MD-[Ala - A]$_{aq}$.

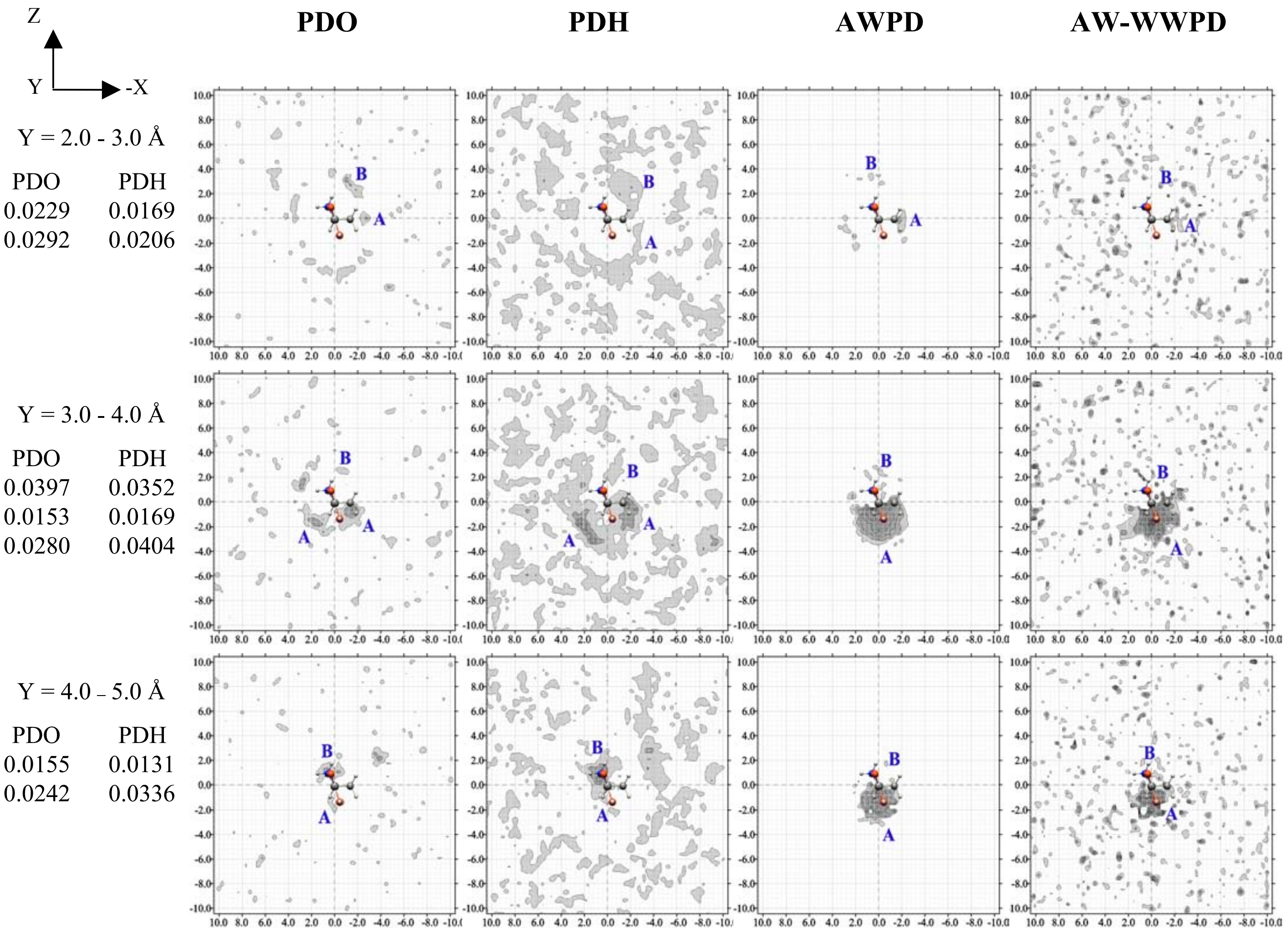

d) Y = 2.0 - 3.0 Å

	PDO	PDH
A	0.0229	0.0169
B	0.0292	0.0206

	AWPD	AW-WWPD
A	-18.2510	-69.6273
B	-11.6296	-68.8364

e) Y = 3.0 - 4.0 Å

	PDO	PDH
A	0.0397	0.0352
B	0.0153	0.0169
A	0.0280	0.0404

	AWPD	AW-WWPD
A	-35.5680	-89.8615
B	-14.1018	-73.4806

f) Y = 4.0 – 5.0 Å

	PDO	PDH
A	0.0155	0.0131
B	0.0242	0.0336

	AWPD	AW-WWPD
A	-32.8237	-83.6766
B	-13.7572	-63.5544

Figure C.3 (continued)

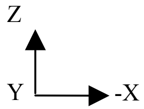

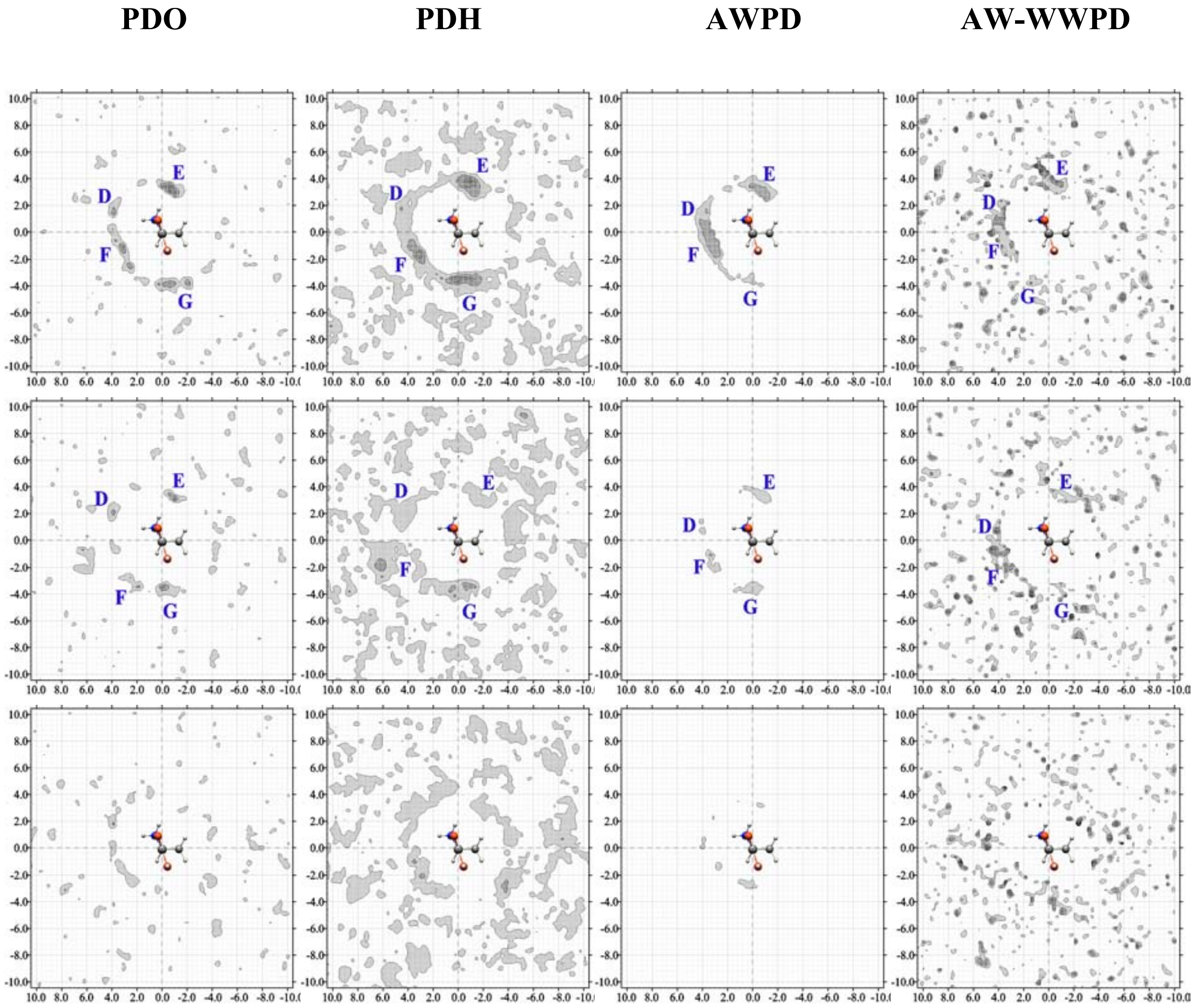

g) Y = -1.0 - 0.0 Å

	PDO	PDH
E	0.0429	0.0424
D	0.0256	0.0222
F	0.0321	0.0339
G	0.0272	0.0401

	AWPD	AW-WWPD
E	-19.1261	-82.0447
D	-14.6403	-72.1481
F	-19.4101	-72.2450
G	-13.2206	-70.7341

h) Y = -2.0 - -1.0 Å

	PDO	PDH
E	0.0345	0.0184
D	0.0235	0.0199
F	0.0181	0.0181
G	0.0300	0.0243

	AWPD	AW-WWPD
E	-12.9952	-74.3640
D	-12.4561	-80.3519
F	-15.0428	-81.7430
G	-13.3233	-78.7734

i) Y = -3.0 - -2.0 Å

Figure C.3 (continued)

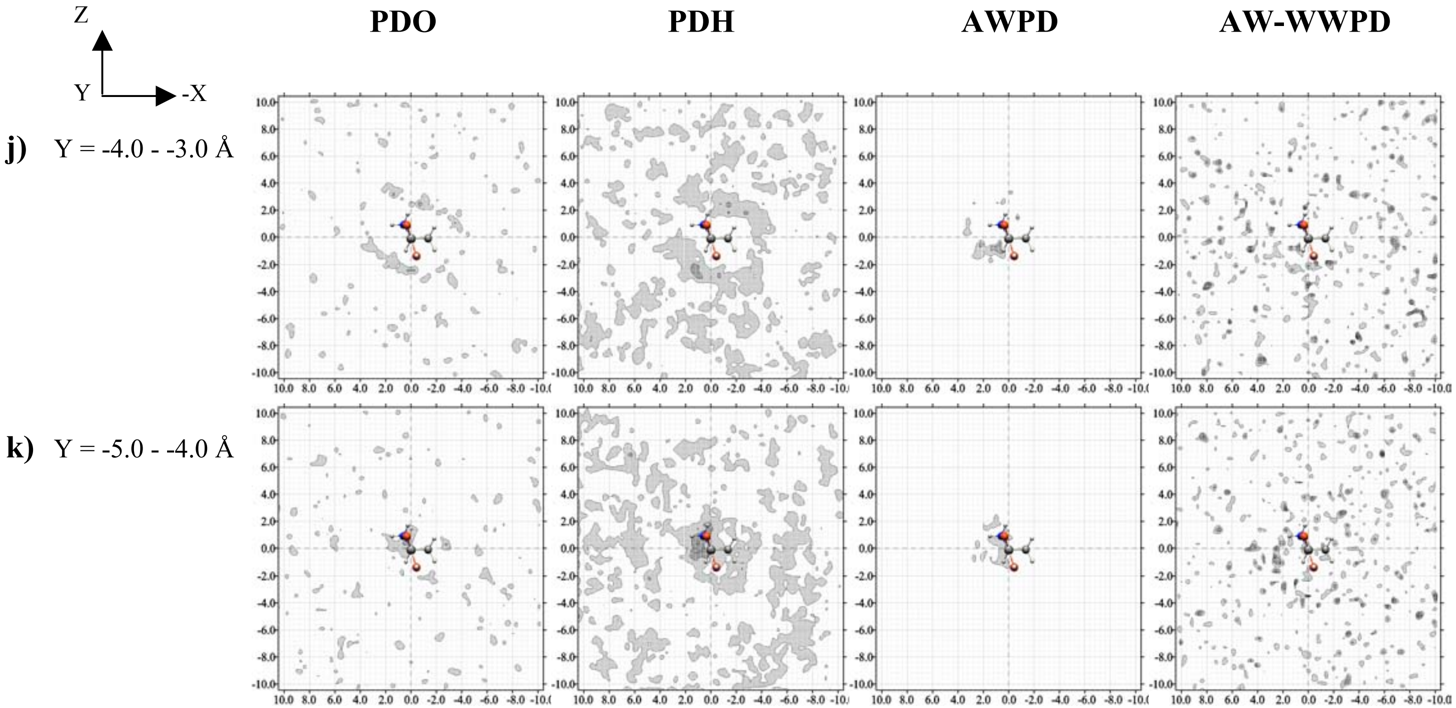

Figure C.3 (continued)

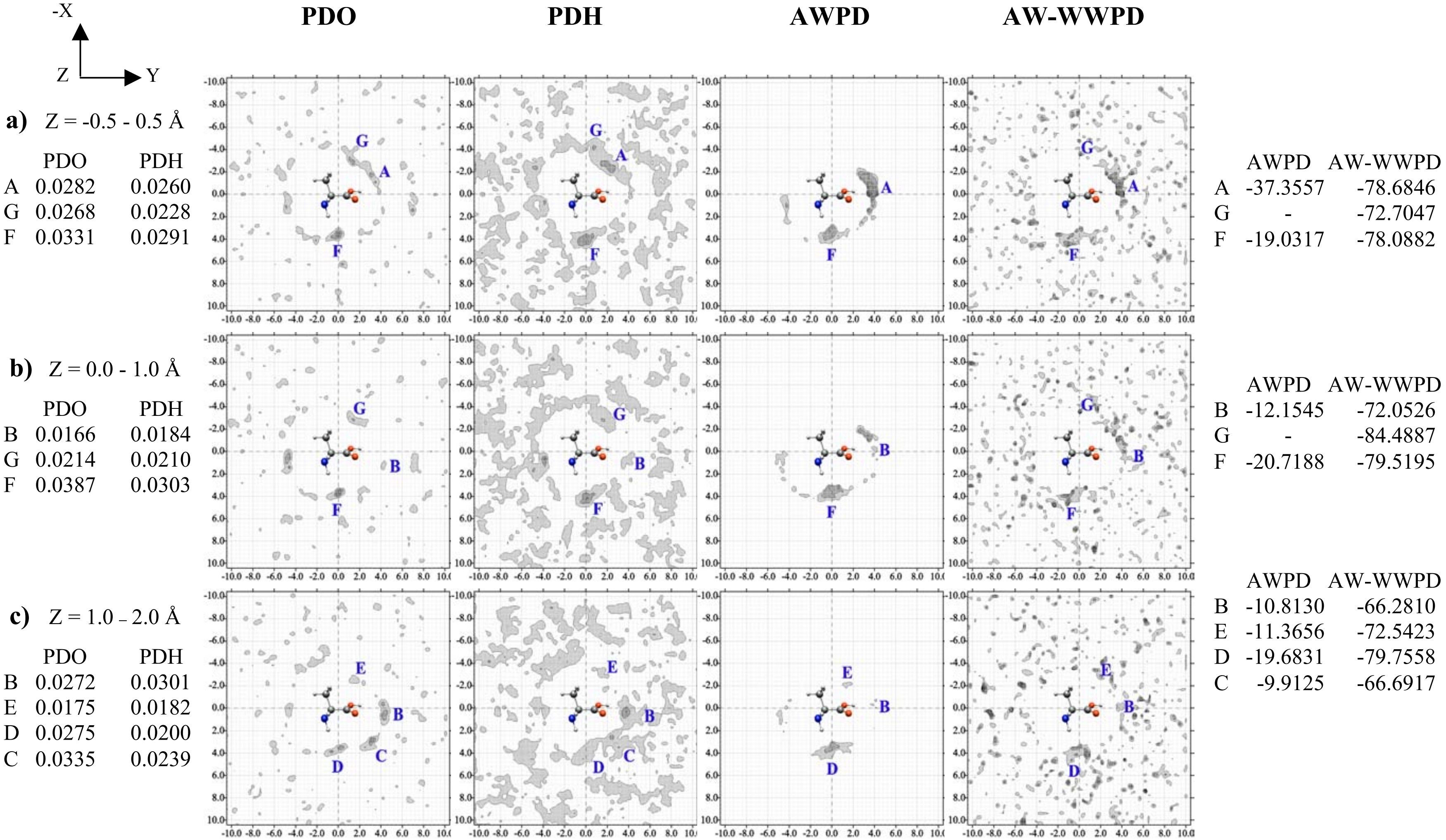

a) Z = -0.5 - 0.5 Å

	PDO	PDH
A	0.0282	0.0260
G	0.0268	0.0228
F	0.0331	0.0291

	AWPD	AW-WWPD
A	-37.3557	-78.6846
G	-	-72.7047
F	-19.0317	-78.0882

b) Z = 0.0 - 1.0 Å

	PDO	PDH
B	0.0166	0.0184
G	0.0214	0.0210
F	0.0387	0.0303

	AWPD	AW-WWPD
B	-12.1545	-72.0526
G	-	-84.4887
F	-20.7188	-79.5195

c) Z = 1.0 – 2.0 Å

	PDO	PDH
B	0.0272	0.0301
E	0.0175	0.0182
D	0.0275	0.0200
C	0.0335	0.0239

	AWPD	AW-WWPD
B	-10.8130	-66.2810
E	-11.3656	-72.5423
D	-19.6831	-79.7558
C	-9.9125	-66.6917

Figure C.4 The PDO, PDH, AWPD and AW-WWPD maps with respect to reference plane III obtained from MD-[Ala - A]$_{aq}$.

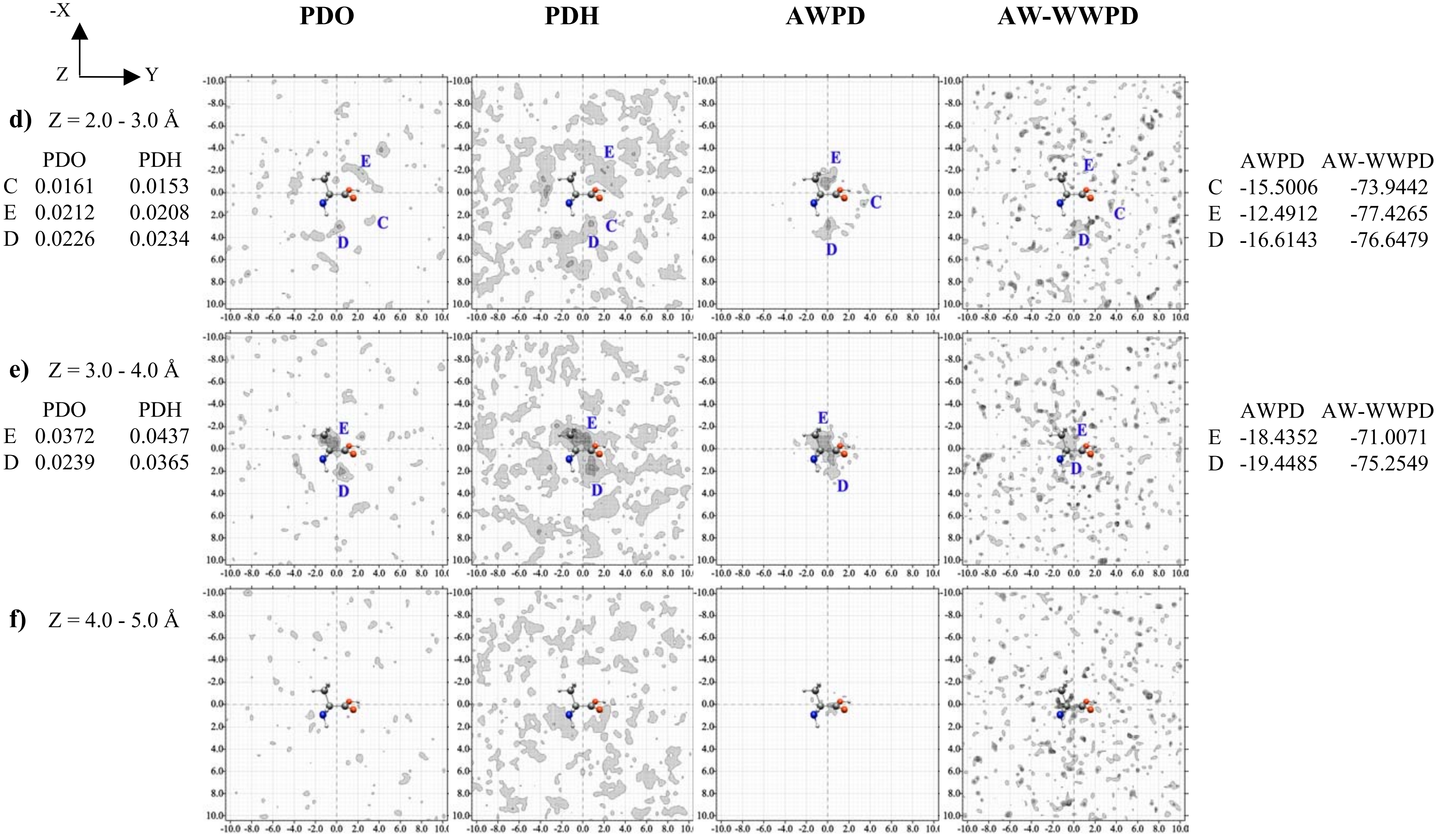

d) Z = 2.0 - 3.0 Å

	PDO	PDH
C	0.0161	0.0153
E	0.0212	0.0208
D	0.0226	0.0234

	AWPD	AW-WWPD
C	-15.5006	-73.9442
E	-12.4912	-77.4265
D	-16.6143	-76.6479

e) Z = 3.0 - 4.0 Å

	PDO	PDH
E	0.0372	0.0437
D	0.0239	0.0365

	AWPD	AW-WWPD
E	-18.4352	-71.0071
D	-19.4485	-75.2549

f) Z = 4.0 - 5.0 Å

Figure C.4 (continued)

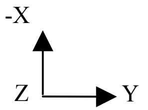

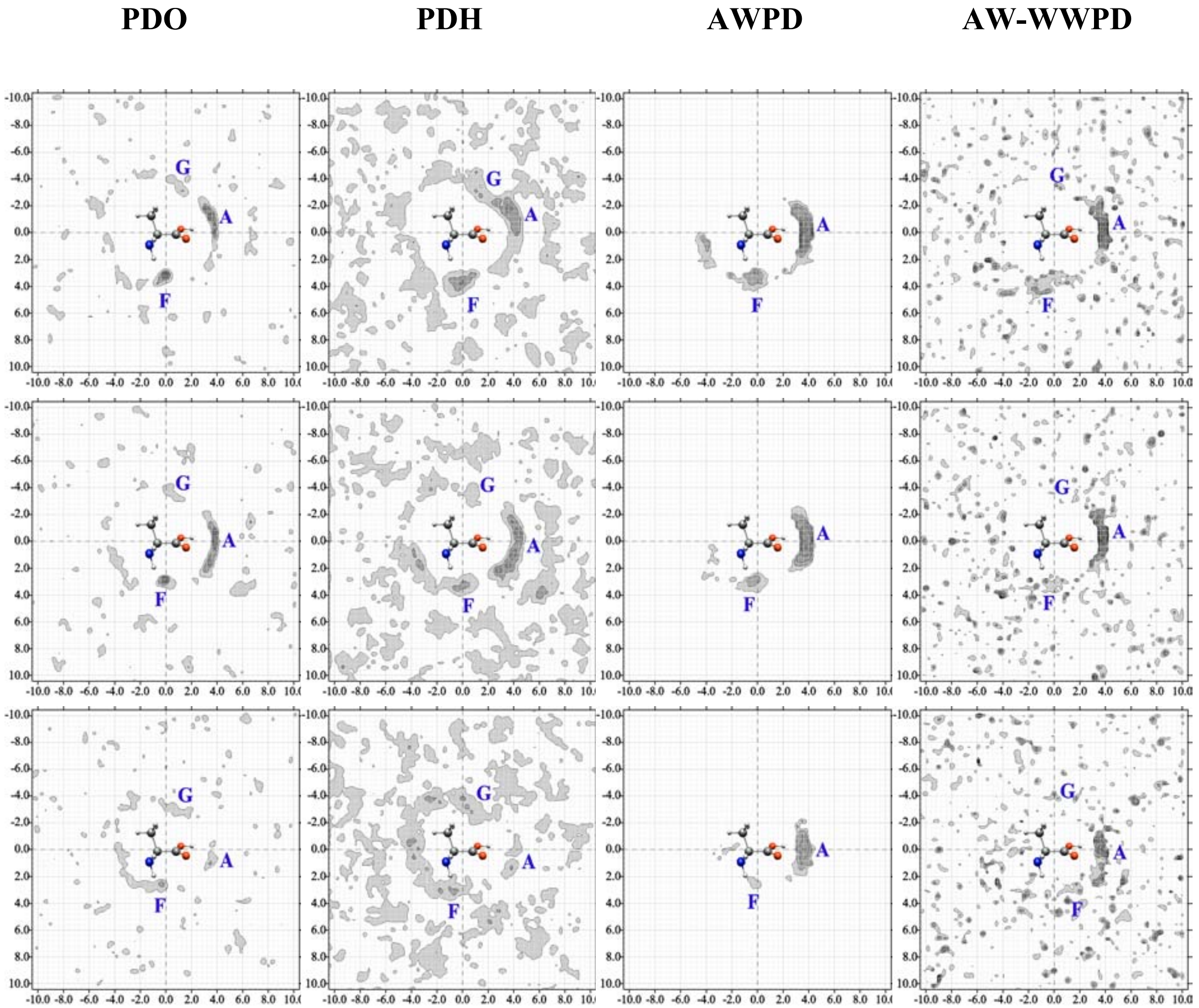

g) Z = -1.0 - 0.0 Å

	PDO	PDH
A	0.0431	0.0316
G	0.0201	0.0219
F	0.0563	0.0295

	AWPD	AW-WWPD
A	-33.4487	-78.5025
G	-	-76.2451
F	-19.4574	-71.2738

h) Z = -2.0 - -1.0 Å

	PDO	PDH
A	0.0501	0.0373
G	0.0193	0.0184
F	0.0489	0.0271

	AWPD	AW-WWPD
A	-30.2922	-81.9560
G	-	-70.2130
F	-17.7586	-76.8307

i) Z = -3.0 - -2.0 Å

	PDO	PDH
A	0.0231	0.0211
G	0.0181	0.0241
F	0.0272	0.0240

	AWPD	AW-WWPD
A	-24.2936	-79.4450
G	-	-65.2682
F	-11.7958	-66.5426

Figure C.4 (continued)

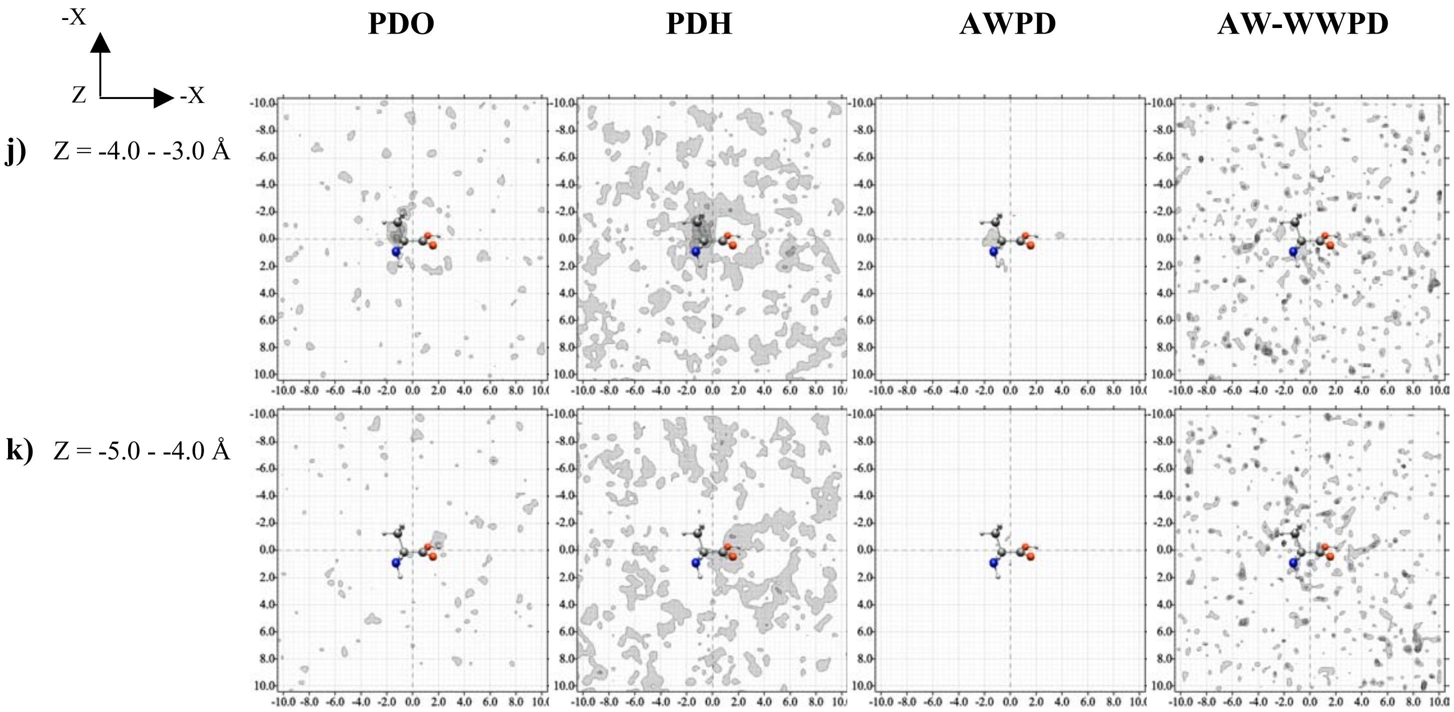

Figure C.4 (continued)

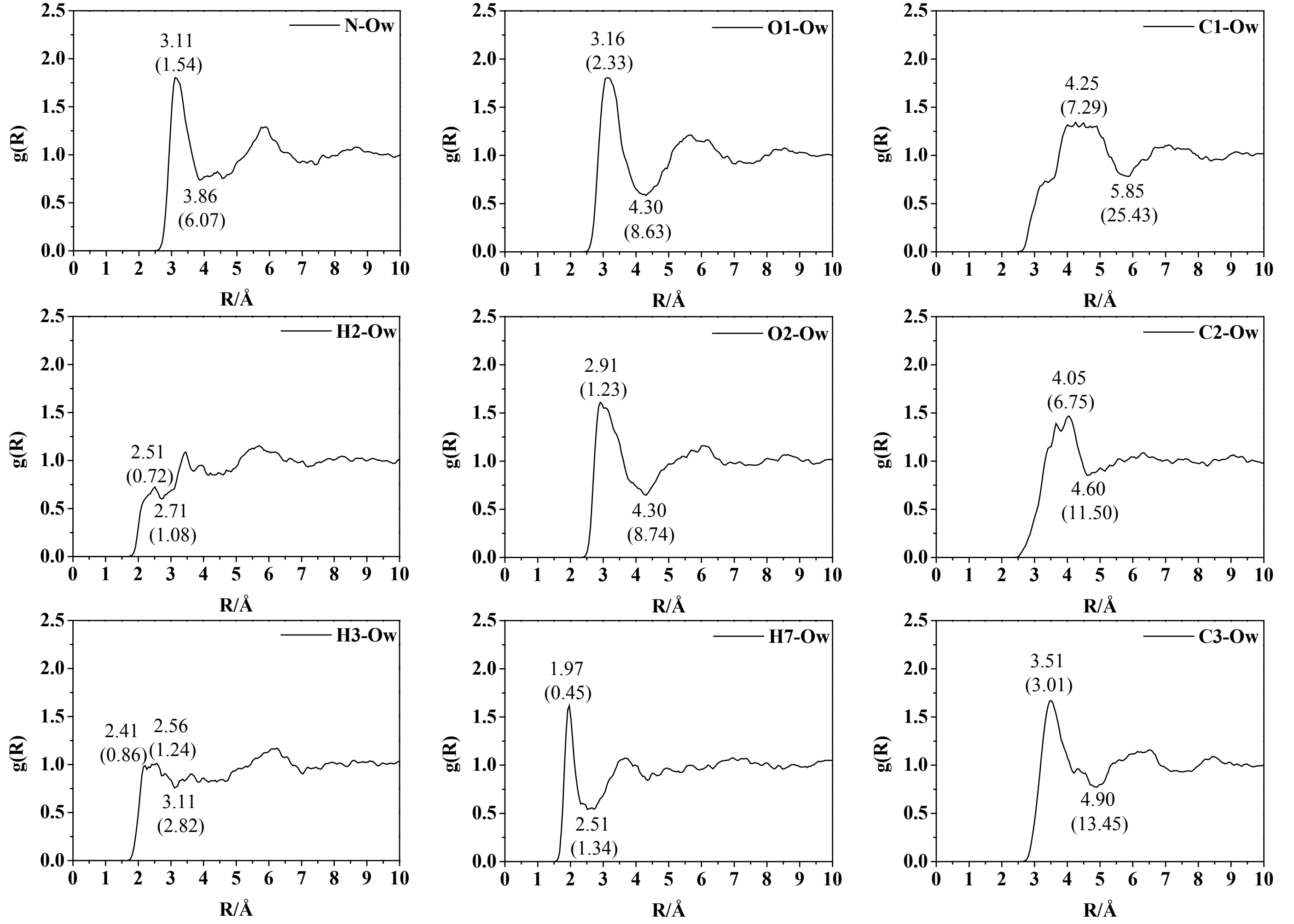

Figure C.5 g(R) obtained from MD-[Ala - B]$_{aq}$. Some characteristic distances are shown, with n(R) in parenthesis.

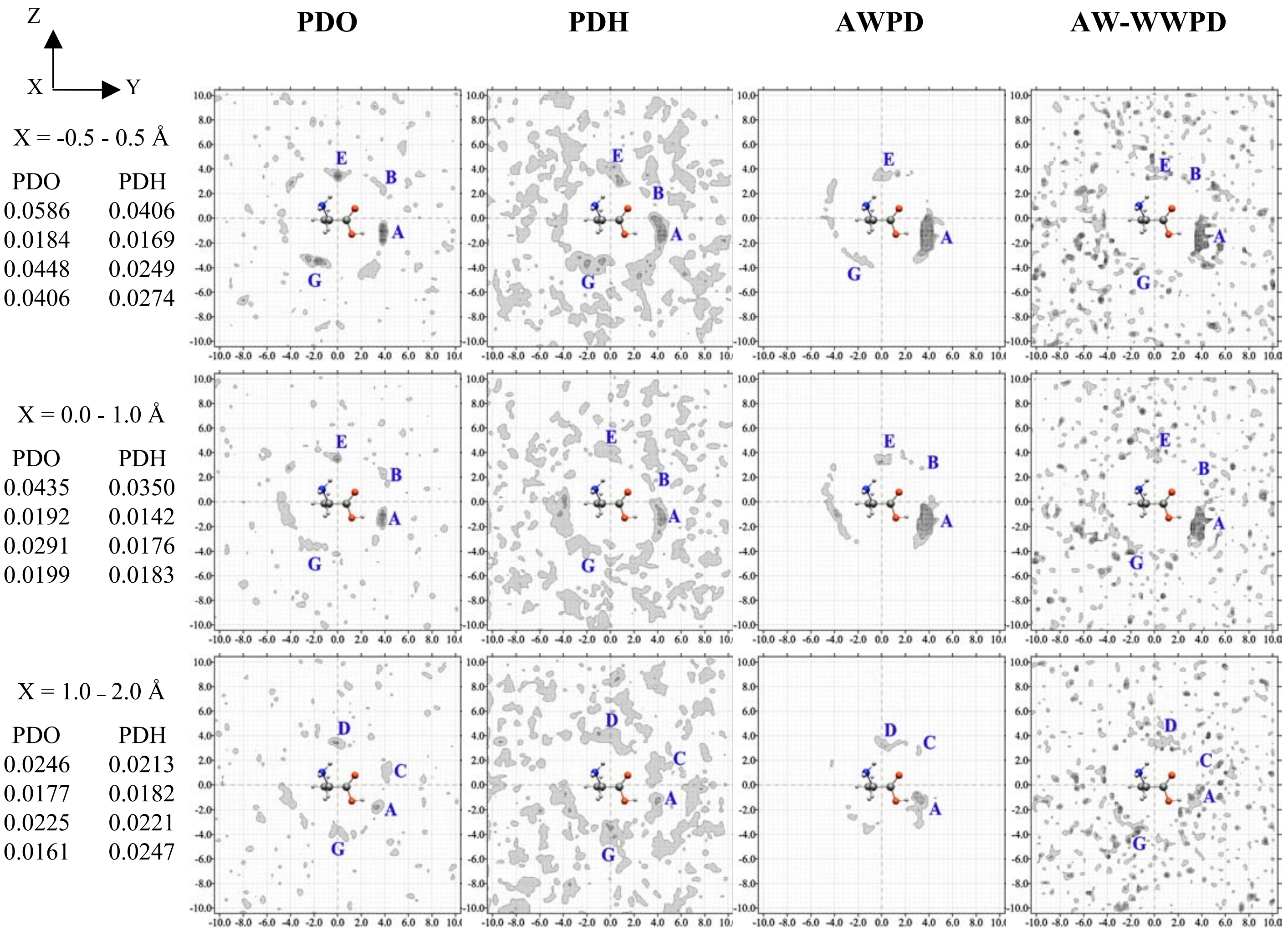

a) X = -0.5 - 0.5 Å

	PDO	PDH
A	0.0586	0.0406
B	0.0184	0.0169
E	0.0448	0.0249
G	0.0406	0.0274

	AWPD	AW-WWPD
A	-30.4110	-84.1717
B	-	-67.1540
E	-16.1176	-71.0394
G	-12.3215	-73.6108

b) X = 0.0 - 1.0 Å

	PDO	PDH
A	0.0435	0.0350
B	0.0192	0.0142
E	0.0291	0.0176
G	0.0199	0.0183

	AWPD	AW-WWPD
A	-28.9225	-80.2858
B	-12.0751	-65.6044
E	-14.5344	-71.3941
G	-	-81.5239

c) X = 1.0 – 2.0 Å

	PDO	PDH
A	0.0246	0.0213
C	0.0177	0.0182
D	0.0225	0.0221
G	0.0161	0.0247

	AWPD	AW-WWPD
A	-18.5593	-76.7231
C	-12.0607	-63.1068
D	-15.4312	-73.5011
G	-	-82.1716

Figure C.6 The PDO, PDH, AWPD and AW-WWPD maps with respect to reference plane I obtained from MD-[Ala - B]$_{aq}$.

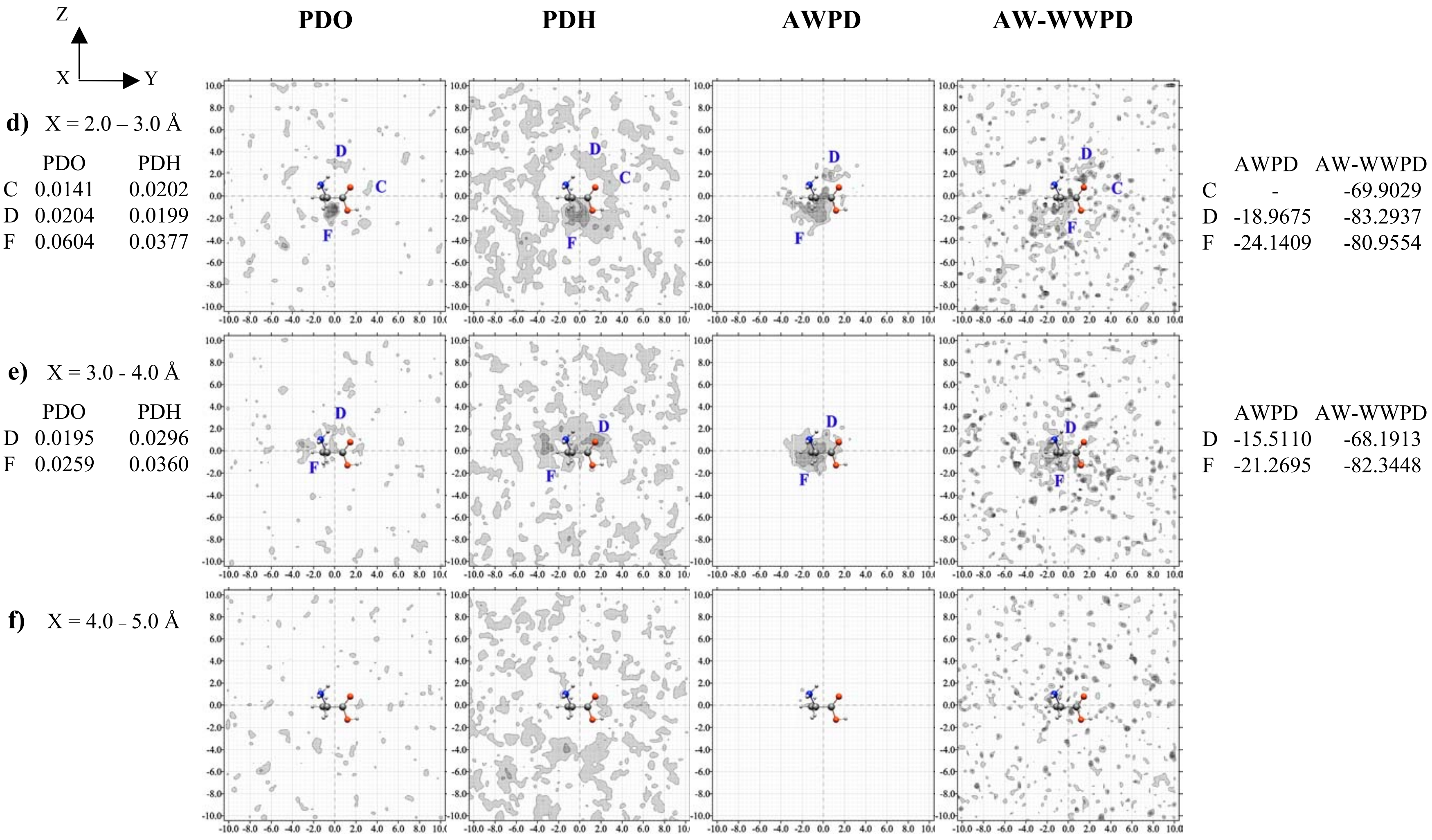

d) X = 2.0 – 3.0 Å

	PDO	PDH
C	0.0141	0.0202
D	0.0204	0.0199
F	0.0604	0.0377

	AWPD	AW-WWPD
C	-	-69.9029
D	-18.9675	-83.2937
F	-24.1409	-80.9554

e) X = 3.0 - 4.0 Å

	PDO	PDH
D	0.0195	0.0296
F	0.0259	0.0360

	AWPD	AW-WWPD
D	-15.5110	-68.1913
F	-21.2695	-82.3448

f) X = 4.0 – 5.0 Å

Figure C.6 (continued)

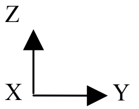

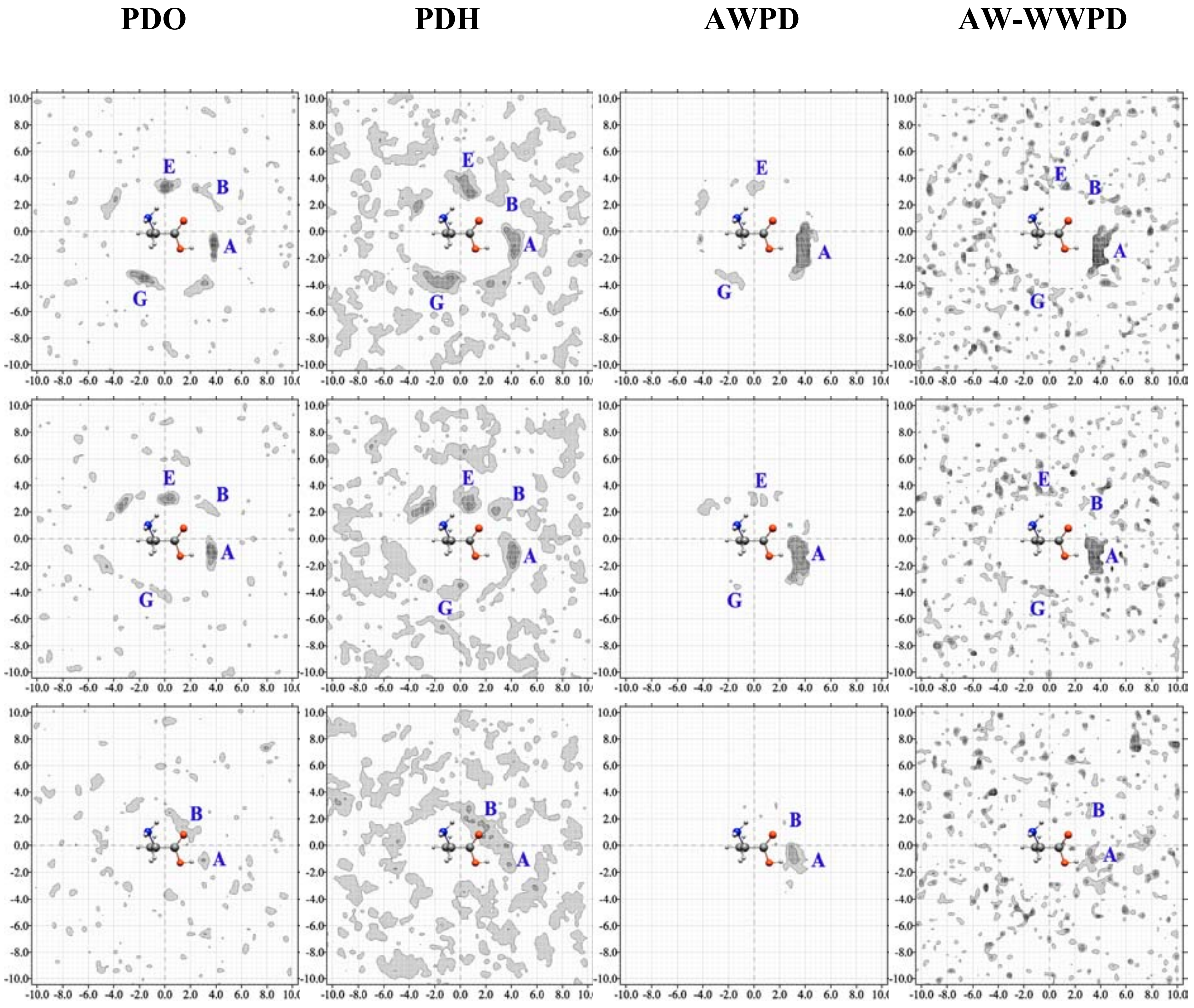

g) X = -1.0 - 0.0 Å

	PDO	PDH
A	0.0583	0.0355
B	0.0265	0.0202
E	0.0437	0.0373
G	0.0477	0.0347

	AWPD	AW-WWPD
A	-31.2628	-86.0436
B	-	-74.4296
E	-13.1341	-77.9172
G	-13.5118	-69.3349

h) X = -2.0 - -1.0 Å

	PDO	PDH
A	0.0440	0.0384
B	0.0188	0.0255
E	0.0344	0.0410
G	0.0146	0.0250

	AWPD	AW-WWPD
A	-26.7609	-80.7813
B	-	-67.7618
E	-11.6414	-72.8147
G	-12.5079	-69.4952

i) X = -3.0 - -2.0 Å

	PDO	PDH
A	0.0207	0.0221
B	0.0201	0.0270

	AWPD	AW-WWPD
A	-19.7968	-74.1541
B	-10.7849	-73.7163

Figure C.6 (continued)

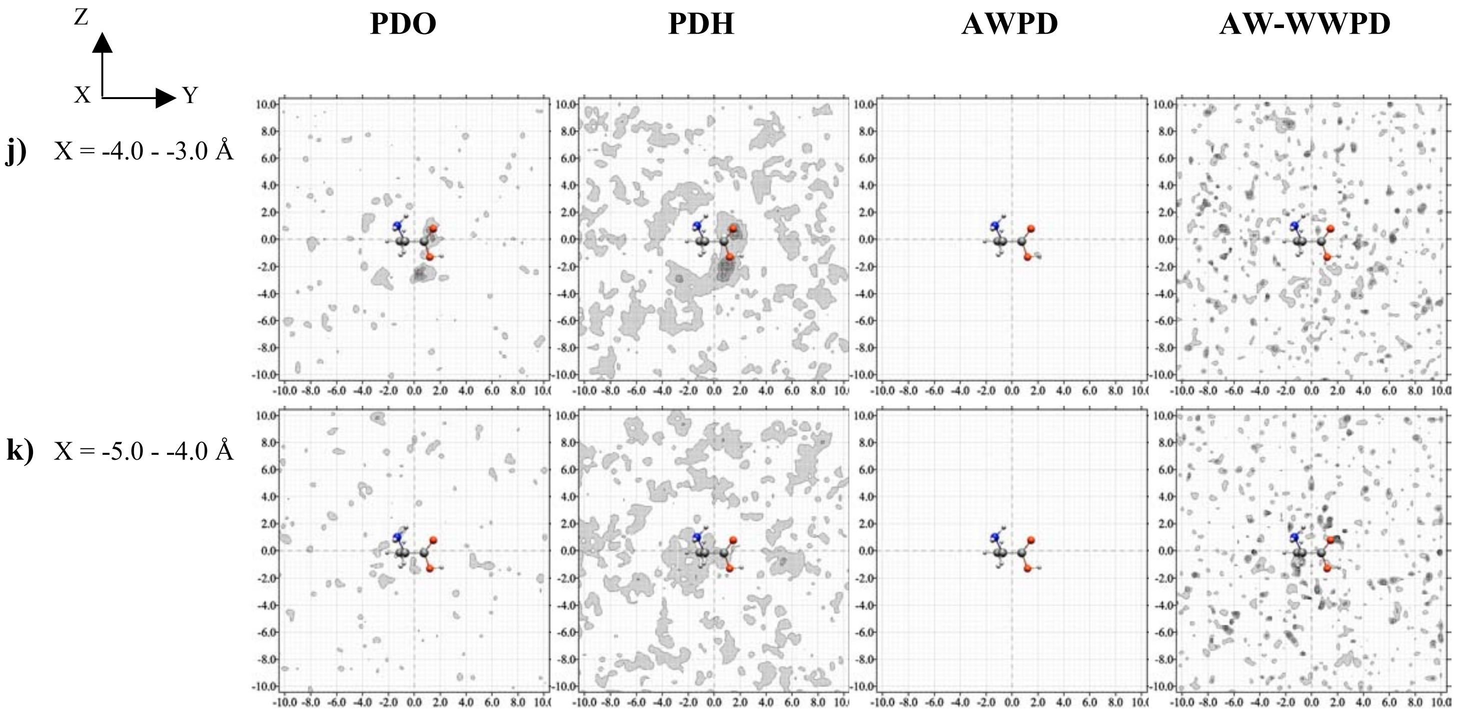

Figure C.6 (continued)

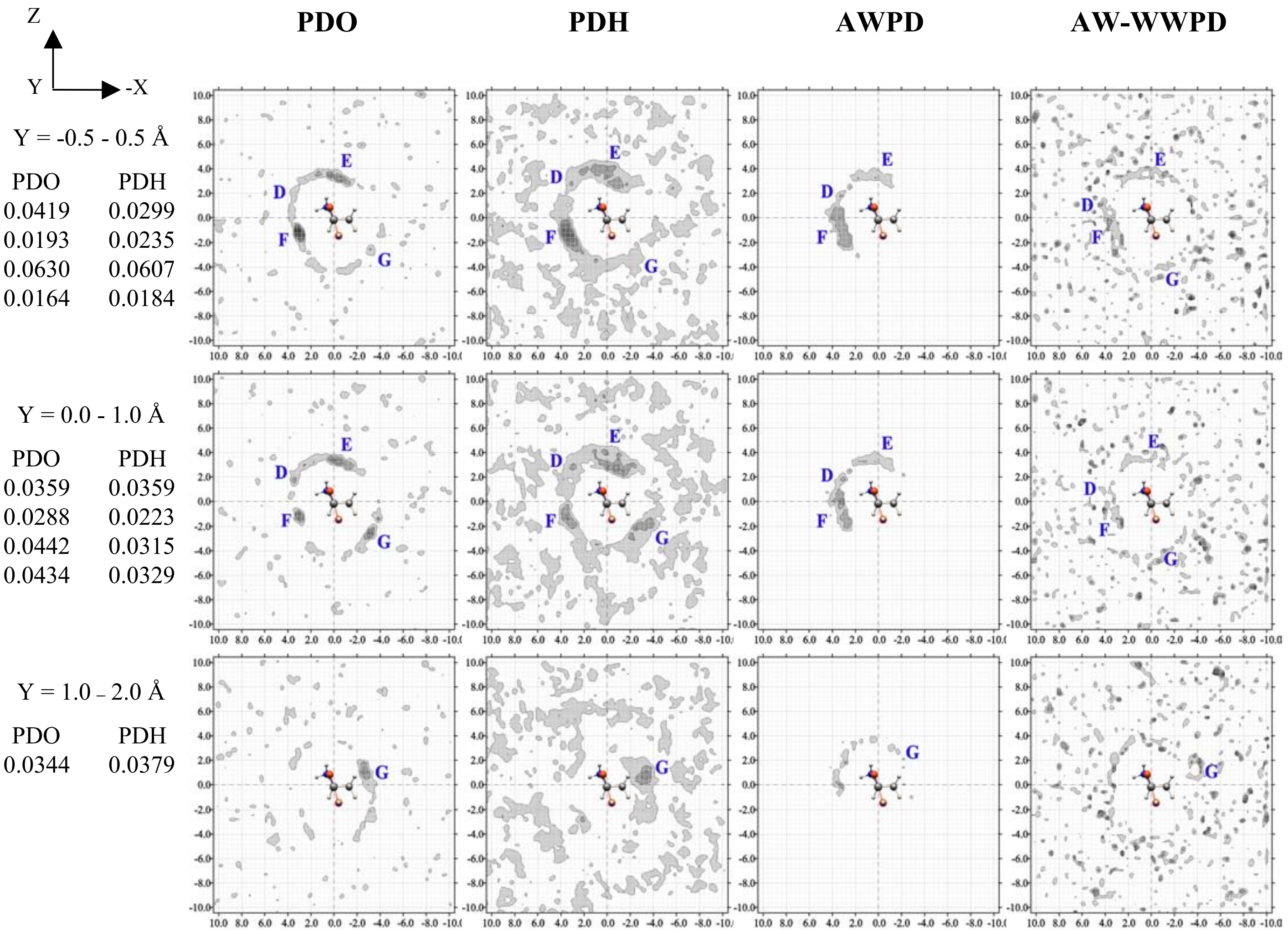

a) Y = -0.5 - 0.5 Å

	PDO	PDH
E	0.0419	0.0299
D	0.0193	0.0235
F	0.0630	0.0607
G	0.0164	0.0184

	AWPD	AW-WWPD
E	-15.1442	-73.3278
D	-15.5061	-73.0784
F	-19.7284	-70.7290
G	-	-68.1850

b) Y = 0.0 - 1.0 Å

	PDO	PDH
E	0.0359	0.0359
D	0.0288	0.0223
F	0.0442	0.0315
G	0.0434	0.0329

	AWPD	AW-WWPD
E	-14.6055	-70.1060
D	-16.8506	-69.3526
F	-23.6271	-72.9094
G	-	-66.4982

c) Y = 1.0 – 2.0 Å

	PDO	PDH
G	0.0344	0.0379

	AWPD	AW-WWPD
G	-11.9069	-75.1923

Figure C.7 The PDO, PDH, AWPD and AW-WWPD maps with respect to reference plane II obtained from MD-[Ala - B]$_{aq}$.

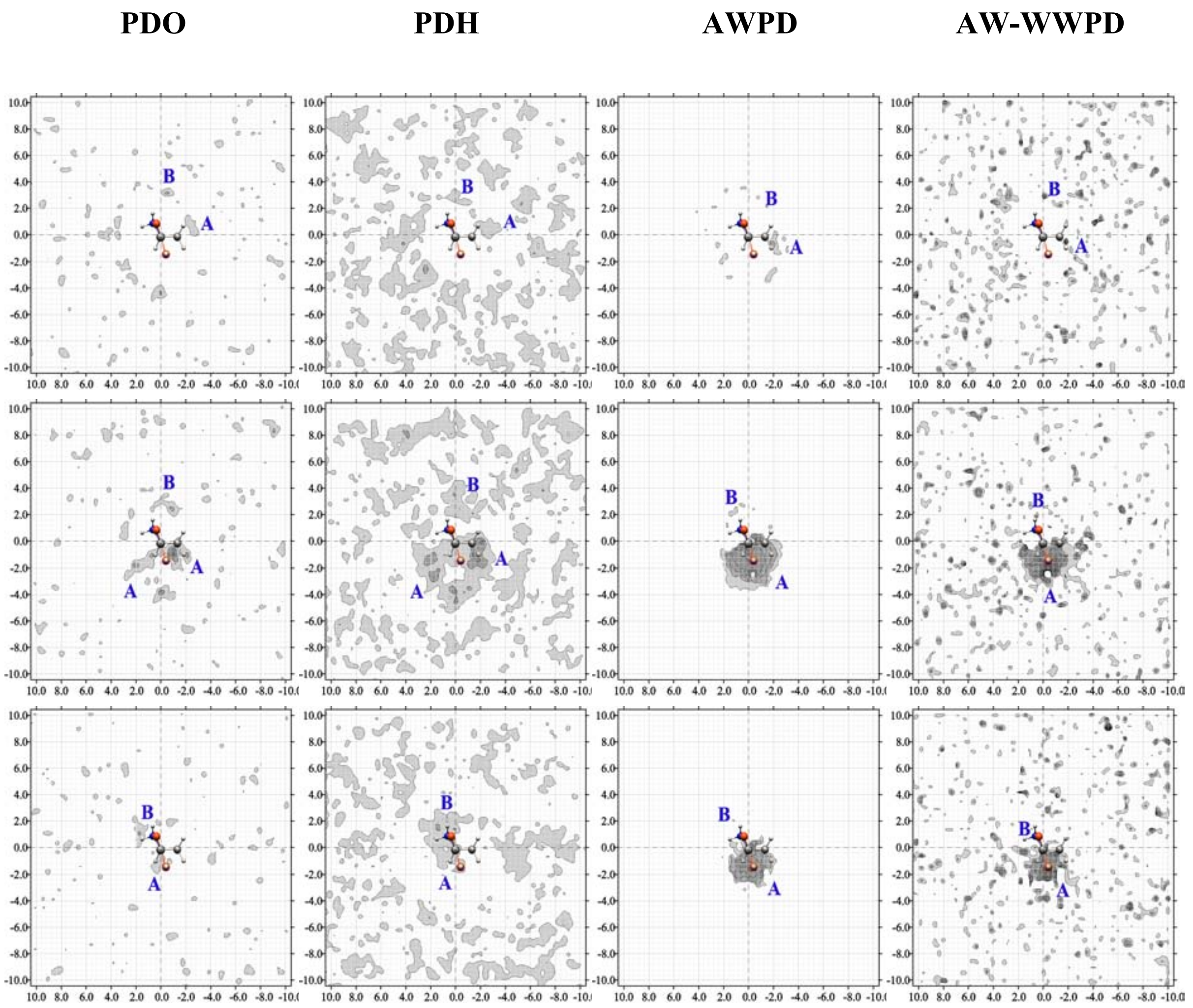

d) Y = 2.0 - 3.0 Å

	PDO	PDH
A	0.0175	0.0175
B	0.0219	0.0159

	AWPD	AW-WWPD
A	-16.7422	-72.9664
B	-11.0484	-78.4185

e) Y = 3.0 - 4.0 Å

	PDO	PDH
A	0.0399	0.0353
B	0.0209	0.0211
A	0.0268	0.0308

	AWPD	AW-WWPD
A	-31.7934	-88.5885
B	-12.9347	-74.2449

f) Y = 4.0 – 5.0 Å

	PDO	PDH
A	0.0190	0.0197
B	0.0243	0.0224

	AWPD	AW-WWPD
A	-30.7692	-84.3607
B	-9.6539	-58.3407

Figure C.7 (continued)

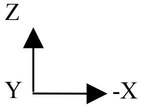

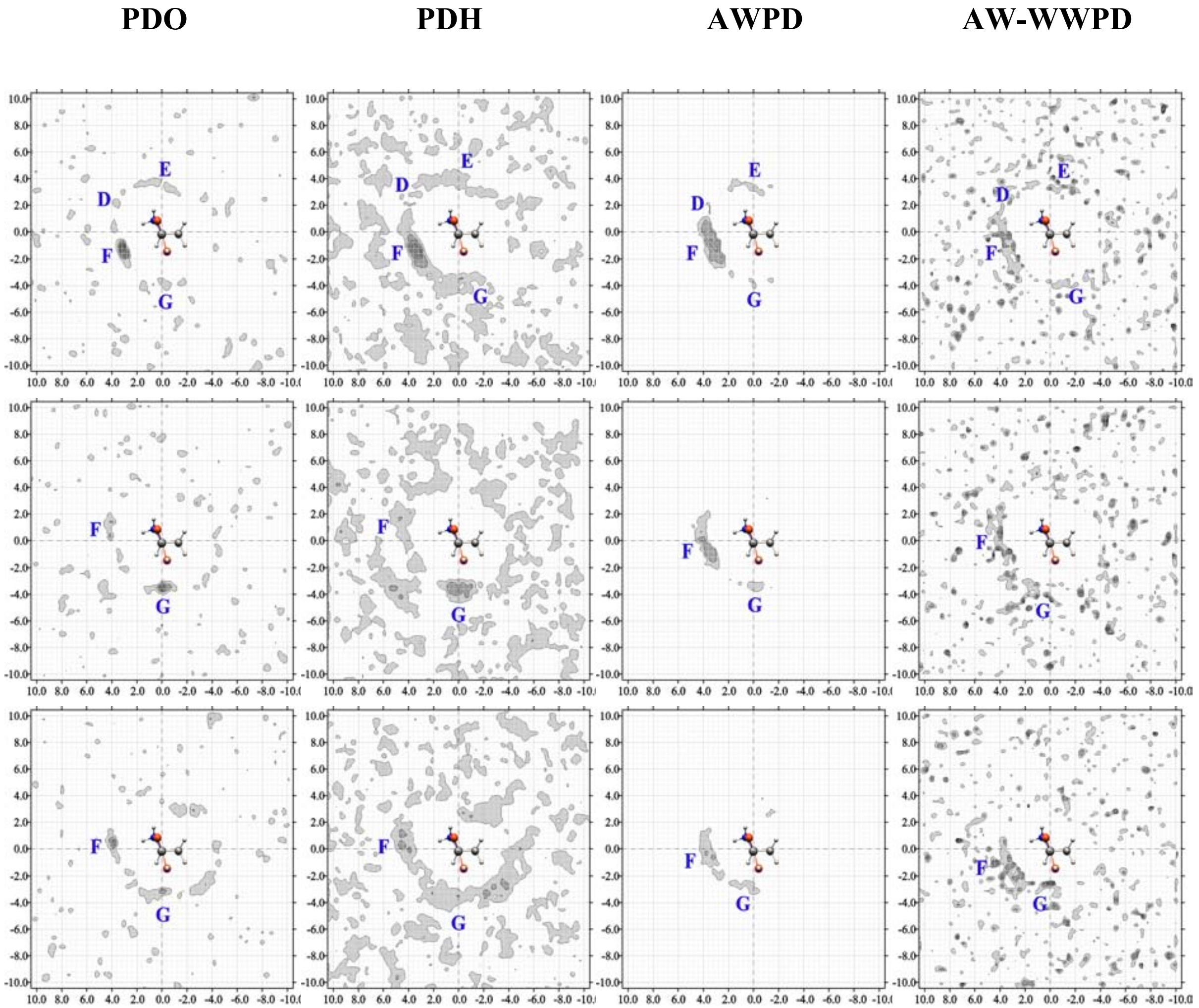

g) Y = -1.0 - 0.0 Å

	PDO	PDH
E	0.0191	0.0185
D	0.0161	0.0153
F	0.0588	0.0475
G	0.0183	0.0203

	AWPD	AW-WWPD
E	-13.1594	-73.0726
D	-10.5058	-71.6055
F	-21.3951	-72.5888
G	-10.9778	-66.5330

h) Y = -2.0 - -1.0 Å

	PDO	PDH
F	0.0241	0.0200
G	0.0481	0.0290

	AWPD	AW-WWPD
F	-18.9254	-79.1724
G	-12.4529	-74.8035

i) Y = -3.0 - -2.0 Å

	PDO	PDH
F	0.0335	0.0251
G	0.0278	0.0205

	AWPD	AW-WWPD
F	-17.4002	-78.5805
G	-13.8129	-78.1918

Figure C.7 (continued)

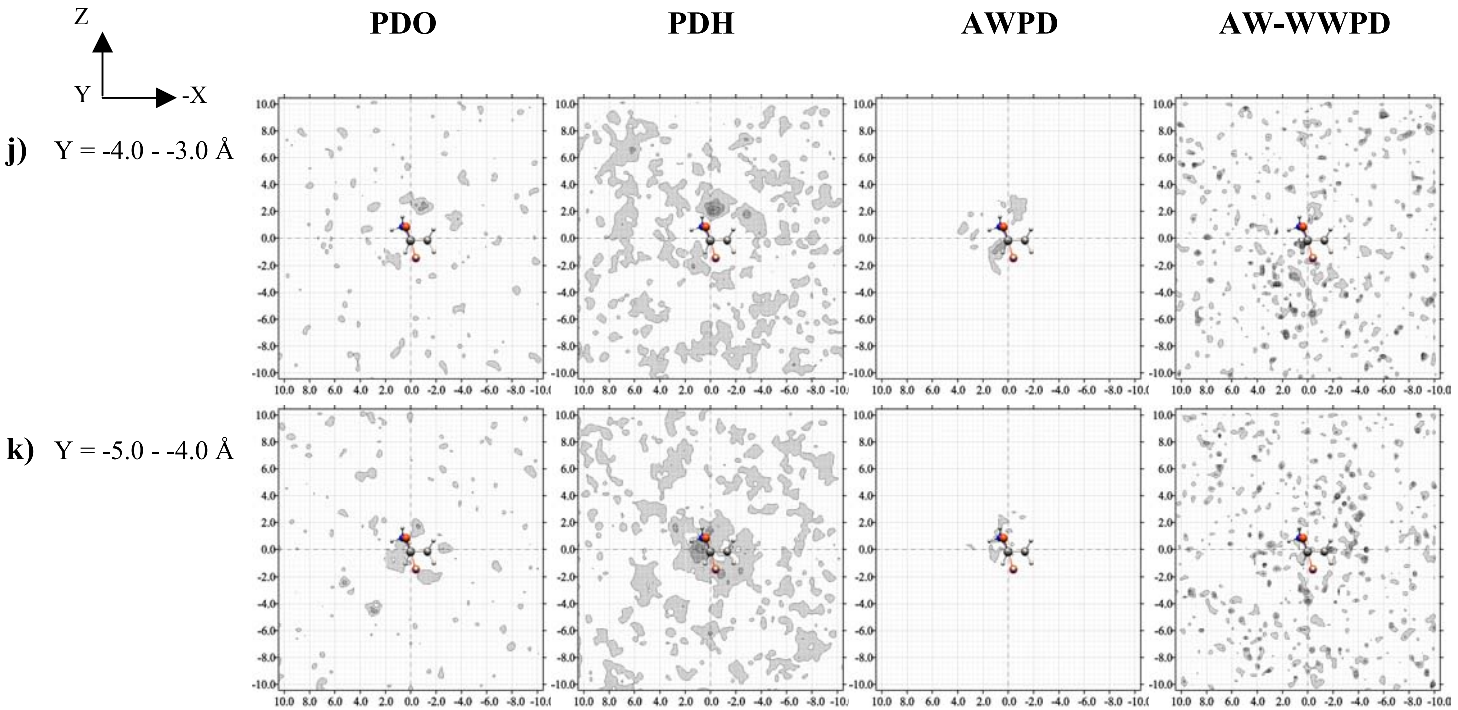

Figure C.7 (continued)

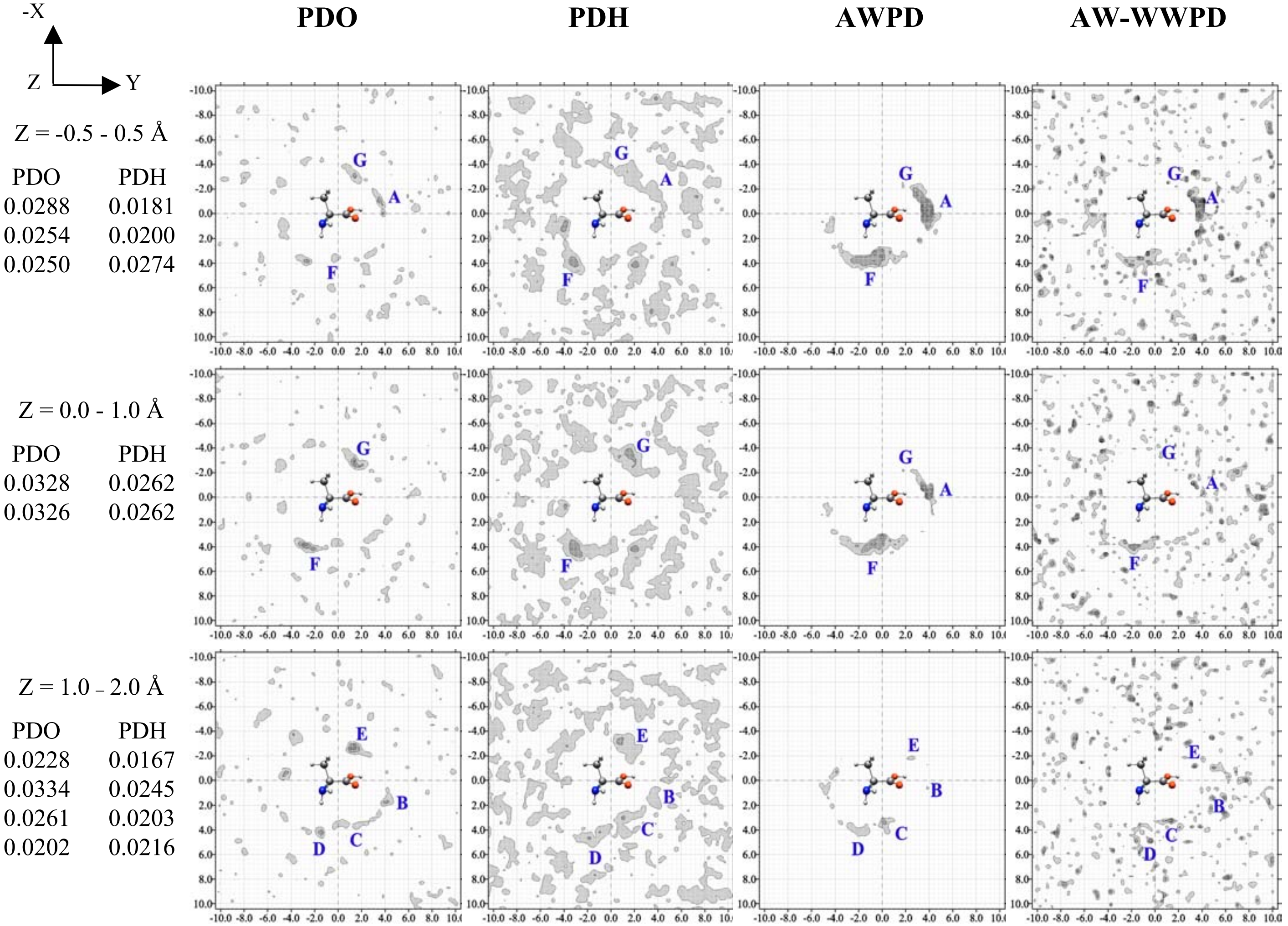

a) Z = -0.5 - 0.5 Å

	PDO	PDH
A	0.0288	0.0181
G	0.0254	0.0200
F	0.0250	0.0274

	AWPD	AW-WWPD
A	-30.1073	-90.0364
G	-10.5333	-70.5165
F	-24.0478	-83.7081

b) Z = 0.0 - 1.0 Å

	PDO	PDH
G	0.0328	0.0262
F	0.0326	0.0262

	AWPD	AW-WWPD
A	-29.6283	-78.3999
G	-10.1895	-65.0339
F	-21.3742	-71.8585

c) Z = 1.0 - 2.0 Å

	PDO	PDH
B	0.0228	0.0167
E	0.0334	0.0245
D	0.0261	0.0203
C	0.0202	0.0216

	AWPD	AW-WWPD
B	-11.1859	-73.9314
E	-12.0690	-69.6205
D	-13.9311	-80.9307
C	-15.3418	-77.1162

Figure C.8 The PDO, PDH, AWPD and AW-WWPD maps with respect to reference plane III obtained from MD-[Ala - B]$_{aq}$.

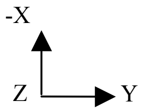

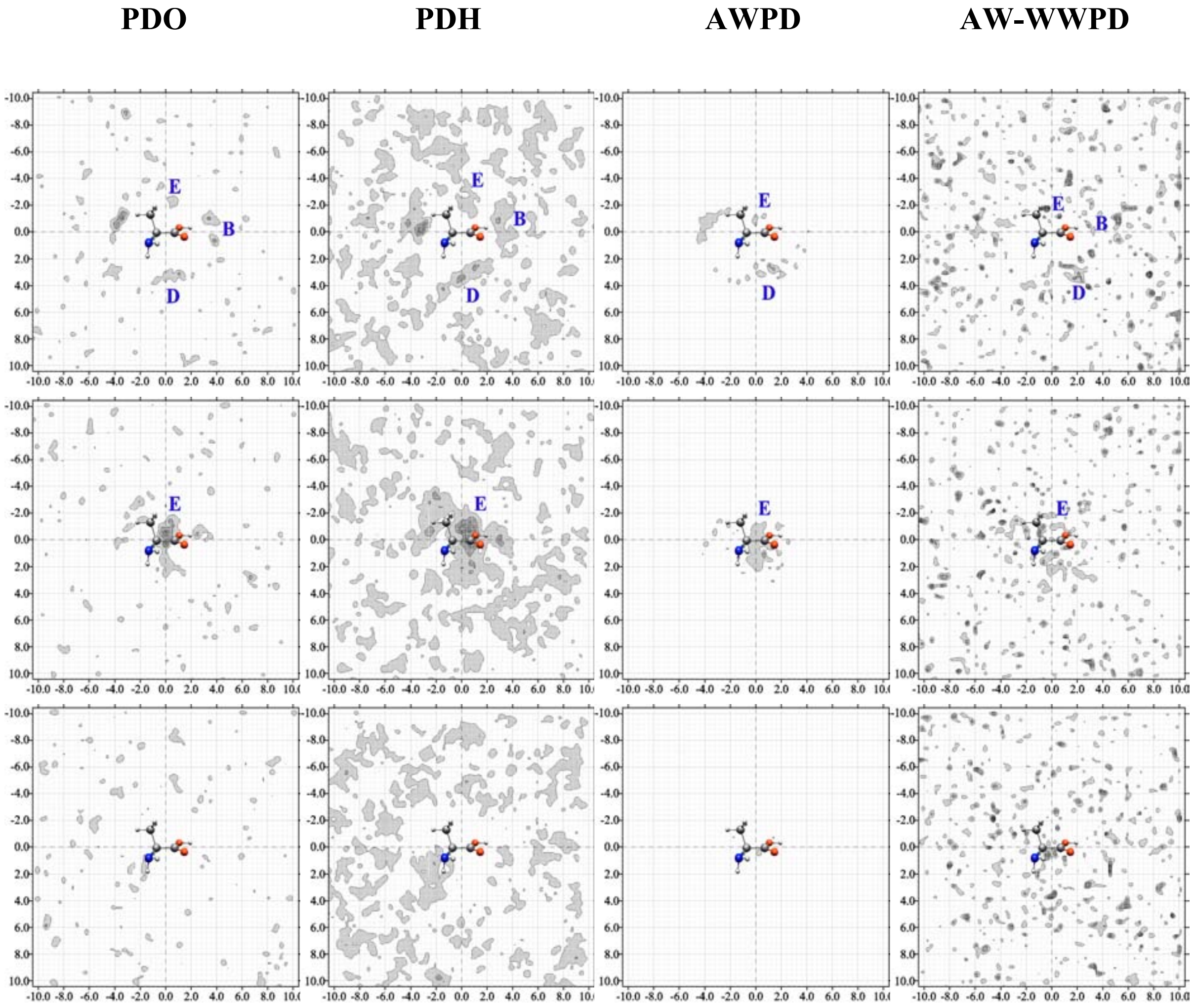

d) Z = 2.0 - 3.0 Å

	PDO	PDH
B	0.0208	0.0214
E	0.0163	0.0161
D	0.0236	0.0256

	AWPD	AW-WWPD
B	-	-68.0617
E	-12.1344	-88.9772
D	-16.4382	-72.5560

e) Z = 3.0 - 4.0 Å

	PDO	PDH
E	0.0319	0.0536

	AWPD	AW-WWPD
E	-17.8058	-75.1135

f) Z = 4.0 - 5.0 Å

Figure C.8 (continued)

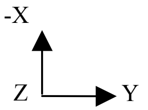

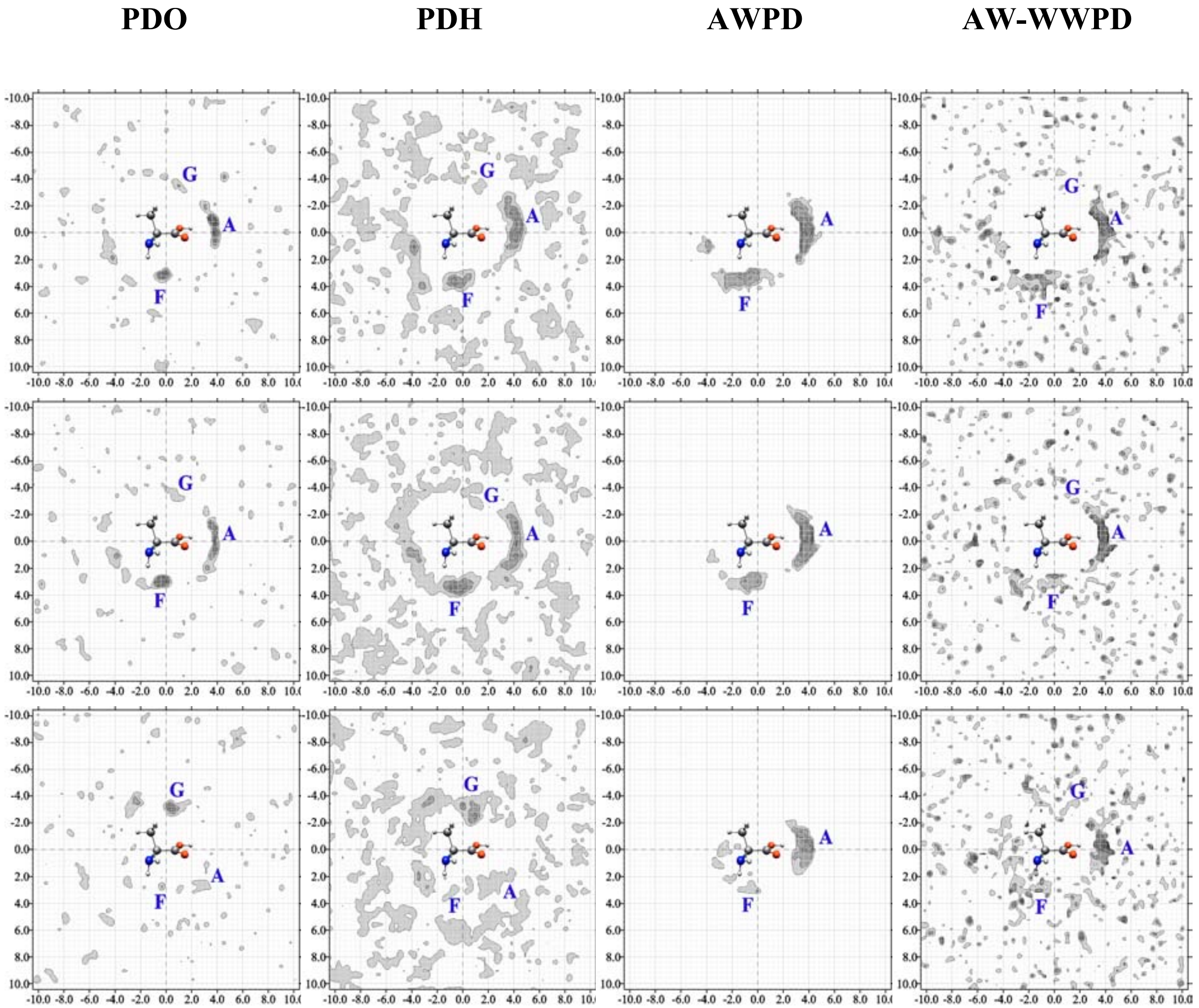

g) Z = -1.0 - 0.0 Å

	PDO	PDH
A	0.0633	0.0395
G	0.0221	0.0153
F	0.0463	0.0373

	AWPD	AW-WWPD
A	-30.9532	-79.4406
G	-	-66.1600
F	-22.2629	-77.1751

h) Z = -2.0 - -1.0 Å

	PDO	PDH
A	0.0406	0.0370
G	0.0192	0.0200
F	0.0468	0.0469

	AWPD	AW-WWPD
A	-34.6299	-84.6454
G	-	-67.8306
F	-19.0008	-71.8275

i) Z = -3.0 - -2.0 Å

	PDO	PDH
A	0.0142	0.0190
G	0.0434	0.0329
F	0.0232	0.0132

	AWPD	AW-WWPD
A	-26.3067	-88.7907
G	-	-70.3191
F	-15.6607	-73.0041

Figure C.8 (continued)

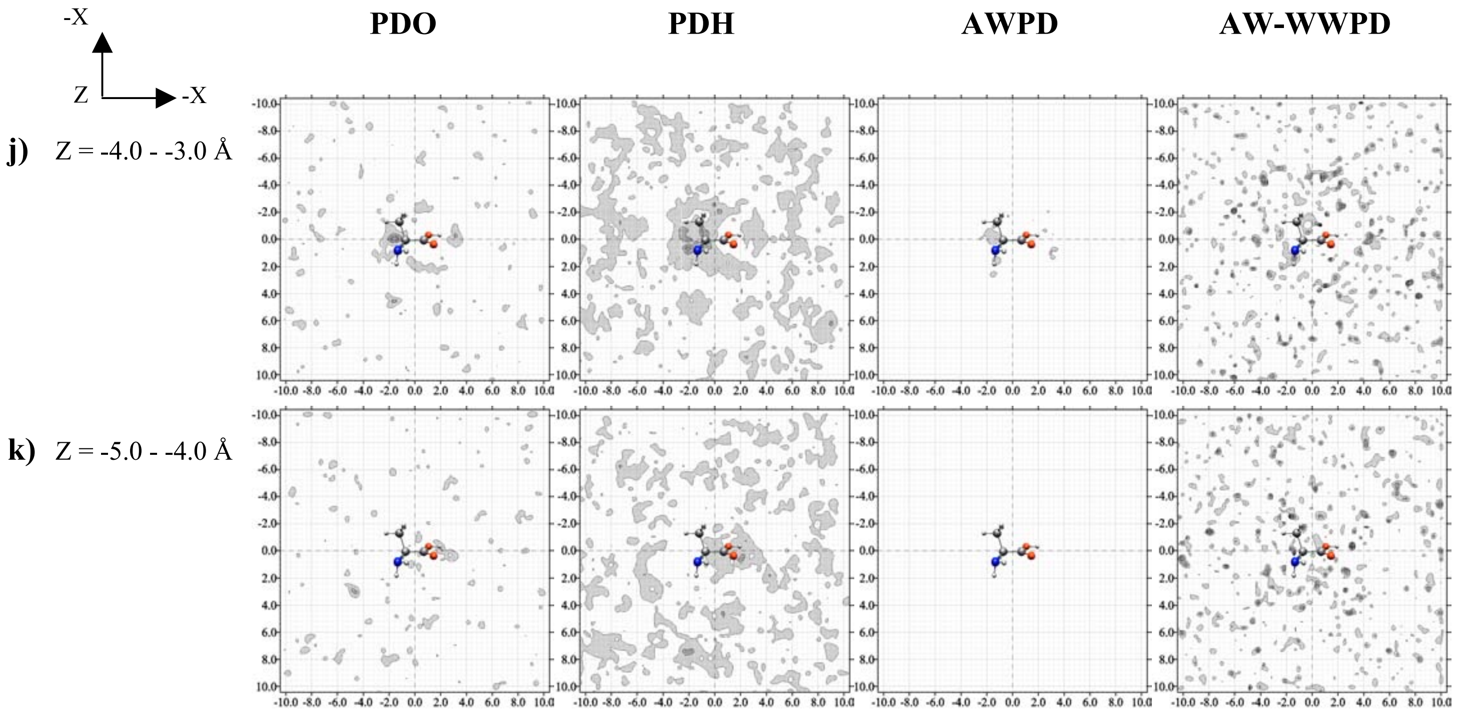

Figure C.8 (continued)

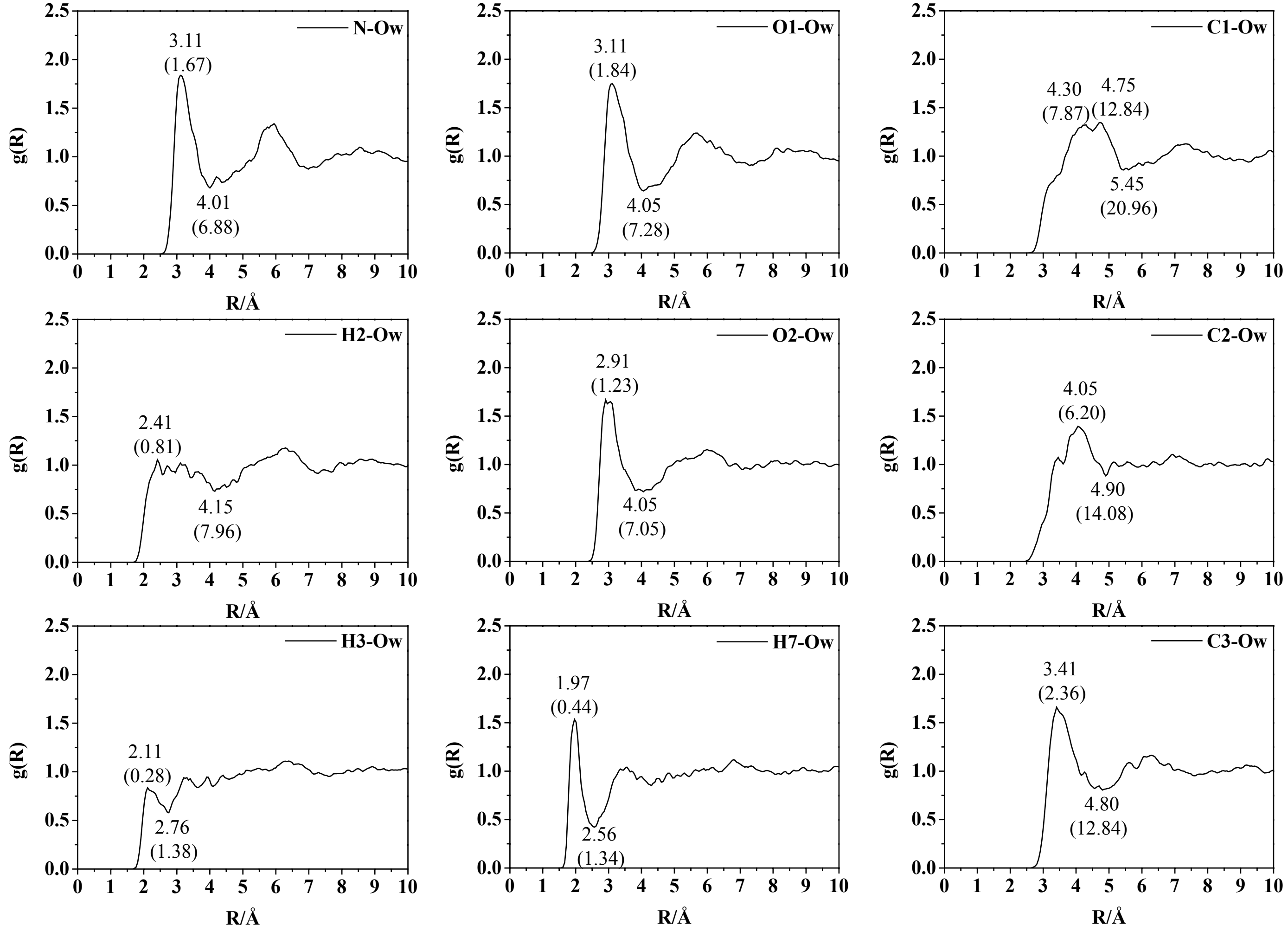

Figure C.9 g(R) obtained from MD-[Ala - C]$_{aq}$. Some characteristic distances are shown, with n(R) in parenthesis.

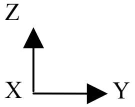

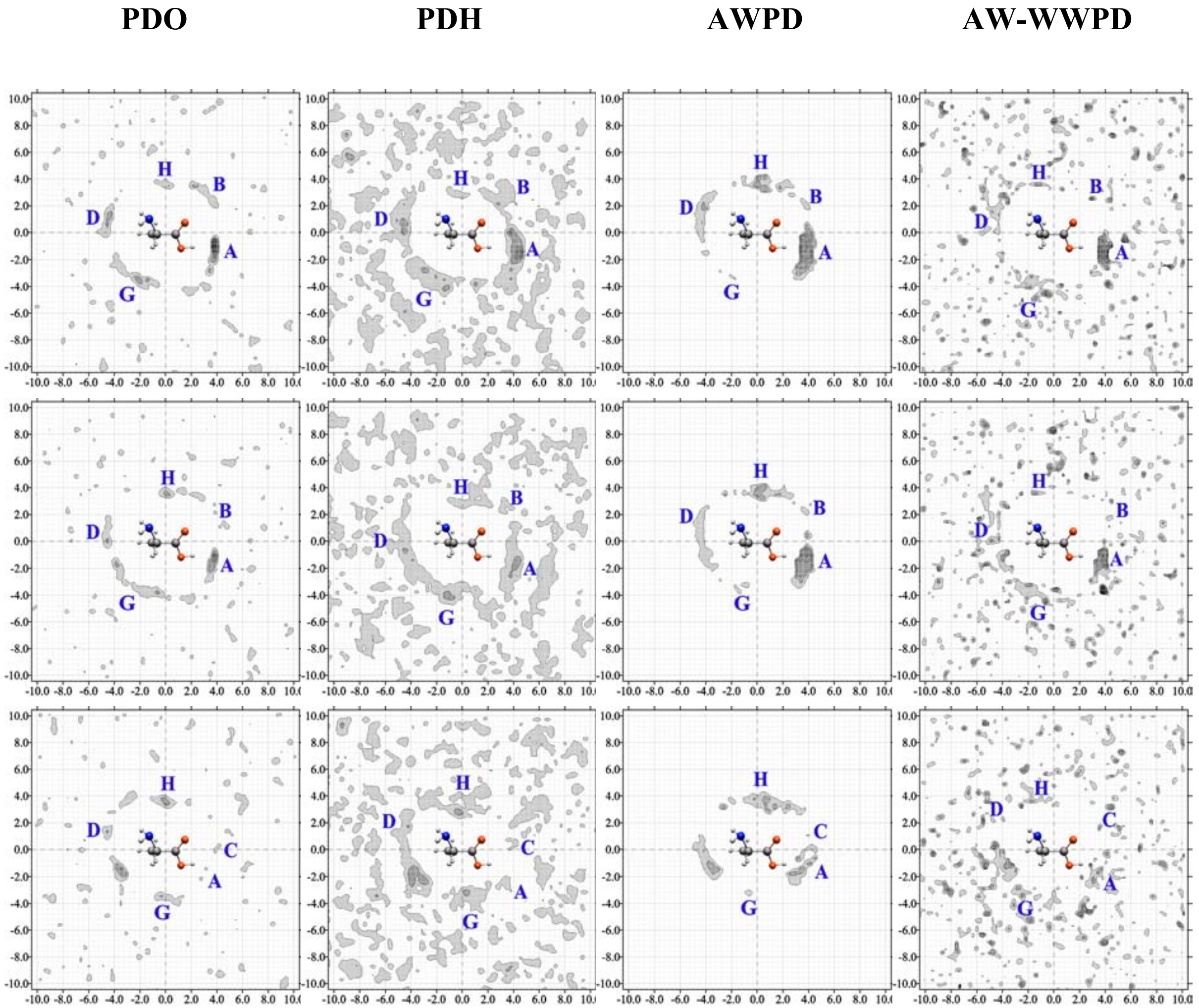

a) X = -0.5 - 0.5 Å

	PDO	PDH
A	0.0716	0.0475
B	0.0236	0.0223
H	0.0201	0.0154
D	0.0232	0.0279
G	0.0259	0.0235

	AWPD	AW-WWPD
A	-31.3260	-81.8260
B	-15.3191	-71.1968
H	-18.9028	-69.5025
D	-15.6913	-75.8639
G	-10.4567	-69.1989

b) X = 0.0 - 1.0 Å

	PDO	PDH
A	0.0450	0.0258
B	0.0129	0.0125
H	0.0224	0.0201
D	0.0228	0.0145
G	0.0228	0.0250

	AWPD	AW-WWPD
A	-30.8685	-76.8345
B	-12.7130	-68.3798
H	-17.5083	-69.1310
D	-13.1778	-71.1349
G	-12.1514	-69.9339

c) X = 1.0 – 2.0 Å

	PDO	PDH
A	0.0118	0.0139
C	0.0116	0.0111
H	0.0256	0.0270
D	0.0211	0.0221
G	0.0219	0.0266

	AWPD	AW-WWPD
A	-19.6442	-71.9594
C	-10.4364	-67.4754
H	-19.3391	-66.5390
D	-	-66.9940
G	-11.7530	-67.1738

Figure C.10 The PDO, PDH, AWPD and AW-WWPD maps with respect to reference plane I obtained from MD-[Ala - C]$_{aq}$.

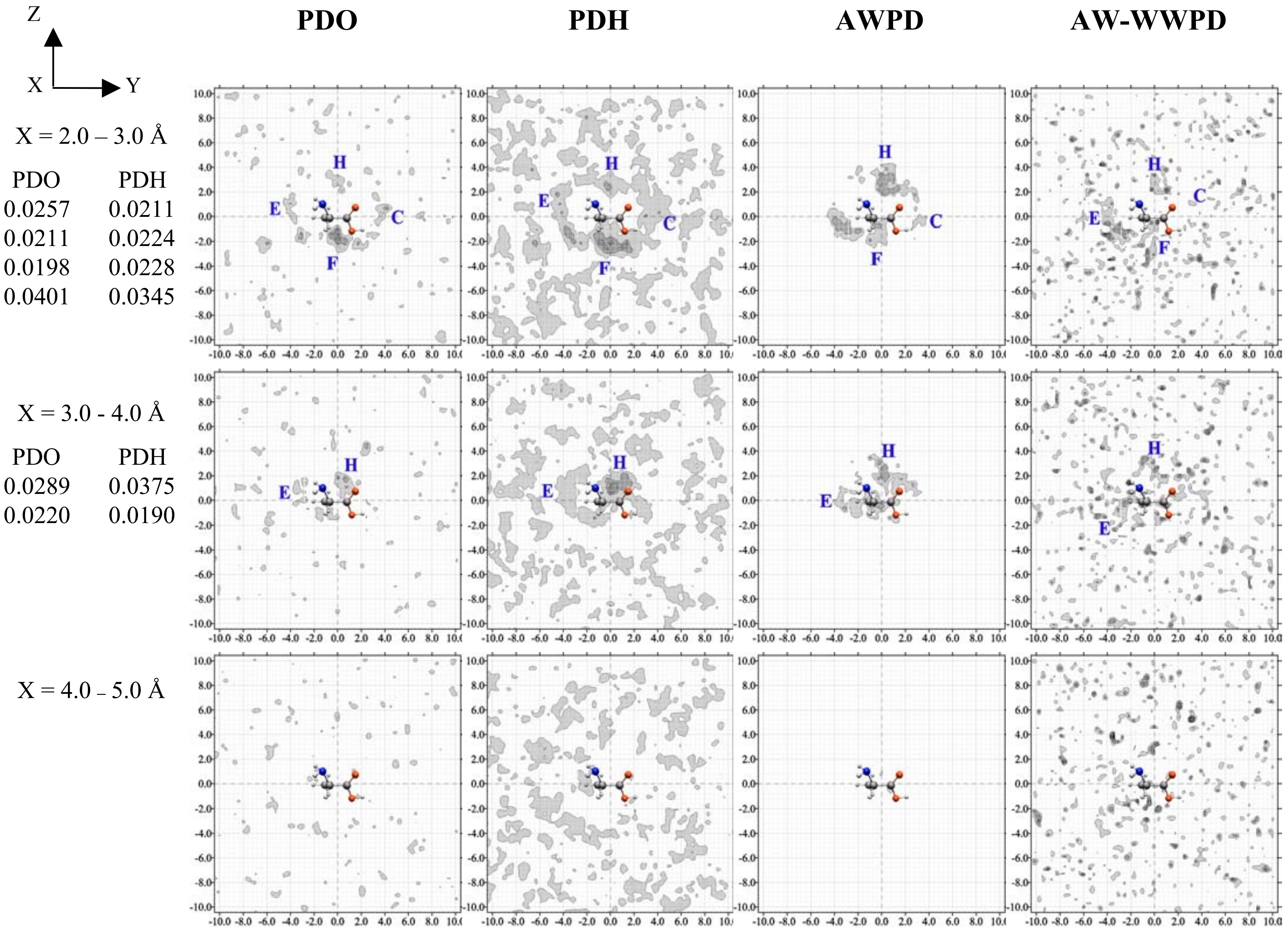

d) X = 2.0 – 3.0 Å

	PDO	PDH
C	0.0257	0.0211
H	0.0211	0.0224
E	0.0198	0.0228
F	0.0401	0.0345

	AWPD	AW-WWPD
C	-14.3262	-66.5419
H	-18.8487	-70.1921
E	-	-70.3969
F	-18.3220	-80.3942

e) X = 3.0 - 4.0 Å

	PDO	PDH
H	0.0289	0.0375
E	0.0220	0.0190

	AWPD	AW-WWPD
H	-18.5317	-73.7014
E	-19.1703	-74.7981

f) X = 4.0 – 5.0 Å

Figure C.10 (continued)

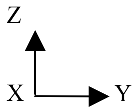

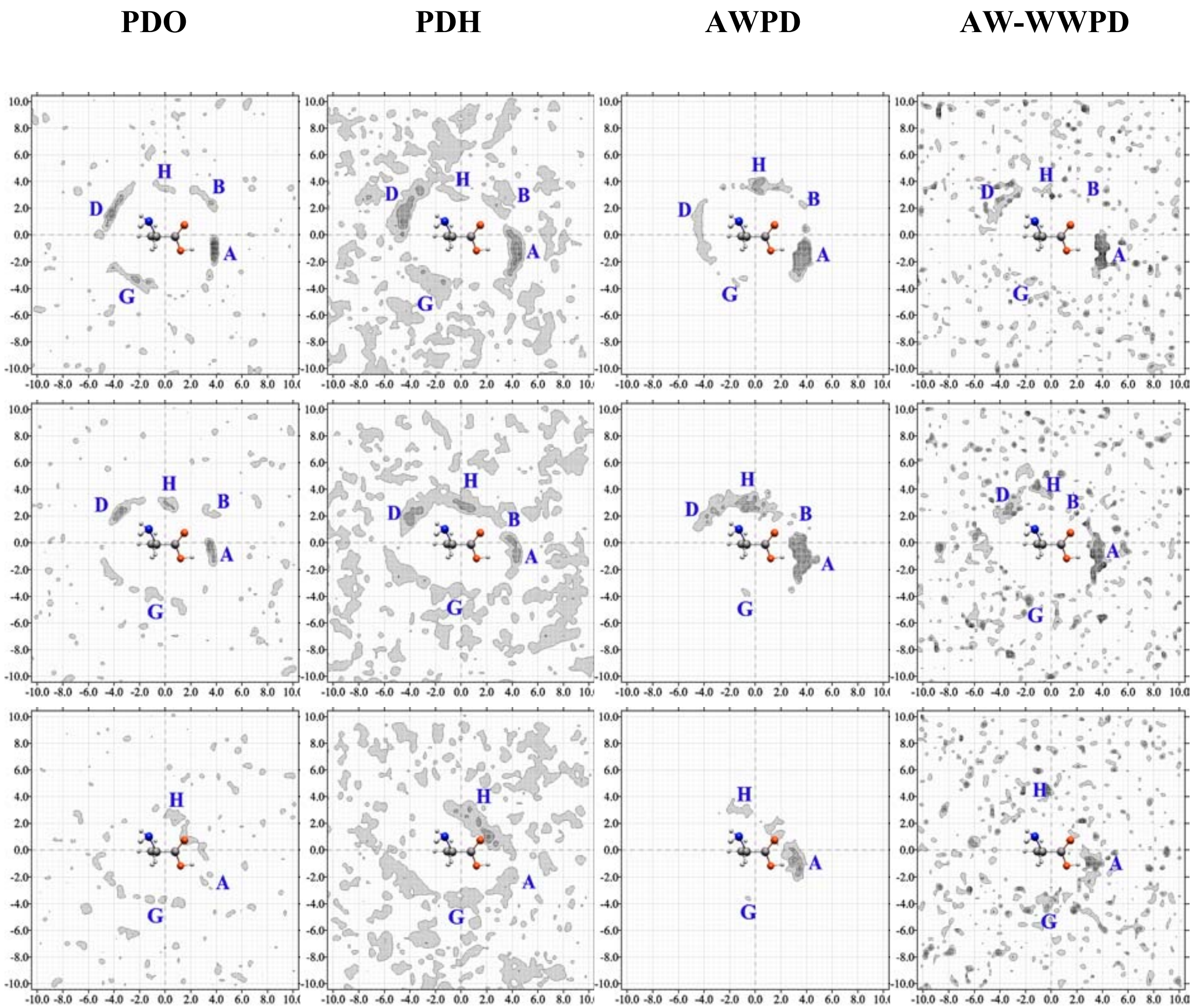

g) X = -1.0 - 0.0 Å

	PDO	PDH
A	0.0653	0.0408
B	0.0236	0.0204
H	0.0168	0.0190
D	0.0389	0.0363
G	0.0237	0.0242

	AWPD	AW-WWPD
A	-30.6826	-81.2862
B	-12.3007	-70.9732
H	-26.0827	-89.0372
D	-16.2363	-72.0821
G	-11.5632	-69.1692

h) X = -2.0 - -1.0 Å

	PDO	PDH
A	0.0362	0.0265
B	0.0188	0.0170
H	0.0213	0.0274
D	0.0320	0.0257
G	0.0185	0.0182

	AWPD	AW-WWPD
A	-26.9367	-79.7026
B	-13.4052	-72.5990
H	-24.1335	-79.4267
D	-15.4896	-73.2884
G	-11.9218	-65.8469

i) X = -3.0 - -2.0 Å

	PDO	PDH
A	0.0153	0.0206
H	0.0198	0.0219
G	0.0145	0.0189

	AWPD	AW-WWPD
A	-20.9917	-77.9030
H	-12.2038	-65.4459
G	-10.4409	-68.6642

Figure C.10 (continued)

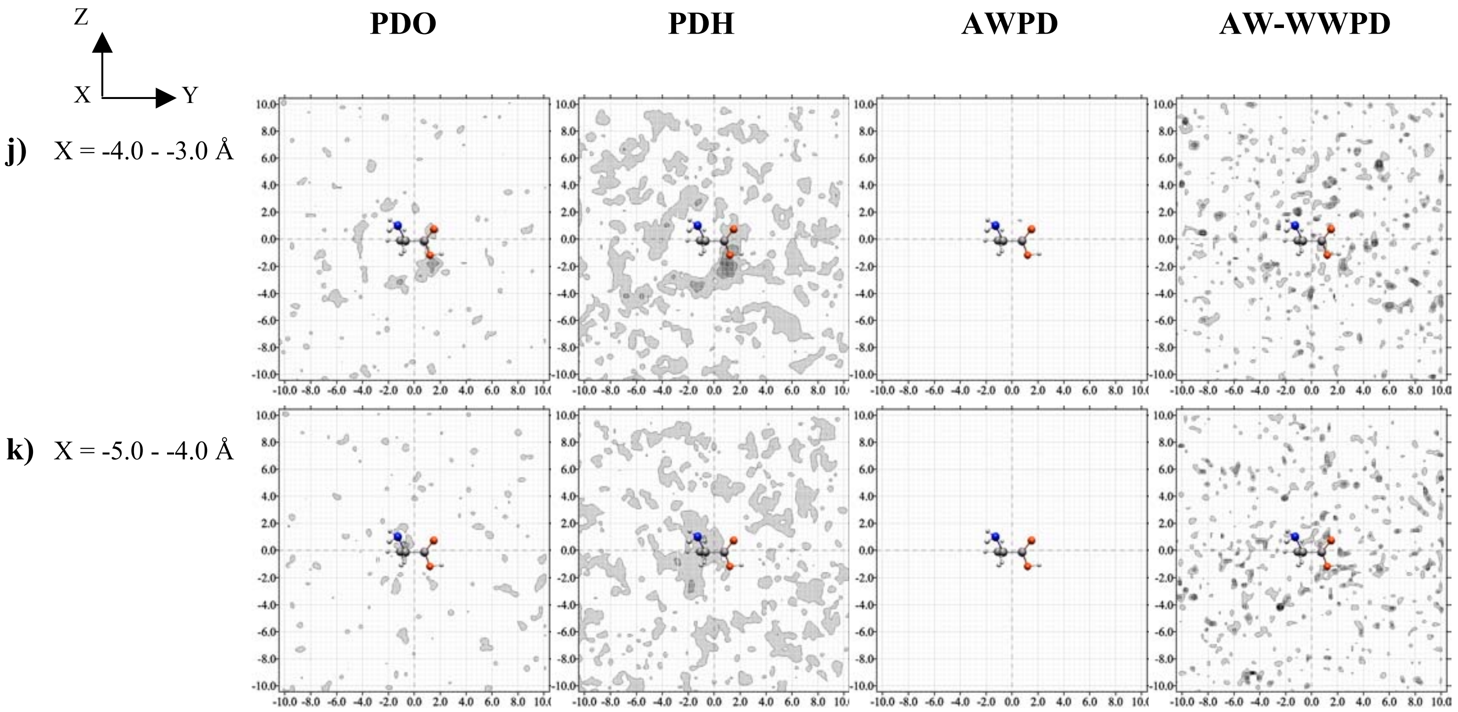

Figure C.10 (continued)

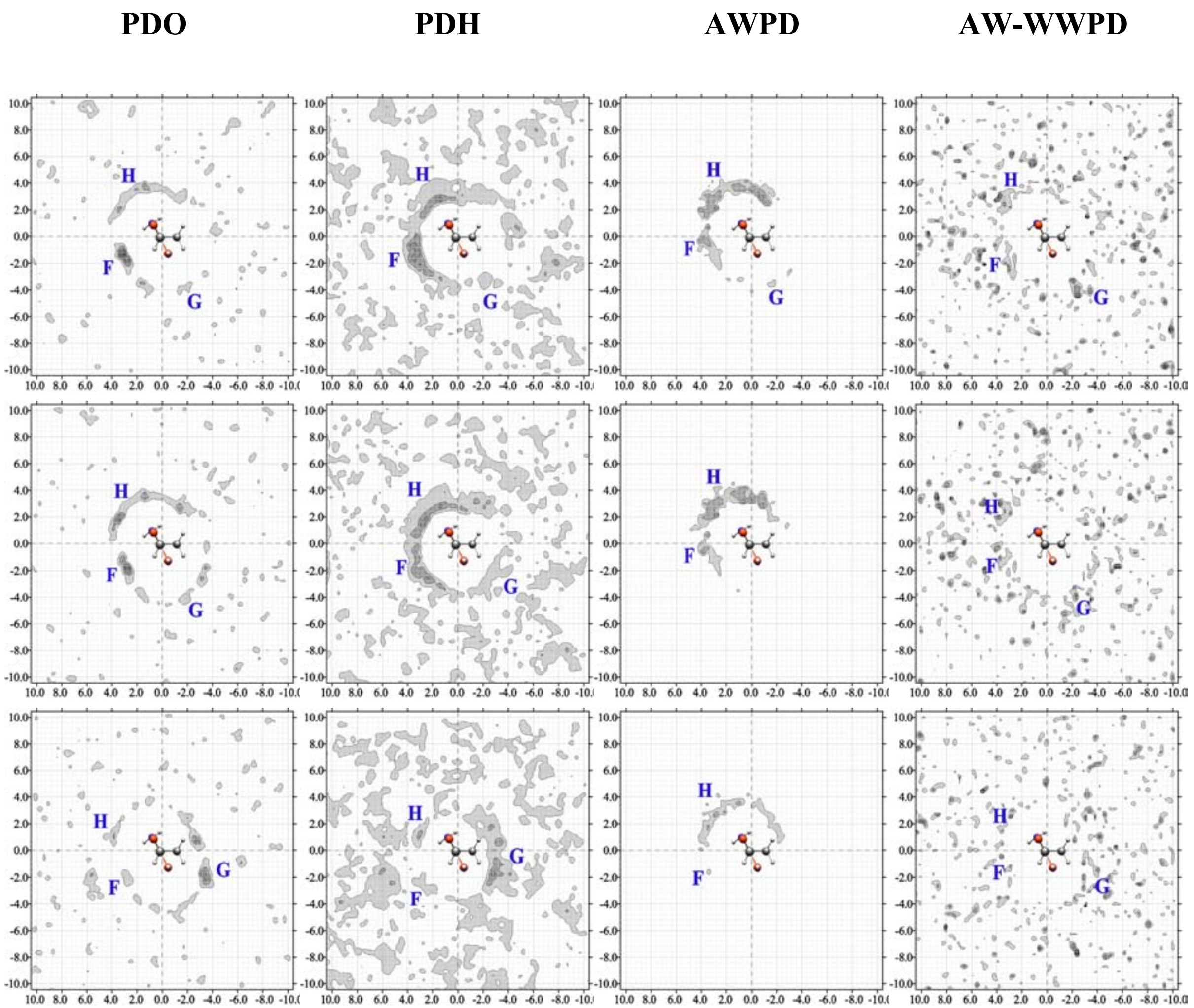

a) Y = -0.5 - 0.5 Å

	PDO	PDH
H	0.0238	0.0366
F	0.0606	0.0345
G	0.0153	0.0163

	AWPD	AW-WWPD
H	-21.0949	-75.7591
F	-20.5029	-70.2815
G	-11.8865	-71.5120

b) Y = 0.0 - 1.0 Å

	PDO	PDH
H	0.0407	0.0363
F	0.0514	0.0318
G	0.0168	0.0173

	AWPD	AW-WWPD
H	-21.0949	-73.7927
F	-19.7607	-71.8541
G	-	-70.7319

c) Y = 1.0 – 2.0 Å

	PDO	PDH
H	0.0205	0.0223
F	0.0189	0.0182
G	0.0341	0.0363

	AWPD	AW-WWPD
H	-16.3109	-71.2429
F	-11.1136	-66.3847
G	-	-70.0958

Figure C.11 The PDO, PDH, AWPD and AW-WWPD maps with respect to reference plane II obtained from MD-[Ala - C]$_{aq}$.

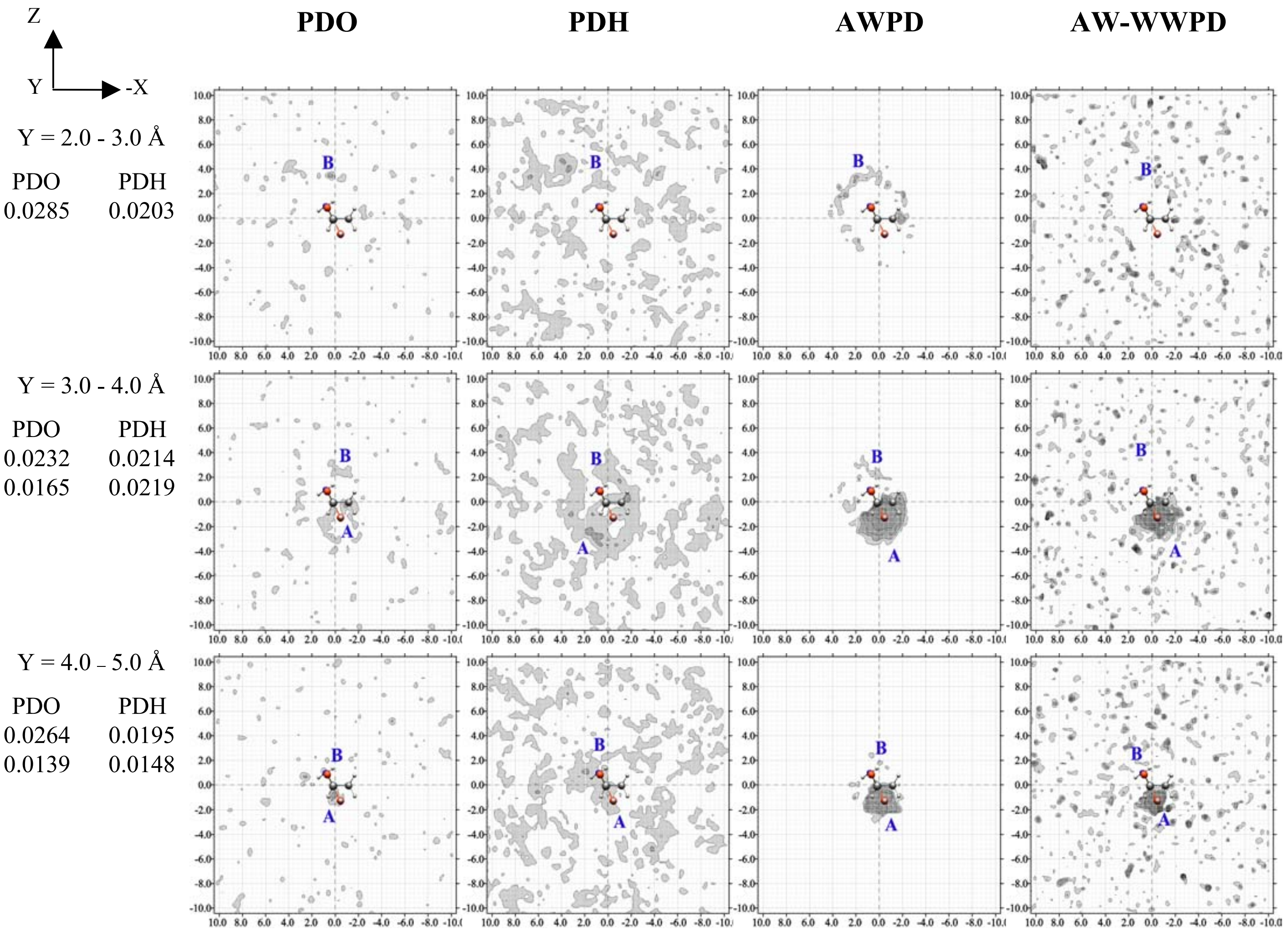

d) Y = 2.0 - 3.0 Å

	PDO	PDH	AWPD	AW-WWPD
B	0.0285	0.0203	-15.1517	-67.7630

e) Y = 3.0 - 4.0 Å

	PDO	PDH	AWPD	AW-WWPD
A	0.0232	0.0214	-33.0249	-86.3783
B	0.0165	0.0219	-13.2974	-70.3245

f) Y = 4.0 – 5.0 Å

	PDO	PDH	AWPD	AW-WWPD
A	0.0264	0.0195	-29.2872	-85.4210
B	0.0139	0.0148	-15.0078	-69.1360

Figure C.11 (continued)

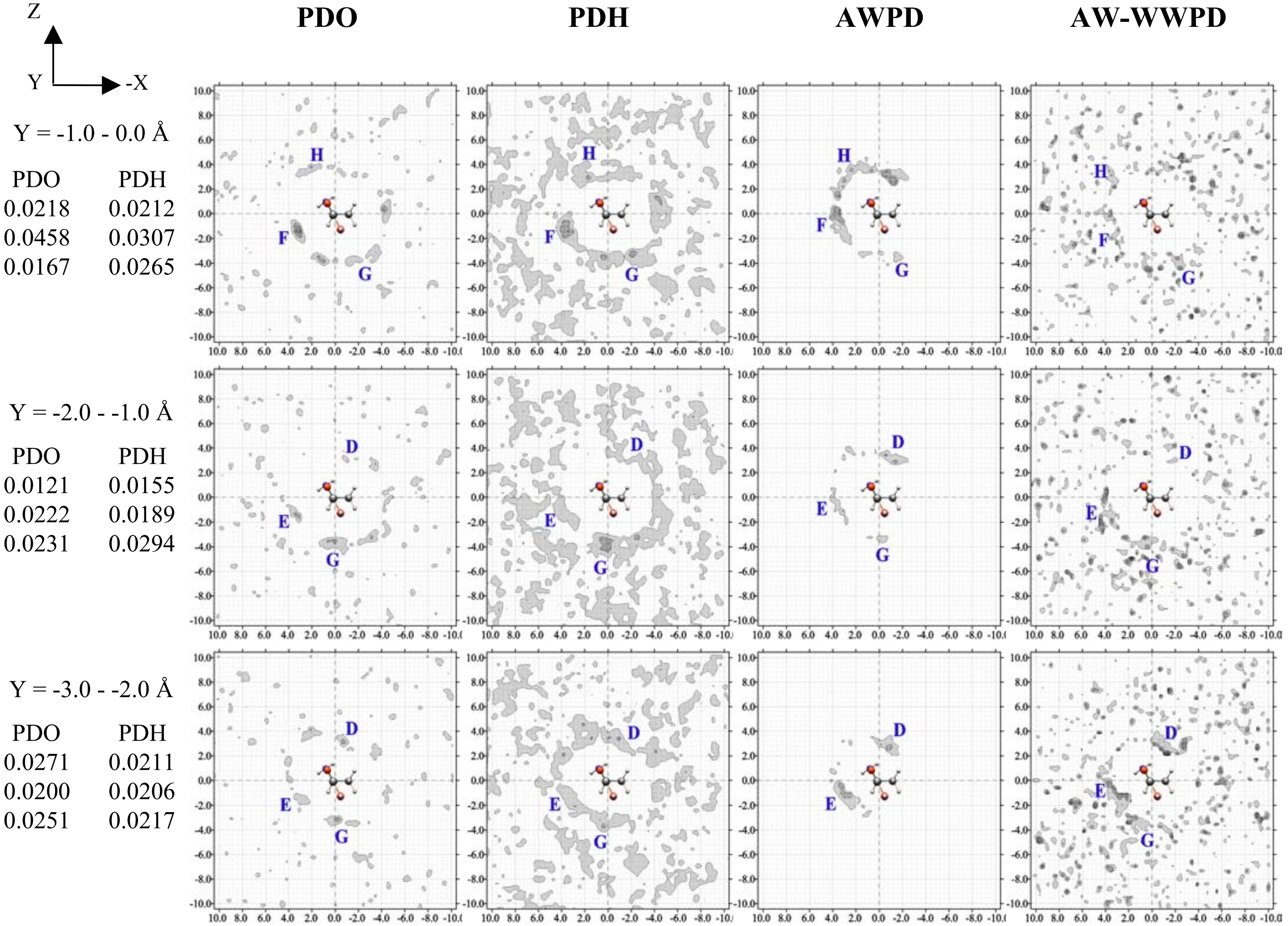

g) Y = -1.0 - 0.0 Å

	PDO	PDH
H	0.0218	0.0212
F	0.0458	0.0307
G	0.0167	0.0265

	AWPD	AW-WWPD
H	-20.2840	-70.3192
F	-21.1742	-70.5840
G	-13.5414	-74.0034

h) Y = -2.0 - -1.0 Å

	PDO	PDH
D	0.0121	0.0155
E	0.0222	0.0189
G	0.0231	0.0294

	AWPD	AW-WWPD
D	-16.0060	-67.6809
E	-15.2678	-76.1202
G	-12.4858	-72.2738

i) Y = -3.0 - -2.0 Å

	PDO	PDH
D	0.0271	0.0211
E	0.0200	0.0206
G	0.0251	0.0217

	AWPD	AW-WWPD
D	-16.3725	-80.5251
E	-17.0127	-74.0402
G	-	-67.8787

Figure C.11 (continued)

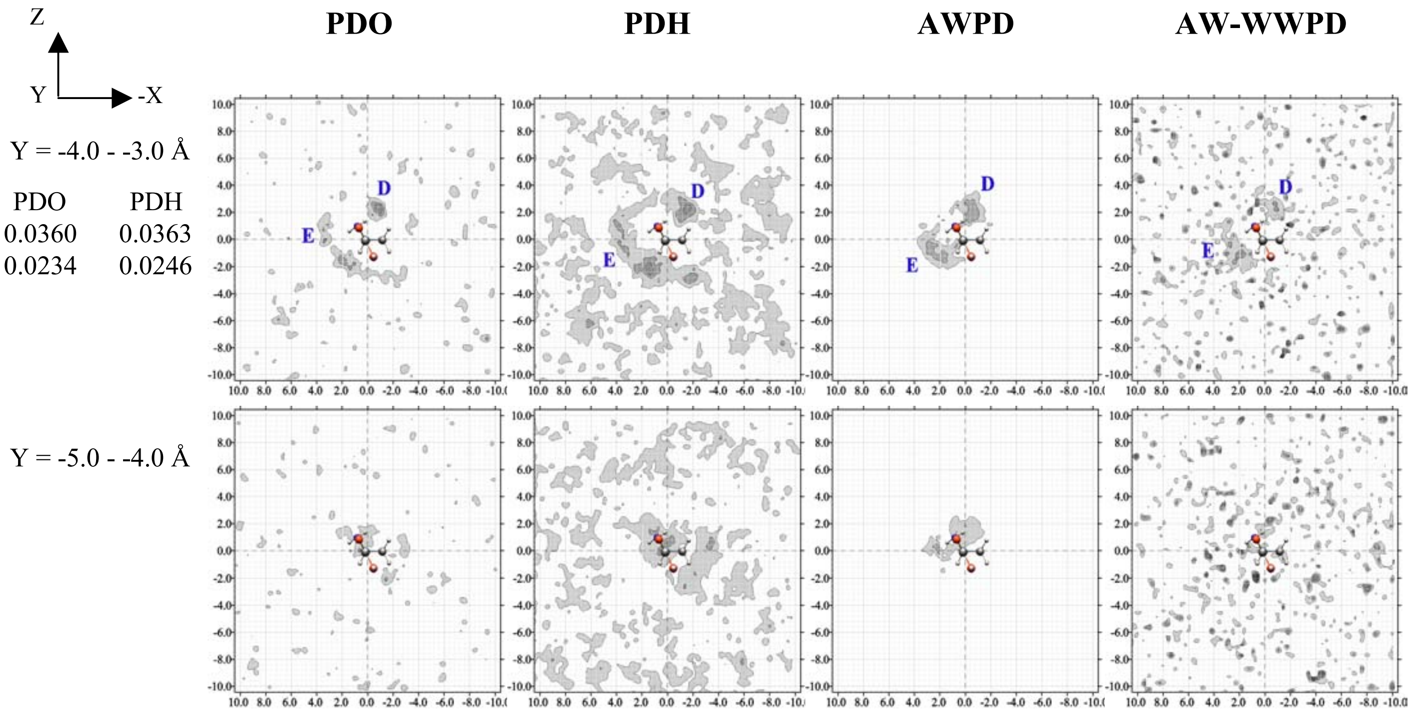

j) Y = -4.0 - -3.0 Å

	PDO	PDH
D	0.0360	0.0363
E	0.0234	0.0246

	AWPD	AW-WWPD
D	-16.6960	-78.0767
E	-16.4381	-74.1860

k) Y = -5.0 - -4.0 Å

Figure C.11 (continued)

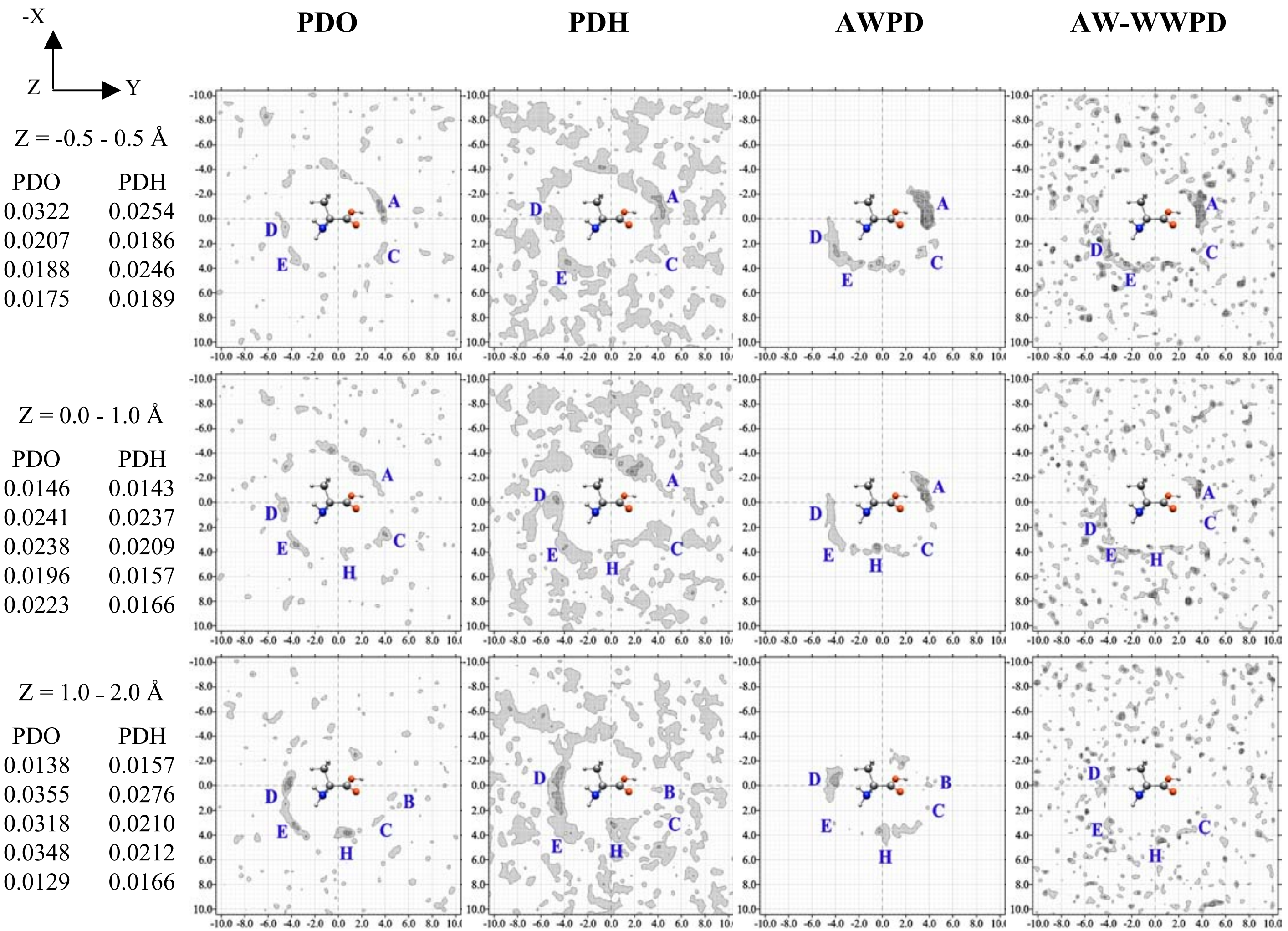

a) Z = -0.5 - 0.5 Å

	PDO	PDH
A	0.0322	0.0254
D	0.0207	0.0186
E	0.0188	0.0246
C	0.0175	0.0189

	AWPD	AW-WWPD
A	-31.0770	-80.5323
D	-13.9285	-70.1861
E	-16.0606	-71.9326
C	-16.3960	-80.6851

b) Z = 0.0 - 1.0 Å

	PDO	PDH
A	0.0146	0.0143
D	0.0241	0.0237
E	0.0238	0.0209
H	0.0196	0.0157
C	0.0223	0.0166

	AWPD	AW-WWPD
A	-28.4364	-76.5807
D	-14.3711	-72.1090
E	-13.7885	-69.4112
H	-20.3950	-70.6389
C	-11.7114	-67.3522

c) Z = 1.0 – 2.0 Å

	PDO	PDH
B	0.0138	0.0157
D	0.0355	0.0276
E	0.0318	0.0210
H	0.0348	0.0212
C	0.0129	0.0166

	AWPD	AW-WWPD
B	-12.9052	-
D	-16.7347	-70.3674
E	-10.1206	-72.0782
H	-17.6549	-78.8325
C	-14.2451	-73.9802

Figure C.12 The PDO, PDH, AWPD and AW-WWPD maps with respect to reference plane III obtained from MD-[Ala - C]$_{aq}$.

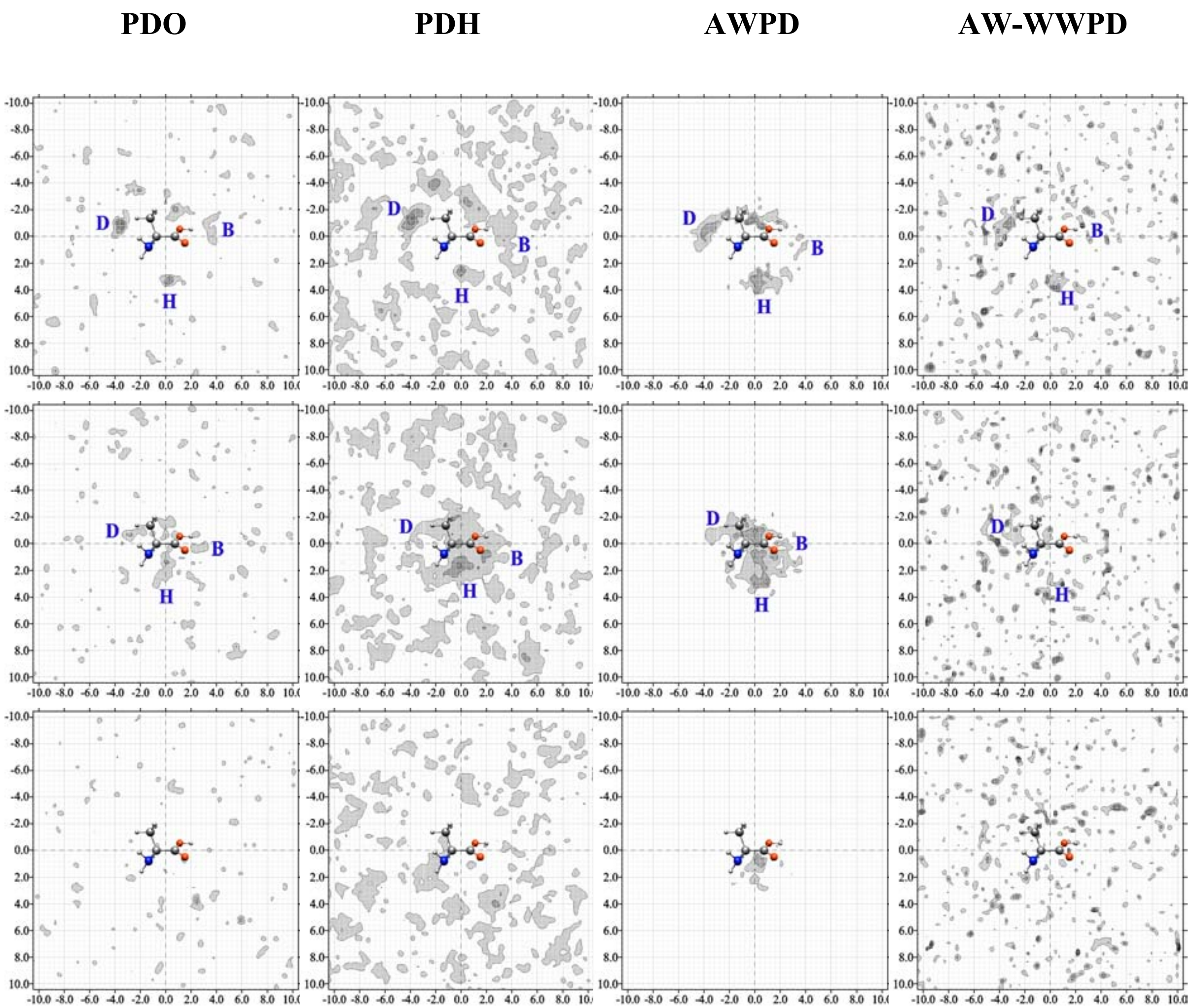

d) Z = 2.0 - 3.0 Å

	PDO	PDH
B	0.0175	0.0197
D	0.0393	0.0409
H	0.0310	0.0305

	AWPD	AW-WWPD
B	-13.3998	-71.6676
D	-17.0512	-71.6840
H	-17.7658	-77.8214

e) Z = 3.0 - 4.0 Å

	PDO	PDH
B	0.0182	0.0240
D	0.0236	0.0186
H	0.0224	0.0312

	AWPD	AW-WWPD
B	-15.2999	-69.7894
D	-14.9604	-73.4474
H	-19.7376	-77.7121

f) Z = 4.0 - 5.0 Å

Figure C.12 (continued)

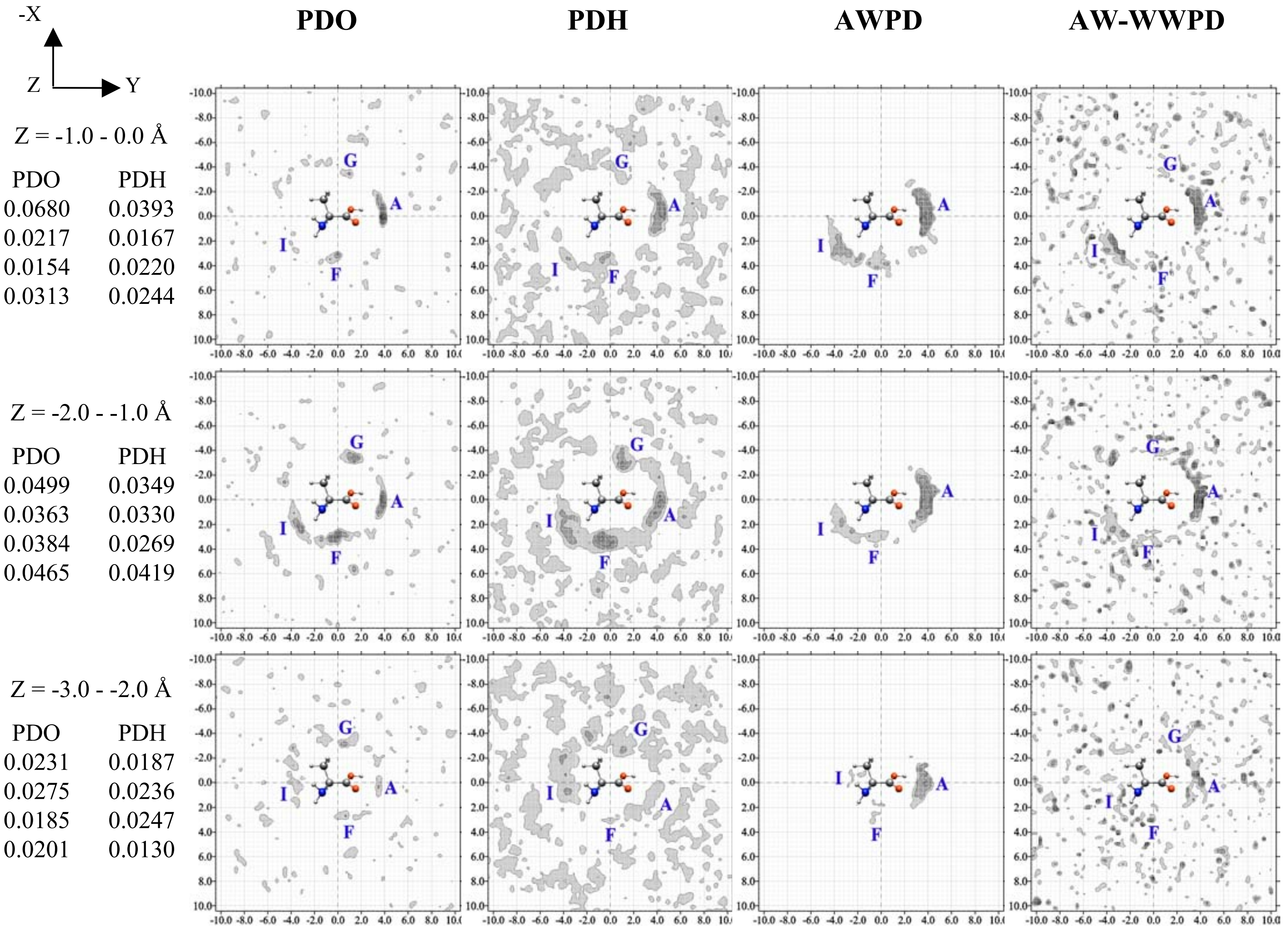

g) Z = -1.0 - 0.0 Å

	PDO	PDH
A	0.0680	0.0393
G	0.0217	0.0167
I	0.0154	0.0220
F	0.0313	0.0244

	AWPD	AW-WWPD
A	-325956	-79.9055
G	-	-67.7084
I	-18.3538	-77.1010
F	-16.7762	-75.1545

h) Z = -2.0 - -1.0 Å

	PDO	PDH
A	0.0499	0.0349
G	0.0363	0.0330
I	0.0384	0.0269
F	0.0465	0.0419

	AWPD	AW-WWPD
A	-28.6435	-80.8745
G	-	-69.9221
I	-15.9736	-74.7128
F	-14.1109	-73.0392

i) Z = -3.0 - -2.0 Å

	PDO	PDH
A	0.0231	0.0187
G	0.0275	0.0236
I	0.0185	0.0247
F	0.0201	0.0130

	AWPD	AW-WWPD
A	-24.4033	-77.6856
G	-	-78.2875
I	-12.4850	-74.6539
F	-13.2742	-78.1299

Figure C.12 (continued)

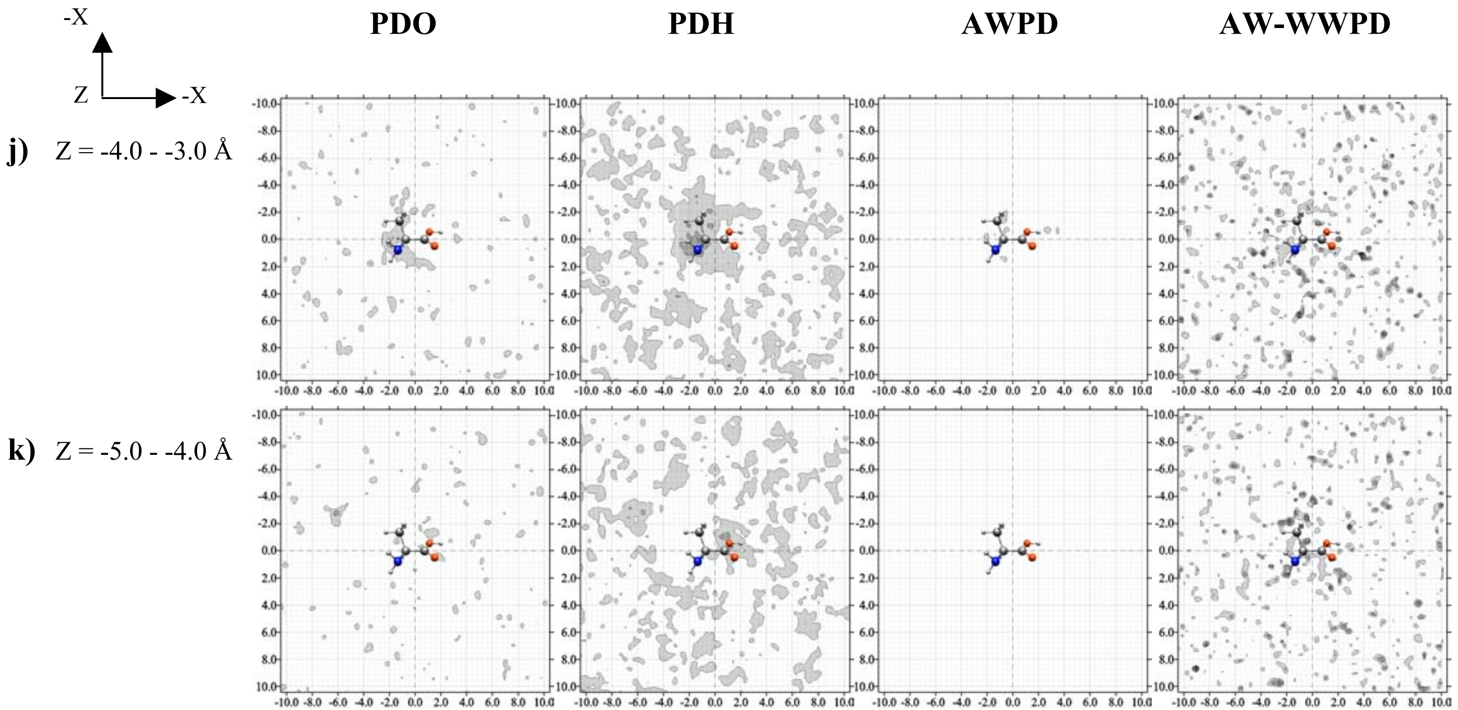

Figure C.12 (continued)

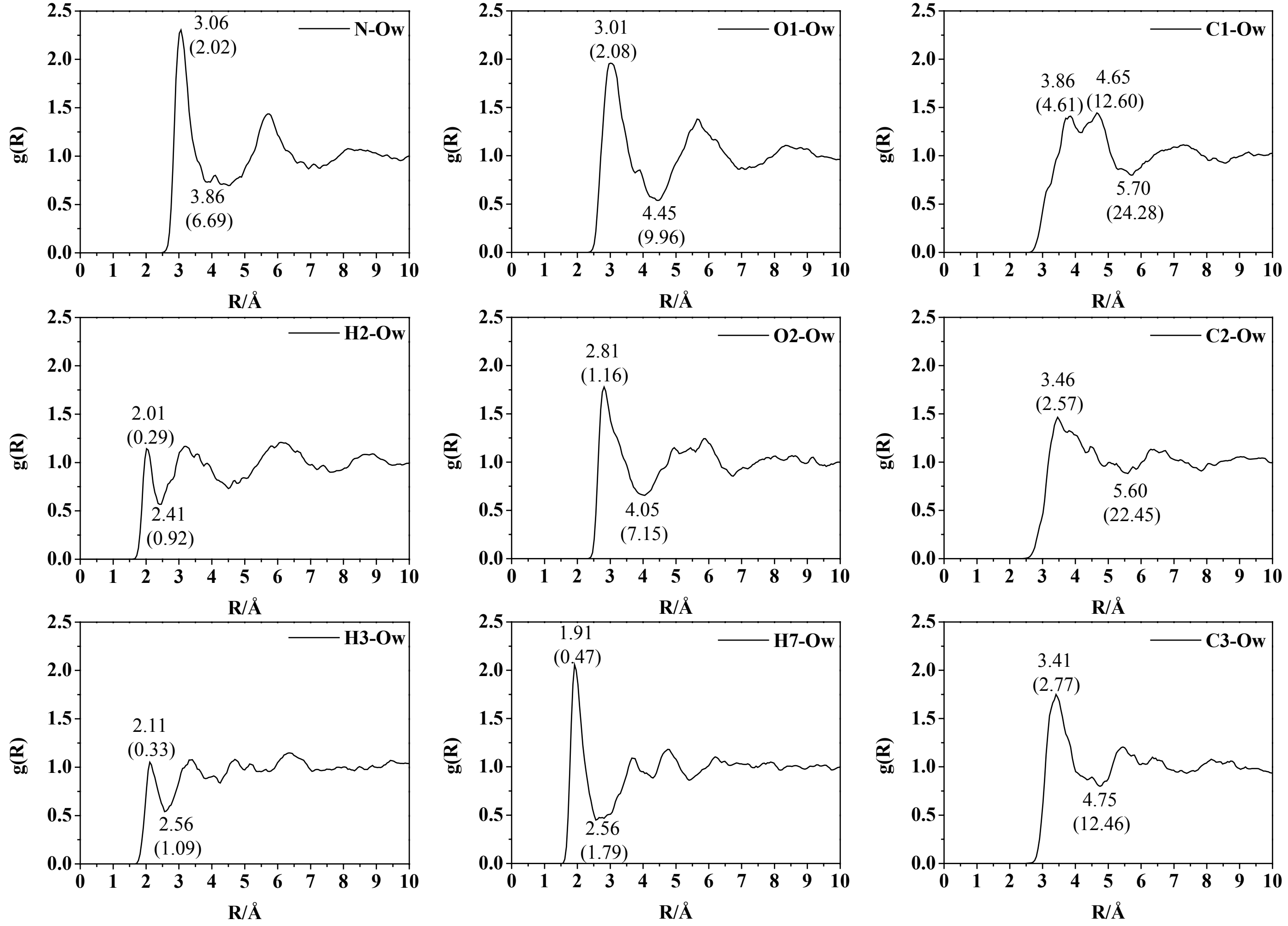

Figure C.13 g(R) obtained from MD-[Li$^+$/Ala - C]$_{aq}$. Some characteristic distances are shown, with n(R) in parenthesis.

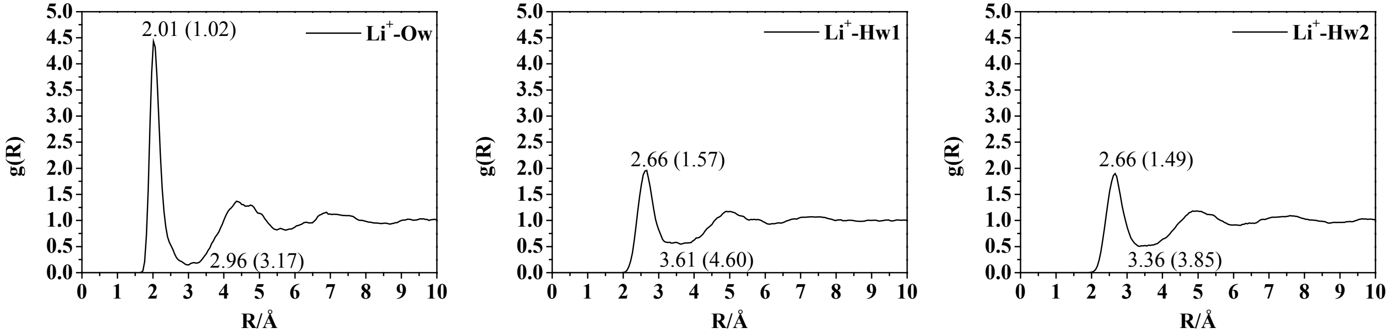

Figure C.13 (continued)

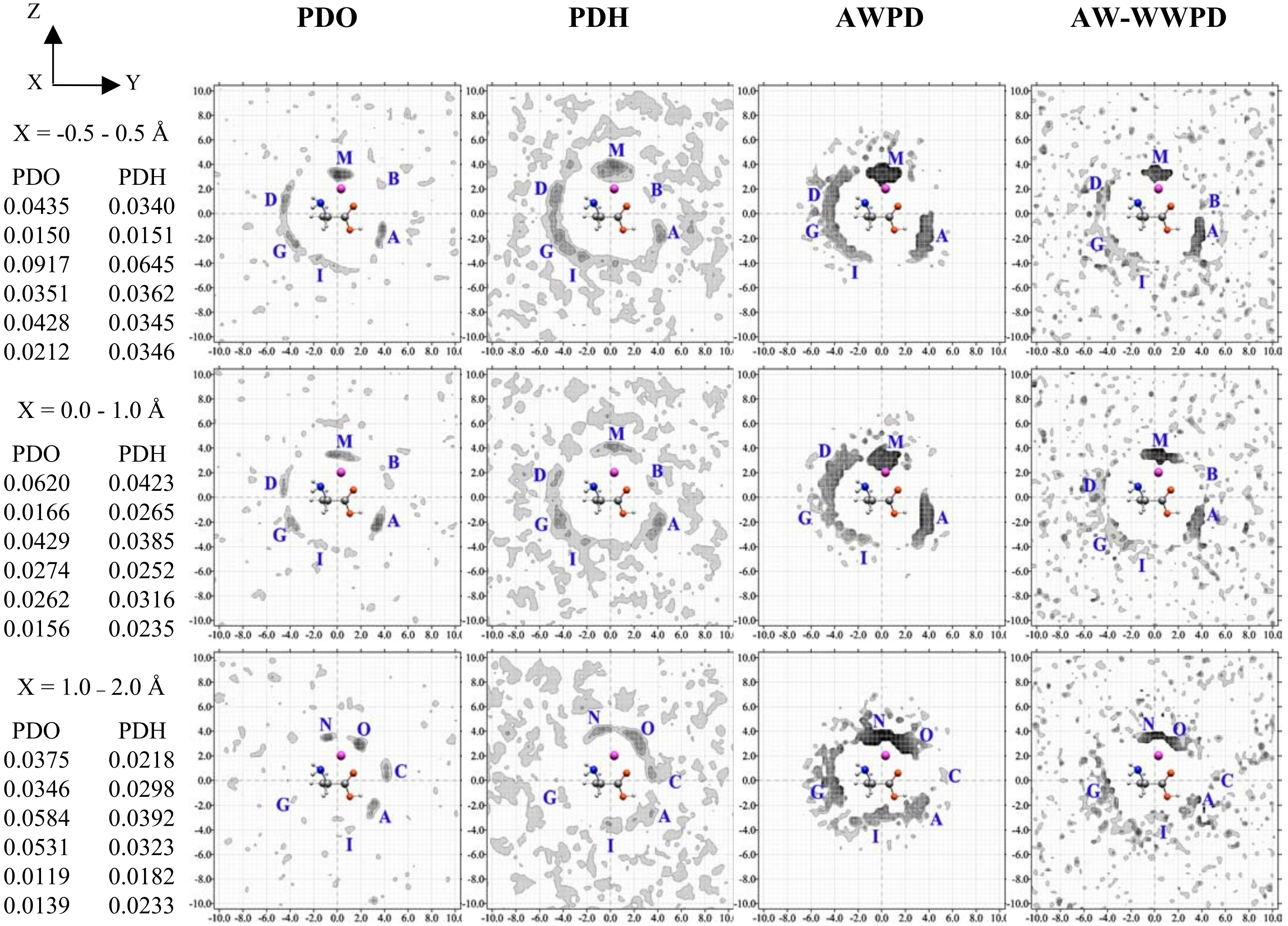

a) X = -0.5 - 0.5 Å

	PDO	PDH
A	0.0435	0.0340
B	0.0150	0.0151
M	0.0917	0.0645
D	0.0351	0.0362
G	0.0428	0.0345
I	0.0212	0.0346

	AWPD	AW-WWPD
A	-46.5555	-88.4220
B	-	-72.8093
M	-77.6275	-93.2631
D	-39.3266	-75.6041
G	-37.9641	-76.5922
I	-29.0012	-73.4805

b) X = 0.0 - 1.0 Å

	PDO	PDH
A	0.0620	0.0423
B	0.0166	0.0265
M	0.0429	0.0385
D	0.0274	0.0252
G	0.0262	0.0316
I	0.0156	0.0235

	AWPD	AW-WWPD
A	-40.1885	-82.2147
B	-	-67.5349
M	-85.4308	-107.119
D	-31.3161	-76.5281
G	-33.5841	-76.5922
I	-22.1413	-73.1394

c) X = 1.0 - 2.0 Å

	PDO	PDH
A	0.0375	0.0218
C	0.0346	0.0298
O	0.0584	0.0392
N	0.0531	0.0323
G	0.0119	0.0182
I	0.0139	0.0233

	AWPD	AW-WWPD
A	-30.0514	-81.6393
C	-13.9507	-75.0848
O	-87.3315	-90.7873
N	-86.8294	-99.3027
G	-48.9149	-85.5050
I	-34.4969	-71.5060

Figure C.14 The PDO, PDH, AWPD and AW-WWPD maps with respect to reference plane I obtained from MD-[Li$^+$/Ala - C]

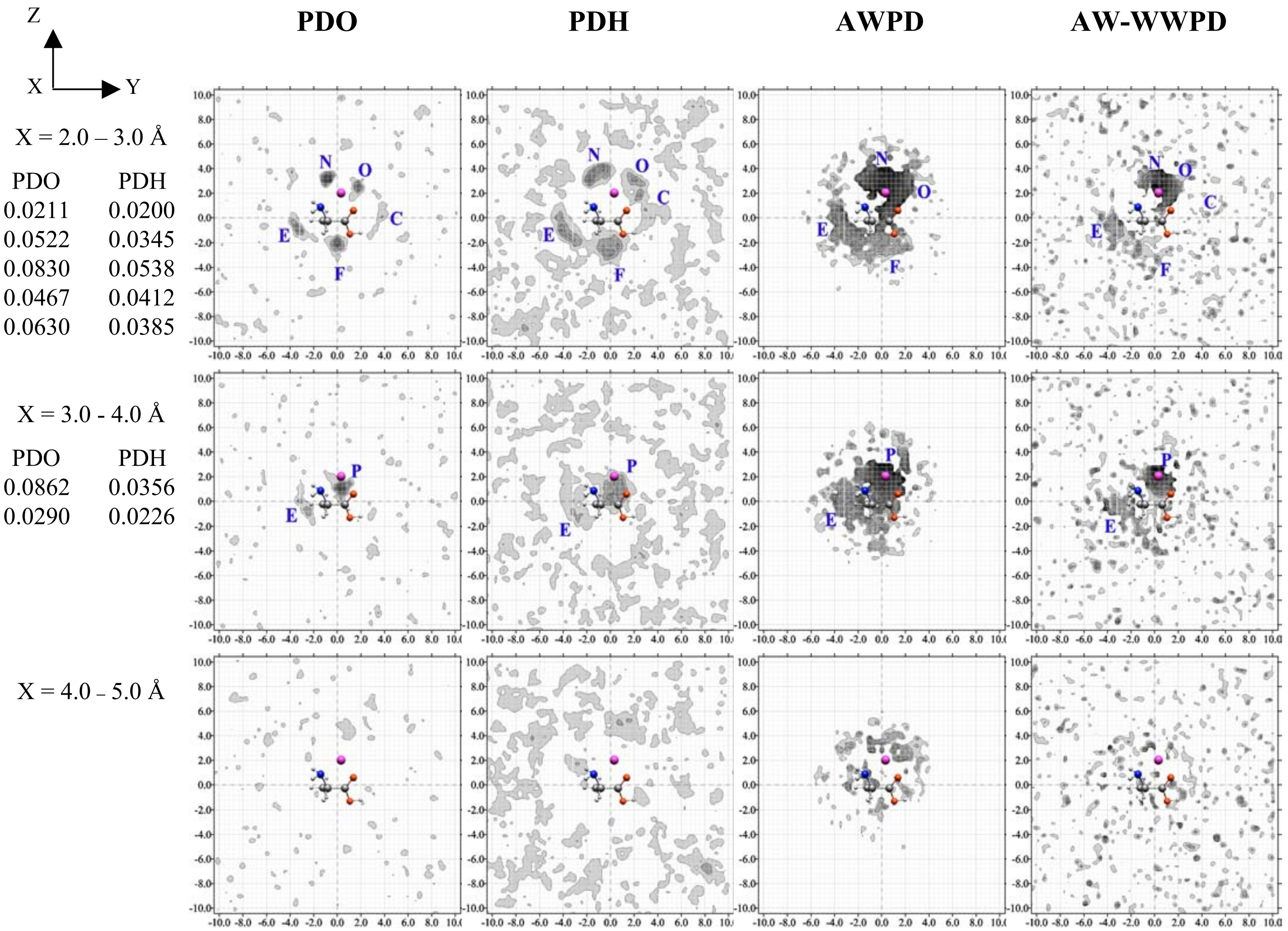

d) X = 2.0 – 3.0 Å

	PDO	PDH
C	0.0211	0.0200
O	0.0522	0.0345
N	0.0830	0.0538
E	0.0467	0.0412
F	0.0630	0.0385

	AWPD	AW-WWPD
C	-	-67.6492
O	-75.5497	-105.159
N	-92.7597	-114.642
E	-45.2805	-87.2224
F	-37.2450	-77.9196

e) X = 3.0 - 4.0 Å

	PDO	PDH
P	0.0862	0.0356
E	0.0290	0.0226

	AWPD	AW-WWPD
P	-88.5118	-111.849
E	-38.2317	-79.9939

f) X = 4.0 - 5.0 Å

Figure C.14 (continued)

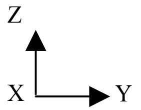

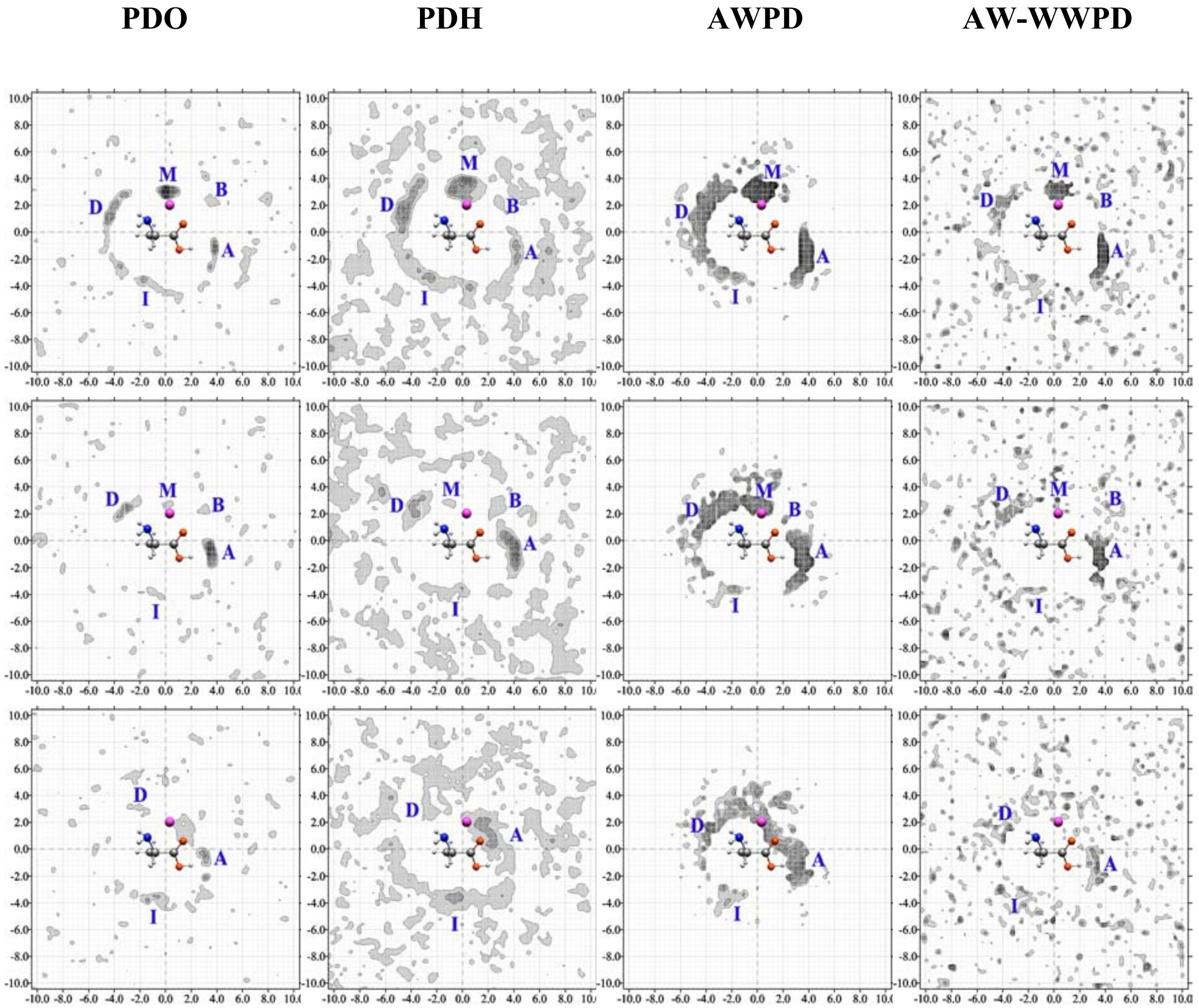

g) X = -1.0 - 0.0 Å

	PDO	PDH
A	0.0464	0.0286
B	0.0193	0.0170
M	0.1017	0.0549
D	0.0350	0.0420
I	0.0297	0.0265

	AWPD	AW-WWPD
A	-49.5756	-91.4350
B	-	-69.4621
M	-69.7434	-87.2767
D	-39.7912	-74.2824
I	-29.0012	-71.2136

h) X = -2.0 - -1.0 Å

	PDO	PDH
A	0.0749	0.0602
B	0.0154	0.0187
M	0.0195	0.0133
D	0.0406	0.0279
I	0.0170	0.0208

	AWPD	AW-WWPD
A	-45.7348	-90.4135
B	-24.9124	-67.0857
M	-41.7630	-84.3769
D	-39.5611	-73.3269
I	-20.5067	-69.3621

i) X = -3.0 - -2.0 Å

	PDO	PDH
A	0.0295	0.0193
D	0.0183	0.0194
I	0.0251	0.0256

	AWPD	AW-WWPD
A	-36.5360	-73.8493
D	-34.2893	-75.2587
I	-19.4170	-70.5464

Figure C.14 (continued)

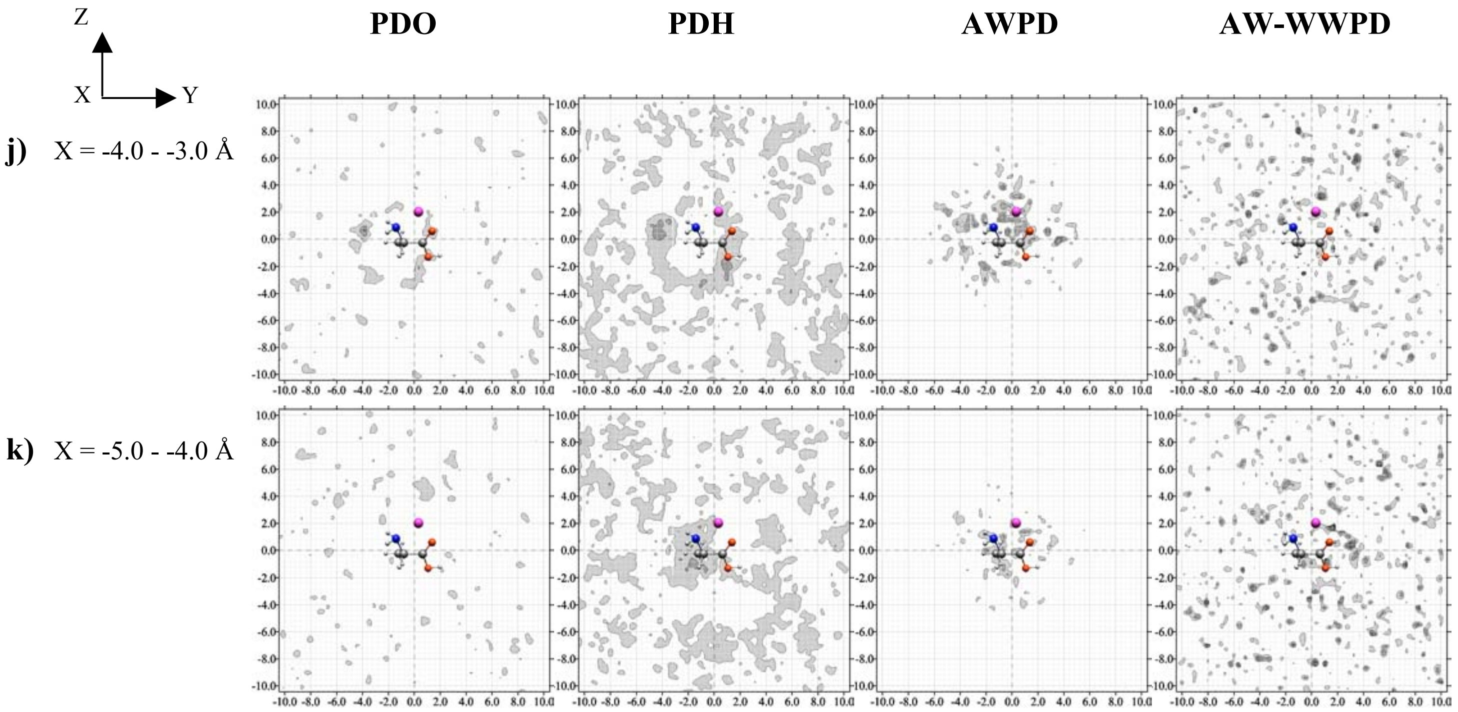

Figure C.14 (continued)

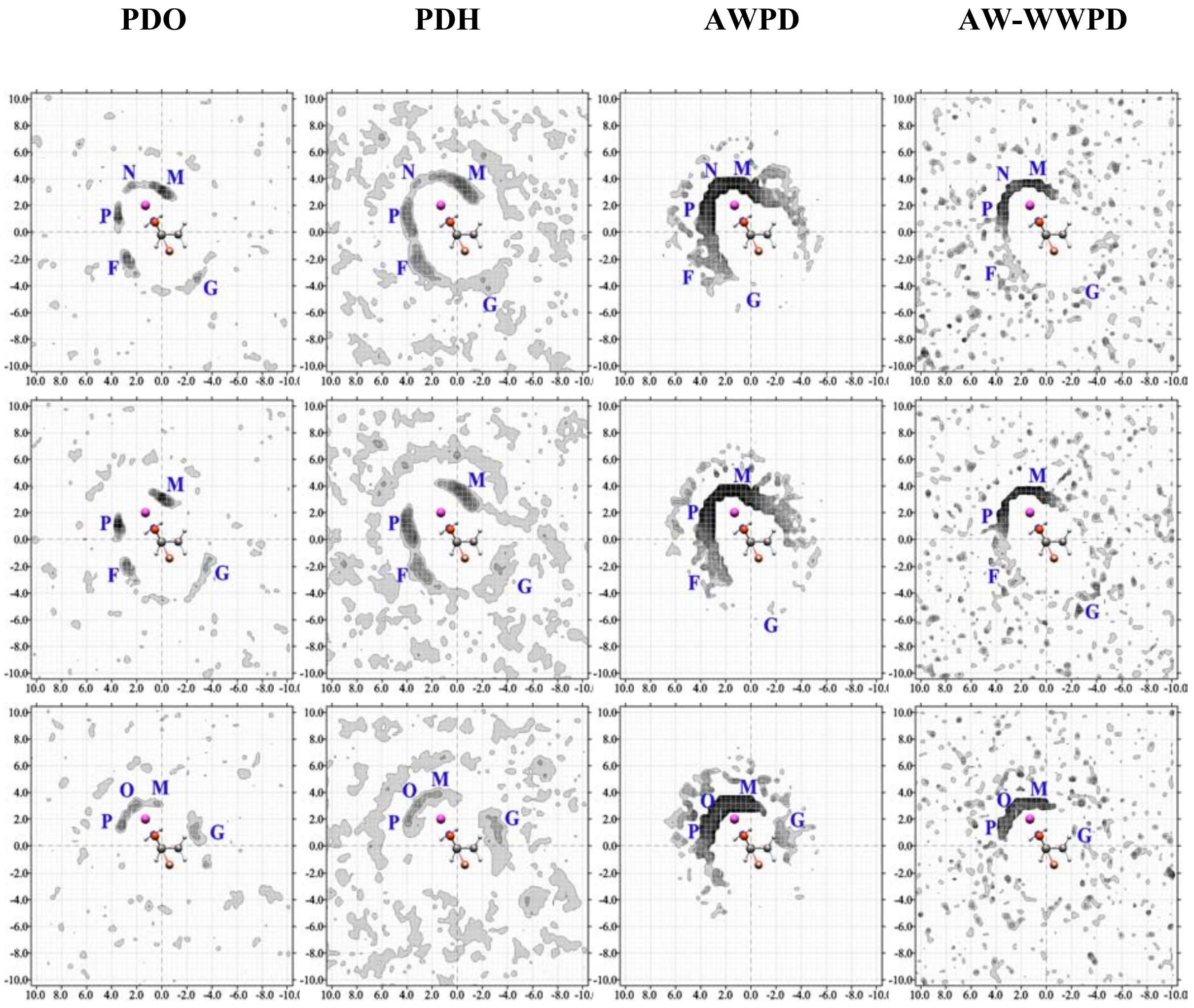

a) Y = -0.5 - 0.5 Å

	PDO	PDH
M	0.1083	0.0771
N	0.0400	0.0261
P	0.0860	0.0456
F	0.0618	0.0477
G	0.0389	0.0226

	AWPD	AW-WWPD
M	-84.2679	-98.6654
N	-82.8616	-98.0326
P	-85.0526	-90.5707
F	-36.4442	-69.3882
G	-11.3757	-67.3782

b) Y = 0.0 - 1.0 Å

	PDO	PDH
M	0.1257	0.0797
P	0.1365	0.0694
F	0.0562	0.0423
G	0.0281	0.0233

	AWPD	AW-WWPD
M	-90.0445	-104.036
P	-87.0257	-100.503
F	-34.2403	-71.1107
G	-12.6426	-69.7811

c) Y = 1.0 – 2.0 Å

	PDO	PDH
M	0.0304	0.0280
O	0.0382	0.0358
P	0.0463	0.0342
G	0.0270	0.0297

	AWPD	AW-WWPD
M	-78.3657	-93.0695
O	-80.4487	-94.0768
P	-76.2313	-97.9132
G	-26.0941	-71.6738

Figure C.15 The PDO, PDH, AWPD and AW-WWPD maps with respect to reference plane II obtained from MD-[Li$^+$/Ala - C]

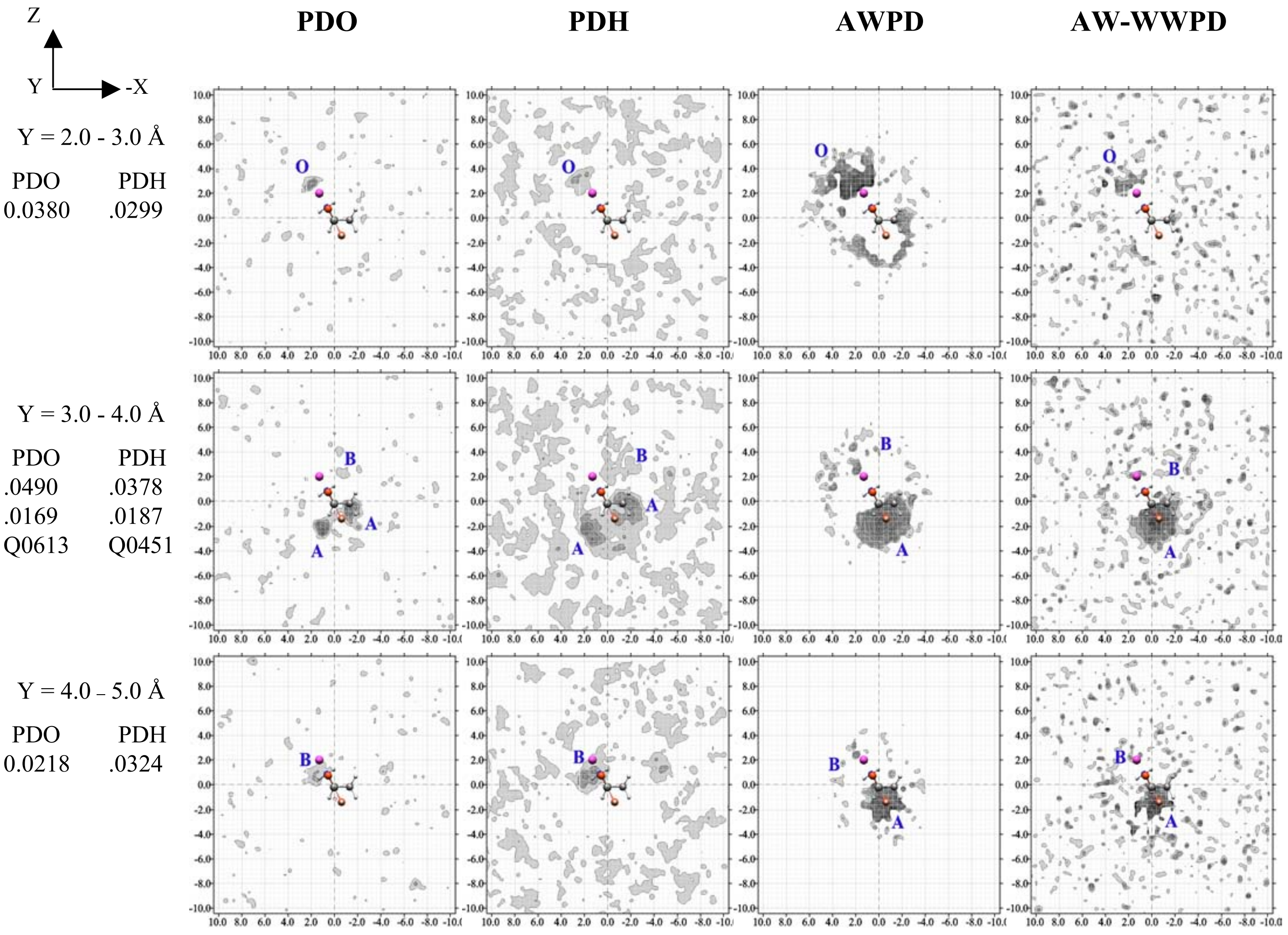

d) Y = 2.0 - 3.0 Å

	PDO	PDH
O	0.0380	.0299

	AWPD	AW-WWPD
O	64.2284	77.8741

e) Y = 3.0 - 4.0 Å

	PDO	PDH
A	.0490	.0378
B	.0169	.0187
A	Q0613	Q0451

	AWPD	AW-WWPD
A	52.7004	95.9092
B	19.0523	67.0963

f) Y = 4.0 – 5.0 Å

	PDO	PDH
B	0.0218	.0324

	AWPD	AW-WWPD
B	-16.6555	71.8270

Figure C.15 (continued)

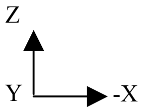

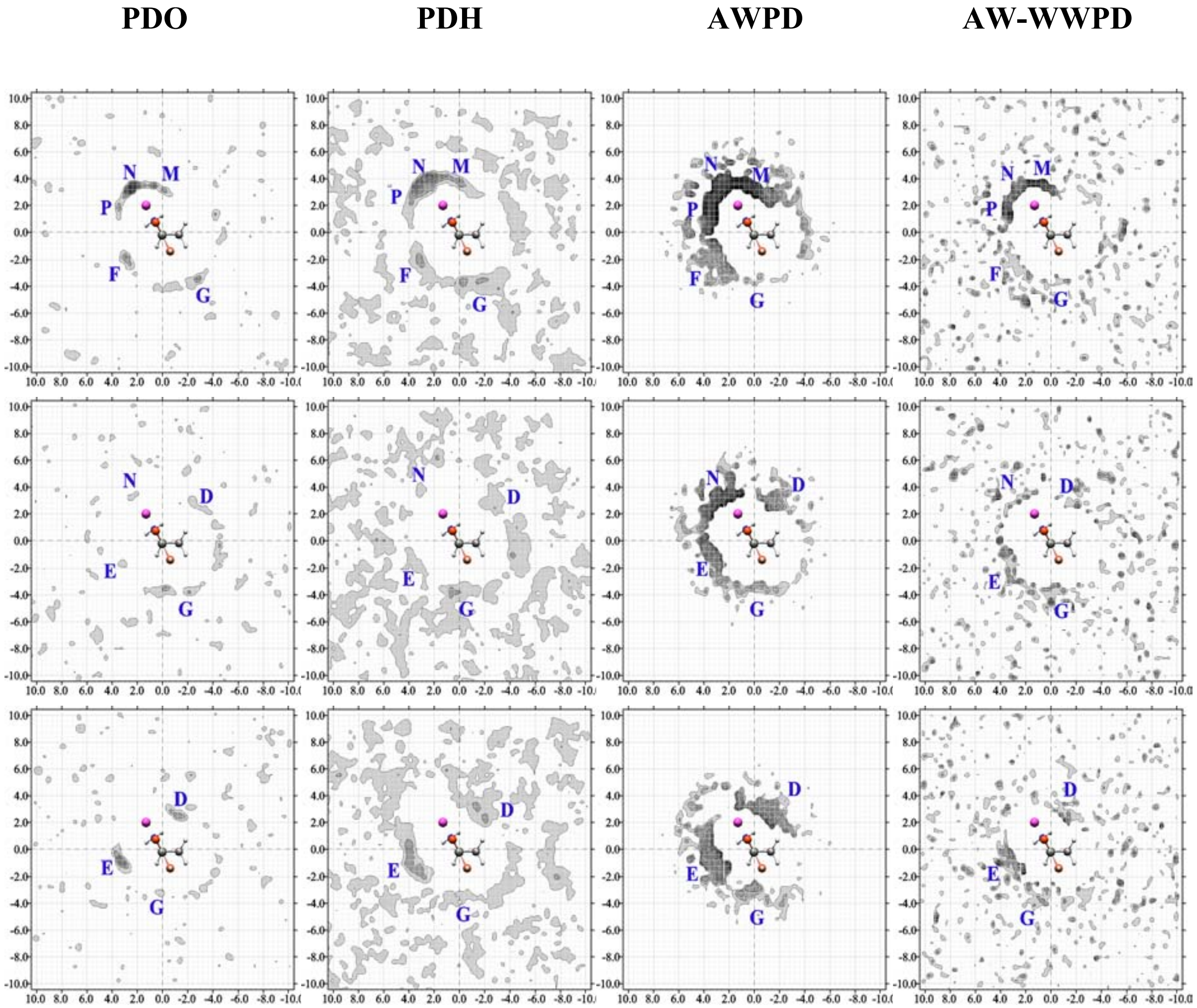

g) Y = -1.0 - 0.0 Å

	PDO	PDH
M	0.0451	0.0304
N	0.0853	0.0578
P	0.0278	0.0573
F	0.0291	0.0255
G	0.0339	0.0278

	AWPD	AW-WWPD
M	-78.1563	-92.5438
N	-73.6018	-80.9028
P	-77.5391	-101.535
F	-41.3764	-75.0901
G	-19.0238	-72.5304

h) Y = -2.0 - -1.0 Å

	PDO	PDH
D	0.0179	0.0218
N	0.0151	0.0143
E	0.0186	0.0190
G	0.0267	0.0237

	AWPD	AW-WWPD
D	-40.7095	-74.6212
N	-61.5928	-75.0705
E	-42.6858	-79.7492
G	-23.1566	-70.5026

i) Y = -3.0 - -2.0 Å

	PDO	PDH
D	0.0272	0.0270
E	0.0469	0.0296
G	0.0142	0.0175

	AWPD	AW-WWPD
D	-41.7913	-76.2283
E	-48.5828	-85.2786
G	-25.0764	-71.0966

Figure C.15 (continued)

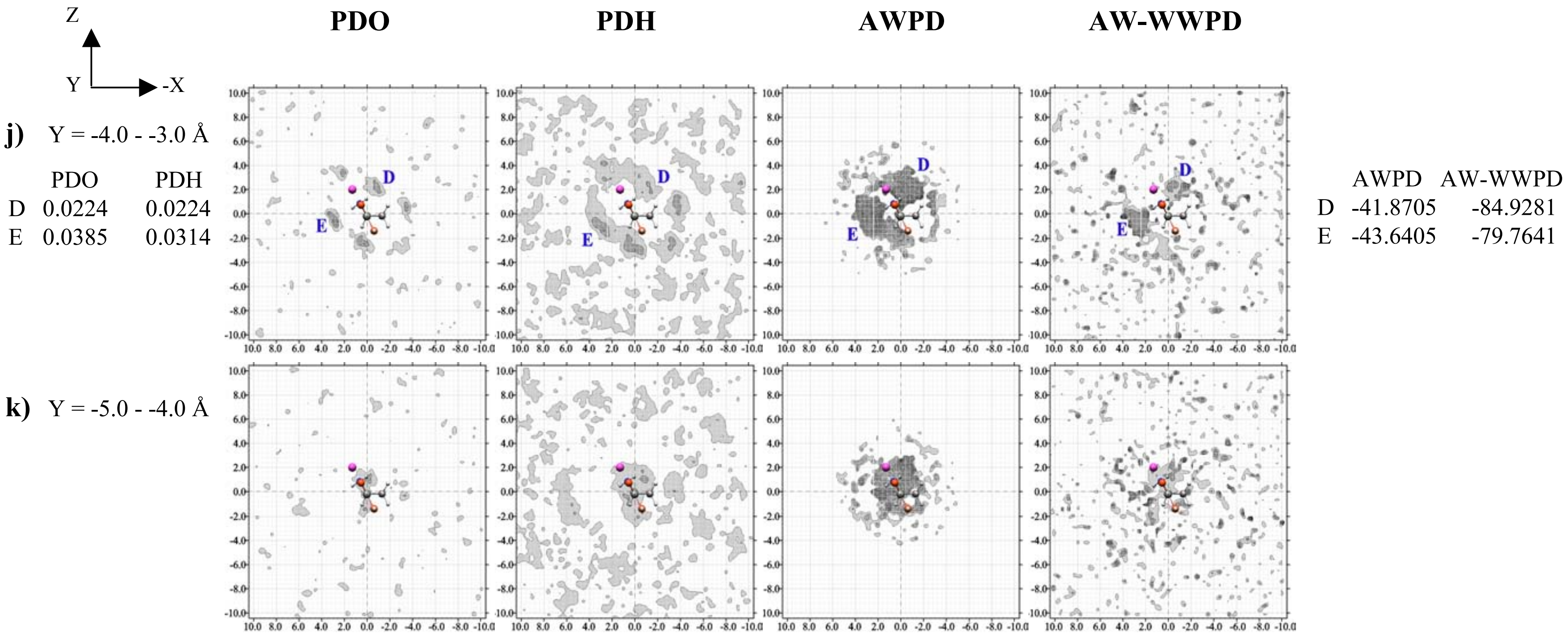

j) Y = -4.0 - -3.0 Å

	PDO	PDH
D	0.0224	0.0224
E	0.0385	0.0314

	AWPD	AW-WWPD
D	-41.8705	-84.9281
E	-43.6405	-79.7641

k) Y = -5.0 - -4.0 Å

Figure C.15 (continued)

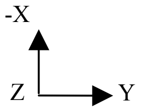

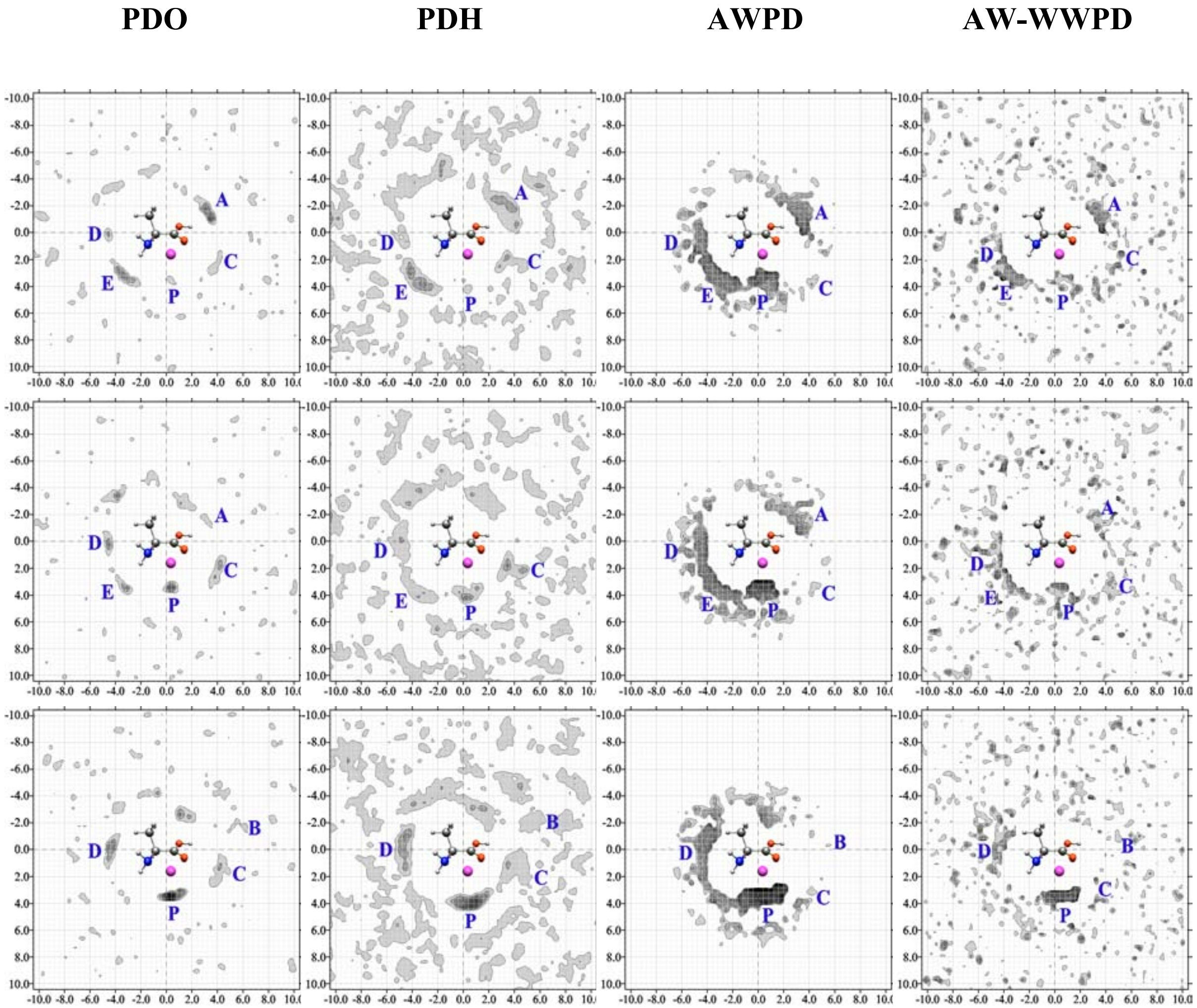

a) Z = -0.5 - 0.5 Å

	PDO	PDH
A	0.0601	0.0268
D	0.0221	0.0148
E	0.0370	0.0354
P	0.0143	0.0130
C	0.0175	0.0268

	AWPD	AW-WWPD
A	-37.4007	-80.8719
D	-31.0716	-72.8881
E	-40.4958	-85.8979
P	-50.4969	-77.6107
C	-16.0913	-81.2036

b) Z = 0.0 - 1.0 Å

	PDO	PDH
A	0.0144	-
D	0.0326	0.0225
E	0.0340	0.0210
P	0.0581	0.0336
C	0.0298	0.0322

	AWPD	AW-WWPD
A	-34.2109	-75.7721
D	-36.7214	-76.7720
E	-40.4181	-75.4874
P	-62.0481	-76.9479
C	-15.8563	-73.6046

c) Z = 1.0 - 2.0 Å

	PDO	PDH
B	0.0136	0.0185
D	0.0370	0.0336
P	0.1265	0.0825
C	0.0212	0.0251

	AWPD	AW-WWPD
B	-13.9789	-67.6386
D	-39.3972	-72.7422
P	-76.9287	-88.2598
C	-13.9691	-71.2906

Figure C.16 The PDO, PDH, AWPD and AW-WWPD maps with respect to reference plane III obtained from MD-[Li^+/Ala - C]

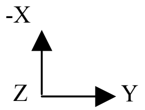

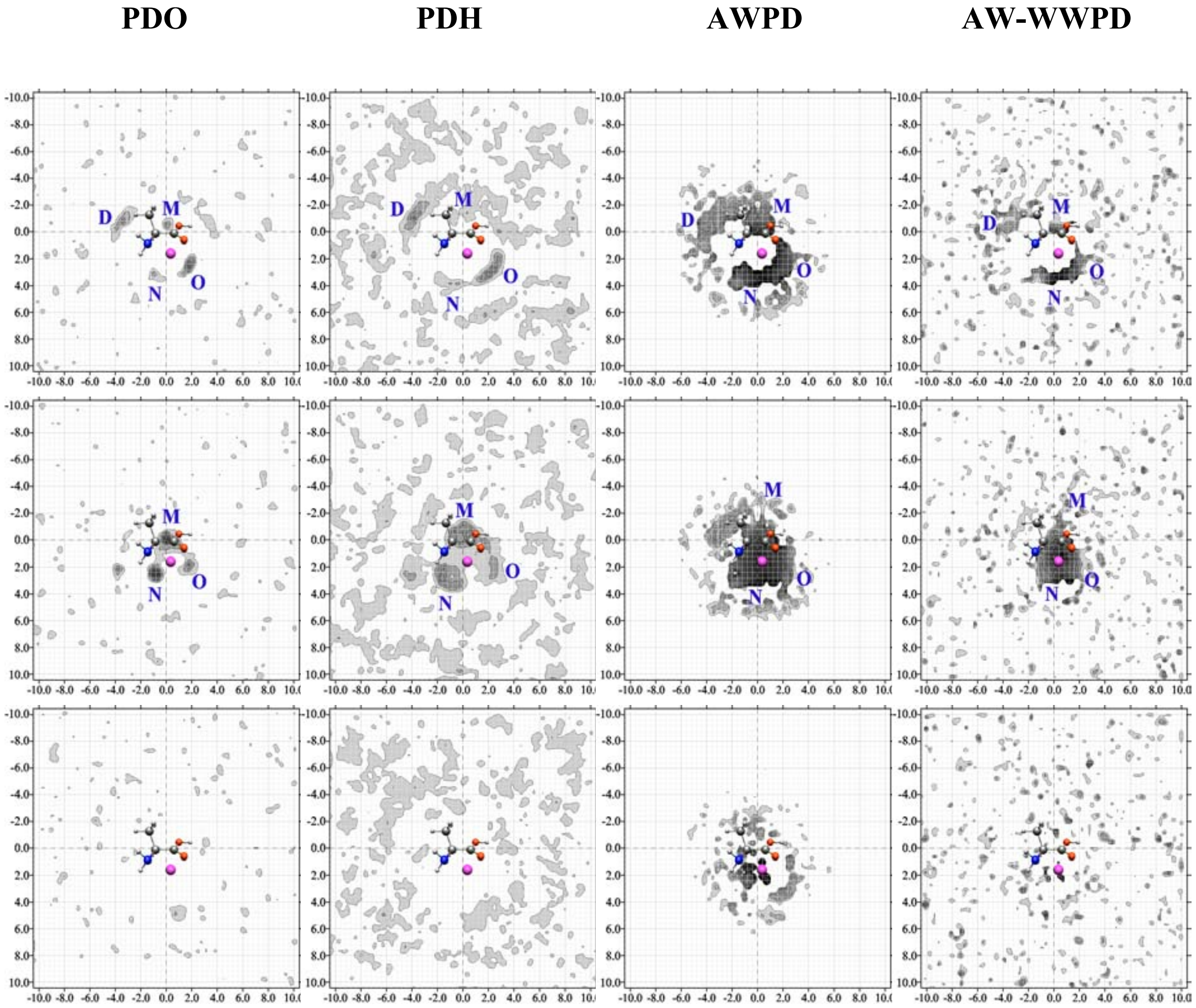

d) Z = 2.0 - 3.0 Å

	PDO	PDH
M	0.0262	0.0178
D	0.0321	0.0433
N	0.0249	0.0219
O	0.0544	0.0478

	AWPD	AW-WWPD
M	-69.3621	-85.7767
D	-37.5264	-76.8941
N	-79.8250	-85.8305
O	-92.5750	-103.796

e) Z = 3.0 - 4.0 Å

	PDO	PDH
M	0.0833	0.0450
N	0.0831	0.0462
O	0.0414	0.0297

	AWPD	AW-WWPD
M	-82.4222	-108.154
N	-91.1624	-96.4325
O	-87.2029	-102.854

f) Z = 4.0 - 5.0 Å

Figure C.16 (continued)

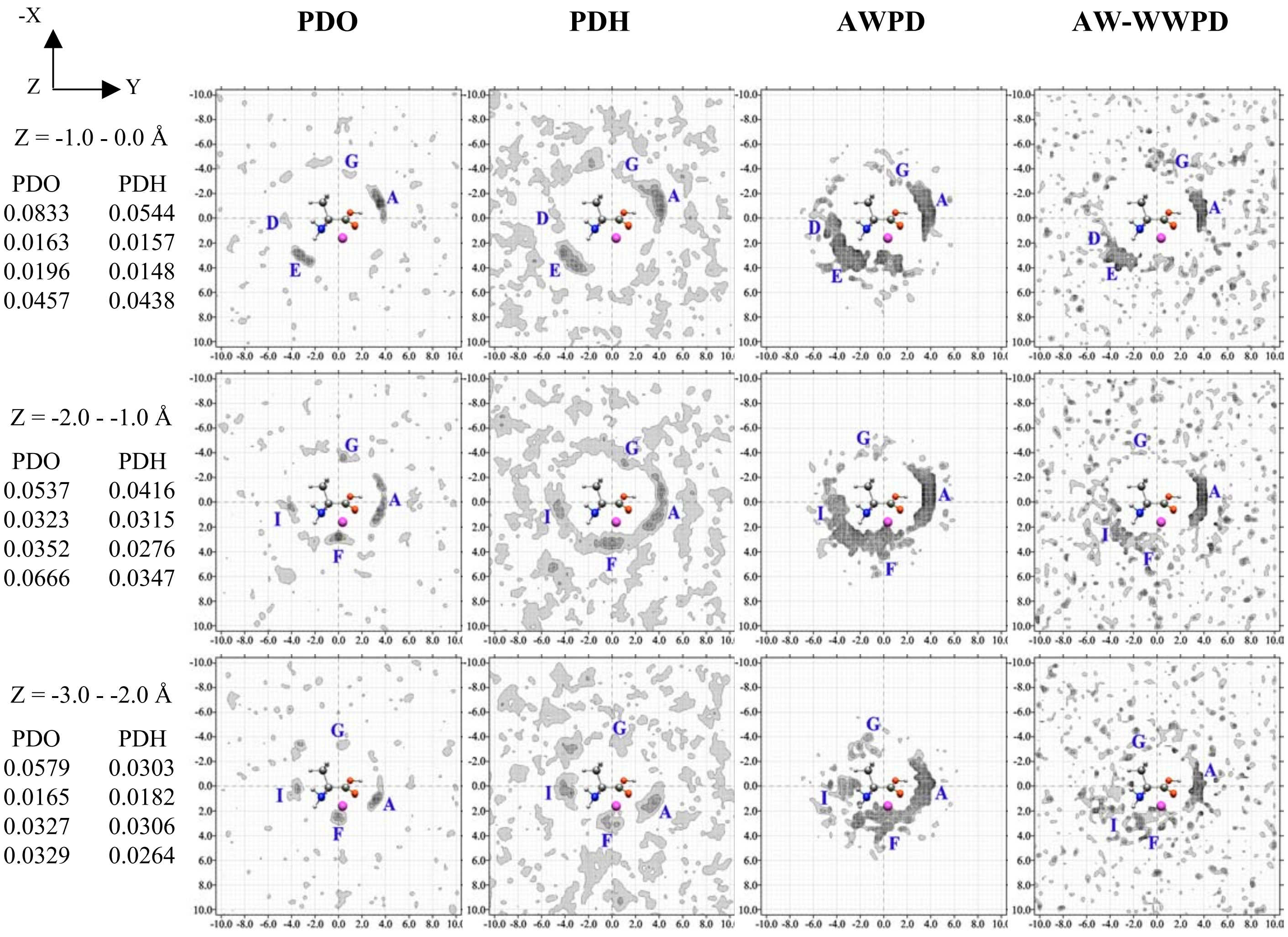

g) Z = -1.0 - 0.0 Å

	PDO	PDH
A	0.0833	0.0544
G	0.0163	0.0157
D	0.0196	0.0148
E	0.0457	0.0438

	AWPD	AW-WWPD
A	-44.8230	-84.5438
G	-23.0001	-74.2719
D	-38.3884	-72.7814
E	-47.0855	-75.7466

h) Z = -2.0 - -1.0 Å

	PDO	PDH
A	0.0537	0.0416
G	0.0323	0.0315
I	0.0352	0.0276
F	0.0666	0.0347

	AWPD	AW-WWPD
A	-51.0153	-90.5487
G	-19.6026	-67.0169
I	-29.6435	-81.4143
F	-32.4229	-77.3832

i) Z = -3.0 - -2.0 Å

	PDO	PDH
A	0.0579	0.0303
G	0.0165	0.0182
I	0.0327	0.0306
F	0.0329	0.0264

	AWPD	AW-WWPD
A	-41.9758	-86.9332
G	-20.6388	-74.6249
I	-24.8283	-82.6202
F	-29.6168	-79.3430

Figure C.16 (continued)

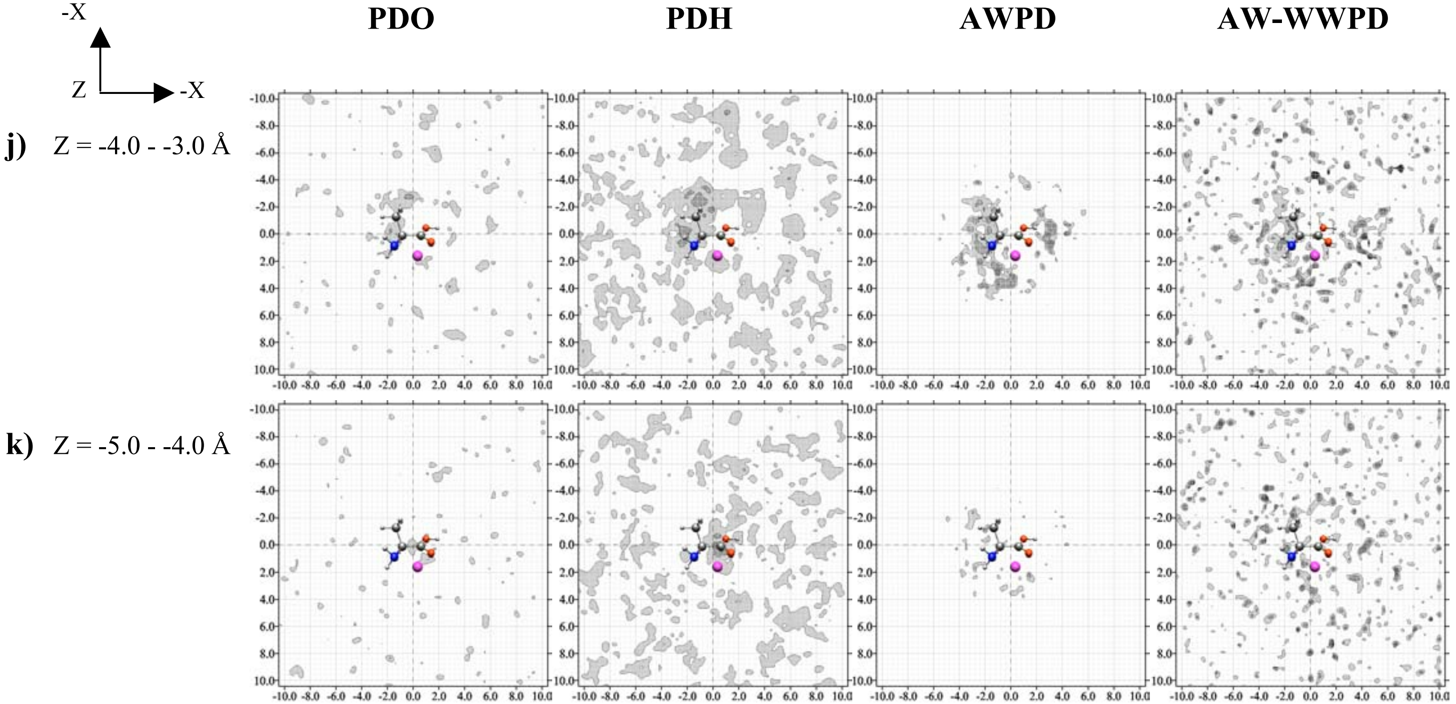

Figure C.16 (continued)

APPENDIX D

SUPPLEMENTARY RESULTS FOR WATER EXCHANGES

MD-[Ala – A]$_{aq}$

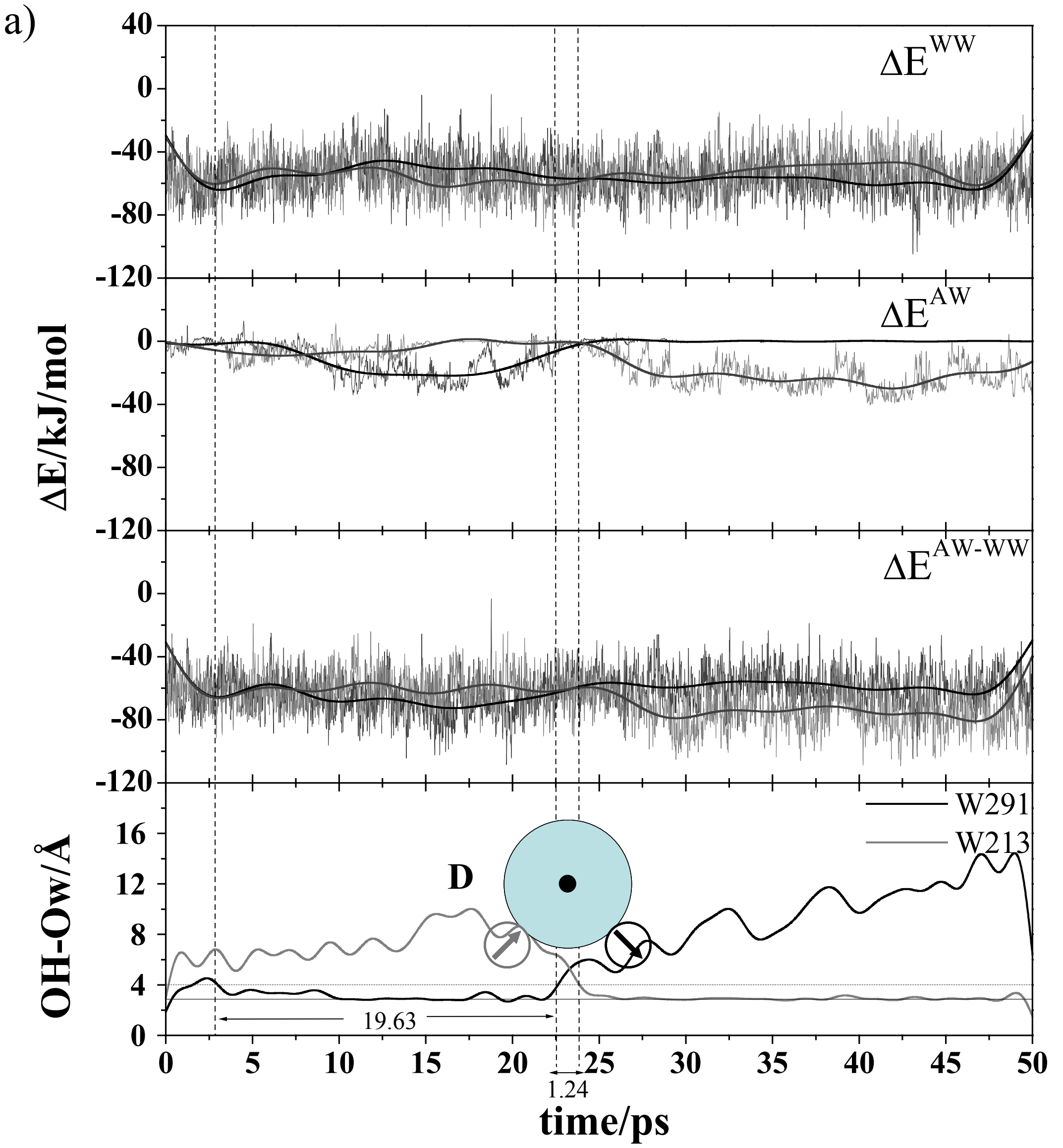

Figure D.1 Additional examples of water exchange diagrams for specific water molecule in the first hydration shell of the O2-H7 group in [Ala - A]$_{aq}$ together with the corresponding total interaction energy (ΔE^{AW-WW}), solute-solvent (ΔE^{AW}) and solvent-solvent (ΔE^{WW}) interaction energy, monitored in course of MD simulations. Some water exchange mechanisms proposed by Langford and Gray (1996) are also included in the figure.

MD-$[\text{Ala} - \text{A}]_{aq}$

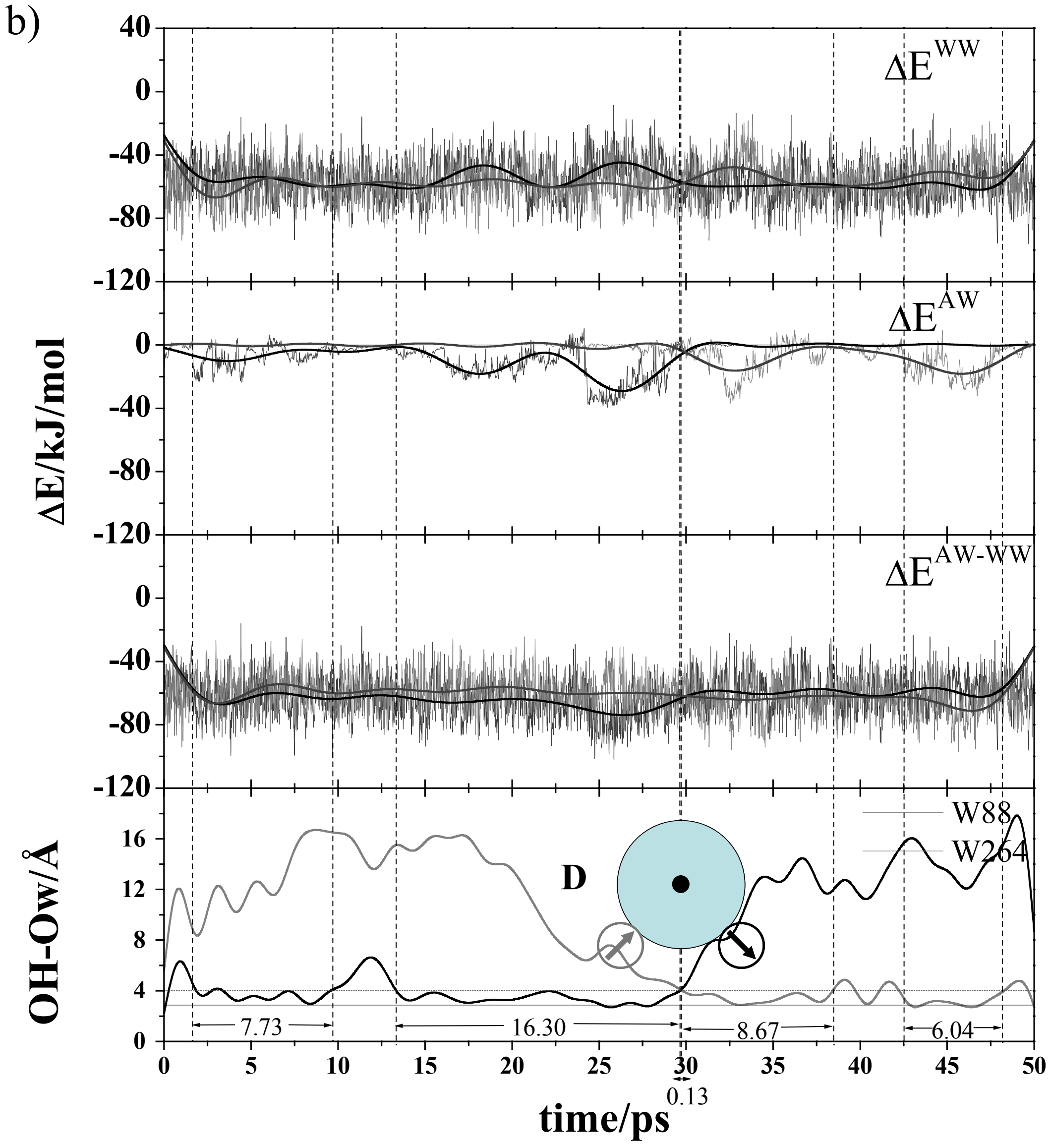

Figure D.1 (continued)

MD-[Ala – B]$_{aq}$

a)

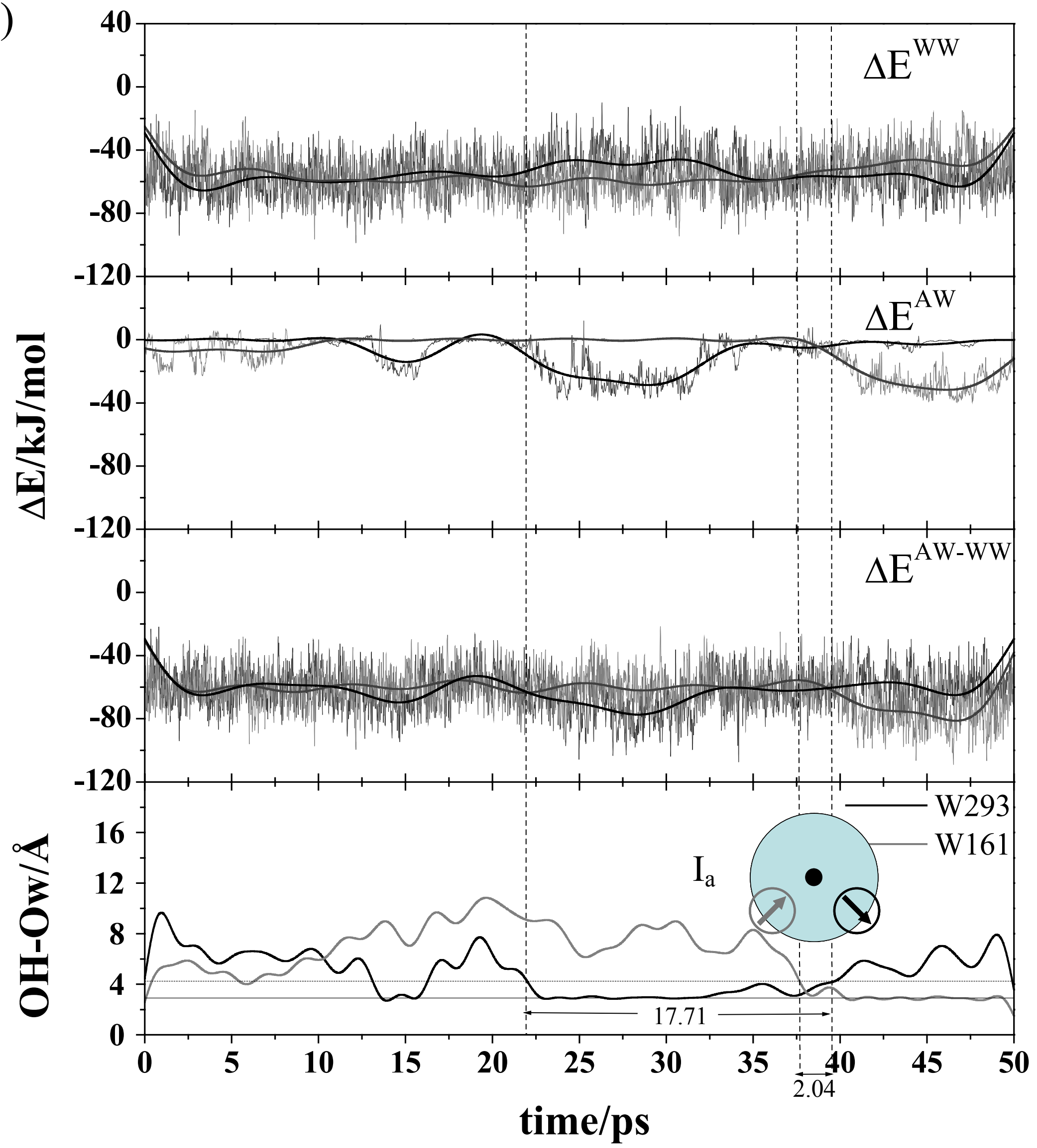

Figure D.2 Additional examples of water exchange diagrams for specific water Molecule in the first hydration shell of the O2-H7 group in [Ala - B]$_{aq}$ Together with the corresponding total interaction energy ($\Delta E^{AW\text{-}WW}$), solute-solvent (ΔE^{AW}) and solvent-solvent (ΔE^{WW}) interaction energy, monitored in course of MD simulations. Some water exchange mechanisms proposed by Langford and Gray (1996) are also included in the figure.

MD-$[Ala – C]_{aq}$

a)

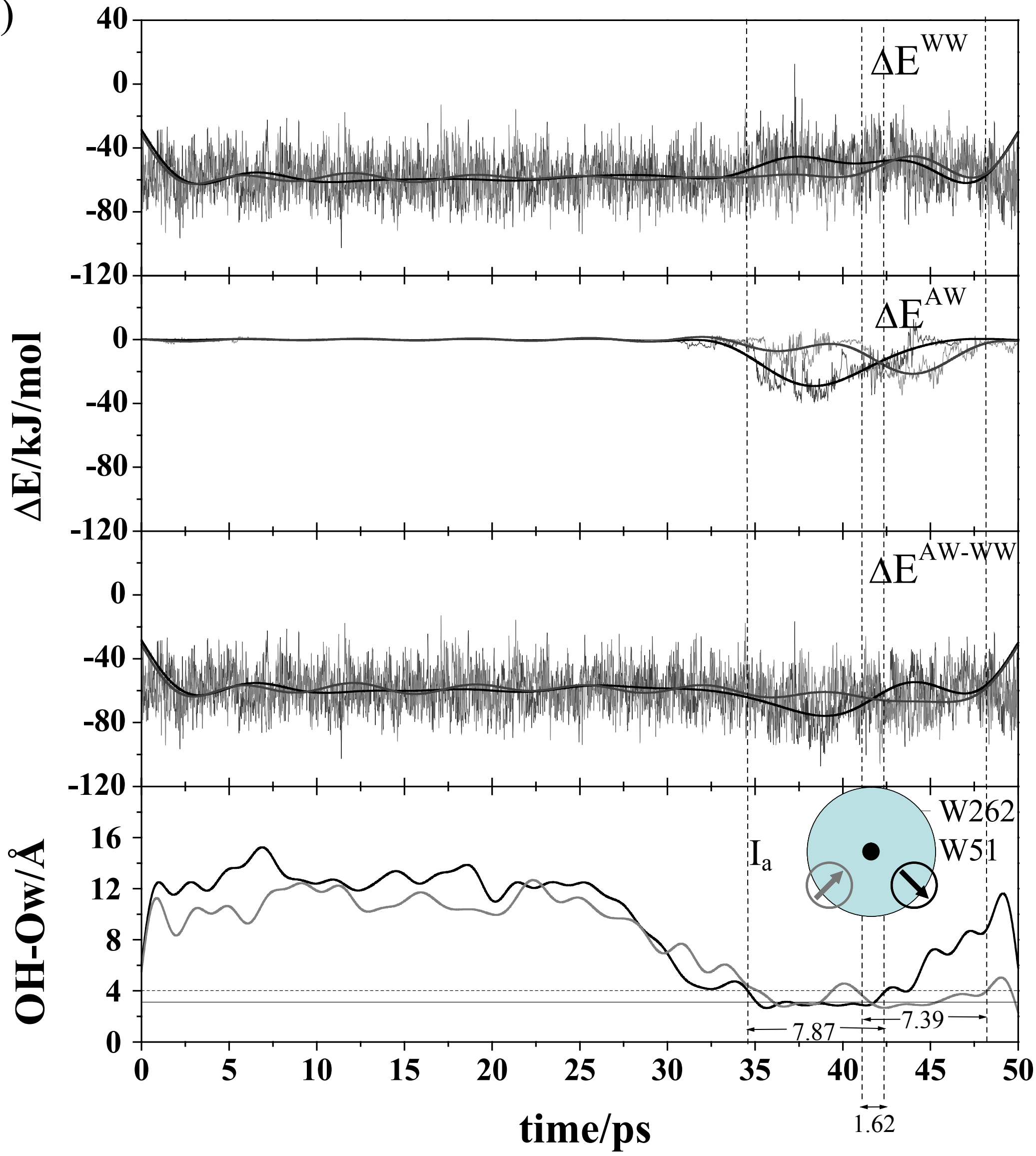

Figure D.3 Additional examples of water exchange diagrams for specific water molecule in the first hydration shell of the O2-H7 group in $[Ala - C]_{aq}$ together with the corresponding total interaction energy (ΔE^{AW-WW}), solute-solvent (ΔE^{AW}) and solvent-solvent (ΔE^{WW}) interaction energy, monitored in course of MD simulations. Some water exchange mechanisms proposed by Langford and Gray (1996) are also included in the figure.

MD-[Ala – C]$_{aq}$

b)

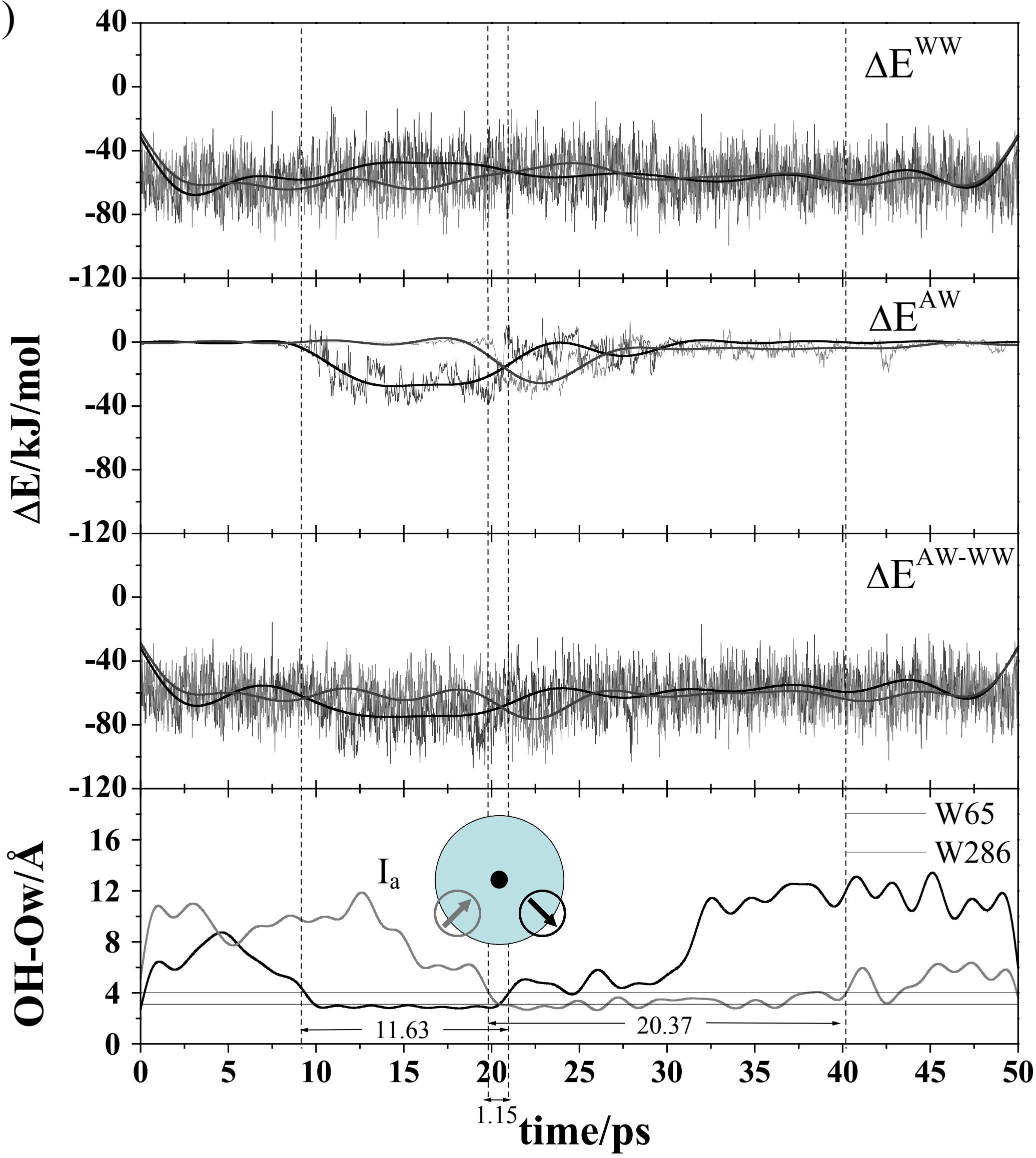

Figure D.3 (continued)

MD-[Ala – C]$_{aq}$

c)

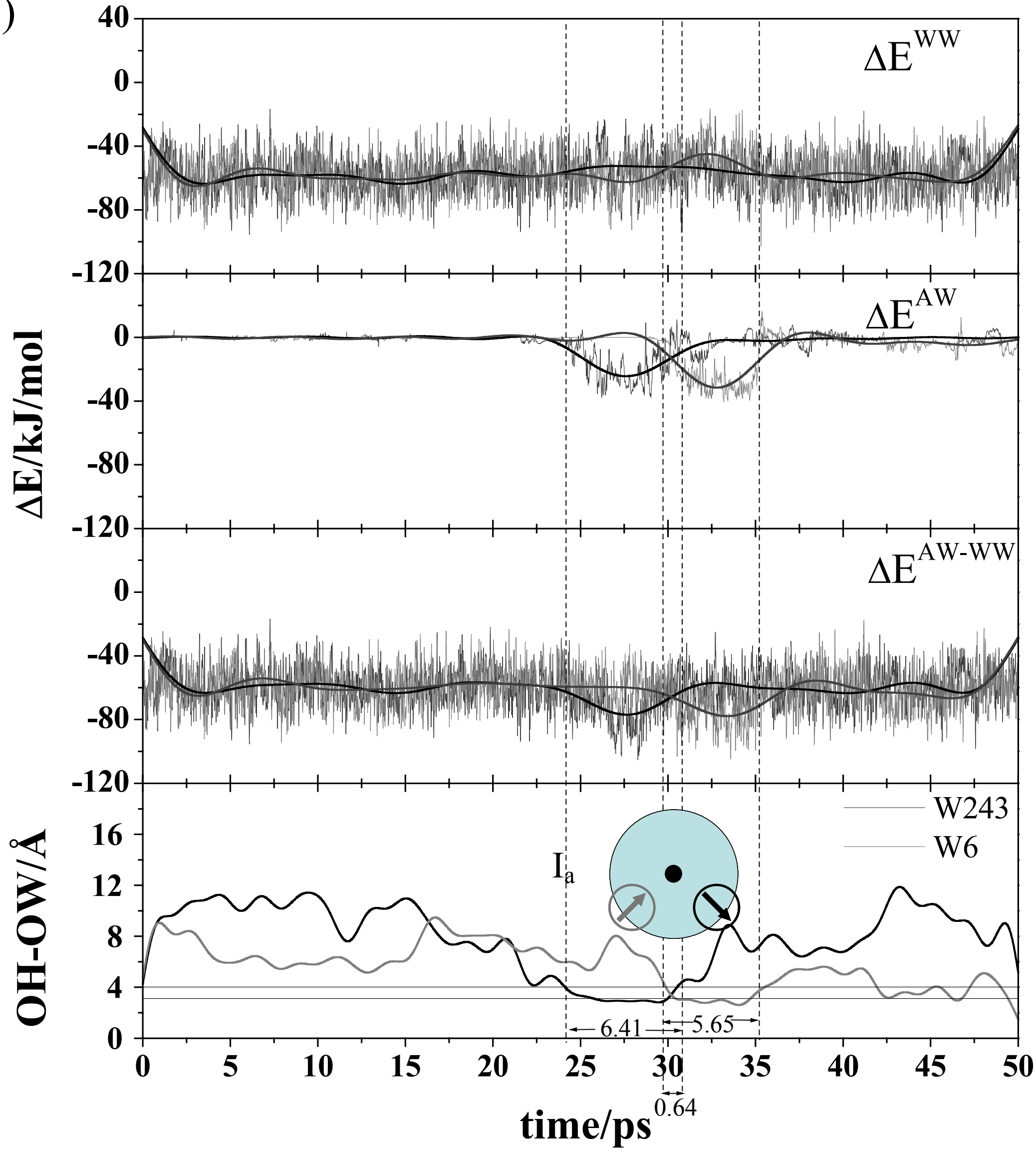

Figure D.3 (continued)

MD-[Ala – C]$_{aq}$

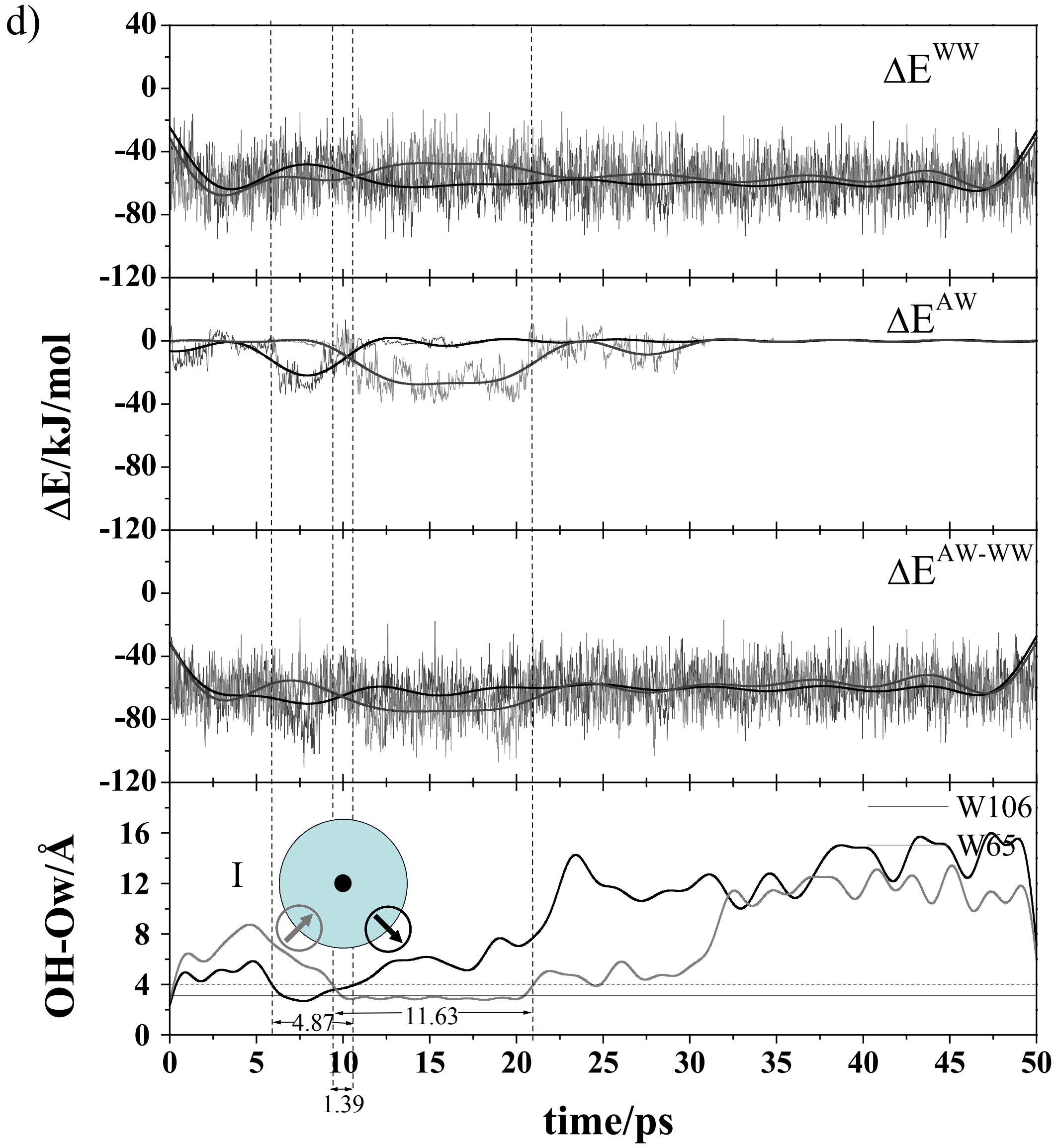

Figure D.3 (continued)

MD-[Li^+/Ala – C]$_{aq}$

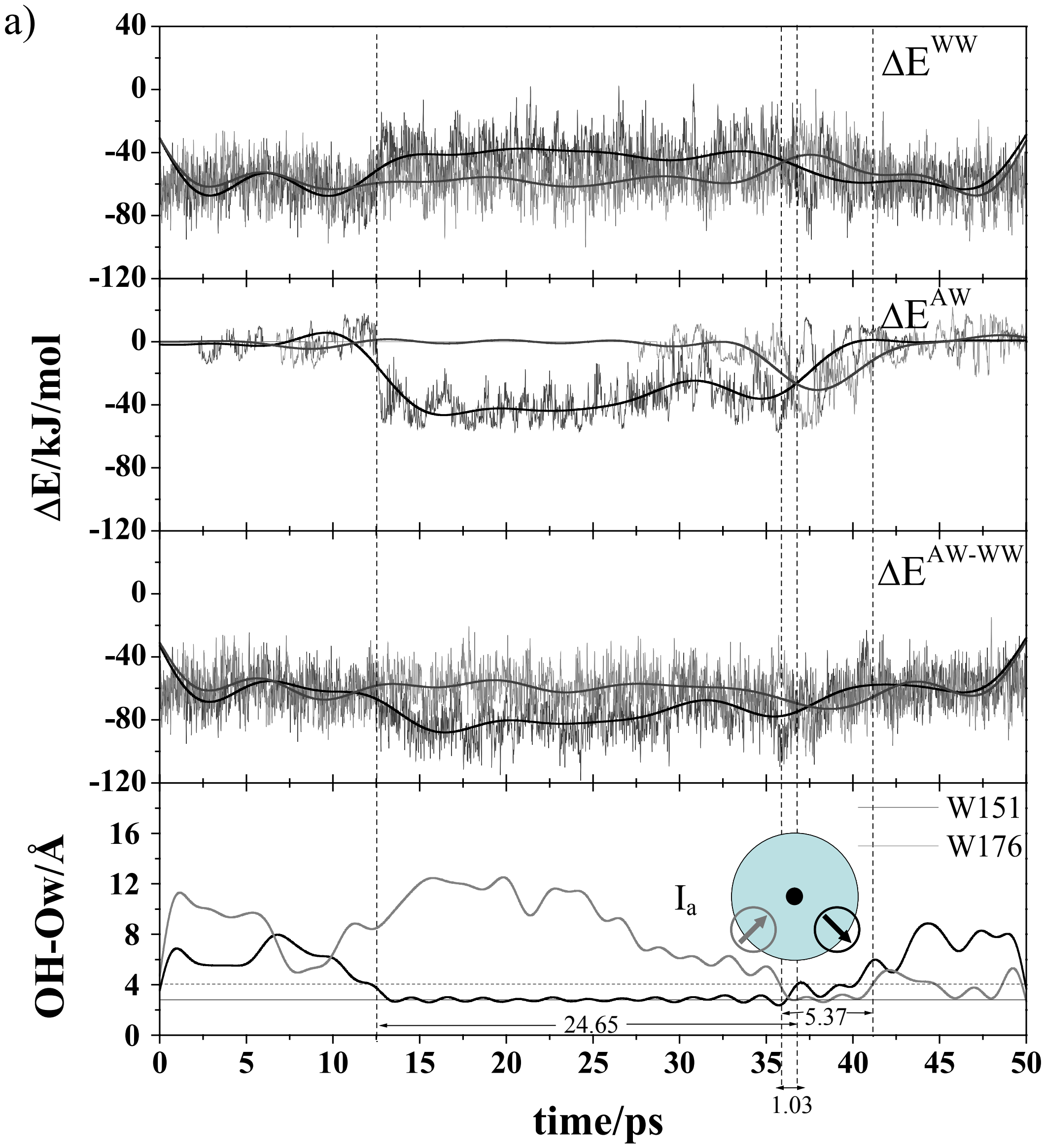

Figure D.4 Additional examples of water exchange diagrams for specific water molecule in the first hydration shell of the O2-H7 group in [Li^+/Ala - C]$_{aq}$ together with the corresponding total interaction energy ($\Delta E^{AW\text{-}WW}$), solute-solvent (ΔE^{AW}) and solvent-solvent (ΔE^{WW}) interaction energy, monitored in course of MD simulations. Some water exchange mechanisms proposed by Langford and Gray (1996) are also included in the figure.

MD-[Li^+/Ala – C]$_{aq}$

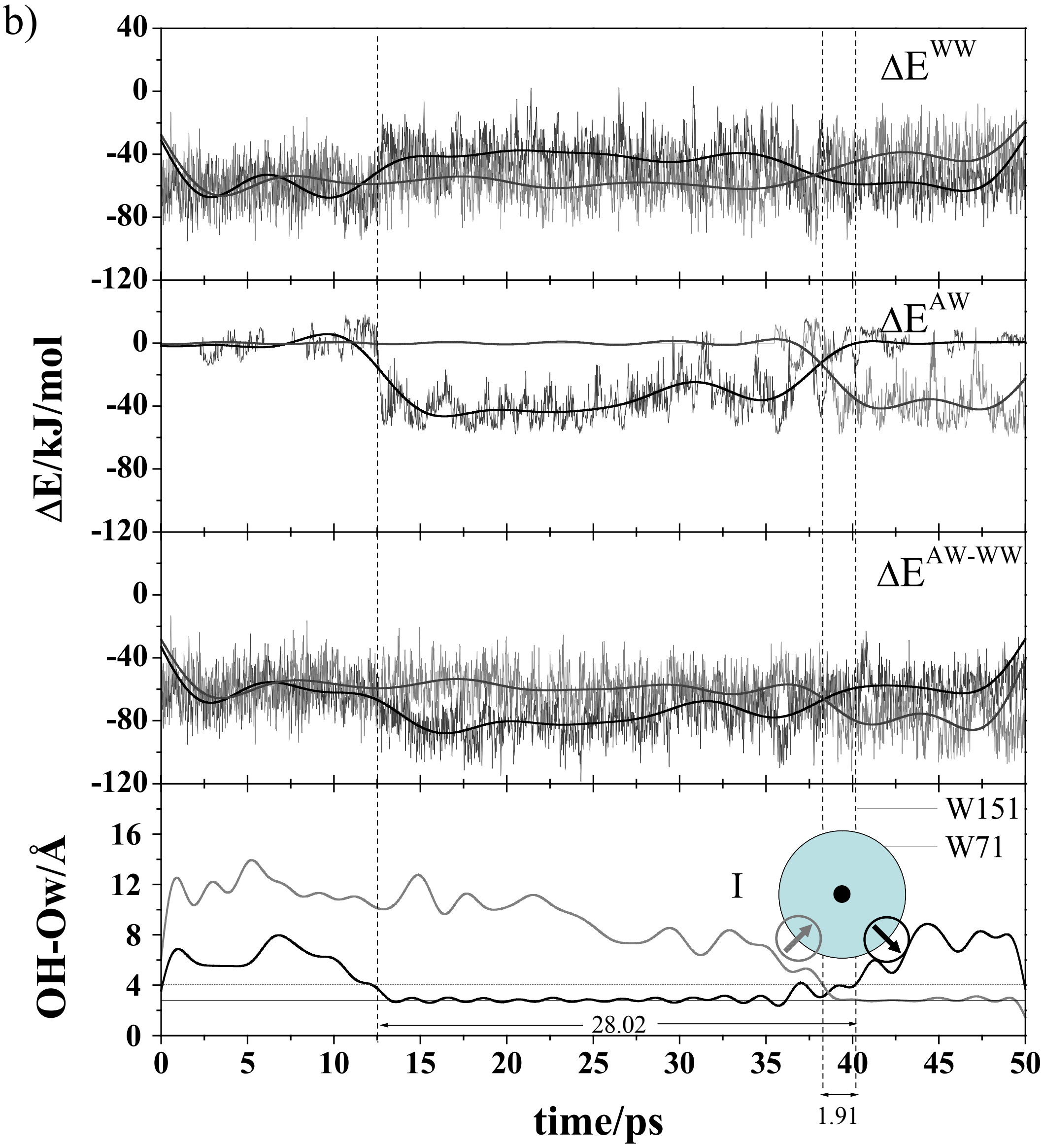

Figure D.4 (continued)

MD-$[Li^+/Ala - C]_{aq}$

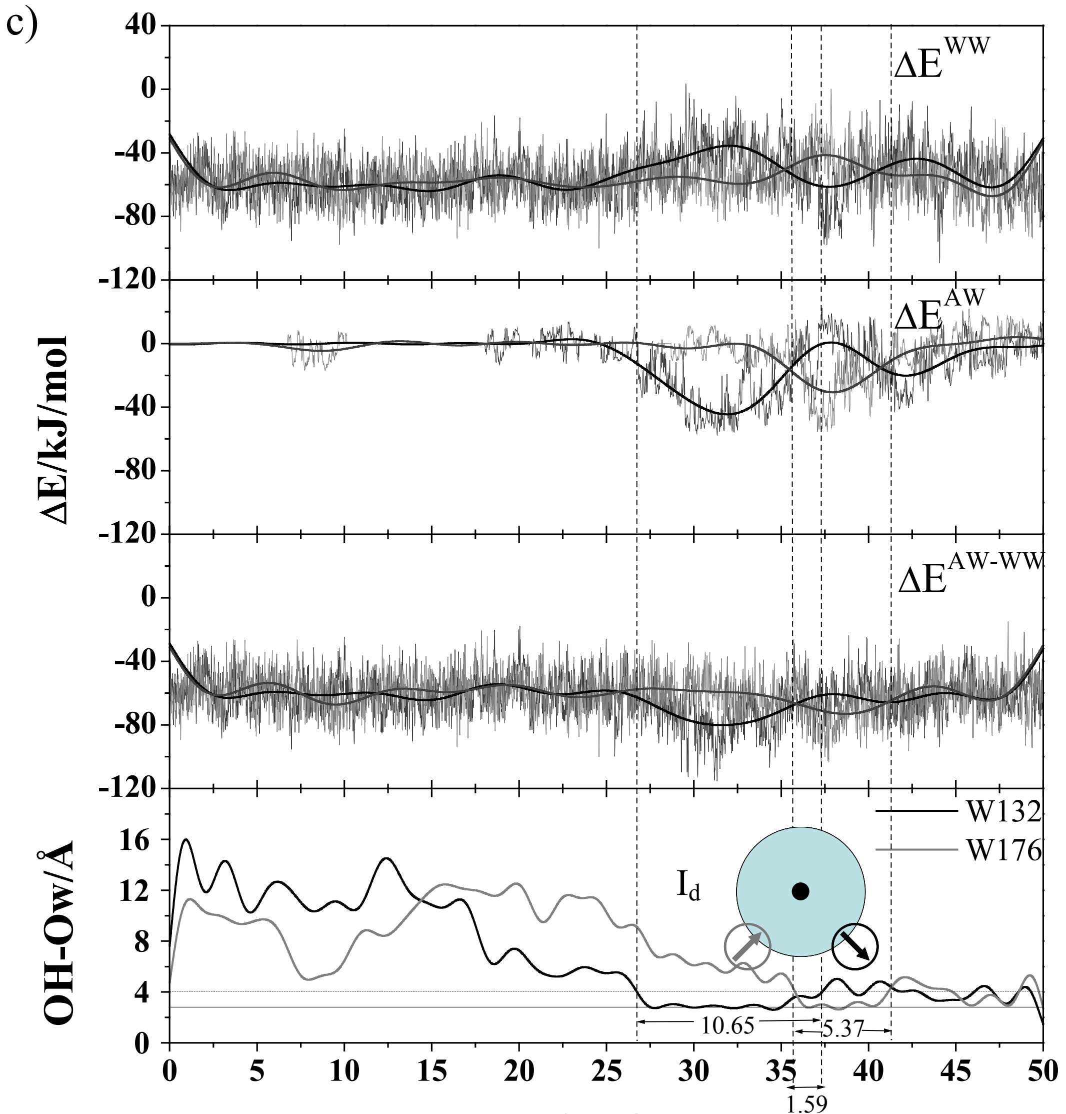

Figure D.4 (continued)

MD-$[Li^+/Ala - C]_{aq}$

a)

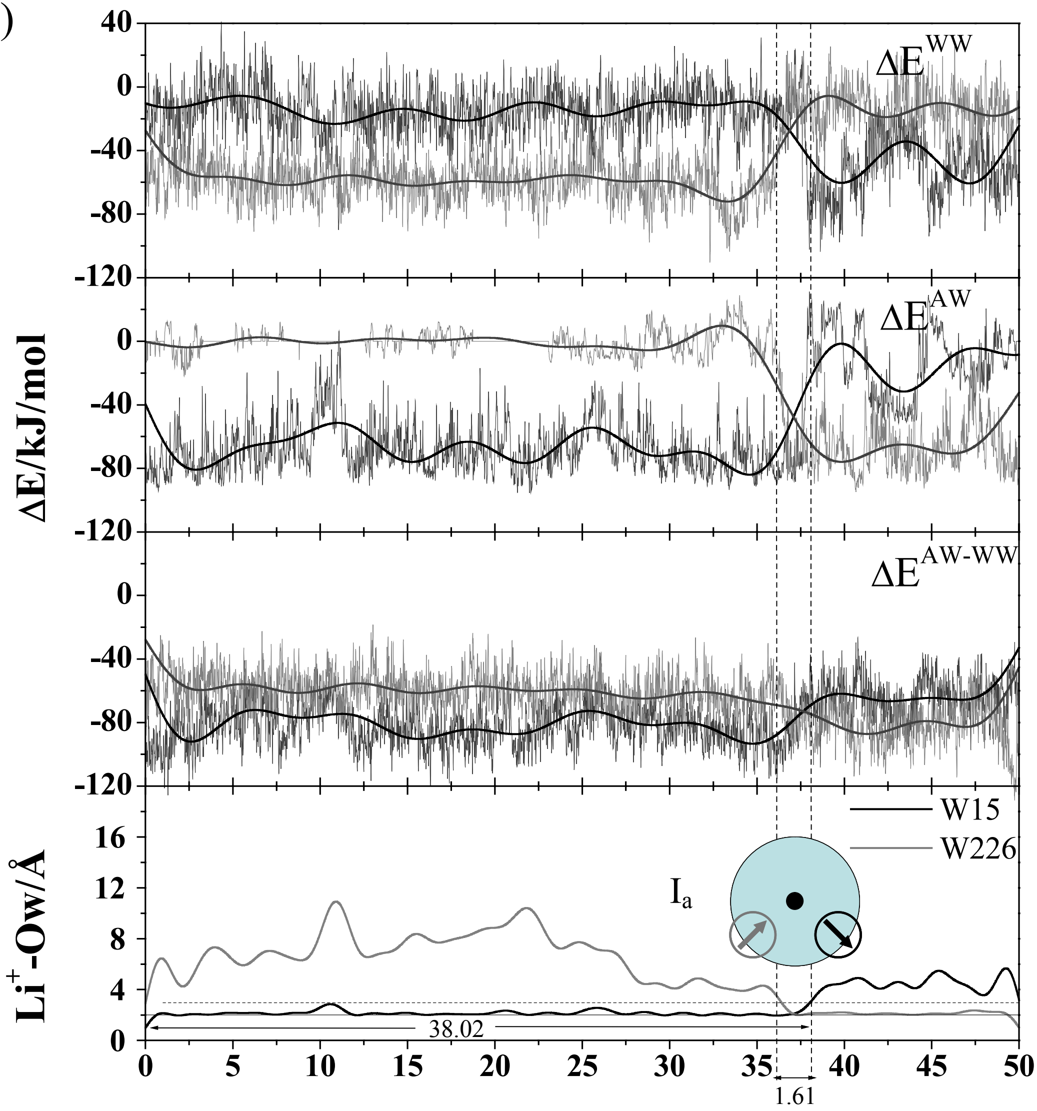

Figure D.5 Additional examples of water exchange diagrams for specific water molecule in the first hydration shell of Li^+ in $[Li^+/Ala - C]_{aq}$ together with the corresponding total interaction energy (ΔE^{AW-WW}), solute-solvent (ΔE^{AW}) and solvent-solvent (ΔE^{WW}) interaction energy, monitored in course of MD simulations. Some water exchange mechanisms proposed by Langford and Gray (1996) are also included in the figure.

MD-$[Li^+/Ala – C]_{aq}$

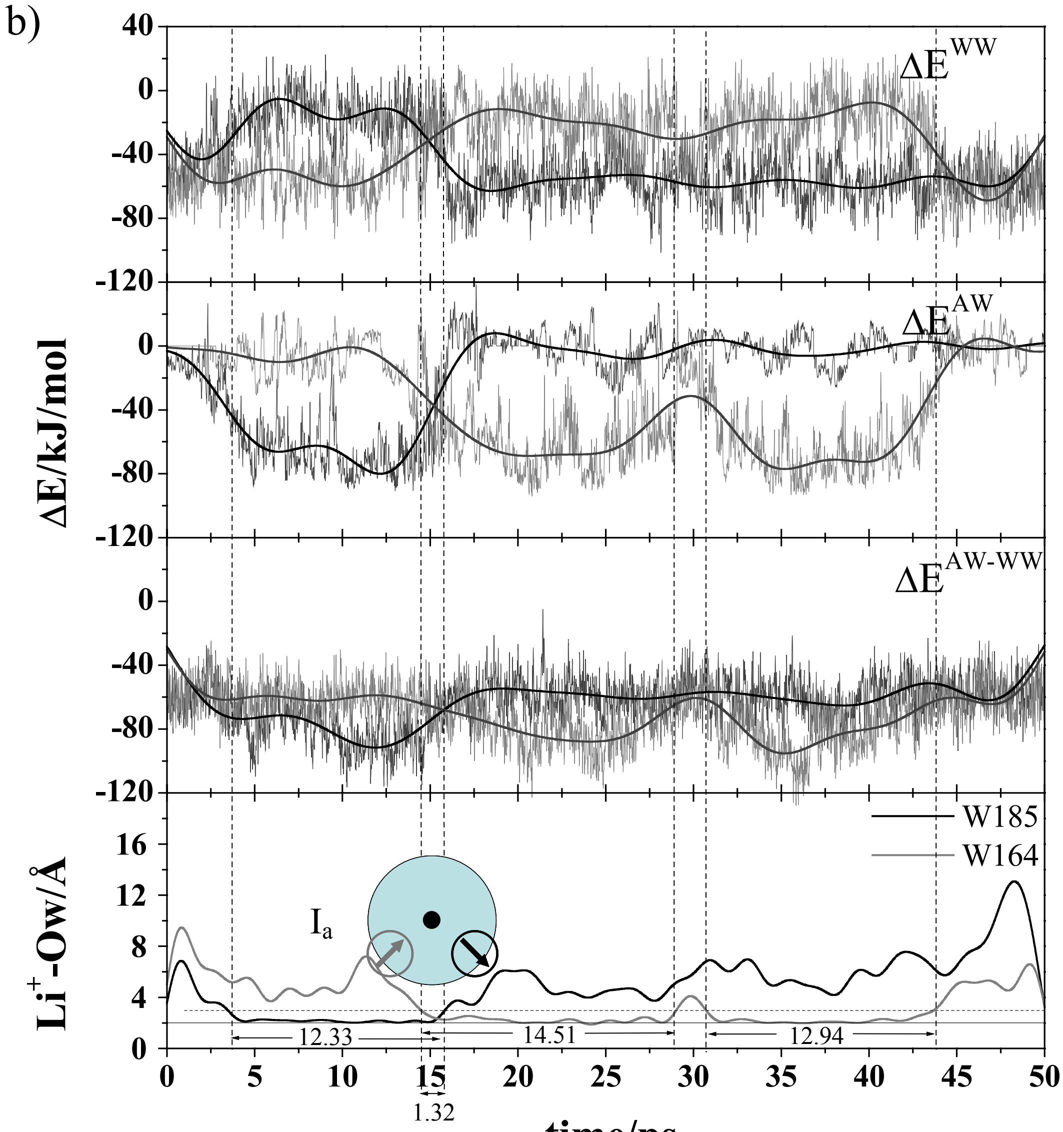

Figure D.5 (continued)

MD-[Li^+/Ala – C]$_{aq}$

c)

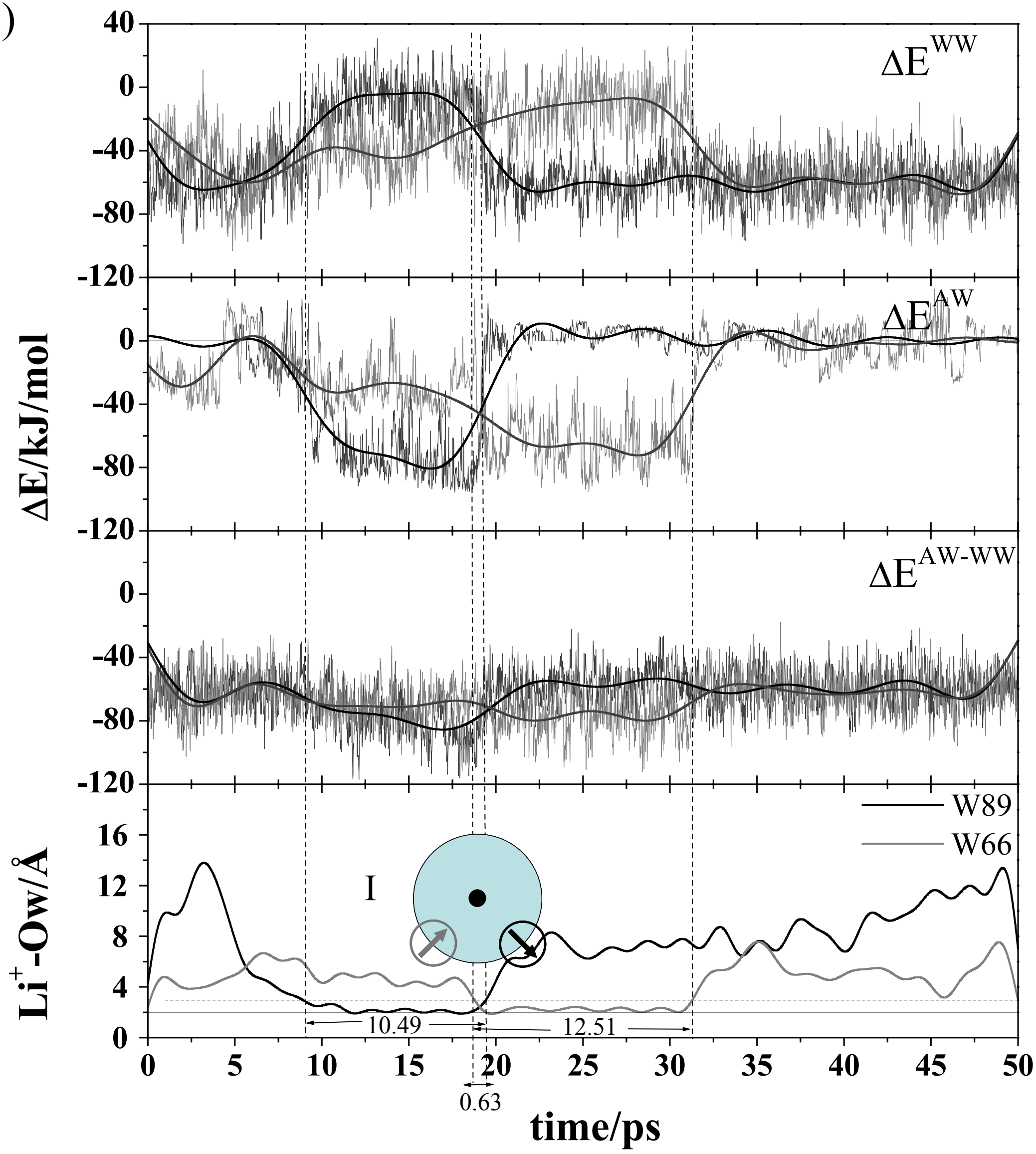

Figure D.5 (continued)

MD-[Li$^+$/Ala – C]$_{aq}$

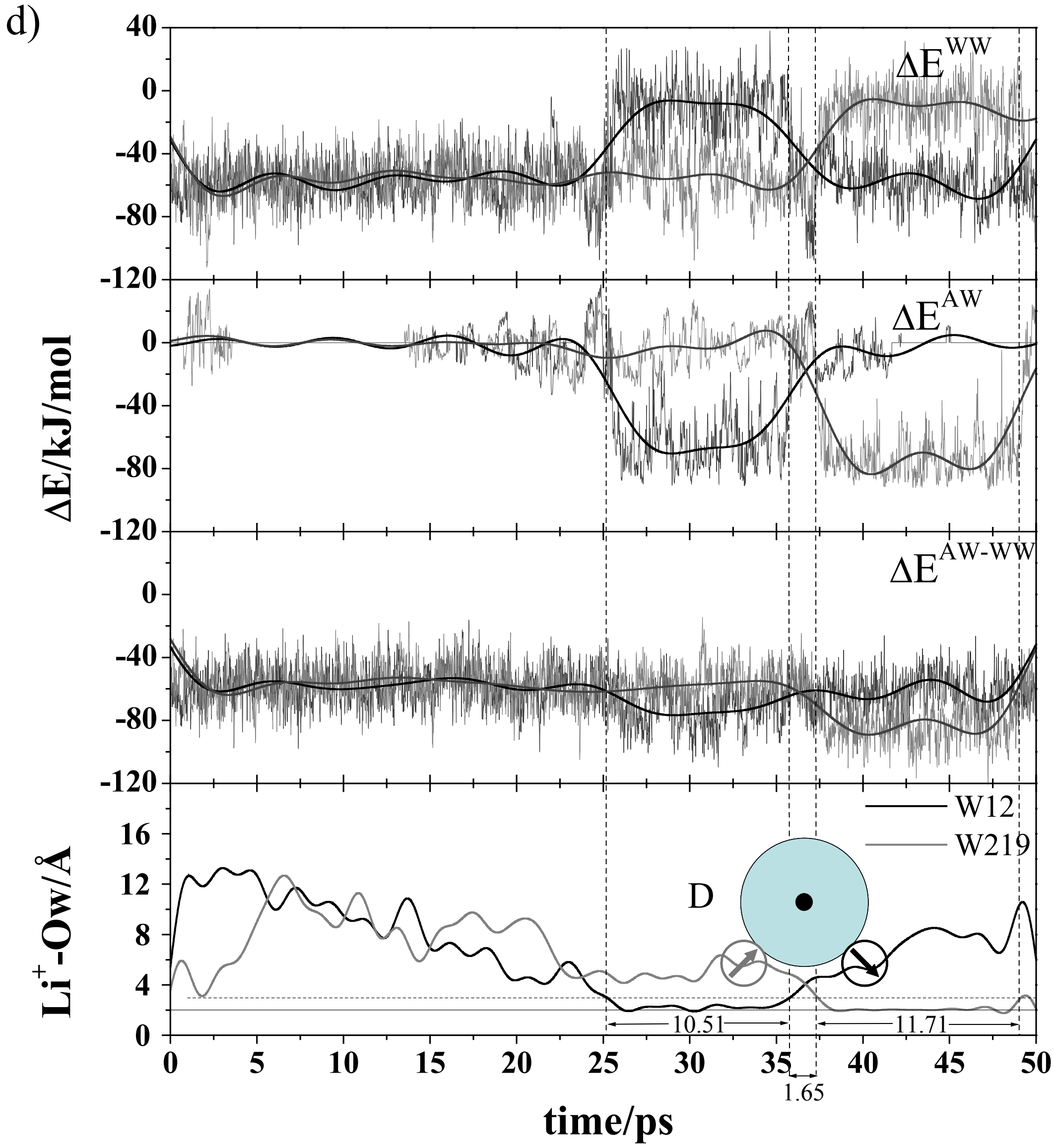

Figure D.5 (continued)

CURRICULUM VITAE

MISS NATTHIYA DEEYING

Born : July 23, 1976, Surin **Citizenship :** Thailand

Education :

1997	B.Sc. (2^{nd} class honor) in Chemistry, Mahasarakham University, Mahasarakham, Thailand
2006	Ph.D. in Chemistry, Suranaree University of Technology, Nakhon Ratchasima, Thailand

Experience :

1998	Teaching Assistant (TA), School of Chemistry, Institute of Science, Suranaree University of Technology, Nakhon Ratchasima, Thailand
2005 - 2006	A research visit, Department of Chemistry and Biochemistry, California State University, Fullerton, Orange, California, USA

Scholarship :

1999 – 2006	The Royal Golden Jubilee (RGJ) Ph.D. research scholarship from Thailand Research Fund (TRF)

Research Publications :

- Deeying, N., and Sagarik, K. (2006). Effects of Metal Ion and Solute Conformation Change on Hydration of Small Amino Acid, **Biophysical Chemistry,** accepted.